TECHNISCHE UNIVERSITÄT MÜNCHEN

Lehrstuhl für Flugsystemdynamik

A New Design Framework For Impact Time Control

Raziye Tekin Erer

Vollständiger Abdruck der von der Fakultät für Maschinenwesen der Technischen Universität München zur Erlangung des akademischen Grades eines

Doktor-Ingenieurs

genehmigten Dissertation.

Vorsitzender: Prof. Dr.-Ing. Hans-Jakob Kaltenbach

Prüfer der Dissertation:
1. Prof. Dr.-Ing. Florian Holzapfel
2. Prof. Dr. Joseph Z. Ben-Asher
   Technion – Israel Institute of Technology, Israel

Die Dissertation wurde am 11.01.2018 bei der Technischen Universität München eingereicht und durch die Fakultät für Maschinenwesen am 24.04.2018 angenommen.

ACKNOWLEDGMENT

I would like to thank

my supervisor Prof. Dr.-Ing. Florian Holzapfel firstly for providing a free working environment and for the endless enthusiasm he shared with me;

Prof. Joseph Z. Ben-Asher who introduced me the latest studies and spared time for me during his visits, which were valuable;

Paul Zarchan for the encouragement he provided during the difficult times and for joining the dissertation presentation;

Dr. Koray Savaş Erer for the strong technical discussions and the support throughout the whole process;

Höhndorf family for their warmest hospitality;

my colleagues at FSD Team for the time we spent together;

Aselsan Academy for supporting the thesis for the last two years;

my family;

and finally to Gocabey whom I do not even know where he eternally rests.

to Hypatia of Alexandria
with my deepest respect,

ABSTRACT

This dissertation focuses on the problem of impact time control by utilizing a new design framework that is stated as shaping the fundamental states of the engagement via polynomials in time. The specific application considered in the study is missile guidance; however, the techniques developed are in principle applicable to any practical setting that concerns the time of arrival. Identifying the range and the look angle as the fundamental states that define the nonlinear engagement kinematics between a missile and a stationary target, three different guidance laws to control the impact time are derived by means of the proposed framework. Through these methods, none of which require the time-to-go to be estimated, the time domain solutions of various engagement variables are made available. The first guidance law is the result of shaping the range as a general form polynomial, whose coefficients are derived for any order. The method can be implemented either as open loop or as closed loop, the latter showing robustness in the presence of disturbing factors such as noise and autopilot lag. The second guidance law is based on a multi-phased look angle profile, where the phases are characterized by straight line segments. This structure makes it possible to calculate the minimum and maximum impact times under the acceleration and look angle constraints. The third guidance law follows from a similar approach as the first one. The look angle is shaped in the form of a general order polynomial. Both open- and closed-loop mechanizations are possible. Unlike the previous ones, the guidance gain must be obtained either by solving an integral equation or by linearizing the system. In addition, the impact time control problem is solved under varying speed, which is typically caused by drag and gravity. For this purpose, a predictive-adaptive algorithm, which adapts the gain of the third guidance law with respect to the predicted mean speed, is proposed.

Keywords: Impact Time Control, Trajectory Shaping, Constrained Guidance, Varying Speed.

CONTENTS

LIST OF FIGURES

LIST OF TABLES

LIST OF SYMBOLS

M : Missile

T : Target

V : Speed

r : Range

γ : Flight path angle

ε : Look angle

λ : LOS angle

$\dot{\gamma}$: Flight path angle rate

a : Control acceleration

t_{d} : Desired time

t_f : Final time

t_{go} : Time to go

t : Time

N : Navigation gain

ε_0 : Initial look angle

R_0 : Initial range

$\dot{\gamma}_f$: Final path angle rate

S : Trajectory length

x_i : Coefficient of the polynomials

n : Order of the polynomials

τ : Time constant

t_f^* : Critical impact time

t_s : Switching time

m : Slope

m_c : Critical slope

$t_{f,c}$: Critical impact time

τ : First order autopilot lag

g : Gravity

1 INTRODUCTION

The fundamental objective of the missile guidance is that it must lead the pursuer to the target. In addition to this, the application of interest might necessitate other objectives. For example, the secondary objective could be approaching the target from a specific direction, which is possible with impact angle control. Another objective might be to capture the target at a specified time, which requires impact time control. Additionally, both of these terminal constraints might be needed together, which can be addressed with a simultaneous control of the impact time and angle. Depending on the application, being able to control the shape of the trajectory and consequently the impact geometry might mean one or a combination of the following advantages: exploiting the weak points of the target, increasing the effector effectiveness, avoiding directional defense mechanisms, or reducing the collateral damage, etc.

Parallel navigation states that two objects will eventually meet if the line of sight (LOS) connecting them does not rotate with respect to an inertial frame of reference [1]. Any successful implementation of this rule is expected to drive the miss distance to zero; such that the pursuer must capture its target, which is the first objective of the missile guidance. Proportional navigation (PN) is a frequently utilized guidance law that implements the parallel navigation rule [1,2]. The basic philosophy behind PN is that the missile acceleration should nullify the LOS rate between the target and the missile [3]. There are several kinds of PN classified according to the direction of the commanded acceleration [4]. True PN [5] and pure PN [6] are the well-known forms. In true PN, the acceleration vector is normal to the LOS whereas in pure PN, it is normal to the velocity vector of the pursuer. The latter is an advantage for endo-atmospheric systems since no change of speed is required [7]. It is known that pure PN can capture a non-maneuvering target for almost all initial conditions [6] and the closed form solution of such an engagement is in the form of a uniformly convergent infinite product

[8]. Another form of PN is ideal PN [8]. In this case, the acceleration vector is normal to the relative velocity vector between the target and the pursuer.

It might be possible to obtain the secondary objectives of the guidance process by constructing the required initial geometry. However, there will be limited authority on the initial conditions in a realistic situation, which makes this approach infeasible. “Trajectory shaping” is an alternative approach to adjust the initial conditions in order to succeed in achieving the secondary objectives [2]. This phrase refers to the control action performed by the missile in order to modify its trajectory rather than following the direct course towards the target.

Among the secondary objectives, impact angle control could be considered the most popular objective of trajectory shaping. It is possible to find a considerable number of works focusing on impact angle guidance in the literature dating back to 1970s. Impact angle control facilitates approaching the target from a certain direction; thus, controlling the impact angle might provide invisibility for a certain time. Furthermore, the effector effectiveness can be increased such as with top attacks. One of the earliest studies on impact angle is the one presented in [9]. There, it is shown that optimal control makes it possible to compensate for the pursuer dynamics in a systematic manner. In [10], optimal impact angle control laws are generalized for arbitrary system order and the time-to-go estimation on the closed form trajectory solutions is discussed. [11] shows that the impact angle can be controlled by means of bias addition to the pure PN guidance with three alternatives and in the end, the guidance laws do not require the time-to-go. The study in [12] is one of the few examples of directly considering the seeker field of view (FOV) limit in the design of an impact angle control law. The FOV limit is handled over the look angle under the small angle of attack assumption. The solution dictates switching action so as to keep the look angle constant in between phases of unconstrained optimal guidance. However, the look angle constraint is not the only constraint to be considered while shaping the trajectory. In addition, maneuverability is another constraint. In [13], a two-phase guidance law, which has a PN-based structure, is presented to handle the look angle and the acceleration constraints. Moreover, a comparison of unbiased and biased formulations of PN was made in [14], where the look angle constraint was considered directly.

In contrast to impact angle control, impact time control did not get much attention. The first impact time paper in the open literature is [15] to the knowledge of the author. It is presented in 2006, which is more than thirty years later with respect to the oldest impact angle paper.

However, in correlation with the increasing complexity of the strategic targets with powerful defensive systems, it could be said that the attention has been increasing in recent years. For instance, most of the modern ships have defense systems against anti-ship missiles and aircraft. These defense systems include surface-to-air missile systems, electronic warfare support systems, electronic counter measures, chaff decoys and close-in weapon systems (CIWS) [16]. CIWS is typically a naval shipboard weapon system against incoming anti-ship missiles and aircraft. It consists of radars, computers, fire control systems, multiple barrel and rotary rapid fire guns, all of which mainly works on the principle of one to one engagement [17]. In order to complete a mission against targets with such defensive systems, the survivability of the missiles needs to be increased. One of the strategies to survive against CIWS is to circumvent the disadvantage of a one-to-one engagement by facilitating a salvo attack. "Salvo" by the dictionary meaning is a discharge of weapons in unison, on a ceremonial occasion [18]. In the salvo attack strategy, the common target is tried to be hit as simultaneously as possible.

A salvo attack could be achieved via at least three different methods. The first solution is a preprogrammed guidance strategy where the launchers are mostly on different platforms. In this configuration, the launch conditions are adjusted according to the desired impact condition in order to provide the same impact time. However, such a manual routine might not be a straightforward task to accomplish. Thus, the guidance problem should be handled in a different way that could provide options to enhance the operational flexibility and survivability. The second approach is cooperative homing where the missiles communicate among themselves to have the same arrival time. In other words, the missiles with larger times-to-go try to accomplish high-g maneuvers to have a direct course, whereas the others curve their trajectories to delay their arrival times. The common impact time is not required to be determined in advance; however, online data links must be available throughout the engagement which might be quite challenging. The third method is individual homing. Here, again a common impact time is desired and commanded to all of the missiles. Thereafter, each missile tries to accomplish the desired impact time independently.

The mentioned attack models directly or indirectly require the control of impact time. In addition to salvo attack, impact time control could be employed to make the missile pass through a certain waypoint at a specified time related to its mission. Moreover, time control could be required for UAVs, drones and for other unmanned systems with or without defense

tactics. The very first purpose of the study is to present feasible guidance laws for impact time control, which could be used for individual homing or any time control oriented missions.

1.1 Literature Review and State of the Art

One of the earliest studies on impact time control is presented in [15] as mentioned previously. The guidance law, which originates from a linear formulation, is based on PN. A feedback term, which is the estimated time-to-go, is added to the PN to regulate the impact time error. The same authors extend the previous work to the nonlinear kinematics in [19]. In [20], a polynomial function of the downrange-to-go is introduced with two coefficients. They are determined to satisfy the terminal miss distance and the impact time for the linearized kinematics. After mathematical manipulations, the guidance command results in the biased PN guidance with an arbitrary navigation constant greater than two to capture the target. Additionally, the bias term is updated at each time step to achieve the impact time. [21] suggest a better time-to-go estimation for pure PN and solves the impact time control problem against stationary targets for the nonlinear kinematics. Here, impact time control is managed with a modified time varying gain rather than a constant one as in [15], [19] and [20]. The disadvantage of the method is related with the bias term. For instance, the guidance command can be discontinuous. The study in [22] applies a virtual leader scheme that transforms the impact time control problem into a nonlinear tracking problem, where the guidance command is composed of a PN term and a flight time error.

The problem of impact time control is treated in the literature also through the coordination of missiles during the engagement. This approach requires the missiles to have data links for communication. One example in this direction is given in [23]. Here, the guidance law in [15] is adopted and the main concern of the study is the derivation of the distributed and centralized coordination algorithms to be used in salvo attack. The work in [24] is another study in the same direction, where a PN tactic with a bias term is considered. In this study, the bias term is a time varying navigation gain that is adjusted based on the time-to-go of the individual missile and the times-to-go of the cooperating missiles.

As well as PN-based impact time guidance laws, there exist numerous studies based on the nonlinear control theory. A Lyapunov-based approach is considered in [25] using the same time-to-go estimation as in [15] for planar engagements. Afterwards, the guidance law is extended to the three dimensional environment. In [26], Lyapunov theory is employed to design

a guidance law with an analytical solution for the impact time, which cannot lead to wide impact time intervals since the look angle is made to decrease monotonously during the engagement. Sliding mode control is also considered for impact time control purposes. In [27], a switching surface as a combination of the impact time error and the LOS rate is used. The same authors enhanced their previous study for large heading errors and negative closing speeds in [28]. Another sliding mode control for impact time is presented in [29]. Unlike [27] and [28], a sliding surface, which is only a function of the impact time error, is suggested in this study. In addition, several modifications are made to deal with the singularity of the guidance command. Nevertheless, the common disadvantage of these guidance laws designed via the nonlinear control theory is the high acceleration demand at the beginning of the engagement.

Thus far, the mentioned impact time control studies do not have any physical constraints in consideration. Independent of any guidance objectives, all missiles are subject to various physical constraints. For instance, for endo-atmospheric missiles equipped with target seekers, the seeker angle and the acceleration limitations are probably the most basic factors. Therefore, they need to be addressed during the process of guidance design. However, impact time control considering physical constraints did not receive much attention from researchers, either. A few recent studies regarding impact time control under the FOV constraint can be seen in [30], [31] and [32]. An impact time control law that has a similar structure as in [19] is developed in [30]. In the study, the bias term is used for controlling the impact time while treating the constraint by a rule of weighted heading angle under monotonically decreasing range assumption. [31] is another study from the authors of [30], which includes autopilot lag and FOV constraint in the design process. [32] proposes an impact time control law that results in a varying gain PN structure. The guidance law decreases the seeker's look angle monotonically from the initial value to zero at intercept; thus, higher initial look angles are preferred for a wider impact time interval.

The methods mentioned so far (except [26]) require time-to-go estimation in their design as a feedback source for impact time control. However, it is not an easy task to have the time-to-go. Additionally, time-to-go estimation is actually necessary not only for impact time control, but also for implementing various optimal and impact angle control guidance laws. It could certainly be said that time-to-go estimation is indeed a separate research topic. Therefore, it would be convenient to mention several studies on this topic. In [33], a recursive time-to-go

computation method is suggested for PN, augmented PN and optimal guidance laws for varying speeds. In [34], time-to-go estimation for the PN guidance is proposed by using the time scaling property of the guidance law. Thus, the method can be used for any initial condition and navigation gain via interpolation from the base solution to other initial conditions. [35] is applicable to the general class of PN guidance laws including negative gains, which is derived as a closed-form approximation of the range, the navigation gain and the heading error. Afterwards, recursive numerical computations are used for time-to-go estimation. It needs to be reminded that although the term "time-to-go estimation" is widely used in the guidance literature, the phrase should be "time-to-go prediction" as mentioned in [35]. In order to be consistent with the literature, it will be used as "estimation" throughout the thesis.

As an alternative to devoting efforts to the potentially problematic estimation process, the impact time control problem can also be solved without relying on the time-to-go information as in [36]-[39]. [36] proposes the idea of shaping of the relative look angle profile to control the impact time. A two-phased guidance scheme for indirect control of impact time against moving targets is devised based on this idea. However, the guidance law requires a controlled change of the missile speed. Motivated by [36], [37] suggests second and third order polynomial guidance laws via look angle shaping. Here, the guidance gain is determined by solving an integral equation in order to satisfy the requirement of zero miss distance at intercept. Additionally, the third order approach produces trajectories close to the optimal ones. The method in [38] utilizes the concept of zero effort miss vector to direct the total acceleration so that the moving target is captured at a specified time. Such as [36], the proposed guidance law does not need time-to-go estimation, but requires speed control. The guidance law in [39] is derived by shaping the range as a quartic polynomial of time. The nonlinear design results in a closed loop guidance law showing robustness under lagged response and seeker noise. In [40], the same authors extend the previous study for any order of the range, providing a feasible guidance law that is also capable of operating under the look angle constraint.

Naturally, the impact time can also be enforced via guidance schemes that aim at simultaneous control of the impact time and angle. In [41], the guidance command is composed of two parts, where the first part is for the impact angle constraint with zero miss distance and the second part is for the impact time constraint. The sliding mode control theory is used in [42], where a LOS rate shaping process as a function of downrange is introduced. Besides, a second-order sliding mode control law is introduced using a back-stepping concept to provide

robustness in the presence of uncertainties. A polynomial guidance law is proposed in [43], where the three unknown coefficients of the polynomial are determined with respect to the terminal conditions accounting for the linearized kinematics. [44] assumes that the acceleration command can be represented as a polynomial function of the downrange with two coefficients. The design is based on the linearized kinematics, too. Apart from these, a numerical energy optimal solution is presented in [45], where the impact time and angle control problem is treated as a two-point boundary value problem. In [46], a practical guidance law is proposed to control the impact time or/and the impact angle under the look angle and the acceleration constraints. Starting with the nonlinear optimal control framework, the solutions dictate the familiar PN guidance law.

The key assumption in all of the cited studies until now is that the speed of the missile is either constant or, in a few occasions, controllable. Since impact time control is mainly applicable to anti-ship missiles, this assumption is not entirely unjustified since such missiles could sustain speed control [47]. Nevertheless, the constant speed assumption restricts the domain of application. In fact, the speed is not even controllable in most of the missile applications. It changes under the action of drag, thrust and the trajectory being followed. The works presented in [49] and [50] consider the impact time control problem under varying speed. In [49], which devises a quad-segment polynomial method via parameterizing the trajectories in terms of the downrange, doing a pre-flight analysis is proposed as a first step in coping with the speed change. In [50], on the other hand, integral sliding mode control is performed, taking into account the rate of change of the speed and its limits. However, a pre-flight analysis as in [49] might not always be feasible and having the terminal acceleration systematically diverging away from zero as in [50] could be prohibitive. Except from these, one of the works mentioned previously tries to cope with the varying speed by using an average speed concept [28]. However, the study assumes that the speed remains constant for the sustain phase and gravity is not included in the average speed calculation. In addition, it covers only supersonic missile systems, where the speed is assumed to be decreasing as an exponential function.

Varying speed is assuredly a problem not only for the impact time problem, but also for the optimal guidance laws, too. There are several studies, which concentrate on this issue for supersonic systems as in [28]. An energy-optimized guidance law is presented in [51], where the guidance gain is varied via a time-to-go-like function. This function considers the future missile speed and adjusts the guidance gain with respect to the predicted speed. In [52], an

extension to the previous study is presented while providing two schemes for the mean speed and general-case cost functions for the varying speed.

In addition to the varying speed, another major concern during the guidance design process is robustness. Autopilot lag and measurement noise are among the factors that impact the mission success. One example in the direction of robustness is the adaptive guidance schemes which are applied for dealing with varying conditions. Here, adaptation means updating the guidance gains with respect to those conditions and no connection with the conventional adaptive control is implied. In this extent, the impact angle control problem is studied in the literature. In [53], a nonlinear parameter adaptation scheme is presented for a hypersonic gliding vehicle. The study in [54] develops two adaptive guidance laws, one of which is based on the conventional PN guidance and the other one is based on controlling the turn rate of the relative velocity vector. In both of these studies, the guidance gains are updated in a closed loop manner; therefore, they are able to deal with the varying conditions. Motivated by the future mean speed concept and adaptation for guidance purposes, [55] presents a predictive-adaptive formulation to deal with these concerns, where the guidance laws in [37] are generalized using an n^{th} order polynomial of the look angle. Unlike [37], the linearized kinematics is used to obtain an analytical solution for the guidance gain. It is then extended to the nonlinear domain by considering an adaptive guidance scheme. Such adaptation through periodically updating the guidance gain is not only able to overcome the unmodeled nonlinearities, but it also provides robustness against disturbing factors. However, adaptation will only be sufficient as long as the speed of the missile remains constant; thus, the mean speed is predicted for the interval between the current time and the final time using an iterative process, where the overall guidance turns into a predictive-adaptive impact time control method.

1.2 Objectives

The main objective of the thesis is to develop feasible guidance laws for impact time control. For that purpose, a design framework different than the current literature is undertaken. Optimization is a common approach that is known to lead to solutions to many engineering problems, providing optimality as a byproduct [56]. However, it is not the only framework that can provide feasible solutions. As stated in [57], another option might be computational guidance and control. However, using brute force during the flight might still be restrictive, in

spite of the rapidly developing technology. Even though, the optimal control theory and numerical routines are indeed used in this study, promoting another design methodology for impact time control is deemed essential.

As it was already mentioned in the literature survey, many methods devote considerable effort to time-to-go estimation. The estimation results enter the guidance algorithm as a potential error source. Therefore, the performance of such impact time control algorithms highly depends on the accuracy of the time-to-go estimate, which might prove to be quite problematic. Additionally, the estimated time-to-go usually corresponds to the PN guidance process. As a result, the trajectory eventually evolves into a PN trajectory. This implies that the missile trajectory could easily be estimated by the defense systems. Thus, the second objective of this work can be summarized as follows: To construct a guidance law that does not require the time-to-go used as a feedback signal for impact time control.

The third objective is related with the assumptions, which are usually made during the design process. The linearized kinematics and constant speed are the two common assumptions used by the guidance algorithms related with the impact time. Although there are several studies considering the nonlinear kinematics, there is not a noteworthy contribution on the topic of impact time control for varying speed. As mentioned, the speed is a time varying parameter in reality. Thus, another objective of this thesis is to design a guidance scheme that is useful not only for vehicles with constant or controlled speed but also for those, whose speed is varying.

The last objective is to present an impact time control solution under the physical constraints, because any guidance law needs to handle these either during the design or the engagement, where the former case is preferred to avoid unexpected saturation. Since this subject has not received the attention it deserves, the thesis aims to provide a practical way of controlling the impact time under the look angle constraint and/or the acceleration constraint.

1.3 Contributions

The following aspects are regarded as the main contributions of this study to advance the current state of the art.

A Novel Design Framework Enabling Three Feasible Guidance Laws:

Identifying the fundamental states of the impact time control problem as the range and the look angle, this study introduces the framework termed as “shaping of the fundamental engagement states”. Relying on this novel framework, in which the shaping functions are time dependent, three guidance laws are proposed. One of these is based on range shaping and the others are based on look angle shaping. Through these guidance laws, various closed form solutions of the engagement states are also made available, which provides precious information for the guidance designer.

Time-to-go Estimation Free

Unlike the widespread guidance methods, none of the techniques presented in the thesis rely on time-to-go estimation. Instead, the difference between the current time and the desired impact time is used in the guidance command.

Impact Time Control Under Varying Speed

This problem is solved in a predictive-adaptive scheme with the help of the time domain solution of the states, which is obtained through the polynomial look angle shaping method.

Solutions Under Physical Constraints

Practically implementable impact time control laws under physical constraints are presented. Both the look angle constraint and the acceleration constraint are treated properly. Either the impact time intervals are defined with respect to the constraints or new guidance structures are suggested that do not violate them.

Many of the novel designs and applications described in this thesis have been published, while this thesis provides more comprehensive details.

Journal Publications

1. **Tekin, R.**, Erer, K. S., and Holzapfel, F., “Impact Time Control with Generalized-Polynomial Range Formulation,” *Journal of Guidance, Control, and Dynamics*, Vol. 41, No. 5, 2018, pp. 1190-1195.

2. **Tekin, R.,** Erer, K. S., and Holzapfel, F., "Adaptive Impact Time Control via Look Angle Shaping Under Varying Velocity," *Journal of Guidance, Control, and Dynamics,* Vol. 40, No. 12, 2017, pp. 3247–3255.
3. **Tekin, R.,** Erer, K. S., and Holzapfel, F., "Polynomial Shaping of the Look Angle for Impact-Time Control," *Journal of Guidance, Control, and Dynamics,* Vol. 40, No. 10, 2017, pp. 2668–2673.
4. **Tekin, R.,** Erer, K. S., and Holzapfel, F., "Control of Impact Time with Increased Robustness via Feedback Linearization," *Journal of Guidance, Control, and Dynamics*, Vol. 39, No. 7, 2016, pp. 1682–1689.
5. Erer, K. S., and **Tekin, R.,** "Impact Time and Angle Control Based on Constrained Optimal Solutions," *Journal of Guidance, Control, and Dynamics*, Vol. 39, No. 10, 2016, pp. 2448–2454.
6. **Tekin, R.,** and Erer, K. S., "Switched-Gain Guidance for Impact Angle Control Under Physical Constraints," *Journal of Guidance, Control, and Dynamics*, Vol. 38, No. 2, 2015, pp. 205–216.

Conference Papers

- **Tekin, R.,** Erer, K. S., and Holzapfel, F., "Quartic Range Shaping for Impact Time Control", Control and Automation (MED), 2017, 25th Mediterranean Conference, Valetta, Malta, 2017.

1.4 Thesis Outline

Chapter 2 identifies the fundamental engagement states and presents the nonlinear differential equation set governing the engagement kinematics between a guided missile and a stationary target. Afterwards, the impact time problem is stated and several fundamental impact time definitions are given.

Chapter 3 introduces the first of the guidance laws, which relies neither on a time-to-go estimate nor on the linearized kinematics. The guidance design assumes that the range, which is the first fundamental state of the nonlinear kinematics, could be described as a polynomial in time. Using range as a shaping state provides a feasible basis, since the polynomial

coefficients are analytically available. Then, the guidance law is expressed as a combination of the rates of the look and the LOS angles. After presenting the open loop structure of the guidance law, the closed loop formulation of the guidance law is derived. Since the maximum look angle is determined by the suggested design methodology, two methods for the look angle constrained impact time control are derived. The performance of the proposed methods is demonstrated in a comparative simulation study that involves the energy optimal guidance solution and [29] from the literature, which is based on sliding mode control and time-to-estimation. Additionally, it is also shown that the adverse effects of sensor noise and lagged response can be avoided with the closed loop implementation of the proposed guidance law. Moreover, instead of the true range information, estimated range is used in the guidance law. Owing to the nature of the closed loop guidance, the guidance law has satisfactory results under these circumstances.

Chapter 4 investigates the guidance problem by focusing on the look angle, which is the second fundamental state of the nonlinear kinematics. The main idea is to provide a time-dependent profile of the look angle to control the impact time without the need for time-to-go estimation. For that purpose, multi-phased look angle structures are designed. First, a two-phased shaping process is expressed, where the analytical derivation of the guidance strategy is divided into cases. Furthermore, the acceleration limit is considered during the design. Second, a three-phased approach leads to another solution that differs from what is available in the literature in the following respect: The impact time control problem is addressed by considering the full extent of the available resources in the form of the look angle and the acceleration constraints. Based on the switched structure of the guidance command, a practical guidance law to control the impact time without violating the constraints is derived. It is then shown that this result is also made possible by the use of the nonlinear optimal control framework, where the cost function does not involve a running cost but it is made up of an endpoint cost aiming to extremize the impact time.

Chapter 5 discusses the impact time problem via a continuous, i.e. no switching, form of look angle shaping. Motivated by the range shaping results and with the knowledge gained from Chapter 4, the design comes up with a function based on the general form of a time dependent polynomial. This shaping function leads to a single gain guidance law while satisfying the general objectives of a nonlinear engagement. The time domain solutions of the engagement states are also provided. Although, the guidance gain could be determined by a

numerical routine, the linearized kinematics are also suggested to provide an analytical expression of the guidance gain. Additionally, the maximum values of the look angle and the acceleration, which are obtained during the engagement, are solved. Comparative simulation runs confirm that the proposed technique is also advantageous in terms of control effort. Owing to the fact that the final look angle rate is constrained to be zero, the results obtained with cubic shaping turn out to be similar to the energy optimal results.

Chapter 6 is devoted for impact time control under time varying speed. First, the solution in Chapter 5 is extended to the nonlinear domain by considering an adaptive guidance scheme. Adaptation through periodically updating is not only able to overcome the unmodeled nonlinearities but it also provides robustness against disturbing factors such as autopilot lag. However, adaptation will only be sufficient as long as the speed of the missile is constant. The situation is indeed more problematic that the speed profile eventually depends on the trajectory, which is the result of the guidance law itself. If the future speed profile, or equivalently, the mean value of this profile can somehow be predicted, this information could be used to feed the adaptive guidance process. For that purpose, an approach to predict the mean speed is developed using the linearized kinematics and then it is modified for the nonlinear kinematics. At each guidance step, the mean speed is predicted for the interval between the current time and the final time using an iterative process, where the eventual objective is the adaptation of the guidance gain based on the predicted mean speed. One of the key points of the design is that it could be applied to any guidance law that somehow provides the time domain solutions of the flight path angle and the guidance command. After presenting examples with constant speed for the adaptive scheme, more realistic ground-to-ground scenarios with non-constant speed profiles including autopilot lag are exemplified for the predictive-adaptive impact time control method. In addition, comparisons with energy optimal solutions are provided.

2 PRELIMINARIES

This chapter aspires to familiarize the reader with the basics of the nonlinear engagement kinematics and the fundamental definitions of impact time control.

2.1 Nonlinear Engagement Geometry

Figure 2.1 depicts the two dimensional, point mass engagement geometry between a stationary target *T* and a missile *M*. The speed of the missile is *V* and the magnitude of its acceleration component perpendicular to the velocity vector is *a*. The speed is free to vary under the action of several factors such as gravity and drag, but not with the control input. The inertial coordinate system is fixed to the surface of a flat-Earth model: x axis is the downrange and y axis can either be altitude or crossrange. $\vec{u}_r$ is the unit vector in the direction of $\vec{r} = \vec{p}_T - \vec{p}_M$. p denotes the position and *r* is the magnitude of the range vector. λ denotes the LOS angle that $\vec{u}_r$ makes with respect to $\vec{u}_x$, where $\vec{u}_x$ is the unit vector in the x direction. The angle between the velocity vector and the LOS is the look angle ε; the angle $\vec{u}_V$ makes with respect to $\vec{u}_r$, where $\vec{u}_V$ is the unit vector in the $\vec{V}$ direction. γ is the flight path angle made by $\vec{u}_V$ with respect to $\vec{u}_x$. All angles are positive in the counter-clockwise direction.

The guidance objective is to design the input a, equivalently $\dot{\gamma}$, in such a way that the target is captured, that is $r_f = 0$ desired value of the final time $t_f = t_d$. Here, the subscript *f* represents the final time and *d* denotes the desired time.

It is clearly observed in Figure 2.1 that the LOS and the flight path angles are measured with respect to an inertial frame of reference. If the reference frame was changed to another one that has a constant angular offset from the current one, the values of these angles would change. On the other hand, the look angle would remain the same because it is measured with respect to the LOS. This implies that the kinematics of a typical guidance problem, in which no direct

external reference is required, can be expressed in terms of the range and the look angle. As with the zero miss distance problem, this is the case with the impact time control problem. Therefore, the range and the look angle are termed as “the fundamental engagement states” in this study. A counter example would be the impact angle control problem, where an external reference is required to define the impact angle.

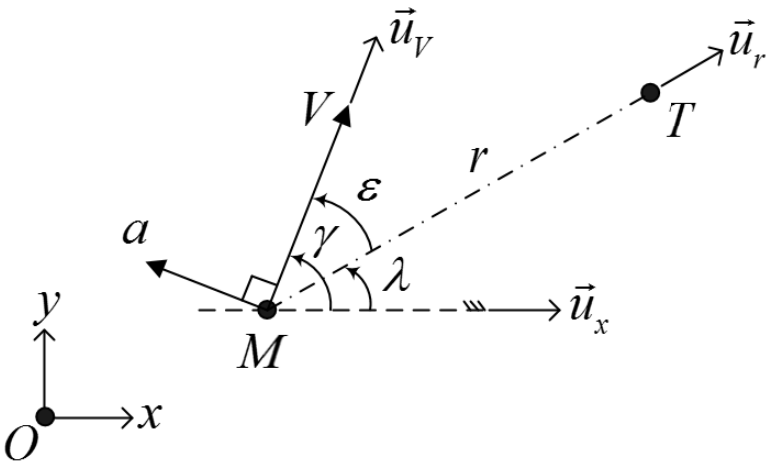

Figure 2.1 Engagement geometry between a stationary target and its pursuer.

2.2 Nonlinear Engagement Kinematics

As there are two degrees of freedom associated with the movement of a point in the plane, two differential equations are required to initiate the mathematical manipulation. A visual inspection of Figure 2.1 suggests that a polar representation with r and λ could be suitable. Accordingly, the first differential equation is directly written as

$$\dot{r} = -V\cos(\gamma - \lambda) \tag{2.1}$$

where the dot operator represents derivative with respect to time, i.e. $\mathrm{d}/\mathrm{d}t$. The derivation of the second differential equation could start with the LOS angle:

$$\lambda = \tan^{-1}\left(\frac{r_y}{r_x}\right) \tag{2.2}$$

where r_x and r_y are respectively the *x* and *y* components of vector $\vec{r}$ that is directed from *M* to *T*. Due to the stationary target, $\dot{r}_x = -V_x$ and $\dot{r}_y = -V_y$. Here, V_x and V_y are respectively the *x* and *y* components of vector $\vec{V}$. The LOS angle rate can be obtained by differentiating Eq. (2.2)

$$\dot{\lambda} = -\frac{r_x V_y - r_y V_x}{r^2} \tag{2.3}$$

The other angle related with the engagement is the look angle:

$$\varepsilon = \gamma - \lambda \tag{2.4}$$

If the sine function is applied to both sides, Eq. (2.4) yields

$$\sin\varepsilon = \sin\gamma\cos\lambda - \cos\gamma\sin\lambda \tag{2.5}$$

This could be rewritten in terms of the range and the velocity components as

$$\sin\varepsilon = \frac{r_x V_y - r_y V_x}{r^2}\frac{r}{V} \tag{2.6}$$

Using Eq. (2.3) in Eq. (2.6) will reveal the second differential equation of the nonlinear engagement kinematics:

$$r\dot{\lambda} = -V\sin\varepsilon \tag{2.7}$$

The first differential equation could be written in a compact form as

$$\dot{r} = -V\cos\varepsilon \tag{2.8}$$

by using Eq. (2.4) in Eq. (2.1). The complementary equation defining the relationship between the angles given in Eq. (2.4) will be one of the main equations that is required to obtain the guidance commands. Thus, the time derivative of Eq. (2.4) is modified to obtain the rate of the flight path angle as

$$\dot{\gamma} = \dot{\varepsilon} + \dot{\lambda} \tag{2.9}$$

2.3 Length of a Trajectory

The length of the trajectory is the point of interest for impact time control and must satisfy the following equality:

$$S = Vt_f \tag{2.10}$$

under the constant speed assumption. The distance along a curve between the points *A* and *B* on the trajectory is called the arc length expressed as

$$S = \int_A^B ds \tag{2.11}$$

The infinitesimal distance traveled ds satisfies

$$ds = \sqrt{dx^2 + dy^2} \tag{2.12}$$

and the total length travelled is

$$S = \int_{t_1}^{t_2} ds = \int_{t_1}^{t_2} \sqrt{\left(\frac{dx}{dt}\right)^2 + \left(\frac{dy}{dt}\right)^2}\, dt \tag{2.13}$$

during the relevant time interval. Eq. (2.12) may be written as

$$ds = \sqrt{1 + \left(\frac{dy}{dx}\right)^2}\, dx \tag{2.14}$$

and the distance travelled may be expressed as

$$S = \int_{x_1}^{x_2} ds = \int_{x_1}^{x_2} \sqrt{1 + \left(\frac{dy}{dx}\right)^2}\, dx \tag{2.15}$$

As it is shown in Eq. (2.15), it could be guessed why the impact time control studies mostly evolve to use the downrange to parametrize their equations during the guidance design process such as in [42], [43] and [44]. However, Eq. (2.15) is nonlinear and analytically not integrable in general. Thus, immense mathematical modifications would have to be made, which yields

the guidance law in an unfeasible final form. Additionally, Eq. (2.15) is not directly used in this study to design the guidance laws.

2.4 Important Impact Time Values

Before proceeding further, several important impact time definitions will be made, each of which is either a limiting or a comparison factor for the designer. The very first definition is the theoretical minimum impact time, which demands unbounded acceleration. Under the assumption of the constant speed, it is expressed as the initial range, R_0, divided by the speed of the missile

$$t_{theo,\min} = \frac{R_0}{V} \tag{2.16}$$

However, this value is impossible to realize while dealing with real applications. Second, if the initial look angle is maintained to the end of the engagement, then no correction impact time becomes

$$t_n = \frac{R_0}{V\cos\varepsilon_0} \tag{2.17}$$

where ε_0 is the initial look angle. Since the guidance laws in this study does not demand sign change of the look angle, the derivations are presented for $\varepsilon_0 \geq 0$ without loss of generality to prevent unnecessary confusion. This equation is obtained by integrating Eq. (2.8) with constant look angle. However, the designer must be aware of the fact that such a guidance routine will result in unbounded acceleration, (see Figure 2.2). Third, the well-known PN guidance law is expressed as

$$\dot{\gamma} = N\dot{\lambda} \tag{2.18}$$

where N is referred to as the navigation gain. The approximate impact time of PN can be obtained as given below [24] (for details see Appendix A):

$$t_{PN} \approx \frac{r}{V}\left(1+\frac{\varepsilon_0^2}{2(2N-1)}\right) \tag{2.19}$$

In order to have a basic awareness, a ground-to-ground engagement is exemplified, where the target is initially 5 km away. The speed of the missile is 200 m/s and the initial look angle is 80°. The look angle is maintained by $\dot{\gamma} = \dot{\lambda}$, which is actually PN with unity gain. The guidance commands are executed without latency and the simulations are terminated when the range is less than 1 m. Whereas Eq. (2.17) gives 143.97 s , the estimated impact time of PN with N = 3 from Eq. (2.19) is 29.87 s. On the other hand, the theoretical minimum impact time is 25 s, obtained via Eq. (2.16). The trajectories corresponding to these three cases are given in Figure 2.2. The theoretical impact time trajectory is essentially a straight line, whereas the no correction trajectory presents a logarithmic spiral behavior [1]. However, these two trajectories demand unbounded acceleration at the beginning or the end of the engagement, neither of which is realistic.

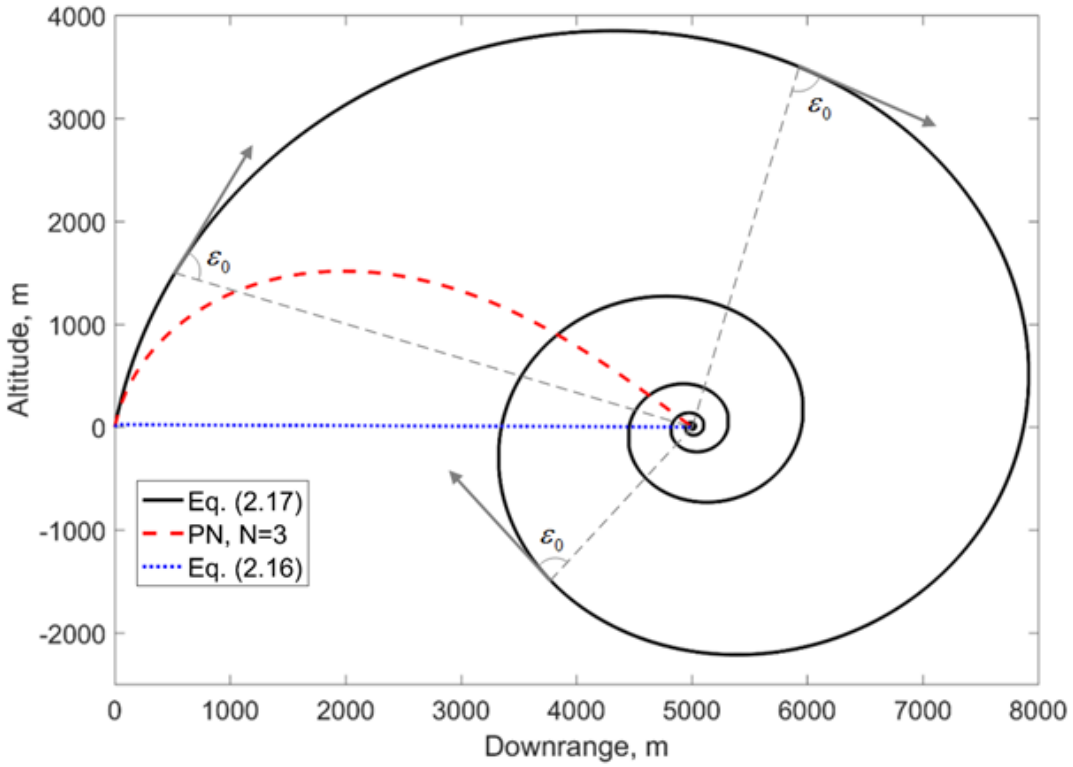

Figure 2.2 Example trajectories of the important impact time values.

3 GENERALIZED POLYNOMIAL RANGE SHAPING FOR IMPACT TIME CONTROL

In the literature, impact time control has been mainly addressed over time-to-go estimation. As mentioned in Chapter 1, PN-based approaches solve the length of the trajectory by means of Taylor expansion in order to obtain the guidance laws. Taylor expansion is essential since an analytical solution under the PN framework is not available. Moreover, linearization of the nonlinear engagement kinematics might be necessary depending on the formulation of the problem. Similarly, solutions based on the nonlinear control theory force the engagement geometry to a PN trajectory. This leads to the desired impact time only with high-g initial maneuvers; in contrast, a solution without high-g maneuvers would be beneficial.

As mentioned earlier, another design approach termed as state shaping might offer solutions for the secondary objectives of the guidance process. Following this direction, a basic shaping process is applied to the LOS and the LOS rate in [42] to control the impact time and angle simultaneously. In this study, the LOS rate is expressed as a function of downrange. The coefficients of the shaping function are determined with respect to the boundary conditions. However, the coefficient that is related with the impact time has to be determined either via trial and error or with an optimization routine. Unfortunately, this offline analysis is a result of the chosen complex function and the handling of the guidance problem is done over an indirect state. These issues make the guidance law inefficient. Another work regarding the shaping approach is [43], where rather than shaping a state, the acceleration command is assumed to be a function of the downrange. However, it requires linearization of the states and Taylor expansion for obtaining the length of the trajectory, all of which results in an infeasible and a complicated guidance law.

As outlined in the previous chapter, the kinematics of a typical impact time guidance problem can entirely be depicted in terms of the range and the look angle. It is also to be noted that as well as the selected state that is to be shaped, the structure of the shaping function is

also important. Since it is preferred to have feasible solutions, this will mainly depend on the existence of an analytical solution of Eq. (2.8). Moreover, shaping the state not as a function of the downrange but as a function of time could provide better solutions without the difficulties mentioned in the previous paragraph. Thus, a new design framework based on the shaping of the fundamental states of the engagement in the form of a time dependent function is introduced.

Motivated by the current state of the literature, the direction of this chapter is towards finding a feasible guidance law to shape the range as a function of time. The design is for the nonlinear kinematics and therefore, the small angle assumption is not applicable. Time-to-go estimation is avoided because a noisy estimate is not desired to be used as a feedback source to the guidance command. Unlike many approaches, it is not desired that the trajectory of the missile evolves into the PN trajectory, which could easily be estimated for counter measures. Furthermore, the time domain solution of any engagement state would be appreciated and the practical applicability of the design would be essential. With the hope of satisfying these requirements, it is assumed that the range equation could be defined as a polynomial of any order of time. Such a generalized range polynomial can be written as

$$r = x_n t^n + x_{n-1} t^{n-1} + ... + x_2 t^2 + x_1 t + x_0 \tag{3.1}$$

where n is the order of the range polynomial and x_i, where $i = 1 \ldots .n$ are the related coefficients of the polynomial.

The main objective of any guidance law is achieving zero miss distance, which happens to be the final condition of Eq. (3.1). As well as this primary condition, the guidance law must also satisfy other boundary conditions. For instance, zero look angle at the impact time is demanded in order to fulfill the necessary condition of having a bounded acceleration. (However, this is not sufficient by itself as will be shown later.) The initial values of the range and the closing speed are also to be satisfied. These four boundary conditions in fact provide the minimum order of Eq. (3.1), which can be expressed as $n \geq 3$. It should be kept in mind that if the order of the range polynomial is increased, then the number of the unknowns will accordingly increase. Hence, more boundary or intermediate conditions must be provided to solve for the coefficients. Thereafter, the engagement kinematics can be used to derive the guidance command.

In the following subsections; first, the general open loop solution of the impact time control problem is derived based on the constant speed assumption. Here, "open loop" refers to the fact that no regulation exists for the impact time error. Afterward, the guidance laws for several orders of the range polynomial are presented, highlighting the acceleration characteristics of each design. The next step is deriving the closed loop form of the guidance command. Furthermore, the impact time interval and the maximum look angle solution are studied. Next, sample simulations with the open loop structure are presented to provide an insight into the proposed impact time control strategy. In order to show a comparison, a guidance law from the literature and the energy optimal solution are included in the study. In addition to these sample scenarios, the simulation results under more realistic conditions such as those with autopilot, seeker lag, noisy measurements and lack of the true range are also presented. Finally, the impact time control method is modified to obtain a solution under the FOV constraint. For that purpose, two alternative solutions are derived and exemplified with simulations.

3.1 Determination of the Guidance Command

In order to obtain the guidance command for the n^{th} order range polynomial, $(n+1)$ equations are required. The very first equation to be mentioned is related with the primary objective of any guidance law: Zero miss distance. Thus, the final range must be zero, which can be written by replacing t in Eq. (3.1) with t_f:

$$x_n t_f^{\,n} + x_{n-1} t_f^{\,n-1} + ... + x_2 t_f^{\,2} + x_1 t_f + x_0 = 0 \tag{3.2}$$

Second, the most trivial boundary condition is the initial range, R_0, which directly gives the first coefficient

$$x_0 = R_0 \tag{3.3}$$

Third, when the final condition of the look angle is zero, then the final closing speed is $-V$. Using this relationship, the first time derivative of Eq. (3.1) is obtained and t is again replaced by t_f, leading to the following

$$\dot{r}\left(t = t_f\right) = n x_n t_f^{\,n-1} + (n-1) x_{n-1} t_f^{\,n-2} + ... + 2x_2 t_f + x_1 = -V \tag{3.4}$$

Afterwards, the fourth equation can be obtained via the initial condition of the closing speed

$$x_1 = -V\cos\varepsilon_0 \tag{3.5}$$

Eq. (3.5) provides x_1 regardless of the order of the range polynomial. So far, four equations are obtained regarding the boundary conditions. However, $(n-3)$ equations are still missing. A viable design decision could be forcing the higher derivatives of the range, i.e. $\ddot{r}, \dddot{r}, \ldots$, to zero at the final time. This leads to

$$\begin{bmatrix} \ddot{r} \\ \dddot{r} \\ . \\ . \\ . \\ \dot{r}^{(n-3)} \end{bmatrix}_{t_f} = \begin{bmatrix} n(n-1)x_n {t_f}^{n-2} + (n-2)(n-1)x_{n-1}{t_f}^{n-3} + \ldots\ldots + 6x_3 t_f + 2x_2 \\ n(n-1)(n-2)x_n {t_f}^{n-3} + (n-3)(n-2)(n-1)x_{n-1}{t_f}^{n-4} + \ldots\ldots + 6x_3 \\ . \\ . \\ . \\ n(n-1)(n-2)(n-3)\ldots\ldots\ldots 3x_n t_f \end{bmatrix} = \bar{0} \tag{3.6}$$

In this structure, the higher the value of *n*, the sooner $\dot{r}$ will converge to $-V$. This will also assist the look angle to converge to zero before intercept.

After the required equation set is obtained to solve for the coefficients of the n^{th} order range polynomial, the next step is to find the guidance command. The first time derivative of Eq. (2.4) gives the guidance command that is $\dot{\gamma} = \dot{\varepsilon} + \dot{\lambda}$. Therefore, $\dot{\varepsilon}$ has to be identified. For that purpose, the second derivative of the range equation is required:

$$\ddot{r} = V\dot{\varepsilon}\sin\varepsilon \tag{3.7}$$

Since $\ddot{r}$ is already available in Eq. (3.6), the look angle rate equation becomes

$$\dot{\varepsilon} = \frac{n(n-1)x_n t^{n-2} + (n-2)(n-1)x_{n-1}t^{n-3} + \ldots\ldots + 6x_3 t + 2x_2}{V\sin\varepsilon} \tag{3.8}$$

Replacing Eq. (3.8) into Eq. (2.9) provides the guidance command as

$$\dot{\gamma} = \frac{n(n-1)x_n t^{n-2} + (n-2)(n-1)x_{n-1}t^{n-3} + \ldots\ldots + 6x_3 t + 2x_2}{V\sin\varepsilon} + \dot{\lambda} \tag{3.9}$$

As seen, the guidance law is not only composed of terms that can be fed back, i.e. ε and $\dot{\lambda}$, but it also involves a purely time-dependent term. This is the reason why this form is referred to as an "open loop" formulation.

3.2 Guidance Laws for 3rd, 4th and 5th Order Polynomials

After presenting the general form of the guidance command, now it is time find the coefficients and analyze the proposed method. First of all, it has already been mentioned that the minimum order of Eq. (3.1) must be three. However, this does not grant the bounded final acceleration yet. Thus, the minimum order of the range polynomial must be discussed in details. For that purpose, the acceleration characteristics needs to be examined. These issues will be introduced in this section.

3.2.1 3rd Order Polynomial

The 3rd order range equation is

$$r = x_3 t^3 + x_2 t^2 + x_1 t + x_0 \tag{3.10}$$

x_0 and x_1 were already found for any order as given in Eq. (3.3) and Eq. (3.5). To find x_2 and x_3, first the time derivative of the range equation is obtained. Next, using the two final boundary conditions $r_f = 0$ and $\dot{r}_f = -V$, the coefficients for the 3rd order polynomial are found:

$$x_2 = \frac{\left(2\cos\varepsilon_0 + 1\right)Vt_f - 3R_0}{{t_f}^2}, \quad x_3 = -\frac{\left(\cos\varepsilon_0 + 1\right)Vt_f - 2R_0}{{t_f}^3} \tag{3.11}$$

These complete the 3rd order range equation. To obtain the analytical form of the look angle, Eq. (2.8) can be written as

$$\varepsilon = \cos^{-1}\left(\frac{-\dot{r}}{V}\right) \tag{3.12}$$

which shows that the derivation requires the time derivative of Eq. (3.10). Thus, the look angle turns out to be the inverse cosine of a quadratic polynomial

$$\varepsilon = \cos^{-1}\left(-\frac{3x_3 {t_f}^2 + 2x_2 t_f + x_1}{V}\right) \tag{3.13}$$

To produce the guidance command, the look angle rate is written from Eq. (3.7) as

$$\dot{\varepsilon} = \frac{\ddot{r}}{V \sin\varepsilon} \tag{3.14}$$

In Eq. (3.14), $\ddot{r}$ is to follow from Eq. (3.10). Then, the guidance command is constructed:

$$\dot{\gamma} = \frac{6x_3 t + 2x_2}{V \sin\varepsilon} + \dot{\lambda} \tag{3.15}$$

The next step is to analyze the guidance command. It is never desired to have an unbounded acceleration requirement. Therefore, the feasibility of the 3rd order polynomial requires careful consideration. From Eq. (3.15), the initial guidance command is as follows

$$\dot{\gamma}_0 = \frac{2x_2}{V \sin\varepsilon_0} + \dot{\lambda} \tag{3.16}$$

When x_2, which is given in Eq. (3.11), is replaced into Eq. (3.16) and the initial LOS rate is found by rearranging Eq. (2.7), then the initial guidance command becomes

$$\dot{\gamma}_0 = \frac{\left(2\cos\varepsilon_0 + 1\right)2Vt_f - 6R_0}{V{t_f}^2 \sin\varepsilon_0} - \frac{V\sin\varepsilon_0}{R_0} \tag{3.17}$$

which is a finite value when $\sin\varepsilon_0 \neq 0$. Then, the final acceleration must be analyzed to clarify the boundedness issue. In order to find the final acceleration, the final time is replaced into Eq. (3.15) with the corresponding coefficients given in Eq. (3.11). It is represented as

$$\dot{\gamma}_{t=t_f} = \frac{f\left(t_f\right)}{g\left(t_f\right)} \tag{3.18}$$

Since ε_f is forced to be zero at the intercept and $\sin\varepsilon_f$ term in $g(t_f)$ happens to be zero at $t = t_f$ as it could be also seen from Eq. (3.15). On the other hand, the numerator is

$$f\left(t_f\right) = 6Vt_f{}^4\left(2Vt_f - 3R_0 + Vt_f\cos\varepsilon_0\right) \tag{3.19}$$

which is a finite value. This result indicates that the final acceleration will be infinite. However, it must first be shown that Eq. (3.18) does not yield the condition of 0/0. For that purpose, it must be determined that $f(t_f)$ is never zero. There are two conditions, under which Eq. (3.19) could be zero. It is apparent that this could happen when t_f is zero, which is not the case for the impact time problem. Second, it could happen when the second part of Eq. (3.19) is zero, providing the final time as

$$t_f \overset{?}{=} \frac{R_0}{V}\frac{3}{\left(2+\cos\varepsilon_0\right)} \tag{3.20}$$

In order to demand a feasible impact time from any engagement geometry, the desired impact time must be greater than the theoretical impact time, which was already mentioned in Eq. (2.16). This requirement results in the condition that $\cos\varepsilon_0$ must be greate than 1, which is not true. Therefore, it is proven that, the condition of 0/0 will never occur. Hence, the final acceleration for the 3rd order is not bounded:

$$\dot{\gamma}_f = \pm\infty \tag{3.21}$$

and it is apparent that such a guidance law is not desirable. Thus, the minimum order for the range equation must be four, which will next be examined.

3.2.2 4th Order Polynomial

After presenting the 3rd order range solution and identifying the minimum order required, now the 4th order range polynomial can be examined. To find the coefficients, an addition to the previous boundary conditions has to be made. In this regard, the second time derivative of the range equation and the related kinematics is constructed

$$\ddot{r} = 12x_4t^2 + 6x_3t + 2x_2 = V\dot{\varepsilon}\sin\varepsilon \tag{3.22}$$

The final look angle is already demanded to be zero at the final time. Hence, this condition results in the following statement: $\ddot{r}_f$ is zero regardless of $\dot{\varepsilon}_f$ as seen in Eq. (3.22). Finally, the

rest of the coefficients could be given in the following form using the related equations and the boundary conditions

$$\begin{bmatrix} 1 & 0 & 0 & 0 & 0 \\ 0 & 1 & 0 & 0 & 0 \\ 1 & t_f & {t_f}^2 & {t_f}^3 & {t_f}^4 \\ 0 & 1 & 2t_f & 3{t_f}^2 & 4{t_f}^3 \\ 0 & 0 & 2 & 6t_f & 12{t_f}^2 \end{bmatrix} \begin{bmatrix} x_0 \\ x_1 \\ x_2 \\ x_3 \\ x_4 \end{bmatrix} = \begin{bmatrix} R_0 \\ -V\cos\varepsilon_0 \\ 0 \\ -V \\ 0 \end{bmatrix} \tag{3.23}$$

Since the equations for the 3rd order was simple enough to solve, this matrix form was not presented. Eq. (3.23) is conducted as

$$A\bar{x} = B \rightarrow \bar{x} = A^{-1}B \tag{3.24}$$

where A includes the related equations of the boundary conditions and B represents the demanded boundary conditions. After solving Eq. (3.24), the coefficients are as follow:

$$x_2 = \frac{3\left(\cos\varepsilon_0 + 1\right)Vt_f - 6R_0}{{t_f}^2}, \quad x_3 = \frac{-\left(3\cos\varepsilon_0 + 5\right)Vt_f + 8R_0}{{t_f}^3}$$
$$x_4 = \frac{\left(\cos\varepsilon_0 + 2\right)Vt_f - 3R_0}{{t_f}^4} \tag{3.25}$$

Second, the look angle equation is given:

$$\varepsilon = \cos^{-1}\left(-\frac{4x_4t^3 + 3x_3t^2 + 2x_2t + x_1}{V}\right) \tag{3.26}$$

The related coefficients could be replaced into Eq. (3.26); however, it turns into a very long equation. Thus, it is not written for the sake of simplicity. At this point, there is one property to be mentioned. Since the look angle equation is derived over $\dot{r}$, the order of the polynomial inside the inverse cosine function will be $\left(n-1\right)$.

The next analysis is about the guidance command. In order to extract it, the same procedure is applied as it was described for the 3rd order. The look angle rate is

$$\dot{\varepsilon} = \frac{12x_4t^2 + 6x_3t + 2x_2}{V\sin\varepsilon} \tag{3.27}$$

Then, the guidance command is obtained as

$$\dot{\gamma} = \frac{12x_4t^2 + 6x_3t + 2x_2}{V\sin\varepsilon} + \dot{\lambda} \tag{3.28}$$

When the corresponding coefficients given in Eq. (3.25) is replaced in Eq. (3.28) and evaluating at t = 0, the initial guidance command of the 4th order is obtained:

$$\dot{\gamma}_0 = \frac{-V^2 {t_f}^2 \sin{\varepsilon_0}^2 - 12{R_0}^2 + 6VR_0t_f\left(1+\cos\varepsilon_0\right)}{VR_0{t_f}^2\sin\varepsilon_0} \tag{3.29}$$

which is a finite value. When the final acceleration is examined, it can be seen that the limit of the guidance command at $t = t_f$ does not exist due to the fact that it has different values from the right and the left hand sides. However, for the guidance command, the limit from the left hand side is meaningful because the time moves forward. The left-hand side limit of the guidance command is available, which is

$$\lim_{t\to t_f^-}\dot{\gamma} = -\frac{36Vt_f - 48R_0 + 12Vt_f\cos\varepsilon_0}{\sqrt{{Vt_f}^3\left(18Vt_f - 24R_0 + 6Vt_f\cos\varepsilon_0\right)}} \tag{3.30}$$

Eq. (3.30) shows that the final acceleration of the 4th order polynomial has a finite value.

3.2.3 5th Order Polynomial

The last example is for the 5th order range shaping. To provide enough equations for the unknowns, in addition to $\ddot{r}_f = 0$, $\dddot{r}_f = 0$ is also added to the equation set. Then, Eq. (3.24) turns into the following form:

$$\begin{bmatrix} 1 & 0 & 0 & 0 & 0 & 0 \\ 0 & 1 & 0 & 0 & 0 & 0 \\ 1 & t_f & {t_f}^2 & {t_f}^3 & {t_f}^4 & {t_f}^5 \\ 0 & 1 & 2t_f & 3{t_f}^2 & 4{t_f}^3 & 5{t_f}^4 \\ 0 & 0 & 2 & 6t_f & 12{t_f}^2 & 20{t_f}^3 \\ 0 & 0 & 0 & 6 & 24t_f & 60{t_f}^2 \end{bmatrix} \begin{bmatrix} x_0 \\ x_1 \\ x_2 \\ x_3 \\ x_4 \\ x_5 \end{bmatrix} = \begin{bmatrix} R_0 \\ -V\cos\varepsilon_0 \\ 0 \\ -V \\ 0 \\ 0 \end{bmatrix} \tag{3.31}$$

Solving these equations for the coefficients results in the following:

$$x_2 = 2\frac{(3+2\cos\varepsilon_0)Vt_f - 5R_0}{{t_f}^2} \qquad x_3 = -2\frac{(7+3\cos\varepsilon_0)Vt_f - 10R_0}{{t_f}^3}$$
$$x_4 = \frac{(11+4\cos\varepsilon_0)Vt_f - 15R_0}{{t_f}^4} \qquad x_5 = -\frac{(3+\cos\varepsilon_0)Vt_f - 4R_0}{{t_f}^5} \tag{3.32}$$

Next, the initial acceleration for the 5th order range polynomial is obtained as it was described for the 4th order:

$$\dot{\gamma}_0 = \frac{V^2{t_f}^2\cos{\varepsilon_0}^2 - V^2{t_f}^2 - 20{R_0}^2 + 12VR_0t_f + 8VR_0t_f\cos\varepsilon_0}{t_f\sqrt{VR_0\left(1-\cos{\varepsilon_0}^2\right)}} \tag{3.33}$$

The second issue related to the guidance commend is the final acceleration. In contrast to the 3rd and the 4th orders, now the limit for the final time exists and it is zero

$$\lim_{t\to t_f}\dot{\gamma} = 0 \tag{3.34}$$

This is certainly a preferred final condition meaning that the missile aligns itself with respect to the target beforehand; therefore, it does not need a maneuver at the time of intercept. If the final guidance command analysis is carried out for the 6th, 7th and the remaining orders, it will be seen that final acceleration is zero. This behavior results in that the increased order of the time derivative of the range provides nulling the final acceleration before intercept, which is not the case for the 3rd and the 4th orders.

So far, the initial and the final guidance commands are described. In addition to these, there is another concern about the guidance command; the maximum value, which is also an important factor since the acceleration capacity of the system is bounded. Unfortunately, the maximum value of the acceleration and when it occurs is not directly available; one needs to resort to numerical means to solve for these.

3.3 Closed Loop Guidance Formulation

The proposed impact time control law could be regarded as an open loop guidance unless the coefficients are updated during the engagement. Consequently, performance degradation will occur under autopilot lag, misinformation or uncertainties. Therefore, an alternative application of the guidance command is proposed here, which results in a closed loop structure

that is robust under the degrading factors. This new form can be obtained by considering the fact that each time instant can actually be regarded as the initial time such that

$$t \to 0,\ R_0 \to r,\ \varepsilon_o \to \varepsilon \tag{3.35}$$

Then, the final time needs to be updated accordingly, i.e.

$$t_f \to t_f - t \tag{3.36}$$

In order to obtain the guidance command, as was done in the previous subsection, first the look angle rate in Eq. (3.8) is rewritten using the conversion defined in Eq. (3.35) and Eq. (3.36) wherever necessary:

$$\dot{\varepsilon} = \frac{2\hat{x}_2}{V \sin \varepsilon} \tag{3.37}$$

These modifications show that the guidance law depends only on the new coefficient $\hat{x}_2$ regardless of *n*. Since $\hat{x}_2$ is obtained from x_2, the next step is to modify x_2 via Eq. (3.35) and Eq. (3.36). For instance, x_2, which is given for the 4th order in Eq. (3.25), turns into the following

$$\hat{x}_2 = \frac{3V\left(\cos\varepsilon + 1\right)}{\left(t_f - t\right)} - \frac{6r}{\left(t_f - t\right)^2} \tag{3.38}$$

Replacing Eq. (3.38) in Eq. (3.37), the guidance law becomes

$$\dot{\gamma} = \frac{6\left(\cos\varepsilon + 1\right)}{\sin\varepsilon\left(t_f - t\right)} - \frac{12r}{V \sin\varepsilon\left(t_f - t\right)^2} + \dot{\lambda} \tag{3.39}$$

After giving this example, the next step is to find the general form of x_2 and then to revise it according to Eq. (3.35) and Eq. (3.36). If x_2 is written for several orders, the following pattern would be observed

$$x_2 = \begin{cases} \left.\begin{matrix} (Vt_f - 3R_0 + 2Vt_f \cos\varepsilon_0)/{t_f}^2 \\ 2(3Vt_f - 5R_0 + 2Vt_f \cos\varepsilon_0)/{t_f}^2 \\ 3(5Vt_f - 7R_0 + 2Vt_f \cos\varepsilon_0)/{t_f}^2 \end{matrix}\right\} n = 3,5,7 \\ \left.\begin{matrix} 1.5(2Vt_f - 4R_0 + 2Vt_f \cos\varepsilon_0)/{t_f}^2 \\ 2.5(4Vt_f - 6R_0 + 2Vt_f \cos\varepsilon_0)/{t_f}^2 \\ 3.5(6Vt_f - 8R_0 + 2Vt_f \cos\varepsilon_0)/{t_f}^2 \end{matrix}\right\} n = 4,6,8 \end{cases} \tag{3.40}$$

Thus, it can be written as

$$x_2 = \frac{(n-1)}{2{t_f}^2}\left[(n-2)Vt_f - nR_0 + 2Vt_f \cos\varepsilon_0\right] \tag{3.41}$$

with respect to general behavior of Eq. (3.40). Thereafter, applying Eq. (3.35) and Eq. (3.36), the general form of the closed loop guidance law is obtained as

$$\dot{\gamma} = \frac{(n-1)}{V\sin\varepsilon\left(t_f - t\right)^2}\left[(n-2)V\left(t_f - t\right) - nr + 2V\left(t_f - t\right)\cos\varepsilon\right] + \dot{\lambda} \tag{3.42}$$

Before going further, it is to be noted that the closed loop guidance command depends on ε, r, t and t_f. $\left(t_f - t\right)$ is also in the guidance command as a feedback term; however, it is not a value to be estimated. In contrast, it is simply the difference between the desired impact time and the elapsed time.

3.4 Solution of the Coefficients

Now, the solution could be extended for every coefficient that is required for the time domain definition of the range. For a brief reminding, the following two conditions were dictated by the initial geometry: $x_0 = R_0$ and $x_1 = -V\cos\varepsilon_0$. The terminal condition of having no miss distance is expressed as $r_f = 0$. In addition, $\varepsilon_f = 0$, which translates into $\dot{r}_f = -V$. These four mandatory conditions, leave $(n-4)$ more conditions to be chosen so that a total of *n* equations are obtained to determine the coefficients of the polynomial. As expressed previously, the proposed approach in this work is to use the following:

$$\left.\frac{d^2r(t)}{dt^2}\right|_{t=t_f} = \left.\frac{d^3r(t)}{dt^3}\right|_{t=t_f} = \cdots = \left.\frac{d^{n-2}r(t)}{dt^{n-2}}\right|_{t=t_f} = 0 \tag{3.43}$$

This system of equations, which is composed of two initial and $(n-2)$ terminal conditions, can be written in matrix form as:

$$A\begin{bmatrix} x_0 & x_1 & \cdots & x_n \end{bmatrix}^T = \begin{bmatrix} R_0 & -V\cos\varepsilon_0 & 0 & -V & 0 & \cdots & 0 \end{bmatrix}^T \tag{3.44}$$

where

$$A = \begin{bmatrix} 1 & 0 & 0 & 0 & 0 & 0 & \cdots & 0 \\ 0 & 1 & 0 & 0 & 0 & 0 & \cdots & 0 \\ 1 & t_f & t_f^2 & t_f^3 & t_f^4 & t_f^5 & \cdots & t_f^n \\ 0 & 1 & 2t_f & 3{t_f}^2 & 4{t_f}^3 & 5{t_f}^4 & \cdots & nt_f^{n-1} \\ 0 & 0 & 2 & 6t_f & 12{t_f}^2 & 20{t_f}^3 & \cdots & \vdots \\ 0 & 0 & 0 & 6 & 24t_f & 60{t_f}^2 & \cdots & \vdots \\ \vdots & \vdots & \vdots & \vdots & \vdots & \vdots & \ddots & \vdots \\ 0 & 0 & 0 & 0 & 0 & 0 & \cdots & 0.5n!t_f^2 \end{bmatrix} \tag{3.45}$$

The steps for finding x_2 could be applied to find the general form of x_n. If x_n is written for several orders, the following pattern would be observed

$$x_n = \begin{cases} \left.\begin{matrix} -(Vt_f - 2R_0 + Vt_f\cos\varepsilon_0)/{t_f}^3 \\ -(3Vt_f - 4R_0 + Vt_f\cos\varepsilon_0)/{t_f}^5 \\ -(5Vt_f - 6R_0 + Vt_f\cos\varepsilon_0)/{t_f}^7 \end{matrix}\right\} n = 3,5,7 \\ \left.\begin{matrix} (2Vt_f - 3R_0 + Vt_f\cos\varepsilon_0)/{t_f}^4 \\ (4Vt_f - 5R_0 + Vt_f\cos\varepsilon_0)/{t_f}^6 \\ (6Vt_f - 7R_0 + Vt_f\cos\varepsilon_0)/{t_f}^8 \end{matrix}\right\} n = 4,6,8 \end{cases} \tag{3.46}$$

Thus, it can be defined as follows

$$x_n = (-1)^n \frac{(n-2)Vt_f - (n-1)R_0 + Vt_f\cos\varepsilon_0}{t_f^n} \tag{3.47}$$

Then, the coefficient x_{n-1} for several orders becomes:

$$x_{n-1}=\left\{\begin{array}{c}\left.\begin{array}{c}(Vt_f-3R_0+2Vt_f\cos\varepsilon_0)/{t_f}^2\\(11Vt_f-15R_0+4Vt_f\cos\varepsilon_0)/{t_f}^4\\(29Vt_f-35R_0+6Vt_f\cos\varepsilon_0)/{t_f}^6\end{array}\right\}n=3,5,7\\\left.\begin{array}{c}-(5Vt_f-8R_0+3Vt_f\cos\varepsilon_0)/{t_f}^3\\-(19Vt_f-24R_0+5Vt_f\cos\varepsilon_0)/{t_f}^5\\-(41Vt_f-48R_0+7Vt_f\cos\varepsilon_0)/{t_f}^7\end{array}\right\}n=4,6,8\end{array}\right. \tag{3.48}$$

where it could be written in general form as the following:

$$x_{n-1}=(-1)^{n-1}\frac{\big((n-1)(n-2)-1\big)Vt_f-n(n-2)R_0+(n-1)Vt_f\cos\varepsilon_0}{t_f^{n-1}} \tag{3.49}$$

The last example is for x_{n-2}

$$x_{n-2}=\left\{\begin{array}{c}\left.\begin{array}{c}(0Vt_f-0R_0+Vt_f\cos\varepsilon_0)/t_f\\2(30Vt_f-10R_0+3Vt_f\cos\varepsilon_0)/{t_f}^3\\3(140Vt_f-28R_0+5Vt_f\cos\varepsilon_0)/{t_f}^5\end{array}\right\}n=3,5,7\\\left.\begin{array}{c}-1.5(8Vt_f-4R_0+2Vt_f\cos\varepsilon_0)/{t_f}^2\\-2.5(72Vt_f-18R_0+4Vt_f\cos\varepsilon_0)/{t_f}^4\\-3.5(240Vt_f-40R_0+6Vt_f\cos\varepsilon_0)/{t_f}^6\end{array}\right\}n=4,6,8\end{array}\right. \tag{3.50}$$

where the general definition for x_{n-2} could be defined

$$x_{n-2}=(-1)^{n-1}\left(\frac{(n-1)}{2}\right)\frac{n(n-2)(n-3)Vt_f-n(n-3)R_0+(n-2)Vt_f\cos\varepsilon_0}{t_f^{n-2}} \tag{3.51}$$

It can be shown that these general form definitions obey the following recursive formulation:

$$x_{(n-m)}=-\frac{1}{(n-m)!}\sum_{k=0}^{m-1}\frac{(n-k)!}{(m-k)!}x_{(n-k)}{t_f}^{(m-k)} \tag{3.52}$$

where $n-1\geq m\geq 2$. Therefore, every coefficient of Eq. (3.1) could be expressed for any order.

Next, the initial acceleration with respect to *n* can be studied. Since the initial LOS rate has nothing to do with *n*, it is avoided in the analysis. Only the look angle rate is investigated, where it only depends on x_2 as described in Eq. (3.37). The partial derivative of x_2 with respect to *n* is

$$\left.\frac{\partial x_2}{\partial n}\right|_{t=0} = \frac{R_0\left(1-2n\right)+Vt_f\left(2n-3+2\cos\varepsilon_0\right)}{2t_f{}^2} \tag{3.53}$$

Yet, the sign of Eq. (3.53) must be analyzed. In Eq. (3.53), there are two terms related with *n*, where the rest depends on the initial conditions and the final time. Since denominator is positive, only the numerator could be investigated for positivity. When mathematical reorganizations are made, the problem will be defined with respect to the result of the inequality

$$R_0\left(1-2n\right) < Vt_f\left(2n-3+2\cos\varepsilon_0\right) \tag{3.54}$$

It is already known that $n \geq 4$. Additionally, Eq. (3.54) also includes the length of the trajectory which is $S = Vt_f$. It is known that the length of the trajectory is more than the initial range

$$S > R_0 \tag{3.55}$$

which is a result of the theoretical minimum impact time presented in Eq. (2.16). Thus, Eq. (3.54) is a true statement, when Eq. (3.55) is applied. Therefore, Eq. (3.53) is a positive quantity. These justifications prove that an increase in *n* increases the demanded acceleration at the initial time.

3.5 Impact Time Interval

The minimum impact time is defined in a such a way that the look angle does not change sign during the engagement. Therefore, the guidance design forces the look angle to be zero only at the final time, which is also an avoidance of the division by zero since $\sin\varepsilon$ is in the denominator of the guidance command. For that purpose, Eq. (2.8) may be considered when the look angle zero, which leads to

$$\dot{r} + V = 0 \tag{3.56}$$

In order to find the time instants where this equality holds, Eq. (3.56) is written from n = 4 to 7 with the corresponding time derivatives of Eq. (3.1):

$$\bar{0} = \begin{cases} (t-t_f)^2 \left(Vt_f{}^2(1-\cos\varepsilon_0) + 4t\left(Vt_f(2+\cos\varepsilon_0) - 3R_0\right) \right) / t_f{}^4 \\ -(t-t_f)^3 \left(Vt_f{}^2(1-\cos\varepsilon_0) + 5t\left(Vt_f(3+\cos\varepsilon_0) - 4R_0\right) \right) / t_f{}^5 \\ (t-t_f)^4 \left(Vt_f{}^2(1-\cos\varepsilon_0) + 6t\left(Vt_f(4+\cos\varepsilon_0) - 5R_0\right) \right) / t_f{}^6 \\ -(t-t_f)^5 \left(Vt_f{}^2(1-\cos\varepsilon_0) + 7t\left(Vt_f(5+\cos\varepsilon_0) - 6R_0\right) \right) / t_f{}^7 \end{cases} \quad n = 4,5,6,7 \qquad (3.57)$$

It is obvious that Eq. (3.57) is zero at $t = t_f$ and at the time instant which makes the second part of the equation zero:

$$t` = -\frac{Vt_f^2(1-\cos\varepsilon_0)}{n\left\{(n-2+\cos\varepsilon_0)Vt_f - (n-1)R_0\right\}} \qquad (3.58)$$

in general form. If Eq. (3.58) is forced to be t_f:

$$t` = t_f \qquad (3.59)$$

with the aim that the solution, which satisfy Eq. (3.57), is only the final time. When Eq. (3.59) is solved, two time instants are obtained, one of which is t_f = 0 and the other is

$$t_f = \frac{R_0}{V}\frac{n}{(n-1+\cos\varepsilon_0)} \qquad (3.60)$$

As it is obvious, t_f = 0 means no engagement. However, if the minimum impact time is defined as Eq. (3.60), then the look angle will not change sign during the engagement. If smaller impact times are desired, then the look angle must change sign, which makes the guidance command singular. The upcoming section will also make use of this no sign change advantage.

In order to make a comparison, the estimated the time-to-go of PN guidance, which is given in Eq. (2.19), is used. Whichever of these guidance laws acquires the smallest impact time could be decided by comparing Eq. (2.19) and Eq. (3.60):

$$\frac{R_0}{V}\left(1+\frac{{\varepsilon_0}^2}{2(2N-1)}\right)\overset{?}{>}\frac{R_0}{V}\left(\frac{n}{(n-1+\cos\varepsilon_0)}\right) \tag{3.61}$$

If Eq. (3.61) is true, then the suggested impact time control method will provide the minimum among the two. Furthermore, it could also be said that smaller impact time could also be possible with the higher orders of *n*. To support this claim, the partial derivative of the minimum impact time with respect to *n* is given:

$$\frac{\partial t_{\min}}{\partial n}=\frac{R_0}{V}\frac{(\cos\varepsilon_0-1)}{(n+\cos\varepsilon_0-1)^2} \tag{3.62}$$

which is negative under the assumption of $\varepsilon_0 \neq 0$, showing that an increment in *n* will result in a smaller $t_{\min}$.

The maximum impact time is a more relaxed term as compared to the minimum impact time. Unless there is a constraint, for instance a look angle or an acceleration constraint, the maximum impact time could be any desired value that does not result in $\sin\varepsilon=0$ during the engagement. However, for very high impact times, which could be considered unrealistic. i.e. for a ground-to-ground pursuer more than 700s, the look angle increases such that it might cross π; moreover, the range might also cross zero before all of the desired conditions are satisfied regarding Eq. (2.8). Nevertheless, it can be argued that such a situation would not be feasible for a realistic engagement.

3.6 Maximum Look Angle Solution

The look angle is one of the concerns of the guidance law design. Together with the acceleration, they form the main physical limits. Under the assumption of small angle of attack, the look angle could be treated to handle the FOV limit [60]. Therefore, when the guidance algorithm takes care of this physical limitation or provides the information of the maximum look angle before intercept, it is quite precious for the overall performance. Fortunately, it is possible to obtain the maximum look angle that will occur before the intercept with the proposed impact time control method and the minimum impact time definition.

After clarifying the general look angle behavior in Section 3.5, it is now possible to make further analysis for the maximum look angle solution. Since the look angle will be zero at the

intercept; there is no need to check the final time for the maximum look angle solution. So, this candidate falls out. The other candidate is the initial time. Next, the local maximum solution must be investigated. For that purpose, the time instants, where the look angle rate equals zero, have to be found:

$$\dot{\varepsilon} = \frac{(n-1)}{2V\sin\varepsilon\left(t_f - t\right)^2}\left[(n-2)V\left(t_f - t\right) - nr + 2V\left(t_f - t\right)\cos\varepsilon\right] = 0 \tag{3.63}$$

If Eq. (3.63) is written for several orders with the corresponding range and look angle definitions, which were explained how to be obtained since far, it will give $t_{\varepsilon,\max} = t_f$ and another time instant. As expressed before, the look angle is zero at the intercept. So, the solution at t_f vanishes, which cannot be a candidate of the maximum look angle. Then, the solution where the look angle rate is zero would be:

$$t_{\varepsilon,\max} = \begin{Bmatrix} (Vt_f{}^2 - 3R_0t_f + 2Vt_f{}^2\cos\varepsilon_0)\Big/\Big(3\left(Vt_f - 2R_0 + Vt_f\cos\varepsilon_0\right)\Big) \\ (3Vt_f{}^2 - 5R_0t_f + 2Vt_f{}^2\cos\varepsilon_0)\Big/\Big(5\left(3Vt_f - 4R_0 + Vt_f\cos\varepsilon_0\right)\Big) \\ (5Vt_f{}^2 - 7R_0t_f + 2Vt_f{}^2\cos\varepsilon_0)\Big/\Big(7\left(5Vt_f - 6R_0 + Vt_f\cos\varepsilon_0\right)\Big) \end{Bmatrix} n = 3,5,7$$
$$\begin{Bmatrix} (2Vt_f{}^2 - 4R_0t_f + 2Vt_f{}^2\cos\varepsilon_0)\Big/\Big(4\left(2Vt_f - 3R_0 + Vt_f\cos\varepsilon_0\right)\Big) \\ (4Vt_f{}^2 - 6R_0t_f + 2Vt_f{}^2\cos\varepsilon_0)\Big/\Big(6\left(4Vt_f - 5R_0 + Vt_f\cos\varepsilon_0\right)\Big) \\ (6Vt_f{}^2 - 8R_0t_f + 2Vt_f{}^2\cos\varepsilon_0)\Big/\Big(8\left(6Vt_f - 7R_0 + Vt_f\cos\varepsilon_0\right)\Big) \end{Bmatrix} n = 4,6,8 \tag{3.64}$$

If the pattern is examined, it will be seen that the time instant of the maximum look angle can be determined as

$$t_{\varepsilon,\max} = \frac{(n-2)Vt_f{}^2 - nR_0t_f + 2Vt_f{}^2\cos\varepsilon_0}{n\left((n-2)Vt_f - (n-1)R_0 + Vt_f\cos\varepsilon_0\right)} \tag{3.65}$$

After finding the time instant, it could be replaced in the look angle equation given in Eq. (3.12) . Notwithstanding, there is not an analytical solution to find the possible impact time under the given look angle constraint, but as seen, a straightforward computing is possible. It is here to be noted that, when $t_{\varepsilon,\max}$ is zero, it means that the maximum look angle is the initial look angle. By equaling the numerator of Eq. (3.65) to zero gives this impact time

$$t_f^* = \frac{nR_0}{(n-2)V + 2V\cos\varepsilon_0} \tag{3.66}$$

which does not demand more look angle than the initial one during the engagement. In other words, if the desired impact time is more than t_f^*, the algorithm will need to increase the look angle to accomplish the desired impact time. So, the maximum look angle will occur at the local maximum. Otherwise, it is the initial look angle.

It is thereon possible to talk about the further characteristics of the look angle. There are things to mention regarding the physical interpretation; such that if the desired impact time increases, the maximum look angle eventually increases whereas the trajectory needs to be curved more. Moreover, if *n* increases, the maximum look angle also increases, because the look angle is driven to zero in a shorter time via curving the trajectory beforehand.

Lastly, a few words could be said about the flight path angle. The impact time control law provides an analytical form for the LOS rate and the look angle rate. Unfortunately, such a solution for the flight path angle is not available. Nevertheless, it is possible to numerically integrate the flight path angle and have the time domain behavior. Generally speaking, the physical interpretation of the flight path angle with respect to *n* would be that; if the order of the range polynomial increases, the final flight path angle decreases in magnitude since the look angle is nulled faster.

3.7 Modification for Terminal Robustness

When Eq. (3.9) is roughly analyzed, it is be seen that the term $\sin\varepsilon$ is in the denominator. Since the look angle will not change sign as expressed in Section 3.5, the singularity condition can only appear at the initial time and the final time when the look angle is zero for feasible desired impact times. The unlikely case of a zero initial condition can easily be handled, for example, by adding a very small bias to the look angle value. As for the final time, it should firstly be noted that guidance algorithms involving such terms in the denominator, e.g. optimal guidance laws with t_{go}, require a similar consideration [58]. Even if the final-time singularity is likely to be dismissed based on the ground that the engagement is already terminated by the time it occurs, division by a very small value will still be a problem since complications are likely to occur in practice long before these terms are identically zero. Accordingly, switching to PN as in [48] may be a viable option in order to provide robustness during the terminal part

of the engagement, where the look angle happens to be small. A practical alleviation of this issue would be as follows. Unless the look angle is less than a threshold, ε_s, Eq. (3.9) will be realized. If it is less than the threshold value, PN guidance will be commanded to circumvent division by zero. However, such a switched structure implies a jump in the guidance command. In order to avoid the jump, the following methodology is suggested. The value of $\dot{\varepsilon}$ at the switching time, $\dot{\varepsilon}^*$, is already known and the ratio with respect to the LOS rate at the switching time, $\dot{\lambda}^*$, can be calculated. Then, PN can be started using this ratio. This ratio is expressed as

$$N' = \frac{\dot{\varepsilon}^*}{\dot{\lambda}^*} \tag{3.67}$$

where N' is part of the PN gain. Since $\dot{\gamma} = \dot{\varepsilon} + \dot{\lambda}$, the final guidance command, which avoids division by zero, is then

$$\dot{\gamma} = \begin{cases} \text{Eq. (3.9)} & \varepsilon \geq \varepsilon_s \\ (N'+1)\dot{\lambda} & \varepsilon < \varepsilon_s \end{cases} \tag{3.68}$$

However, this approach may not be desirable for realistic applications, since the ratio is the division of two noisy variables. The switching is to happen towards the end; so, analyzing the limit of Eq. (3.67) would facilitate an alternative solution. From Eq. (2.7) and Eq. (2.8), it is seen that

$$\lim_{t \to t_f} \frac{\dot{\varepsilon}}{\dot{\lambda}} = -\frac{1}{V^2} \lim_{t \to t_f} \frac{r\ddot{r}}{\sin^2 \varepsilon} = \frac{0}{0} \tag{3.69}$$

which makes use of the fact $r_f = \varepsilon_f = 0$. The application of L'Hôpital's rule leads to

$$\lim_{t \to t_f} \frac{\dot{\varepsilon}}{\dot{\lambda}} = -\frac{1}{2V} \lim_{t \to t_f} \left(\frac{\dot{r}\ddot{r}}{V\dot{\varepsilon} \sin\varepsilon \cos\varepsilon} + \frac{r\dddot{r}}{V\dot{\varepsilon} \sin\varepsilon \cos\varepsilon} \right) = -\frac{1}{2V} \lim_{t \to t_f} \left(\frac{\dot{r}\ddot{r}}{\ddot{r} \cos\varepsilon} + \frac{r\dddot{r}}{\ddot{r} \cos\varepsilon} \right) \tag{3.70}$$

where $V\dot{\varepsilon}\sin\varepsilon$ is indeed $\ddot{r}$ as given in Eq. (3.7). Since the final look angle is zero, this equation becomes as

$$\lim_{t \to t_f} \frac{\dot{\varepsilon}}{\dot{\lambda}} = -\frac{1}{2V} \lim_{t \to t_f} \left(\dot{r} + \frac{r\dddot{r}}{\ddot{r}} \right) \tag{3.71}$$

Since the coefficients of the range is now available in general form, a compact form of the corresponding range derivatives can be written. First, range is rewritten as

$$r(t) = \frac{(t_f - t)}{t_f^n} f(t) \tag{3.72}$$

where $f(t)$ is not a simple compact form function; however, it turns out to be $f(t_f) = Vt_f^n$ at the final time. Then, range derivative is obtained in the following form

$$\dot{r}(t) + V = \frac{(t_f - t)^{n-2}}{t_f^n}\left\{ct + (1 - \cos\varepsilon_0)Vt_f^2\right\} \tag{3.73}$$

where *c* is

$$c = n\left\{(n - 2 + \cos\varepsilon_0)Vt_f - (n-1)R_0\right\} \tag{3.74}$$

Next, the second derivative of range is found

$$\ddot{r}(t) = \frac{(n-1)(t_f - t)^{n-3}}{t_f^n}\left\{-ct + (n - 2 + 2\cos\varepsilon_0)Vt_f^2 - nR_0t_f\right\} \tag{3.75}$$

Last, the third derivative of range is obtained as the previous equations:

$$\dddot{r}(t) = \frac{(n-1)(n-2)(t_f - t)^{n-4}}{t_f^n}\left\{ct - (2n - 3 + 3\cos\varepsilon_0)Vt_f^2 + 2nR_0t_f\right\} \tag{3.76}$$

When these equations replaced in Eq. (3.71), the limit can finally be obtained by summoning the range and its derivatives

$$\lim_{t\to t_f}\frac{\dot{\varepsilon}}{\dot{\lambda}} = \frac{n-2}{2} \tag{3.77}$$

This result makes it possible to express the modified guidance law as follows:

$$\dot{\gamma} = \begin{cases} \text{Eq. (3.42)} & \varepsilon \geq \varepsilon_s \\ \dfrac{n\dot{\lambda}}{2} & \varepsilon < \varepsilon_s \end{cases} \tag{3.78}$$

With this strategy, the amount of the command jump will be negligible. Finally, it is important to ensure $n/2 = N \geq 4$ so that no miss distance occurs [2], which is only possible with $n \geq 4$.

3.8 Simulations of Generalized Range Formulation

In order to demonstrate the efficiency of the proposed impact time guidance law, simulations are divided into three categories. First, the open loop application for several orders is investigated in an ideal environment, where all the required coefficients are calculated at the beginning of the engagement. For comparison purposes, an impact time control method via sliding mode is exemplified as given in [29], whose details can be found in Appendix B. Furthermore, the energy optimal solution is included, where the cost function is $\int a^2 dt$. Second, the closed loop formulation given in Eq. (3.42) is run under autopilot lag for different initial conditions and desired impact times. Last, the closed loop application is studied in a more realistic scenario with autopilot and seeker lag including noisy measurements. In addition to these, the range is now an estimated variable, which is used in the guidance command instead of the true range.

In simulations, the ground-launched pursuer, which attacks a target 5 km away, travels with a constant speed of 200 m/s. In order to avoid division by zero, the guidance is switched to PN when the look angle is less than ε_s = 0.25° as described in Eq. (3.78). The simulations are terminated when range is less than 1 m. To simulate the seeker saturation for the realistic scenario, the last guidance command is held when the range is below 50 m.

3.8.1 Example Simulations and Comparison Between Methods

This subsection is reserved for the demonstration of the basic properties of the proposed guidance structure. The ground-launched pursuer executes the guidance commands with no latency and has 15 *g* acceleration saturation. The initial flight path angle is 20° and the impact time is 30 s. *n* is varied between 4 to 7. The optimal guidance command that minimizes the time integral of acceleration squared in this specific engagement geometry is calculated by applying the optimal control procedure given in Appendix C. To this end, the differential state

and co-state equations that formulate the nonlinear two-point boundary problem was numerically solved via the MATLAB function *bvp4c*.

The related coefficients of the open loop simulations are presented in Table 3.1. In Table 3.2, important results of the simulations are summarized. The maximum acceleration and the maximum look angle magnitudes increase when a higher order *n* is chosen. The maximum acceleration is obtained at the beginning of the engagement.

Table 3.1 Coefficients for the scenarios.

Scenario	**n**	x_2	x_3	x_4	x_5	x_6	x_7
1	4	5.4605	-0.2561	0.0033	-	-	-
2	5	9.5029	-0.6603	0.0167	$-1.497.10^{-4}$	-	-
3	6	14.6564	-1.3475	0.0511	$-9.132.10^{-4}$	$6.362.10^{-6}$	-
4	7	20.9210	-2.3916	0.1207	$-3.2.10^{-3}$	$4.503.10^{-5}$	$-2.58.10^{-7}$

Moreover, the increase in the initial acceleration is correlated with Eq. (3.53). However, for this specific example the cost does not hold the same tendency. The minimum cost function belongs to the 5^{th} order not the 4^{th}, and it is closer to the energy optimal result. However, [29] has the maximum cost value and the look angle among all.

Table 3.2 Summary of the simulation results for various *n*

Scenario	***n***	**Max. Acc., m/s^2**	**Max. Look Angle, deg**	**Cost, m^2/s^3**
1	4	29.19	44.63	8080
2	5	52.83	49.15	7100
3	6	82.97	53.51	8456
5	7	119.6	57.68	10913
6	Optimal	22.14	49.92	6296
7	[29]	147.15	69.62	26022

The visual summary of the simulations is presented in Figures 3.1-3.6. The maximum altitude increases with respect the order of the polynomial as it can be observed in Figure 3.1,

in which the trajectory of the optimal solution lies within the proposed guidance law trajectories. The range histories could be seen in Figure 3.2, where the differences with respect to different n values can be observed. Figure 3.3 provides the information that the increment in the order of the polynomial results in the following consequence: The closing speed reaches the missile speed sooner. For instance, when n is 4, $\dot{r}$ reaches the speed approximately at the time of the impact; however, for $n = 7$, this happens just after $t = 26$ s. The cost of this behavior can be observed in Figure 3.4. If the initial accelerations of the proposed method are compared, it is seen that the 7^{th} order holds the maximum. Nevertheless, this value is still less than the acceleration required by [29]. It is also apparent how the optimal guidance puts in a more uniform control effort compared with these results. It is necessary to remind that when $n = 4$, the final acceleration is not zero. On the other hand, it was described that the final acceleration of the proposed guidance law will be zero for $n > 4$ as presented in Eq. (3.34). This can also be confirmed in Figure 3.4. Furthermore, the look angle behaviors are displayed in Figure 3.5. The optimal solution nulls the look angle towards the end of the engagement. In addition, the maximum look angle obtained by the optimal solution is close to the one obtained by the 5^{th} order. Nevertheless, [29] is the fastest one among the methods to null the look angle and also the one that requires the maximum look angle. The last figure is reserved for the flight path angle histories. In Figure 3.6, it is seen that the increment in the order of the range polynomial leads to higher final path angle magnitudes. When $n = 4$, the maximum final path angle magnitude is obtained. Figure 3.6 actually presents a precious result. It shows that different impact angles can be obtained via changing the order of the range polynomial.

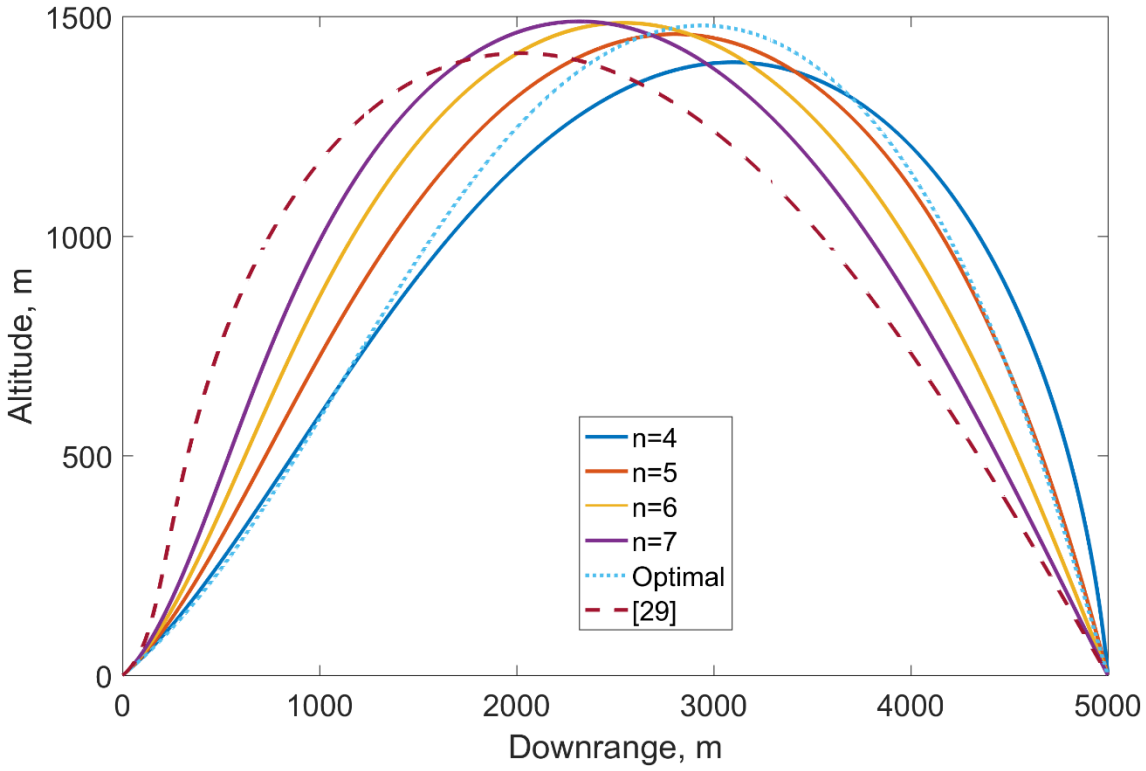

Figure 3.1 Trajectories of the scenarios.

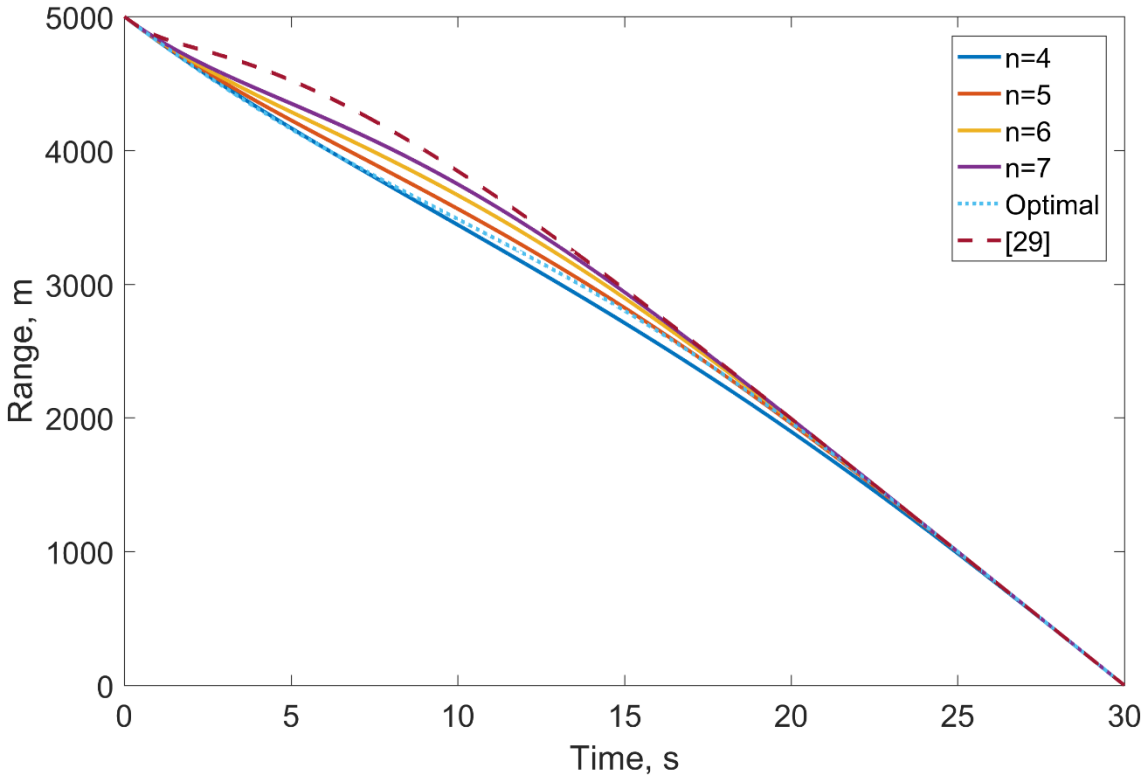

Figure 3.2 Range histories of the scenarios.

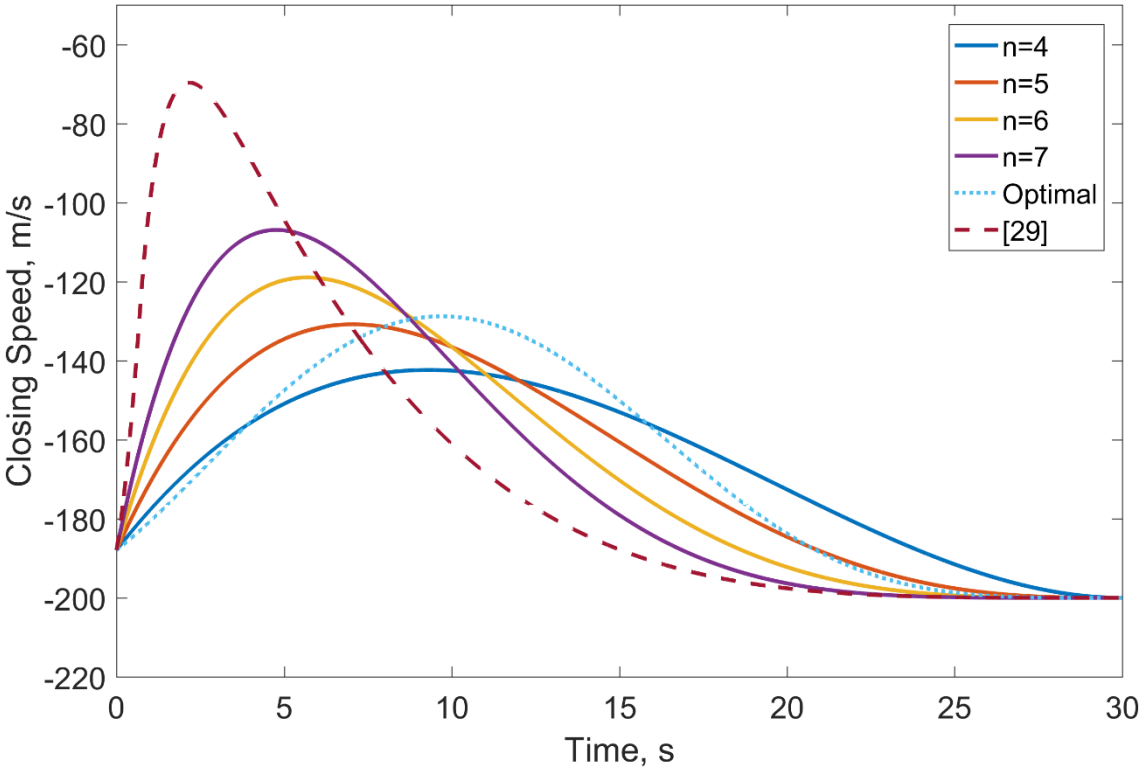

Figure 3.3 Closing speed histories of the scenarios.

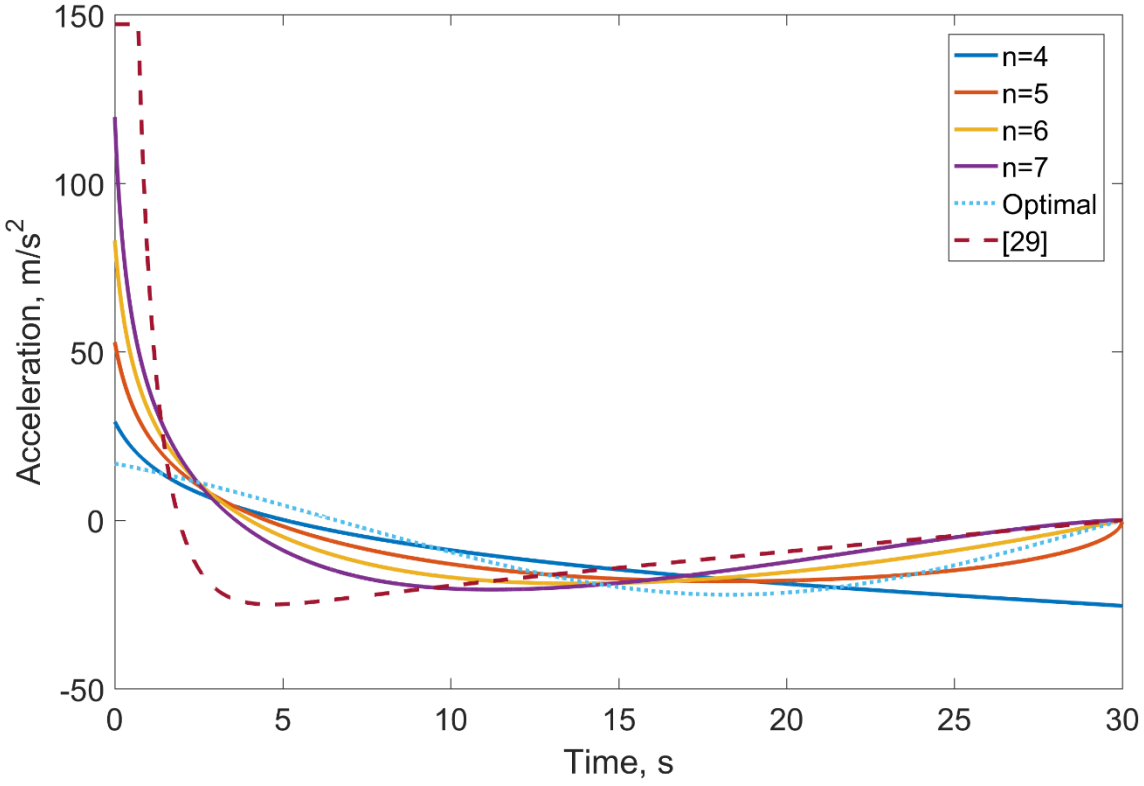

Figure 3.4 Acceleration histories of the scenarios.

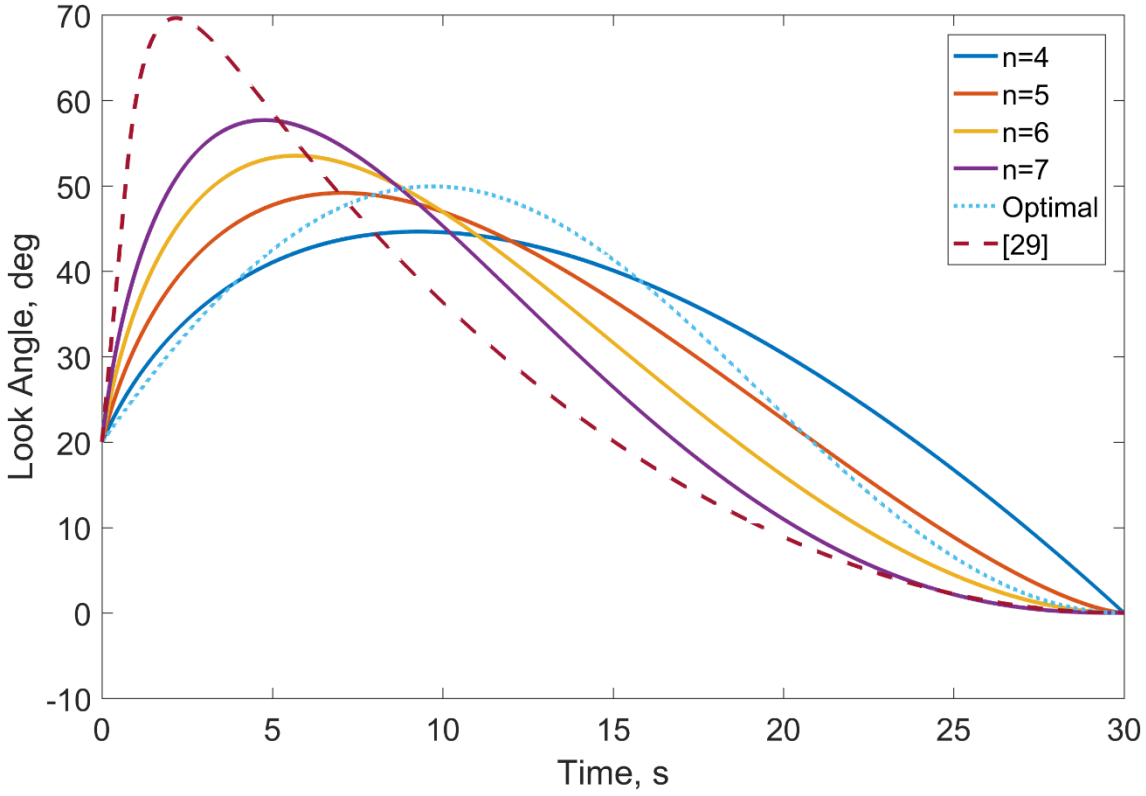

Figure 3.5 Look angle histories of the scenarios.

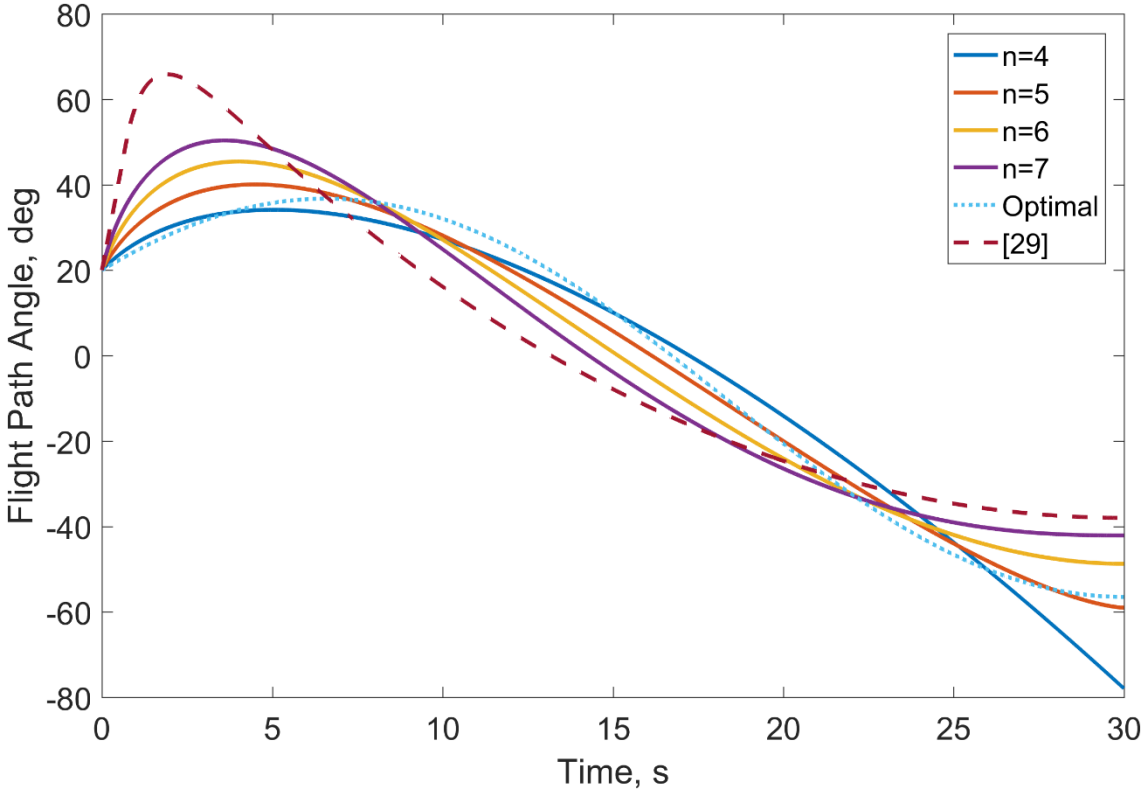

Figure 3.6 Flight path angle histories of the scenarios.

3.8.2 Autopilot Lagged Simulation with Closed Loop Guidance

The proposed impact time control is tested under varied initial look angles for a bunch of desired impact times under first order autopilot lag. The autopilot lag is characterized by the transfer function $1/(\tau s+1)$ as used in many guidance studies [59]. The details of the simulations could be seen in Table 3.3. The range is defined by a 5th order polynomial. The proposed impact time control accomplishes the task successfully within miss distance and impact time requirements. The trajectories and the look angles are presented in Figure 3.7 and Figure 3.8. The increased latency in the guidance command results in small variations in the neighborhood of the ideal cases. Figure 3.9 is reserved for $\hat{x}_2$ of the first simulation in order to give an insight about its variation throughout the engagement, which starts at some value and ends up at zero. The final behavior of $\hat{x}_2$ is due to the autopilot lag which is an expected characteristics.

Table 3.3 Simulation variation for the robustness analysis.

Initial Look Angle, ε_0	$[5 \quad 15 \quad 25 \quad 35 \quad 45 \quad 55 \quad 65 \quad 75]^\circ$
Autopilot Time Constant, τ	$[0.1 \quad 0.2 \quad 0.3 \quad 0.4 \quad 0.5]$ s
Desired Impact Time, t_d	$[30 \quad 32 \quad 34 \quad 36 \quad 38 \quad 40]$ s

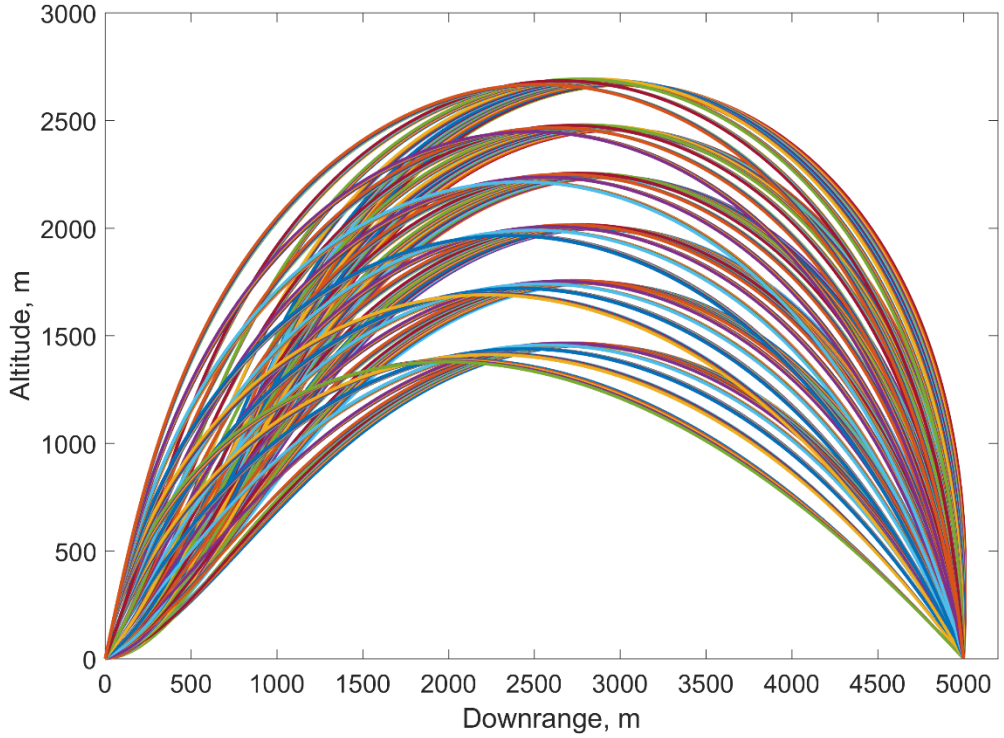

Figure 3.7 Trajectory histories with autopilot lag.

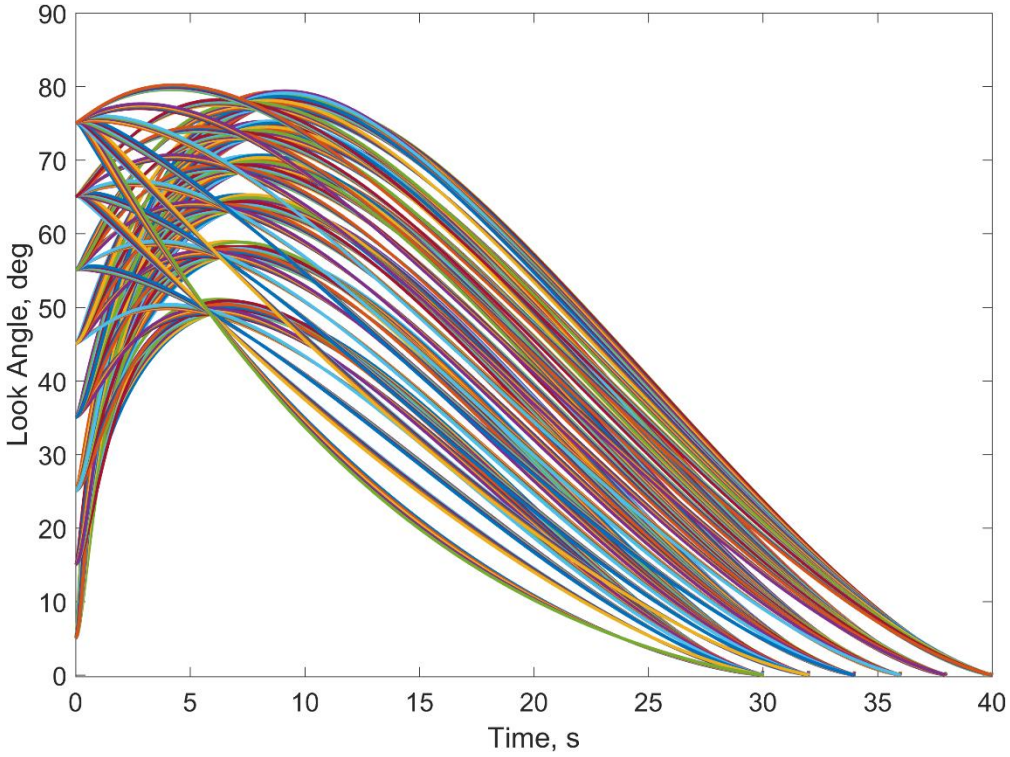

Figure 3.8 Look angle histories with autopilot lag.

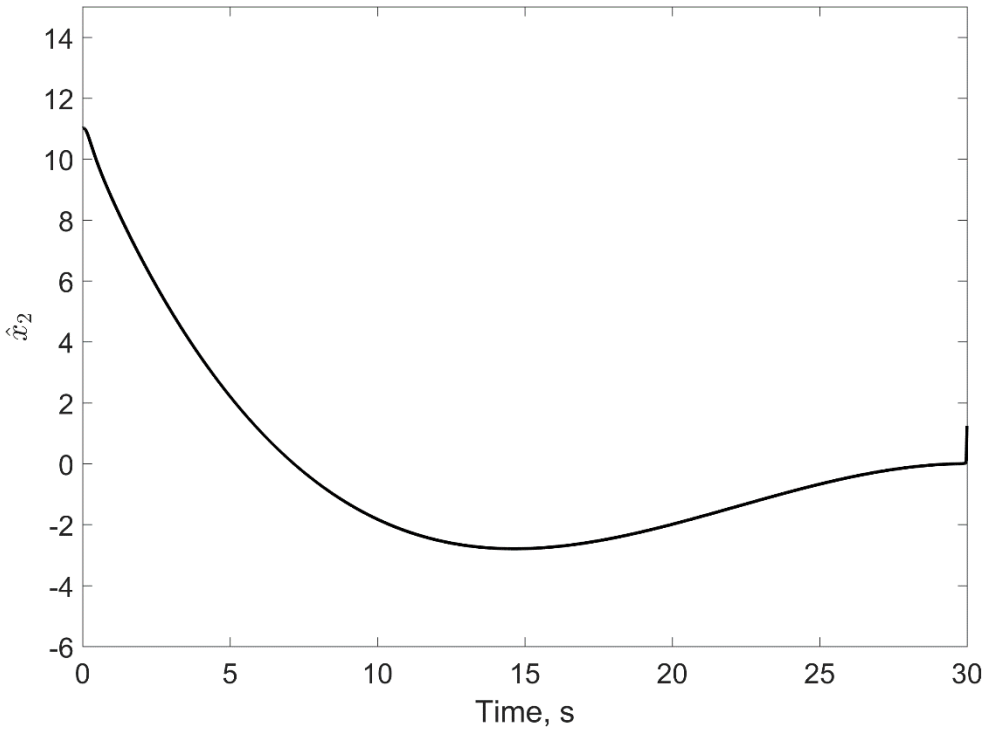

Figure 3.9 $\hat{x}_2$ history of the first simulation.

3.8.3 Realistic Simulations with Closed Loop Guidance

Thus far, the proposed guidance law is evaluated under autopilot lag. However, in an actual environment, this is not the only consideration. For instance, the variables required for the implementation of the guidance law could be noisy. Furthermore, some variables may not be measured and they need to be estimated. As a consequence, the performance of the guidance law might degrade. In order to show the performance, this subsection is reserved for a more realistic implementation with the same initial conditions of the first simulation study. The impact time is 30 s and *n* is 5. In addition to the autopilot lag with τ = 0.3 s , the LOS rate is obtained via a seeker head providing outputs at 40 Hz. For this purpose, Gaussian noise with a standard deviation of 0.025° is added to the LOS angle. Afterwards, it is passed through the following transfer function to obtain the LOS rate: $s/(\tau_a s+1)$, where τ_a simulates a bandwidth of 2 Hz. This way, both the look angle and the LOS rate become contaminated. Figure 3.10 shows how the LOS rate is generated as an input to the guidance algorithm.

The range to the target is another variable that is used by the proposed guidance law. For range estimation, the range observer detailed in [13] is borrowed and briefly expressed in Appendix D. One feature of this observer is that its open-loop, i.e. zero-gain, output can still

be used provided that it has already converged before the zeroing of the gain. This is useful in the current context because it would be wise to avoid the noisy dynamics of the observer towards the end of the engagement, where the sensitivity of the guidance loop is increased due to the look angle being small. Thus, the observer gain is uniformly decreased from 1.5 to zero in twenty-five seconds, which means that the estimation is open loop during the last five seconds. The observer starts with an initial guess which is 3000 m. Simulation is terminated as in the previous studies, when the range is less than 1 m and the time when this condition is realized is 29.95 s. Thus, the impact time error is negligible with respect to the overall simulation time. The results confirm that the algorithm is still applicable under these realistic conditions.

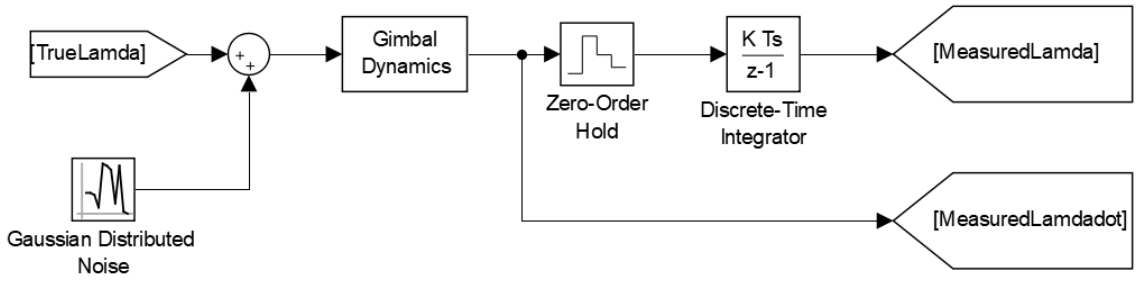

Figure 3.10 Measured LOS rate model for the guidance algorithm.

Figure 3.11 reveals the acceleration and the look angle histories of the simulation. The most important feature of the acceleration trend is the slightly higher magnitudes at the beginning of the engagement, where the range information is not fully correct. Actually, the estimated range magnitude is quite less than the true range, which can be observed in Figure 3.12. Hence; the guidance law curves the trajectory more in order to accomplish the desired impact time. It is evident that if the initial value of the estimated range is better, the magnitude of the initial acceleration will be less. The other option is to start the guidance later, since the duration of this passivity could be subtracted from the desired impact time. In addition to the initial acceleration behavior, another notable aspect is visible at the end of the engagement, where the noisy measurements become more effective. As seen, the final acceleration would be zero for the ideal conditions under the true range and the perfect measurements, but this is not so for the realistic scenario. It should lastly be noted that the final behavior of the look angle is as expected and the autopilot lag has the major role in that.

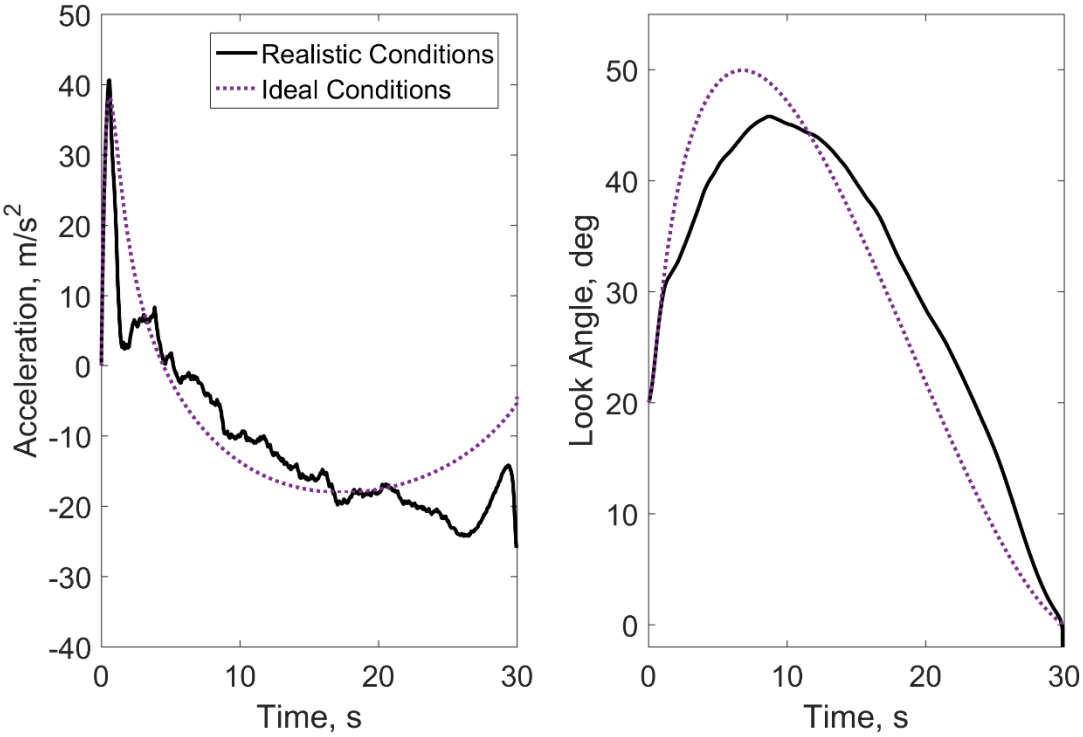

Figure 3.11 Acceleration and look angle histories of a realistic simulation.

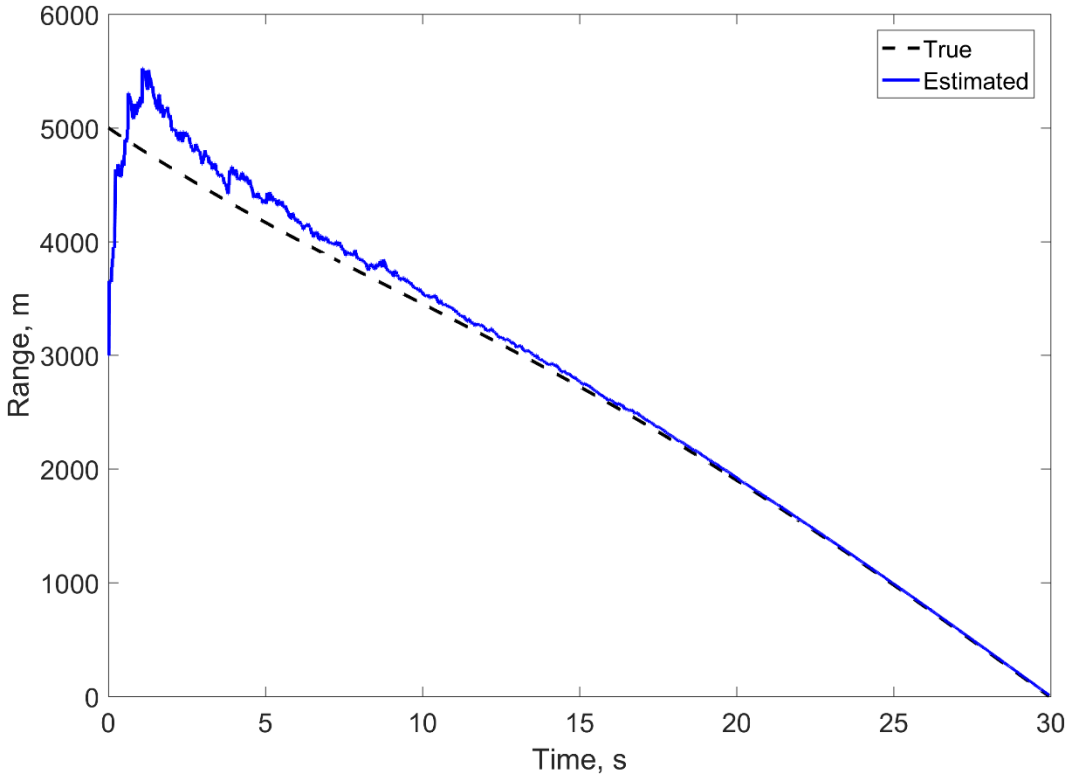

Figure 3.12 True and estimated range histories of a realistic simulation.

3.9 Impact Time Control Under Field of View Constraint

Shaping the trajectory is an expensive task as far as the required resources are considered. Satisfying the terminal constraints causes the missile trajectory to be shaped in such a way that the risk to violate the FOV constraint is increased. When the angle of attack is sufficiently small, the FOV angle may be approximated by the look angle. Thus, the FOV angle can be constrained via the look angle. The objective of this section is to reveal the relationship between this physical limit and the impact time, and then to offer a guidance methodology for the constrained system.

Generally speaking, the impact time control consists of three phases to prevent the violation of the FOV constraint. This switched guidance structure is presented in Figure 3.13. The first phase is where the guidance command brings the system up to the maximum look angle. The second phase holds the maximum look angle for some time duration until the final phase begins. The third phase finally captures the target at the desired impact time, decreasing the look angle to zero. As an additional information, the three phased-guidance structure could also be observed in impact angle control studies that considers the FOV limit such as in [60] and [61].

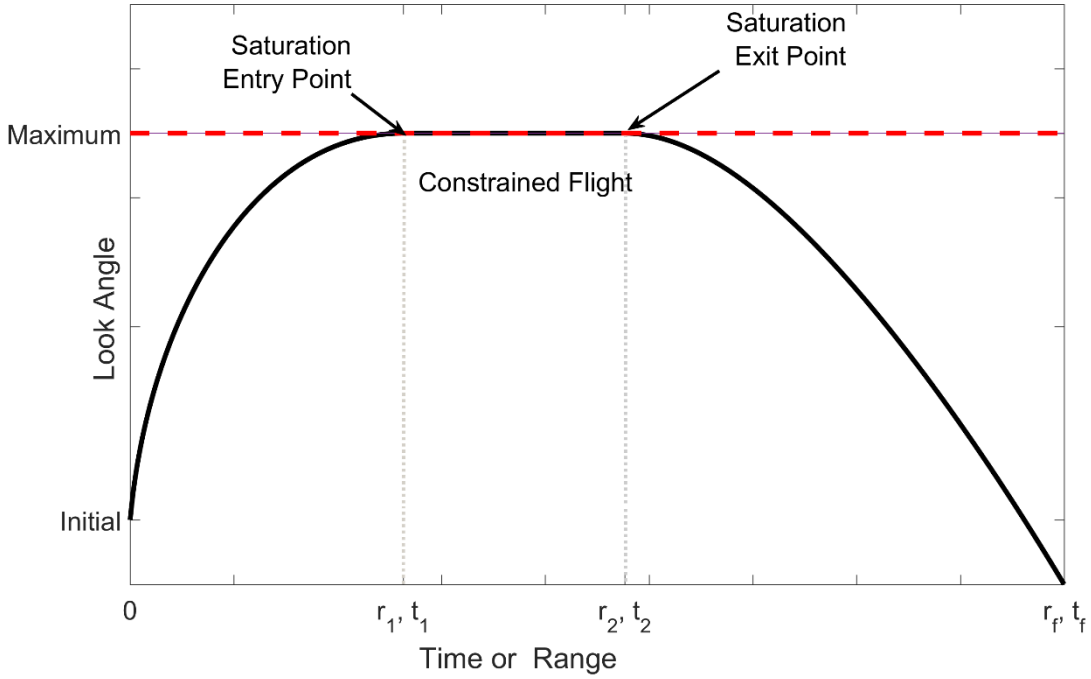

Figure 3.13 Typical saturated look angle history.

Two different solutions will be introduced for the impact time control under the FOV constraint, both of which are practically applicable. The first method completes the first phase regardless of the desired impact time whereas the second method calculates the time instant, where the FOV limit is reached.

3.9.1 Method I

The overall structure of the guidance law can be described as in Eq. (3.79). The first step is to find the switching instants of the guidance algorithm. t_1 is for Phase I, where the guidance law only depends on the initial conditions and the maximum look angle of the system. It is calculated with respect to the allowable engagement time under the given physical constraint. It is to be noted that it has yet nothing directly to do with the desired impact time.

$$\dot{\gamma} = \begin{cases} \text{Phase I} & t <= t_1\left(r_0, \varepsilon_0, \varepsilon_{\max}\right) \\ \text{Phase II} & t_1 < t <= t_2 \\ \text{Phase III} & t > t_2\left(r_0, \varepsilon_0, \varepsilon_{\max}, t_d\right) \end{cases} \tag{3.79}$$

The time instant, where the maximum look angle is obtained, is available by Eq. (3.65). The range covered until t_1 is represented as R_1 and it is the same for any desired impact time that makes the look angle overshoot the limit. Then, the duration and the range, over which the look angle is kept constant, are to be determined. These quantities are denoted as R_2 and $t_2 - t_1$, respectively. Here, t_2 marks the end of the constant look angle phase. Before that, the definitions for the final phase also have to be provided because the second and the third phases of the engagement have to be considered together. The corresponding range from t_2 to end of the capture is R_3. To have solutions for the second and the third phases, at least two equations are required. First of all, when the look angle is constant and at its maximum, Eq. (2.8) becomes

$$\dot{r} = -V\cos\varepsilon_{\max} \tag{3.80}$$

and the distance covered during $\left(t_2 - t_1\right)$ is

$$R_2 - R_1 = -V\cos\varepsilon_{\max}\left(t_2 - t_1\right) \tag{3.81}$$

Afterwards, the distance covered during the final phase, R_3, is required. Unfortunately, it is not a straightforward task. The only known quantities are the final and the initial $\dot{r}$ values. It could be assumed that $\dot{r}$ is a linear function rather than a polynomial function as shown in Figure 3.14. Since the impact time control is applied in the closed loop form, the error caused by this assumption could be circumvented.

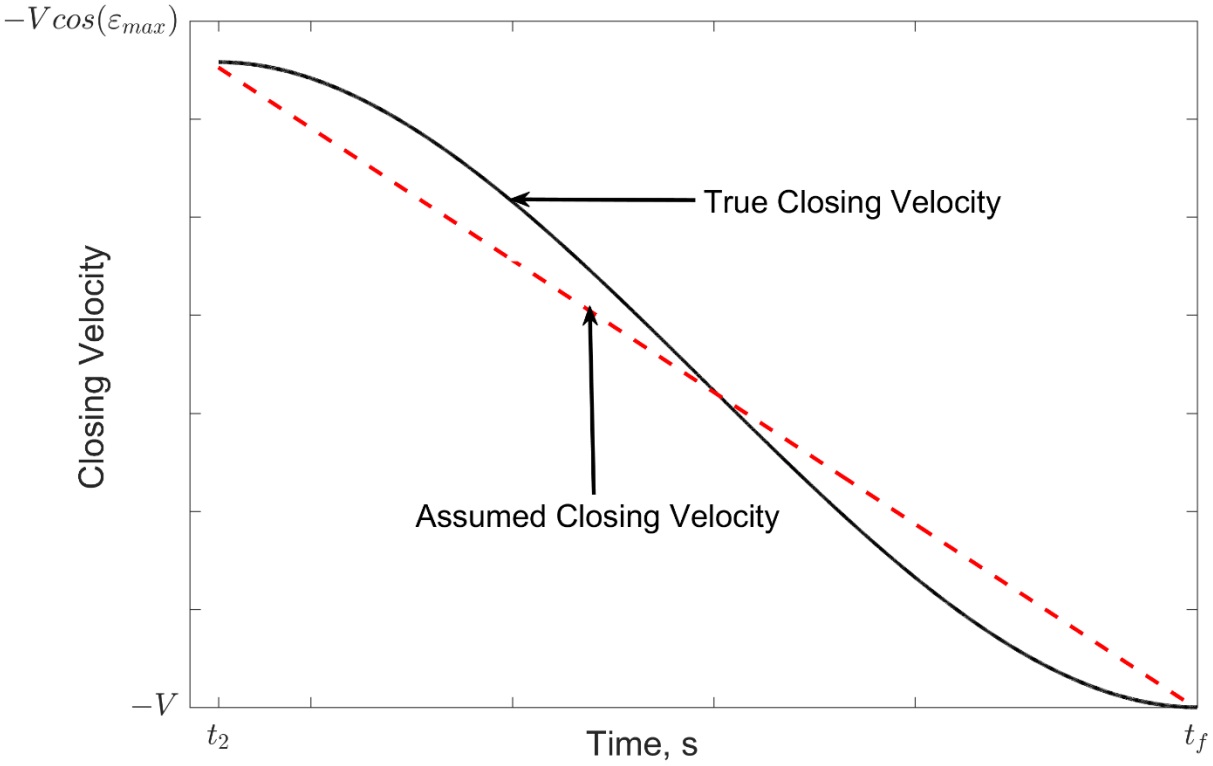

Figure 3.14 Typical $\dot{r}$ profile of the final phase.

Based on Figure 3.14, the approximated range covered in the final phase is

$$R_3 \approx \frac{V\left(\cos\varepsilon_{\max}+1\right)\left(t_d-t_2\right)}{2} \tag{3.82}$$

Actually, the true R_3 is

$$R_3 = R_0 - R_1 - V\left(t_2-t_1\right)\cos\varepsilon_{\max} \tag{3.83}$$

Thereafter, t_2 is found by using Eq.(3.82) in Eq. (3.83):

$$t_2 = \frac{t_d - \dfrac{2\left(R_0 - R_1\right)}{V\left(\cos\varepsilon_{\max}+1\right)} - t_1 \dfrac{2\cos\varepsilon_{\max}}{\cos\varepsilon_{\max}+1}}{1 - \dfrac{2\cos\varepsilon_{\max}}{\cos\varepsilon_{\max}+1}} \tag{3.84}$$

Finally, the guidance law to control the impact time under the FOV constraint can be written. Here, the 4th order guidance command, which is given in Eq. (3.39), is used since it requires the lowest maximum look angle as already shown in the sample simulations. Thus, the closed loop guidance command becomes as given in Eq. (3.85).

$$\dot{\gamma} = \begin{cases} \dfrac{6\left(\cos\varepsilon+1\right)V\left(\hat{t}_f - t\right) - 12r}{V\sin\varepsilon\left(\hat{t}_f - t\right)^2} + \dot{\lambda} & t <= t_1\left(r_0, \varepsilon_0, \varepsilon_{\max}\right) \\ \dot{\lambda} & t_1 < t <= t_2 \\ \dfrac{6\left(\cos\varepsilon+1\right)V\left(t_d - t\right) - 12r}{V\sin\varepsilon\left(t_d - t\right)^2} + \dot{\lambda} & t > t_2\left(r_0, \varepsilon_0, \varepsilon_{\max}, t_d\right) \end{cases} \tag{3.85}$$

Here, $\hat{t}_f$ represents the maximum impact time, which can be reached without saturating the look angle obtained by Eq. (3.65) and the corresponding numerical routine.

It is to be noted that the desired impact time must be feasible. The first constraint related to this feasibility is the bounded acceleration requirement. Thus, the duration of each phase must have a solution. In this regard, the maximum impact time under the FOV constraint could be connected with respect to the no correction impact time, which was given in Eq. (2.17). Since R_1 and t_1 are already known with respect to $\varepsilon_{\max}$, $t_{2,\max}$ must satisfy the following inequality

$$t_{2,\max} < \frac{R_0 - R_1}{V\cos\varepsilon_{\max}} \tag{3.86}$$

which is obtained by rearranging Eq. (2.17). Even though the acceleration demand might be high when this condition is satisfied, there is enough time for the look angle to be driven to zero at the time of intercept, which provides a bounded acceleration.

To investigate the performance of the proposed method, nonlinear simulations are performed with different impact times for a ground-to-ground scenario where $n = 4$. The missile is located at the origin and the initial flight path angle is 10°. The speed of the missile is 200 m/s and the target is 5 km away. The simulations are stopped when the range is less than 1 m.

The maximum look angle is constrained to 70° and the time instant when the maximum occurs is 13.165 s and $\hat{t}_f$ = 39.769 s.

The summary of the scenarios is presented in Table 3.4, showing the switching instants and the final flight path angles for the desired impact times. It is as expected that in order to satisfy the higher impact times, the duration of the saturated phase increases and the duration of the final phase decreases. Figure 3.15 displays the trajectories and the range histories, where it is seen that the variation starts after t_1. The flight path angles could be seen in Figure 3.16, where the increased impact time results in a higher impact angle magnitude. The initial accelerations are same since they have the same trajectory until t_1. In contrast, a higher impact time demand results in a higher maximum acceleration at the final time.

Table 3.4 Summary of the simulation results under the FOV constraint.

Impact Time, s	**Duration of Phase II, *s***	**Distance Covered in Phase II, *m***	**Duration of Phase III, *s***	**Distance Covered in Phase III, *m***	**Final Path Angle, °**
42	4.5508	311.29	24.2846	3259.04	-141.2
44	8.6300	590.33	22.2054	2980	-155.3
46	12.7092	869.36	20.1262	2700.97	-170.8

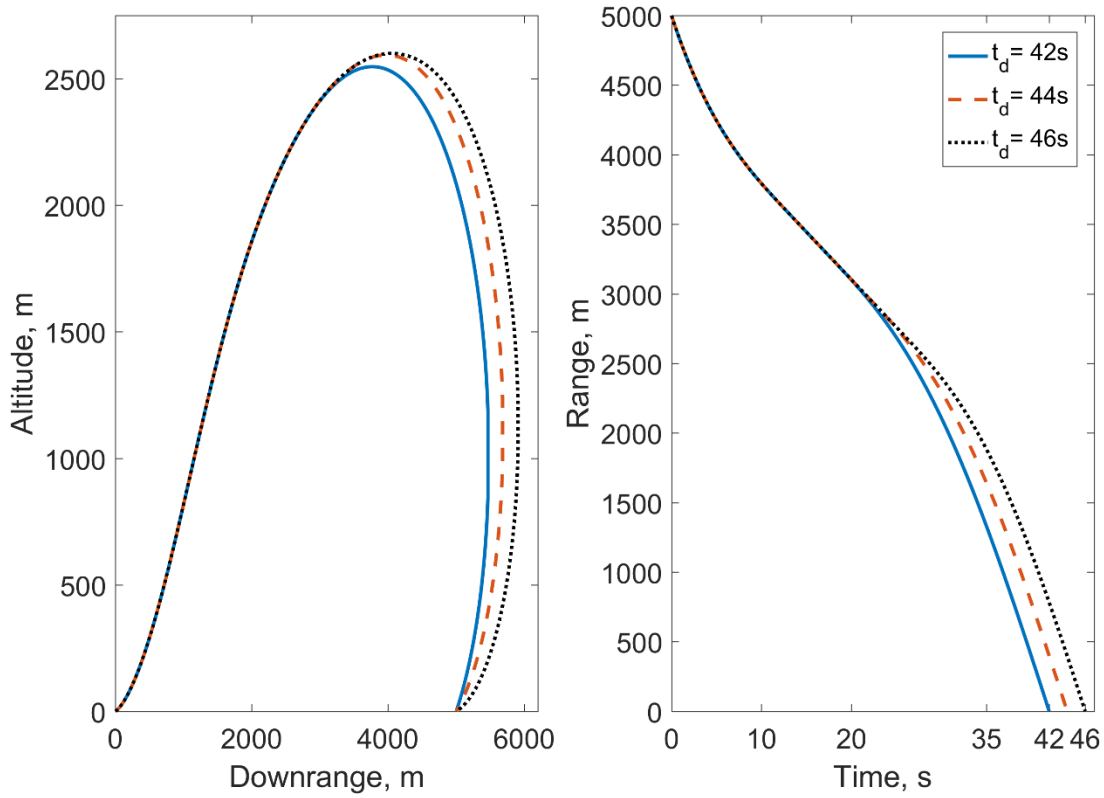

Figure 3.15 Trajectory and range histories under the FOV constraint.

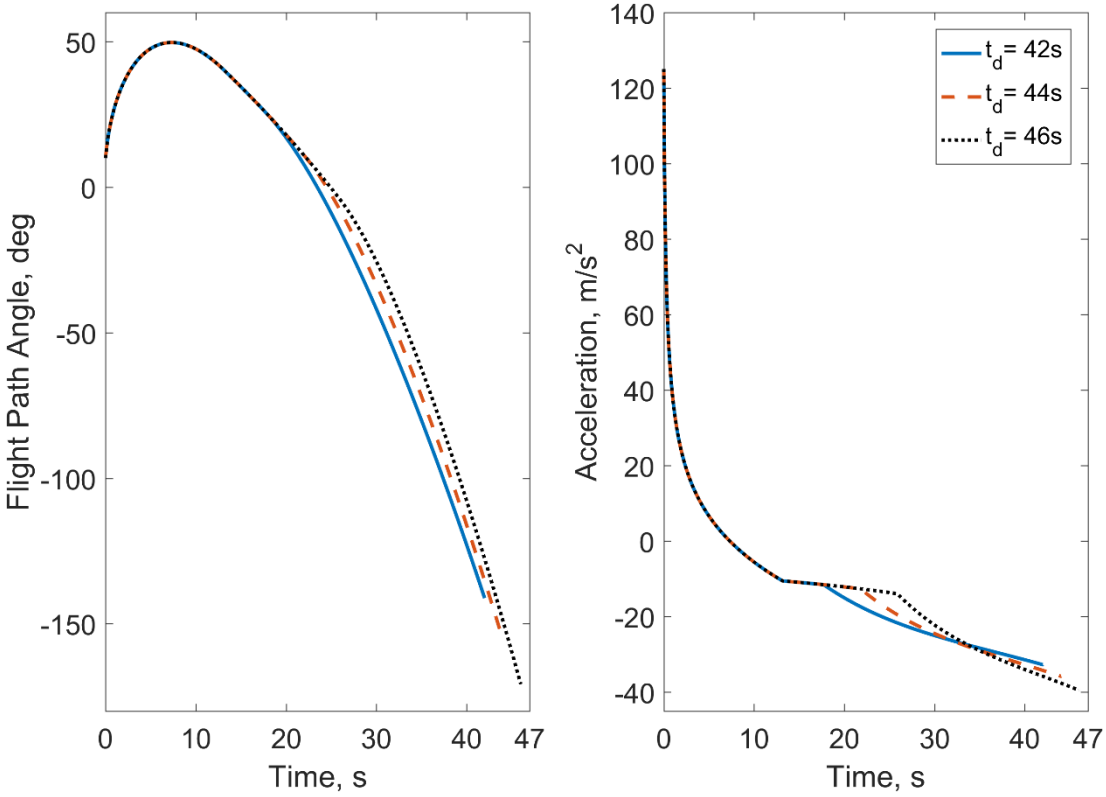

Figure 3.16 Flight path angle and acceleration histories under the FOV constraint.

In addition to the ideal simulations, the performance under autopilot lag is also tested to see whether the look angle constraint is violated or not. It can be said that the impact time values confirm that in each case, the guidance objective is met with sufficient accuracy. It is observed that the overall behavior is not affected much by the lagged response. Therefore, all of the figures are not presented to prevent complexity. Only the look angle behaviors under autopilot lag are given in Figure 3.17. The continuous lines show the results without any latency and the dashed ones are with autopilot lag, where $\tau = 0.3$ s. As described, the look angle increases until 70°, the limit. After that, it stays constant until the final phase starts which depends on the desired impact time. It is seen that the limit is slightly violated when the pursuer dynamics is on. The simple remedy would be to assume a slightly lower value than the actual limit. Last, the guidance coefficients, $\hat{x}_2$, are displayed in Figure 3.18 including the history under autopilot lag for each scenario. It is seen that when there is autopilot, instead of remaining in the neighborhood of zero, it diverges towards the final time, which is a typical guidance law response under autopilot lag [62].

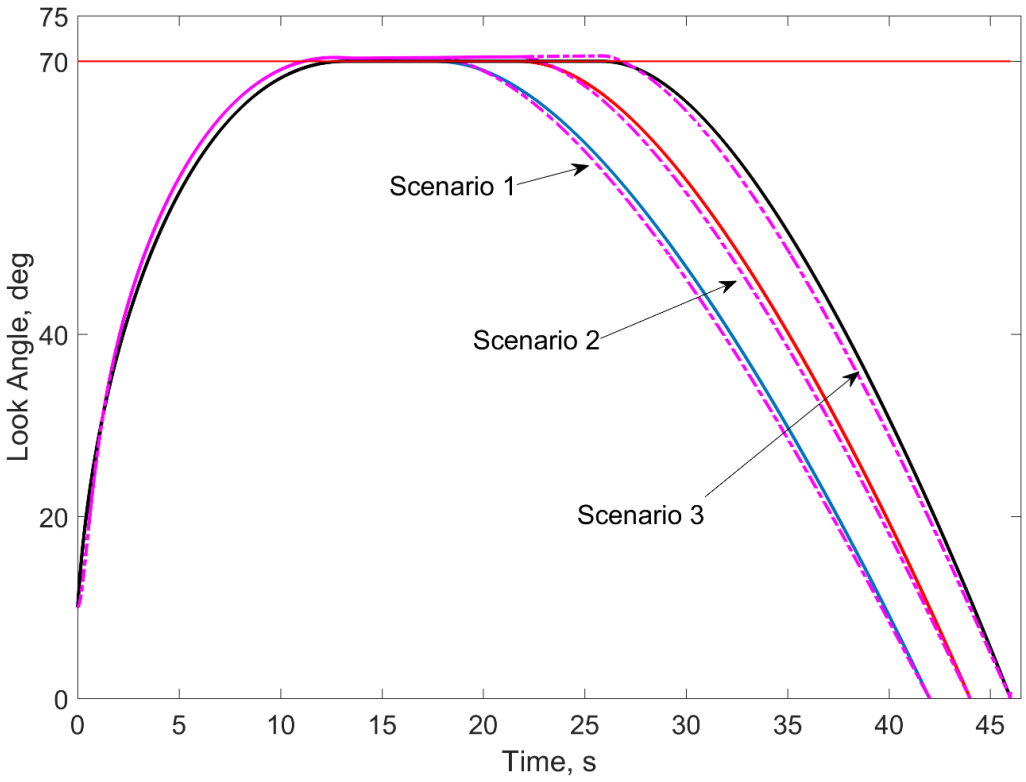

Figure 3.17 Look angle histories with and without autopilot lag.

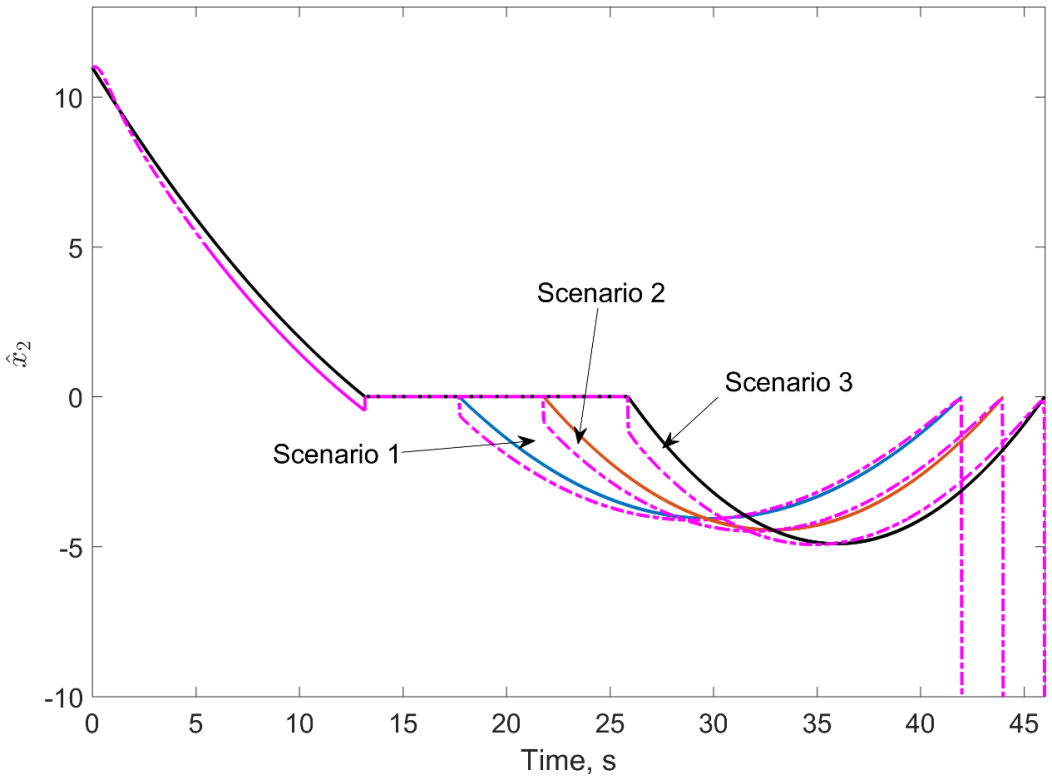

Figure 3.18 $\hat{x}_2$ histories with and without autopilot lag.

3.9.2 Method II

In this subsection, FOV constrained impact time control is presented with a different design approach. In contrast to the previous approach, there is not an assumption in this method. The problem is solved by mainly investigating the characteristics of the look angle during an engagement. In an impact time control problem, the look angle will increase to curve the trajectory. When it is time to decrease the look angle, the look angle rate will change sign. In other words, the look angle rate will cross zero when it is time to decrease the look angle. Motivated by that behavior, the second approach is presented for the 4th order.

Since the guidance law is in a switched structure as presented in Figure 3.13, the first step is to find the time when the maximum look angle occurs. The solution of the time instant could be found via equaling Eq. (2.8) and $\dot{r}$ such as

$$-V\cos\varepsilon_{\max} = 4x_4 t_1^{\,3} + 3x_3 t_1^{\,2} + 2x_2 t_1 + x_1 \tag{3.87}$$

The roots of Eq. (3.87) will provide t_1 and it will then give the corresponding range, R_1, all of which are numerically calculated. Second, the range covered during the constant look angle phase will be

$$R_2 = R_1 - V\cos\varepsilon_{\max}\left(t_2 - t_1\right) \tag{3.88}$$

where t_2 is the time to decrease the look angle and switch to the final phase. At the switching instant, the look angle rate is meant to be zero, where it depends only on $\hat{x}_2$ as given in Eq. (3.38). When Eq. (3.38) is equaled to zero and the following changes

$$\varepsilon \to \varepsilon_{\max} \qquad t \to t_2 \qquad r \to R_2 \tag{3.89}$$

are made, then Eq. (3.38) yields the following equation to find the second switching instant:

$$3\left(\cos\varepsilon_{\max} + 1\right)V\left(t_f - t_2\right) - 6R_2 = 0 \tag{3.90}$$

This equation with Eq. (3.88) gives the time instant to switch to the final phase:

$$t_2 = \frac{\left(1+\cos\varepsilon_{\max}\right)Vt_f - 2\left(R_1 + V\cos\varepsilon_{\max}t_1\right)}{\left(1-\cos\varepsilon_{\max}\right)V} \tag{3.91}$$

After providing t_2, the second method is finalized. Here, it is to be noted that the feasibility condition described in Eq. (3.86) is still valid.

To the extent of comparison between the methods for impact time control under the FOV constraint, simulations are run with the same initial conditions of the previous method. Moreover, to provide a clear understanding, the guidance commands are executed without latency. The desired impact time is 45 s. The two important features are shown in Figure 3.19 and Figure 3.20. In Figure 3.19, it is seen that Method II has sharp transition to the constant look angle phase in comparison to Method I. Furthermore, it reaches the maximum faster than Method I. Besides, the third phase of Method II starts before Method I. As expected, Method II has slightly more acceleration at the beginning. Additionally, the switching instants of Method II are sharper as seen in Figure 3.20. However, Method II finalizes the engagement with slightly less acceleration. To sum up, although there is some difference between the

methods, both of them are satisfactory and applicable for impact time control under the FOV constraint.

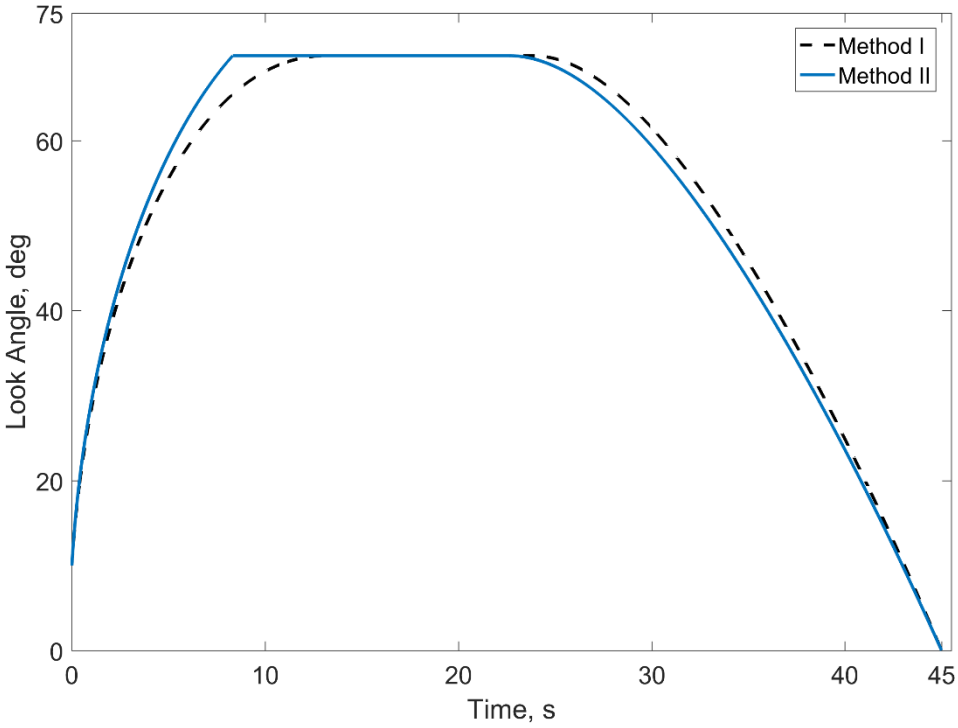

Figure 3.19 Comparison of the look angle histories.

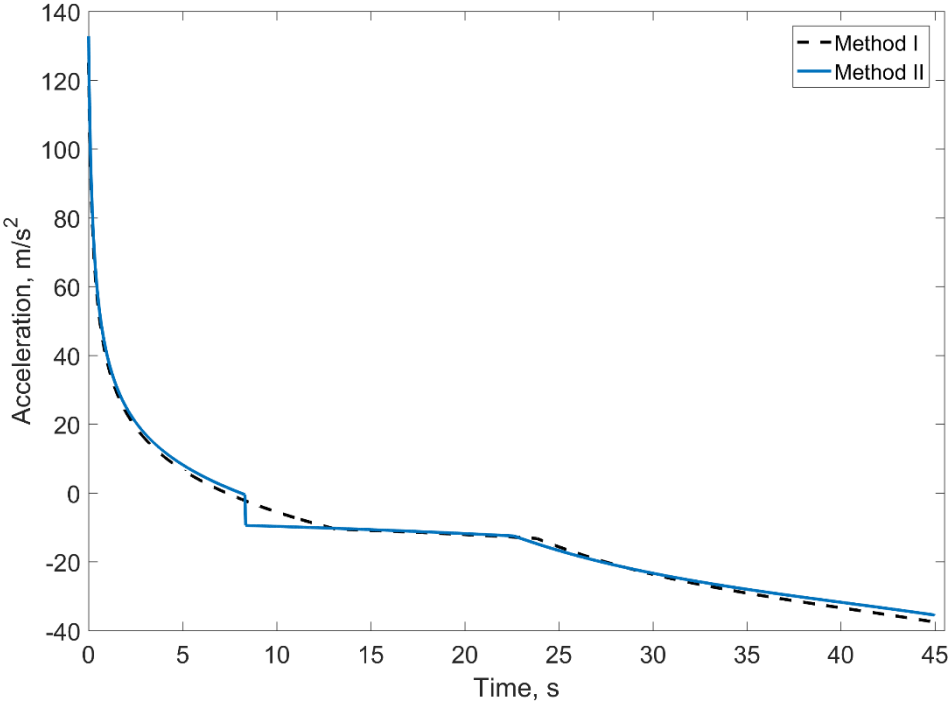

Figure 3.20 Comparision of the acceleration histories.

4 MULTI-PHASE LOOK ANGLE SHAPING FOR IMPACT TIME CONTROL

In the previous chapter, the range was described in terms of a time dependent polynomial, which resulted in a closed loop guidance law. Since the other fundamental state regarding the impact time control problem is the look angle, a solution over look angle shaping could be considered. The very first solution that comes to mind is to keep the look angle constant until capture. This case; however, provides one impact time as presented in Eq. (2.17). Although it might be possible to arrange the initial look angle at the beginning of the engagement, this manual approach would not be feasible. Moreover, for a successful capture, it is necessary to have zero look angle at the time of intercept. Under the constant speed assumption, Eq. (2.8) must have an analytical solution in order to provide a feasible guidance command. However, this would not be straightforward as in the range shaping, since the look angle is located in the cosine function. Nevertheless, at least two alternative and feasible solutions could be presented with a multi-phased guidance structure.

In this chapter, a solution that is based on shaping the look angle as a combination of straight line segments is introduced as a means of capturing the target at the desired time. First, to have an understanding of the relation between the look angle and the impact time, the number of the line segments is kept at two, which is the minimum number required to impose an impact time. The two-phased guidance structure suggested in the first place has two different implementation cases. Whichever of these cases is applicable depends on whether the desired impact time is lower or higher than a critical value. This scheme allows the acceleration limit to be considered in the derivation of the minimum and the maximum achievable impact times. A straightforward way to implement the guidance law turns out to be the utilization of the PN guidance law with specific gains or with a bias.

However, the impact time interval would be limited with this two-phased method. As an improvement, the number of the line segments could be increased for a wider impact time

interval. For that purpose, the three-phased approach is proposed, where the guidance command is constructed by considering the full extent of the available resources in the form of the look angle and the acceleration constraints. In the previous two-phased impact time control structure, the engagement starts either with the constant or with the decreasing look angle phase. However, it is also possible to increase the look angle up to a certain value, which could be the physical limit, (unless it already starts from the limit). Then, the look angle could be kept constant until the moment that it must start decreasing. The question here becomes how to accomplish this initial maneuver. As mentioned, the aim is to increase the impact time interval; thus, the time spent during the constant look angle phase must be kept as long as possible. This interpretation brings in the full effort maneuver for the first phase so that the second phase could last longer. After the first phase, the last two phases can be mechanized by the PN guidance law.

4.1 Two-Phased Look Angle Shaping for Impact Time Control

One direct way to calculate the impact time is implied by Eq. (2.8). Knowing that the target must finally be captured, the integrated form of this equation can be written as

$$R_0 = V\int_0^{t_f} \cos\varepsilon dt \tag{4.1}$$

As seen, the impact time could readily be obtained if an analytical solution to the integral on the right-hand side of the expression above was available.

The very first practical way to obtain the range equation could be considering a ramp-type profile for the look angle such as

$$R_0 = V\int_0^{t_f} \cos\left(\varepsilon_0 + mt\right) dt \tag{4.2}$$

where m is the slope of the ramp function. This equation leads to

$$R_0 = V\frac{\sin\left(\varepsilon_0 + mt_f\right) - \sin\varepsilon_0}{m} \tag{4.3}$$

Here, it appears that there is a solution corresponding to any impact time value. However, as implied, if the look angle is different than zero at the instant of impact, the corresponding value of the LOS rate will not be finite. Therefore, the final value of the look angle needs to be demanded to be zero, i.e. $\sin(\varepsilon_0 + mt_f) = \sin\varepsilon_f = 0$. Following this realization, Eq. (4.3) degenerates to yield the critical slope as

$$m_c = -V\frac{\sin\varepsilon_0}{R_0} \tag{4.4}$$

which can immediately be identified as the initial LOS rate from Eq. (2.7) . So, after replacing Eq. (4.4) in Eq. (4.3), the critical impact time becomes

$$t_{f,c} = -\frac{\varepsilon_0}{m_c} \tag{4.5}$$

As seen, the slope of the ramp function and consequently the final time happen to be dictated by the geometry of the problem; so, it seems that the proposed practice of having a ramp-type profile is fruitless in terms of impact time control. It can provide only one impact time value. The described situation may dramatically be altered by considering a two-phased scheme and accordingly adjusting the start time and/or the slope of the ramp function. It is reasonable to expect that the total engagement duration will be less than the critical impact time if the slope is steepened. Similarly, the engagement should last longer if the start of the ramp is delayed. From this point on, these former and latter cases will be referred to as Case I and Case II, respectively. The general profiles of the look angle applicable to these cases and the critical impact time, which decides whichever of the cases is applicable, is presented in Figure 4.1.

Before proceeding further, it would be convenient to state that Eq. (2.7), Eq. (2.8) and Eq. (4.4) may be utilized to show that $\dot{\lambda} = \dot{\lambda}_0 = m_c$ during the critical case. This result, when combined with Eq. (2.4) and Eq. (4.2) produces

$$\dot{\gamma} = m_c + \dot{\lambda} = 2\dot{\lambda} \tag{4.6}$$

which means that the critical case corresponds to PN with a navigation gain of 2.

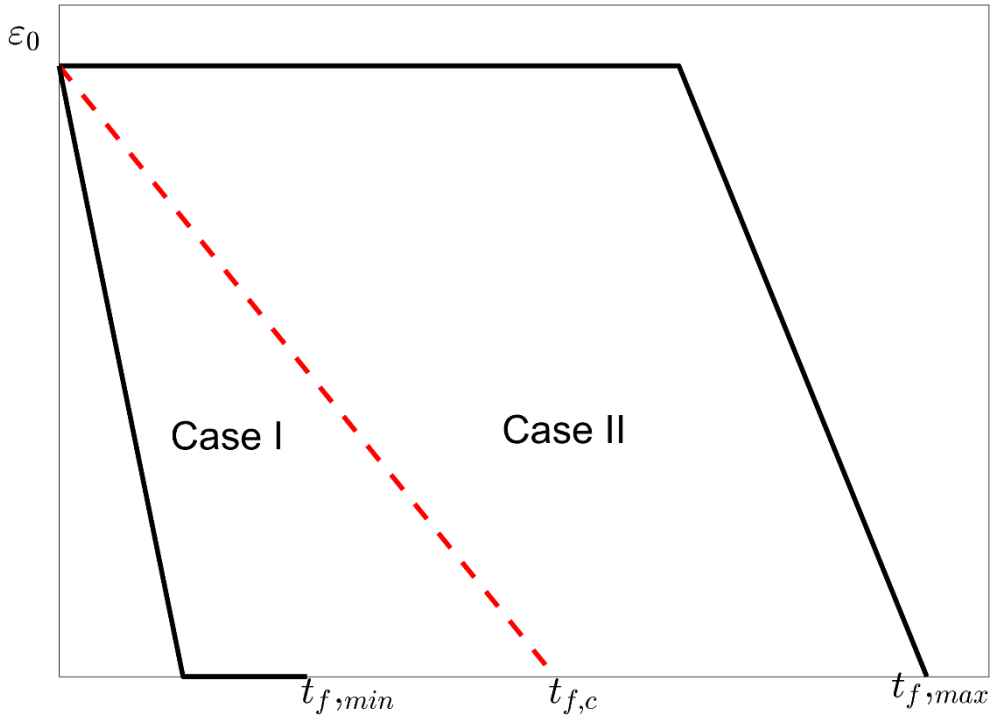

Figure 4.1 Look angle profiles for the two guidance cases.

4.1.1 Case I

Case I is a two-phased approach that involves decreasing the look angle at a rate $|m|>|m_c|$ and maintaining its value once it reaches zero:

$$\varepsilon = \begin{cases} \varepsilon_0 + mt, & t < t_s \\ 0, & t \geq t_s \end{cases} \tag{4.7}$$

From Eq. (4.7), the switching time, t_s, at which the zero value is reached is

$$t_s = -\frac{\varepsilon_0}{m} \tag{4.8}$$

Then, Eq. (2.8) can be integrated between $t = 0$ and $t = t_s$ to obtain the corresponding range value as

$$R_s = R_0 + \frac{V}{m}\sin\varepsilon_0 \tag{4.9}$$

Noting that the pursuer will follow a straight-line trajectory after $t = t_s$ until the intercept, the impact time is simply

$$t_d = t_s + \frac{R_s}{V} \tag{4.10}$$

Replacing the impact time with the desired one, the preceding equation may be combined with Eq. (4.8) and Eq. (4.9) to obtain the slope as

$$m = \frac{\sin \varepsilon_0 - \varepsilon_0}{t_d - R_0 / V} \tag{4.11}$$

This is the slope of the look angle profile during the first phase of Case I that corresponds to a desired impact time. When there is no acceleration constraint, the condition $t_{f,\min} < t_d < t_{f,c}$ must be satisfied, where Eq. (2.16) gives the minimum impact time. The combination of Eq. (4.8) and Eq. (4.11) provides the switching time:

$$t_s = -\frac{t_d - R_0 / V}{\sin \varepsilon_0 - \varepsilon_0} \varepsilon_0 \tag{4.12}$$

Due to Eq. (2.4) and Eq. (4.11), the guidance command of Case I may be written as

$$\dot{\gamma} = \begin{cases} m + \dot{\lambda}, & t < t_s \\ 0, & t \geq t_s \end{cases} \tag{4.13}$$

This shows that the look angle profile of Case I can be tracked by means of a two-phased biased PN guidance process, in which the unity navigation gain and the bias term are both removed at the switching instant. Furthermore, it can be shown that the LOS rate assumes the following form:

$$\dot{\lambda} = \begin{cases} \dfrac{m \sin \varepsilon}{\sin \varepsilon - \dfrac{R_0}{V}\left(m - \dot{\lambda}_0\right)}, & t < t_s \\ 0, & t \geq t_s \end{cases} \tag{4.14}$$

by integrating Eq. (2.8), where the look angle is as described in Eq. (4.7).

4.1.2 Case II

Case II first maintains the initial value of the look angle and afterward decreases the look angle to zero at intercept with a ramp function. This strategy is suggested in order to increase the impact time interval. Here, the look angle can be expressed as

$$\varepsilon = \begin{cases} \varepsilon_0, & t < t_s \\ \varepsilon_0 + m\left(t - t_s\right), & t \geq t_s \end{cases} \tag{4.15}$$

To find the range at the instant of phase switching, Eq. (2.8) can be integrated between $t = 0$ and $t = t_s$, which is yet unknown. This yields the switching range:

$$R_s = R_0 - V \cos \varepsilon_0 t_s \tag{4.16}$$

The structure of the second phase is the same as the critical case. As in Case I, the slope is steeper than the critical slope, i.e. $|m| > |m_c|$; but now for a different reason. In Case I, the reason was the requirement to quickly nullify the look angle; yet this time, it is the higher LOS rate due to the decreased range. Accordingly, Eq. (4.4) may be modified as

$$m = -V \frac{\sin \varepsilon_0}{R_s} \tag{4.17}$$

which is equal to the LOS rate at the switching instant from Eq. (2.7). The duration of the second phase is

$$t_f - t_s = -\frac{\varepsilon_0}{m} \tag{4.18}$$

as in Eq. (4.8). Replacing the impact time with the desired impact time, this equation can be combined with Eq. (4.16) and Eq. (4.17) to produce the slope as

$$m = -V \frac{\sin \varepsilon_0 + \varepsilon_0 \cos \varepsilon_0}{R_0 - V \cos \varepsilon_0 t_d} \tag{4.19}$$

This is the slope of the look angle profile during the second phase of Case II that corresponds to a desired impact time. If there is no acceleration constraint, the condition $t_{f,c} < t_d < t_{f,\max}$

must hold, where $t_{f,\max}$ is defined by no correction impact time as given in Eq. (2.17). The switching instant can be obtained by inserting Eq. (4.19) into Eq. (4.18):

$$t_s = t_d + \frac{\cos\varepsilon_0 t_d - R_0/V}{\sin\varepsilon_0 + \varepsilon_0\cos\varepsilon_0}\varepsilon_0 \tag{4.20}$$

Now, the guidance command may be presented. Noting the slope is zero during the first phase and the second phase is equivalent to the critical case, it follows from Eq. (2.4) and Eq. Eq. (4.6) that

$$\dot{\gamma} = \begin{cases} \dot{\lambda}, & t < t_s \\ 2\dot{\lambda}, & t \geq t_s \end{cases} \tag{4.21}$$

As seen, the look angle profile of Case II can be tracked by means of a two-phased PN guidance process, in which the navigation gain is switched from 1 to 2. As for the LOS rate, one can show that it can be expressed as follows:

$$\dot{\lambda} = \begin{cases} -\dfrac{V\sin\varepsilon}{r - Vt\cos\varepsilon}, & t < t_s \\ \text{Eq. (4.19)}, & t \geq t_s \end{cases} \tag{4.22}$$

using Eq. (4.15) and Eq. (2.7).

4.1.3 Impact Time Interval Determined by the Acceleration Constraint

The objective of this section is to derive the expressions corresponding to the minimum and maximum impact times for an acceleration constrained pursuer. The minimum impact time can be achieved with Case I by bringing the look angle to zero as quickly as possible. Using Eq. (4.14) in Eq. (4.13), the guidance command of the first phase of this case can be obtained as

$$\dot{\gamma} = \left(1 + \frac{\sin\varepsilon}{\sin\varepsilon - \dfrac{R_0}{V}\left(m - m_c\right)}\right) m \tag{4.23}$$

Then, the second derivative happens to be

$$\ddot{\gamma} = -\frac{R_0}{V}\frac{\left(m - m_c\right)}{\left\{\sin\varepsilon - \frac{R_0}{V}\left(m - m_c\right)\right\}^2} m^2 \cos\varepsilon \tag{4.24}$$

Neglecting the trivial solutions $m = 0$ and $m = m_c$, this quantity becomes zero when the look angle satisfies the equality: $\varepsilon = \pi / 2$. To see whether this value corresponds to a local extremum, the third derivative

$$\dddot{\gamma} = \frac{R_0}{V}\frac{\cos^2\varepsilon - \frac{R_0}{V}\left(m - m_c\right)\sin\varepsilon + 1}{\left\{\sin\varepsilon - \frac{R_0}{V}\left(m - m_c\right)\right\}^3}\left(m - m_c\right)m^3 \tag{4.25}$$

can be employed. Noting that $m - m_c = -|\,m - m_c\,|$, it is apparent that the signs of Eq. (4.23) and Eq. (4.25) are opposite. It can hence be concluded that the acceleration reaches its extreme value when $\varepsilon = \pi / 2$ and furthermore, the extreme acceleration is experienced at the initial instant if ε_0 is less than $\pi / 2$. In Eq. (4.23), Replacing $\sin\varepsilon$ with one and $\dot{\gamma}$ with $-\dot{\gamma}_{\max}$, where $a_{\max} = V\dot{\gamma}_{\max} > 0$ is the maximum acceleration capacity, the following is obtained:

$$m^{*2} - \left(\frac{2V}{R_0} + m_c - \dot{\gamma}_{\max}\right)m^* - \left(\frac{V}{R_0} + m_c\right)\dot{\gamma}_{\max} = 0 \tag{4.26}$$

As a result, the steepest slope can be presented as

$$m^* = \begin{cases} \text{root of Eq. (4.26)}, & \varepsilon_0 > \pi/2 \\ V\dfrac{\sin\varepsilon_0}{R_0} - \dot{\gamma}_{\max} & \varepsilon_0 \le \pi/2 \end{cases} \tag{4.27}$$

So, manipulating Eq. (4.11) using the steepest slope, the minimum-achievable impact time becomes

$$t_{f,\min}^* = \frac{R_0}{V} + \frac{\sin\varepsilon_0 - \varepsilon_0}{m^*} \tag{4.28}$$

On the other hand, the maximum impact time can be achieved with Case II by delaying the switching instant as much as possible. According to Eq. (4.22), the extreme value of the LOS

rate will be experienced throughout the second phase. As a result, the switching instant may be investigated for the current purpose. Utilizing Eq. (4.16) in Eq. (4.18) and enforcing $\dot{\gamma}_{\max} = -2\dot{\lambda}_s$ in Eq. (4.17), the maximum-achievable impact time can be found as follows:

$$t_{f,\max}^{*} = \frac{R_0}{V\cos\varepsilon_0} + \frac{2}{\dot{\gamma}_{\max}}\left(\varepsilon_0 - \tan\varepsilon_0\right) \tag{4.29}$$

Finally, the interval of achievable impact times follows from Eq. (4.28) and Eq. (4.29) as

$$\frac{R_0}{V} + \frac{\sin\varepsilon_0 - \varepsilon_0}{m^{*}} \le t_d \le \frac{R_0}{V\cos\varepsilon_0} + \frac{2}{\dot{\gamma}_{\max}}\left(\varepsilon_0 - \tan\varepsilon_0\right) \tag{4.30}$$

Provided that the desired impact time stays within this interval, Eq. (4.11) and Eq. (4.19) and the associated formulations presented in the previous subsections are all applicable.

4.1.4 Simulations for Two-Phased Look Angle Shaping

In this section, the performance of the proposed impact time control structure is demonstrated through various engagement scenarios. In the simulations, the ground-launched missile, which attacks a target 5 km away, travels with a constant speed of 200 m/s. The initial flight path angle is 45°. The simulations are terminated when the range is less than 1 m.

The minimum and maximum impact times assuming no acceleration limit can be calculated as $t_{f,\min} = 25$ s and $t_{f,\max} = 31.063$ s, respectively from Eq. (2.16) and Eq. (2.17). Noting this, the desired impact times are chosen to be 26 s as an example of Case I, 27.77 s, which is the critical impact time obtained from Eq. (4.5), and 30 s for Case II .

In Figure 4.2, the missile trajectories are presented. As seen, increasing the desired impact time increases the curvature of the missile trajectory. The closing speed variations are given in Figure 4.3. It is important to remember that these are analytically integrable, which is the backbone of the guidance design. Figure 4.4 illustrates the missile look angle profiles. In Case I, the look angle is nulled first and kept at zero afterwards. On the other hand, during the first phase of Case II, the look angle is kept constant, then it is driven to zero. The critical impact time solution linearly decreases the initial look angle with the critical slope. Lastly, Figure 4.5 displays the histories of the acceleration. As seen, Case I has zero acceleration for the final phase, meanwhile Case II has a constant acceleration.

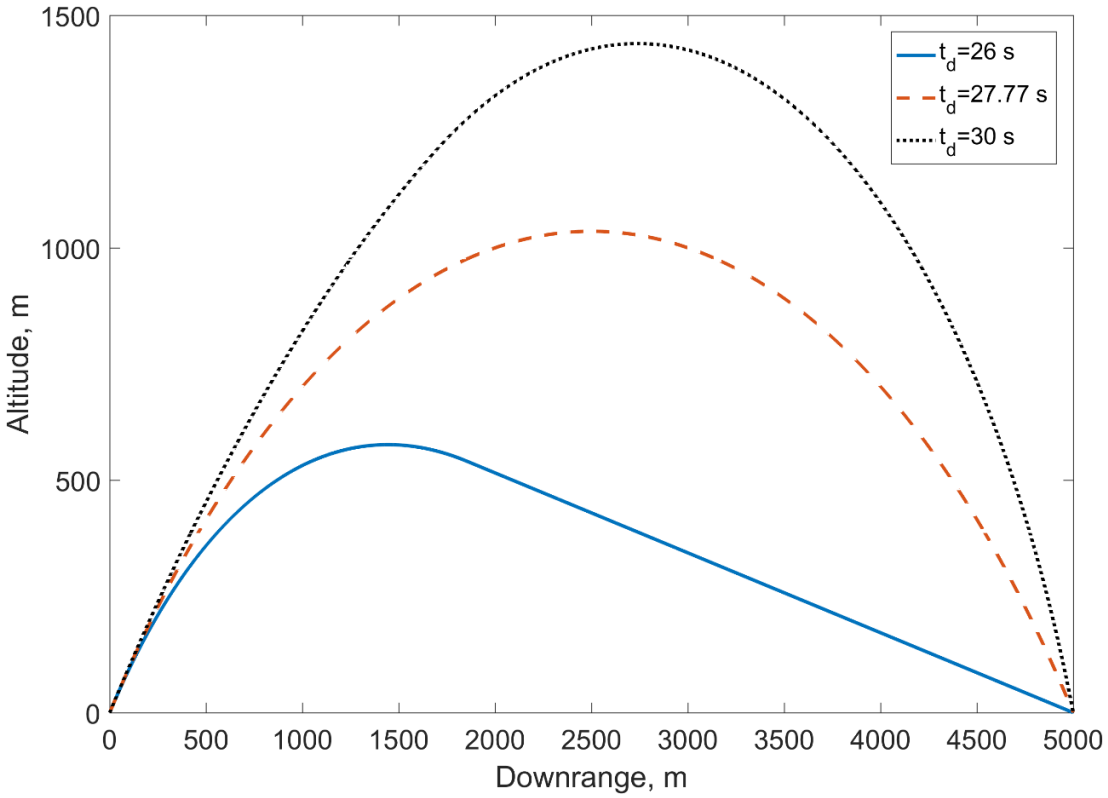

Figure 4.2 Trajectories produced by the two-phased guidance law.

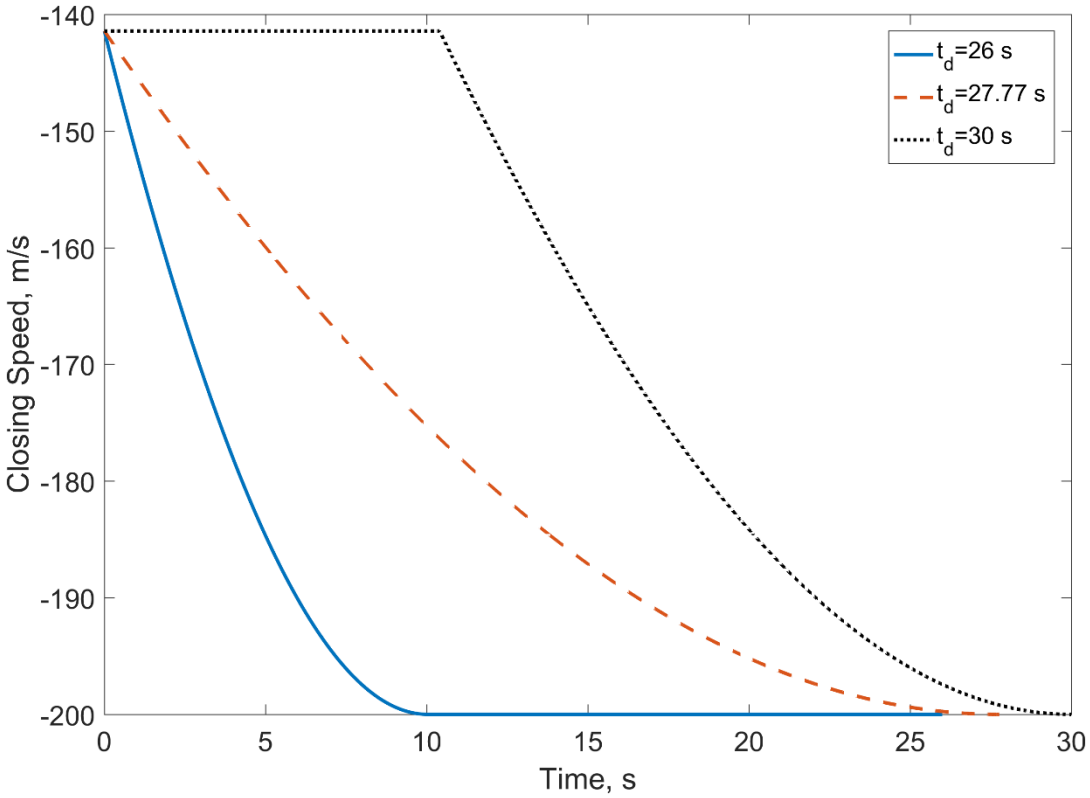

Figure 4.3 Closing speed histories produced by the two-phased guidance law.

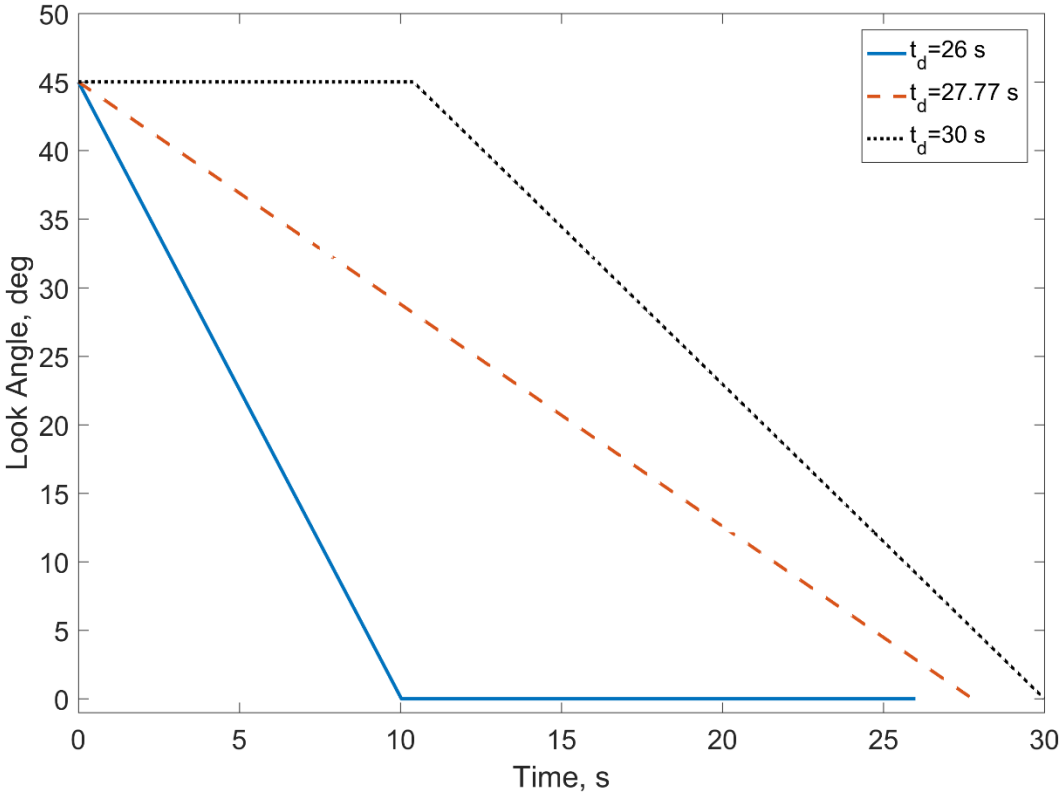

Figure 4.4 Look angle histories produced by the two-phased guidance law.

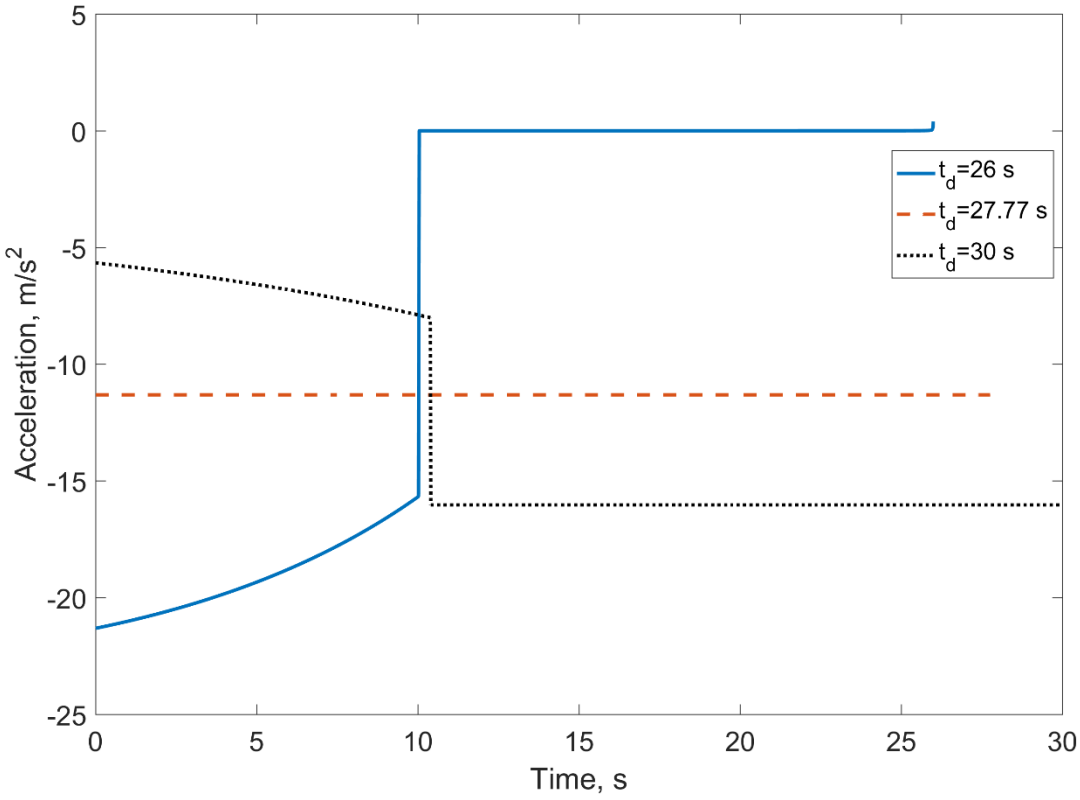

Figure 4.5 Acceleration histories produced by the two-phased guidance law.

4.2 Constrained Impact Time Control with Three-Phased Look Angle Shaping

The objective of this section is to develop guidance schemes to increase the impact time interval and not to violate the look angle and the acceleration constraints in the meantime. As briefly mentioned in Section 4.1, when there are constraints to be considered, the achievable impact times become limited; such that an engagement cannot last shorter than $t_{\mathrm{f,min}}$ or longer than $t_{\mathrm{f,max}}$. This implies that any impact time between these values should be achievable. Obviously, there might be quite a number of alternative approaches to solve the problem. Unlike the previous section, where the look angle was initially kept constant for a while, this section presents an impact time control strategy that starts by changing the look angle using the maximum effort. The guidance laws are once again separated into two cases: Case I and Case II. Figure 4.6 presents a clear picture of these cases and the corresponding time instants. As seen, the first phase of Case I involves a full effort maneuver until $\hat{t}$ and specifically until $\hat{t}_c$ for $t_{\mathrm{f,min}}$. Then in the second phase, the look angle is decreased with a constant slope, which is obtained by applying $\dot{\gamma} = 2\dot{\lambda}$. On the other hand, Case II is realized by rapidly reaching the maximum look angle in the first phase at $t = \tilde{t}_c$, and remaining there until $\breve{t}$ during the second phase. As for $t_{\mathrm{f,min}}$, there is critical $\breve{t}_c$ for $t_{\mathrm{f,max}}$. Thereon, the look angle is decreased with a constant slope by means of $\dot{\gamma} = 2\dot{\lambda}$ in the third phase. It should be noted that the slope of the look angle during the first phases of Case I and Case II is not constant although it might appear so in the figure. So, the cases are classified with respect to the initial behavior of the look angle; decreasing or increasing. This decision is given by the critical impact time, $t_{\mathrm{f,c}}$, as in the previous two-phased approach. If the desired impact time is less than $t_{\mathrm{f,c}}$, Case I will be valid and if not, Case II will be valid. Additionally, there is another impact time definition, t^*, which is in the domain of Case II. Having the desired impact time less than t^* means that the maximum look angle phase will not be experienced. In between t^* and $t_{\mathrm{f,max}}$, both of the constraints will be required.

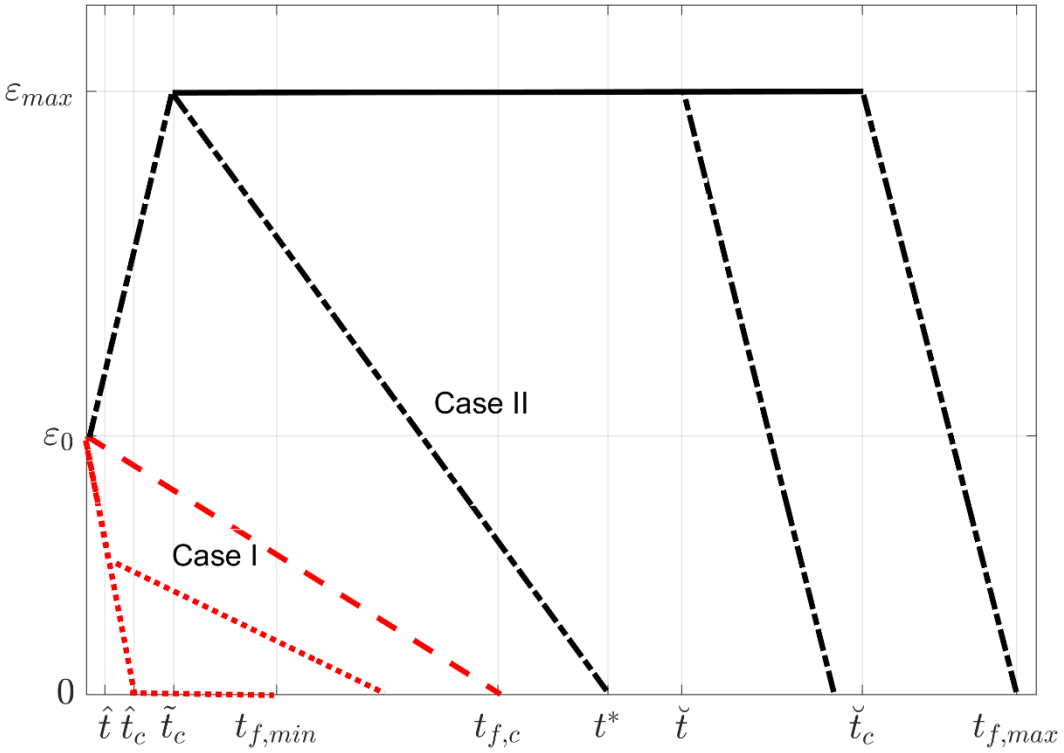

Figure 4.6 Multi-phased look angle shaping for impact time control.

4.2.1 Impact Time Interval

Before investigating Case I and Case II, the minimum and the maximum impact time values under the constraints need to be found. For Case I, the engagement will last longer than $t_{\text{f,min}}$ if the switching was performed earlier than $\hat{t}_c$. On the other hand for Case II, the engagement would last shorter than $t_{\text{f,max}}$ if the final switching was performed earlier than $\breve{t}_c$, as also shown in Figure 4.6. In addition to $\breve{t}_c$, there is another critical time for Case II. $\tilde{t}_c$ denotes the duration of the first phase of Case II to reach up to the look angle limit. The corresponding definitions and the guidance commands are shown in Figure 4.7. The critical switching instants are defined with respect to the look angle and the acceleration constraints in such way that these constraints are not violated. The next step will be to find these values.

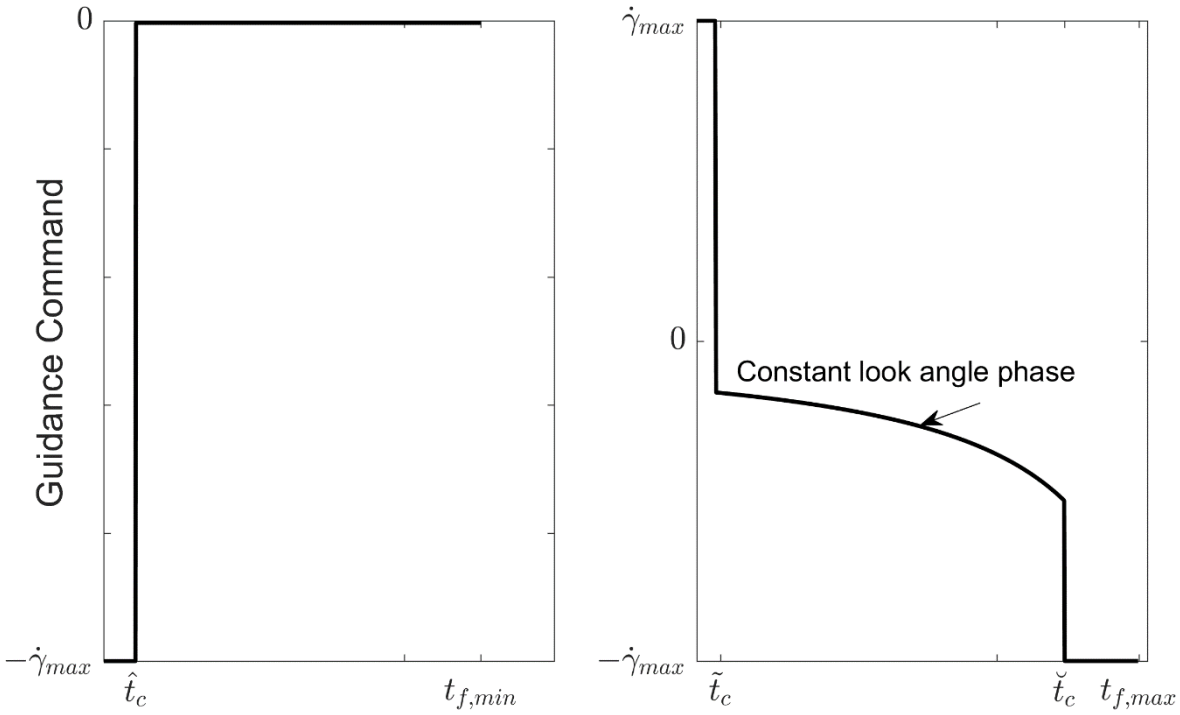

Figure 4.7 The guidance command definitions of the minimum and the maximum impact time.

First, the horizontal and the vertical speeds are written:

$$\dot{x} = V\cos\gamma, \quad \dot{y} = V\sin\gamma \tag{4.31}$$

where the flight path angle for the minimum time problem is:

$$\gamma(t) = \gamma_0 - \dot{\gamma}_{\max} t, \quad t < \hat{t}_c \tag{4.32}$$

When Eq. (4.32) is replaced in Eq. (4.31) and integrated, the following equations are obtained:

$$\begin{aligned} x(t) &= X_0 - \frac{V}{\dot{\gamma}_{\max}}\left\{\sin\left(\gamma_0 - \dot{\gamma}_{\max} t\right) - \sin\gamma_0\right\} \\ y(t) &= Y_0 + \frac{V}{\dot{\gamma}_{\max}}\left\{\cos\left(\gamma_0 - \dot{\gamma}_{\max} t\right) - \cos\gamma_0\right\} \end{aligned} \tag{4.33}$$

Here, γ_0 is the initial flight path angle and X_0, Y_0 are the initial positions, respectively. When Eq. (2.4) is rewritten with the knowledge of zero look angle at $\hat{t}_c$, the flight path angle becomes

equal to the LOS angle, $\hat{\gamma} = \hat{\lambda}$. To obtain $\hat{t}_c$, now this relation needs to be written using the geometric relations based on Figure 4.8, where the missile moves from the point *A* to *B*.

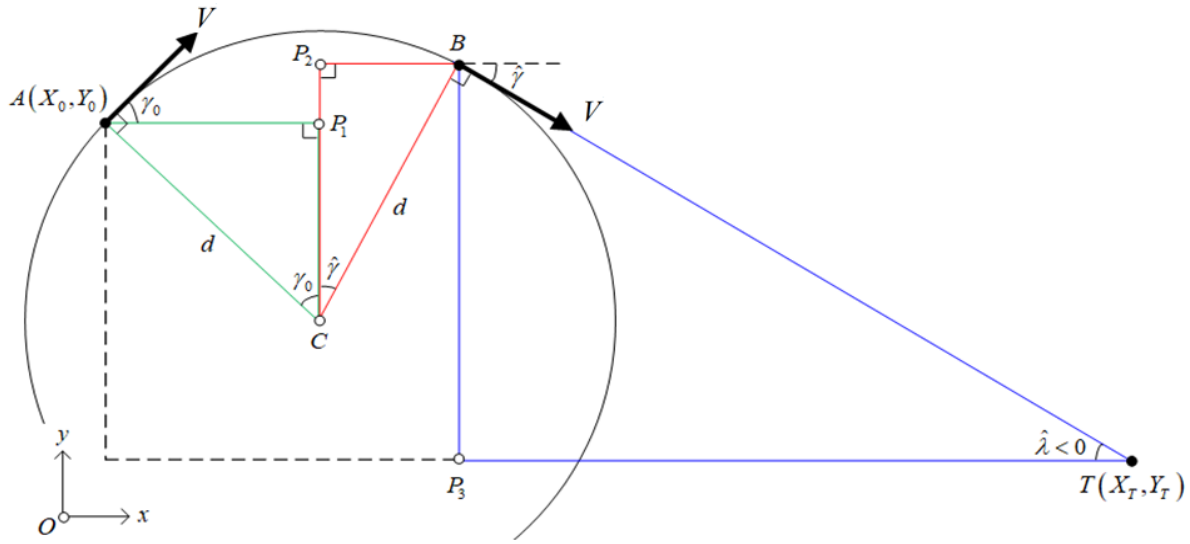

Figure 4.8 Minimum time geometry.

The LOS angle at $\hat{t}_c$ is found from the following equation:

$$\tan\hat{\lambda} = -\frac{|BP_3|}{|TP_3|} \tag{4.34}$$

The distances in Eq. (4.34) are written as

$$\begin{aligned} |TP_3| &= X_T - X_0 - |AB|_x \\ |BP_3| &= Y_0 - Y_T + |P_1P_2| \end{aligned} \tag{4.35}$$

The next step is to find $|P_1P_2|$ and $|AB|_x$, which is the distance along the *x* axis. The horizontal distance covered until $\hat{t}_c$ is composed as follows

$$|AB|_x = |AP_1| + |BP_2| = d\sin\gamma_0 - d\sin\hat{\gamma} \tag{4.36}$$

and the vertical distance is

$$|P_1P_2| = d\cos\hat{\gamma} - d\cos\gamma_0 \tag{4.37}$$

d denotes the minimum radius, which is obtained with the maximum effort

$$d = \frac{V}{\dot{\gamma}_{\max}} \tag{4.38}$$

Since γ is already known from Eq. (4.32), it is possible to rewrite $\hat{\gamma}$:

$$\hat{\gamma} = \gamma_0 - \hat{t}_c \dot{\gamma}_{\max} \tag{4.39}$$

As mentioned, the look angle is zero at $\hat{t}_c$. Replacing Eq. (4.38) in Eq. (4.36) and Eq. (4.37) yields Eq. (4.35) as

$$\begin{aligned} \left|TP_3\right| &= X_T - X_0 + \frac{V}{\dot{\gamma}_{\max}}\left(\sin\hat{\gamma} - \sin\gamma_0\right) \\ \left|BP_3\right| &= Y_0 - Y_T + \frac{V}{\dot{\gamma}_{\max}}\left(\cos\hat{\gamma} - \cos\gamma_0\right) \end{aligned} \tag{4.40}$$

Then, using Eq. (4.40) and Eq. (4.39) in Eq. (4.34) gives the following equality, which can be solved numerically to obtain $\hat{t}_c$

$$\tan^{-1}\left(\frac{-\left|BP_3\right|}{\left|TP_3\right|}\right) = \tan^{-1}\frac{Y_T - Y_0 - \frac{V}{\dot{\gamma}_{\max}}\left\{\cos\left(\gamma_0 - \hat{t}_c\dot{\gamma}_{\max}\right) - \cos\gamma_0\right\}}{X_T - X_0 + \frac{V}{\dot{\gamma}_{\max}}\left\{\sin\left(\gamma_0 - \hat{t}_c\dot{\gamma}_{\max}\right) - \sin\gamma_0\right\}} = \gamma_0 - \hat{t}_c\dot{\gamma}_{\max} = \hat{\lambda} \tag{4.41}$$

If $\hat{t}_c$ is replaced into Eq. (4.33), the range at $\hat{t}_c$ will be found:

$$r\left(\hat{t}\right) = \sqrt{\left\{X_T - X\left(\hat{t}_c\right)\right\}^2 + \left\{Y_T - Y\left(\hat{t}_c\right)\right\}^2} \tag{4.42}$$

Finally, the minimum impact time is the sum of $\hat{t}_c$, which is the end of the first phase of Case I, and the remaining range divided by the speed:

$$t_{\text{f,min}} = \hat{t}_c + \frac{r\left(\hat{t}_c\right)}{V} \tag{4.43}$$

One may immediately appreciate that the look angle constraint is inactive in the minimum time problem. This is because the look angle never increases during the engagement. However, the situation entirely changes when the maximum time is concerned.

Before the maximum time definition, another important time definition, $t_{\mathrm{f,c}}$, has to be clarified. This quantity decides whether the desired impact time is in Case I or in Case II. It is defined as

$$t_{\mathrm{f,c}} = -\frac{\varepsilon_0}{\dot{\lambda}_0} \tag{4.44}$$

which is the impact time of a single-phased engagement governed by $\dot{\gamma} = 2\dot{\lambda}$. It is actually the impact time given in Eq. (4.8) for the critical slope in the previous design methodology, where $m = \dot{\lambda}_0$.

The engagement for the maximum impact time problem comprises of three phases as shown in Figure 4.6 and Figure 4.7. First, the maximum effort is applied until the maximum look angle is reached, which results in moving away from the target over a circle like in the minimum impact time problem. Then, the constant look angle phase starts. Finally, the maximum effort in the opposite direction until impact is employed. In order to obtain $t_{\mathrm{f,max}}$, $\tilde{t}_c$ may be found with the same procedure as it was explained for $\hat{t}_c$, using the required geometric relations based on Figure 4.9.

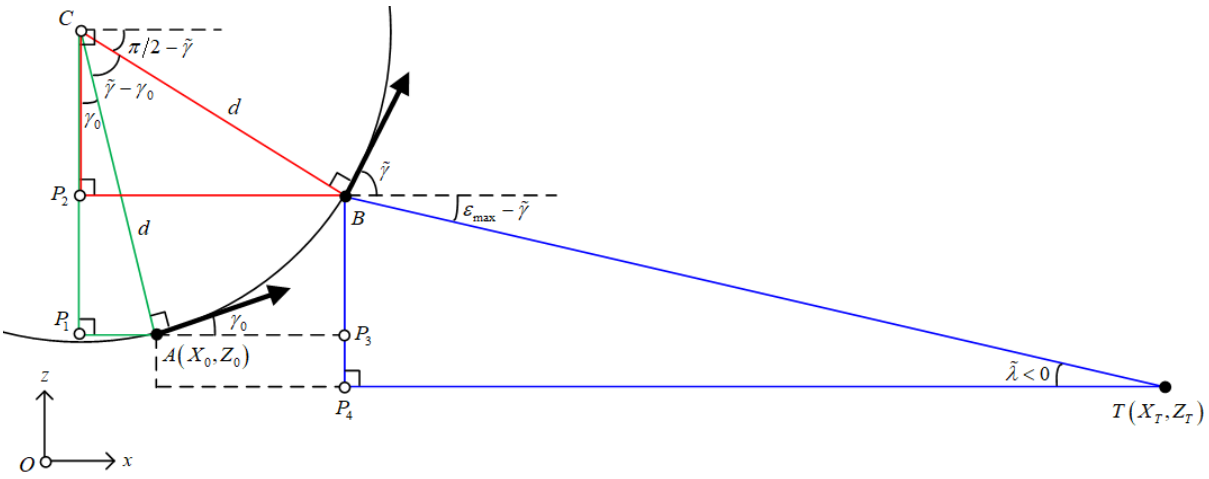

Figure 4.9 Maximum time geometry.

Now, the corresponding relation of the LOS angle at $\tilde{t}_c$ is

$$\tan\tilde{\lambda} = -\frac{|BP_4|}{|TP_4|} \tag{4.45}$$

where the distances are defined as

$$\begin{aligned} |TP_4| &= X_T - X_0 - |AP_3| \\ |BP_4| &= Y_0 - Y_T + |BP_3| \end{aligned} \tag{4.46}$$

The horizontal displacement is

$$|AP_3| = |BP_2| - |AP_1| = d\sin\tilde{\gamma} - d\sin\gamma_0 \tag{4.47}$$

and the vertical displacement is

$$|BP_3| = |CP_1| - |CP_2| = d\cos\gamma_0 - d\cos\tilde{\gamma} \tag{4.48}$$

d is the minimum radius, which was already given in Eq. (4.38) and $\tilde{\gamma}$ represents the flight path angle at $\tilde{t}_c$

$$\tilde{\gamma} = \gamma_0 + \tilde{t}_c\dot{\gamma}_{\max} \tag{4.49}$$

Then, the LOS angle at $\tilde{t}$ is found by Eq. (2.4) and Eq. (4.49)

$$\tilde{\lambda} = \gamma_0 - \left(\varepsilon_{\max} - \tilde{t}_c\dot{\gamma}_{\max}\right) \tag{4.50}$$

Replacing Eq. (4.47) and Eq. (4.48) in Eq. (4.46) yields the following

$$\begin{aligned} |TP_4| &= X_T - X_0 - \frac{V}{\dot{\gamma}_{\max}}\left(\sin\tilde{\gamma} - \sin\gamma_0\right) \\ |BP_4| &= Y_0 - Y_T - \frac{V}{\dot{\gamma}_{\max}}\left(\cos\tilde{\gamma} - \cos\gamma_0\right) \end{aligned} \tag{4.51}$$

When Eq. (4.51), Eq. (4.50) and Eq. (4.49) are used in Eq. (4.45), the final form of the equation for $\tilde{t}_c$ becomes

$$\tan^{-1}\left(\frac{-|BP_4|}{|TP_4|}\right)=\tan^{-1}\frac{Y_T-Y_0+\dfrac{V}{\dot{\gamma}_{\max}}\left\{\cos\left(\gamma_0+\tilde{t}_c\dot{\gamma}_{\max}\right)-\cos\gamma_0\right\}}{X_T-X_0-\dfrac{V}{\dot{\gamma}_{\max}}\left\{\sin\left(\gamma_0+\tilde{t}_c\dot{\gamma}_{\max}\right)-\sin\gamma_0\right\}}=\tilde{\lambda} \tag{4.52}$$

Then, $\tilde{t}_c$ is used to obtain $r\left(\tilde{t}_c\right)$. After solving $\tilde{t}_c$, $\breve{t}_c$ is the second unknown to be found. Following the fact that, the second phase is characterized by the constant look angle, the range equation leads to

$$r\left(\breve{t}_c\right)-r\left(\tilde{t}_c\right)=-V\cos\varepsilon_{\max}\left(\breve{t}_c-\tilde{t}_c\right) \tag{4.53}$$

One needs to notice that after $t=\breve{t}_c$, the guidance law dictates a constant maneuver that eventually leads to the stationary target being captured. Under its action, the guidance command is:

$$-\dot{\gamma}_{\max}=2\dot{\lambda}\left(\breve{t}_c\right) \tag{4.54}$$

where the maximum effort is applied in the opposite direction to decrease the look angle. Eq. (2.7) at $t=\breve{t}_c$ yields

$$r\left(\breve{t}_c\right)\dot{\lambda}\left(\breve{t}_c\right)=-V\sin\left(\varepsilon_{\max}\right) \tag{4.55}$$

Using Eq. (4.54) in Eq. (4.55), the range when the constant look angle phase ends is found:

$$r\left(\breve{t}_c\right)=\frac{2V\sin\varepsilon_{\max}}{\dot{\gamma}_{\max}} \tag{4.56}$$

After mathematical forming of Eq. (4.53) and using Eq. (4.55), the duration of the constant look angle phase is determined as

$$\breve{t}_c-\tilde{t}_c=\frac{r\left(\tilde{t}_c\right)-r\left(\breve{t}_c\right)}{V\cos\varepsilon_{\max}}=\frac{r\left(\tilde{t}_c\right)}{V\cos\varepsilon_{\max}}-\frac{2\sin\varepsilon_{\max}}{\dot{\gamma}_{\max}\cos\varepsilon_{\max}} \tag{4.57}$$

The duration of the last phase can once more be found by Eq. (4.44) :

$$t_{\mathrm{f,max}} - \breve{t}_c = \frac{2\varepsilon_{\max}}{\dot{\gamma}_{\max}} \tag{4.58}$$

As a result, the maximum impact time is obtained using Eq. (4.57) and Eq. (4.58) as

$$t_{\mathrm{f,max}} = \tilde{t}_c + \frac{r\left(\tilde{t}_c\right)}{V\cos\varepsilon_{\max}} + \frac{2\left(\varepsilon_{\max} - \tan\varepsilon_{\max}\right)}{\dot{\gamma}_{\max}} \tag{4.59}$$

4.2.2 Case I

After obtaining $t_{\mathrm{f,min}}$ and $t_{\mathrm{f,max}}$, Case I and the corresponding guidance commands can be expressed. This case covers the impact time interval between $t_{\mathrm{f,min}}$ and $t_{\mathrm{f,c}}$. As already stated, the maximum acceleration is applied at the beginning of the engagement. Depending on the desired impact time, the duration of the first phase changes. $\hat{t}$ is always smaller than $\hat{t}_c$ as it could also be seen in Figure 4.6. In the second phase, the guidance law is $\dot{\gamma} = 2\dot{\lambda}$. The guidance command for Case I is:

$$\dot{\gamma} = \begin{cases} -\dot{\gamma}_{\max}, & t_{\mathrm{f,c}} - t_d > t \\ 2\dot{\lambda}, & \text{otherwise} \end{cases} \tag{4.60}$$

When this command is compared to Eq. (4.13), it is seen that the second phase was zero until the end of the engagement, whereas it is now $2\dot{\lambda}$. Moreover, Eq. (4.13) does not provide a closed loop guidance law. However, the current one could be expressed in a partially closed loop form by replacing the current critical impact time into the guidance command by modifying with Eq. (4.44) via the instant values. So, the switching condition throughout the first phase is controlled. In the end, Eq. (4.60) can be rewritten as

$$\dot{\gamma} = \begin{cases} -\dot{\gamma}_{\max}, & \left(t_{\mathrm{d}} + \dfrac{\varepsilon}{\dot{\lambda}}\right) - t < 0 \\ 2\dot{\lambda}, & \text{otherwise} \end{cases} \tag{4.61}$$

It should also be noted that the second phase is open loop in terms of regulating the impact time error.

4.2.3 Case II

Case II covers the impact time intervals from the critical impact time up to the maximum impact time such as $t_{f,c} < t_d \leq t_{f,max}$. It consists of a two- or three-phased trajectory. First, the maximum effort is applied, which results in rapidly diverging from the target as long as required. Then, it might follow a path that directly starts decreasing the look angle from the value reached or another one that maintains the maximum look angle value. The number of the phases is determined based on t_d. If $t_d > t^*$, then the guidance law is three-phased, as seen in Figure 4.6. Otherwise, there are only two phases. The corresponding guidance command for two-phased guidance is

$$\dot{\gamma} = \begin{cases} \dot{\gamma}_{max}, & t < \tilde{t} \\ 2\dot{\lambda}, & \text{otherwise} \end{cases} \tag{4.62}$$

which could be named as Case II.1 without saturating the look angle. On the other hand, when the look angle is required to be kept at its limit for a while, the corresponding guidance command is $\dot{\gamma} = \dot{\lambda}$ as mentioned in Section 3.9.2. Then, the following three-phased guidance law is summoned:

$$\dot{\gamma} = \begin{cases} \dot{\gamma}_{max}, & t \leq \tilde{t} \\ \dot{\lambda}, & \tilde{t} < t \leq \breve{t} \\ 2\dot{\lambda}, & \text{otherwise} \end{cases} \tag{4.63}$$

This three-phased could be named as Case II.2, which demands saturation of the look angle. Although the corresponding switching instants could be computed at each time step, it is also possible to reformulate Eq. (4.62) and Eq. (4.63) and provide a partially closed loop form as in Section 4.2.2 with the critical impact time given in Eq. (4.44). When Eq. (4.62) and Eq. (4.63) are modified, the guidance laws turn into the following compact form:

$$\dot{\gamma} = \begin{cases} \begin{bmatrix} \dot{\gamma}_{max}, & \varepsilon < \varepsilon_{max} \\ \dot{\lambda}, & \text{otherwise} \end{bmatrix}, & t < \left(t_d + \dfrac{\varepsilon}{\dot{\lambda}} \right) \\ 2\dot{\lambda}, & \text{otherwise} \end{cases} \tag{4.64}$$

Motivated by the structure of the guidance command in Eq. (4.64), it is fortunately possible to rewrite the guidance commands of Case I and Case II in a unified structure:

$$\dot{\gamma} = \begin{cases} \begin{bmatrix} \varsigma\dot{\gamma}_{\max}, & \varsigma\varepsilon < \varepsilon_{\max} \\ \dot{\lambda}, & \text{otherwise} \end{bmatrix}, & \varphi < 0 \\ 2\dot{\lambda}, & \text{otherwise} \end{cases} \tag{4.65}$$

where

$$\varphi = \varsigma t - \varsigma\left(t_{\mathrm{d}} + \frac{\varepsilon}{\dot{\lambda}}\right) \tag{4.66}$$

Here, ς represents the following relation

$$\varsigma = \begin{cases} -1, & t_{\mathrm{d}} \le t_{\mathrm{f,c}} \\ 1, & t_{\mathrm{d}} > t_{\mathrm{f,c}} \end{cases} \tag{4.67}$$

It should be underlined that the outer switching condition in Eq. (4.65) has priority over the one inside the brackets. This is natural since the outer one is governed by φ, which acts as the error signal of the guidance loop. Lastly, it is noted that the guidance law in Eq. (4.65) regulates the error in closed loop form only until the terminal phase commences.

Additionally, the three-phased approach is associated with the nonlinear optimal control framework. The formulation of the optimal control problem through the unconventional endpoint cost by considering the physical limits of the system leads to the same intuitive three-phased guidance structure as presented in Appendix E.

4.2.4 Simulations for Constrained Impact Time Control

In this subsection, a simulation case is carried out for several impact times to show the performance of the guidance law. The selected impact times are chosen on purpose to have two- and three-phased guidance commands in order to show the differences within Case II. Afterwards, a comparison study is carried out between the designs outlined in Section 4.1.1 and Section 4.2.2.

A pursuer, which has a speed of 200 m/s, aims to shape its trajectory against a stationary target located 5 km away from the point of launch. The initial LOS angle is zero whereas the

initial flight path angle is 30°. The look angle limit of the pursuer is $\varepsilon_{\max} = 70^{\circ}$ and the acceleration limit is $a_{\max} = 50$ m/s^2 resulting in $\dot{\gamma}_{\max} = 0.25$ rad/s^2 = 14.324 $^{\circ}$/s^2. The constraints bring about the following impact time interval: $t_{\min} = 25.101$ s from Eq. (4.43), and $t_{\max}$ = 58.766 s from Eq. (4.59), whereas $t_{f,c}$ = 26.175 s from Eq. (4.44). It is to be noted that a performance beyond the minimum and the maximum values listed here is not possible under the given constraints. This statement is independent of the guidance law, which is also clarified in Appendix E. The desired impact times are chosen as 30 s for Case II.1, 35 s and 40 s, which fall into Case II.2 of the constrained impact time control. In addition to these impact times, the maximum impact time is also exemplified.

In Figure 4.10, one can observe how the trajectories become more curved as the impact time is increased and as seen the maximum impact time results in negative altitude. Figure 4.11 shows the look angle variations. It is seen that the first impact time demand results in a two-phased look angle profile whereas the remaining ones are three phased. The first scenario does not have a third phase because the desired impact time does not need the maximum look angle. On the other hand, the second and the third impact times demand the look angle limit. Figure 4.12 and Figure 4.13 present the range and the closing speed. It is expected that the look angle has the same behavior tendency as the closing speed. When the look angle is saturated at a certain value, the closing speed is constant as a consequence of the saturated look angle. The acceleration histories are illustrated in Figure 4.14, where it is seen that there is no violation of the acceleration constraint. The two- or three-phased nature of the proposed guidance scheme can also be observed here. As expected, the maximum effort is applied during the first phase of the engagements, after which the acceleration requirements drop to moderate levels and for the maximum impact time, the maximum effort in the opposite direction is demanded. Figure 4.15 is reserved for the flight path angle histories to show that a higher impact time results in a higher final flight path angle magnitude.

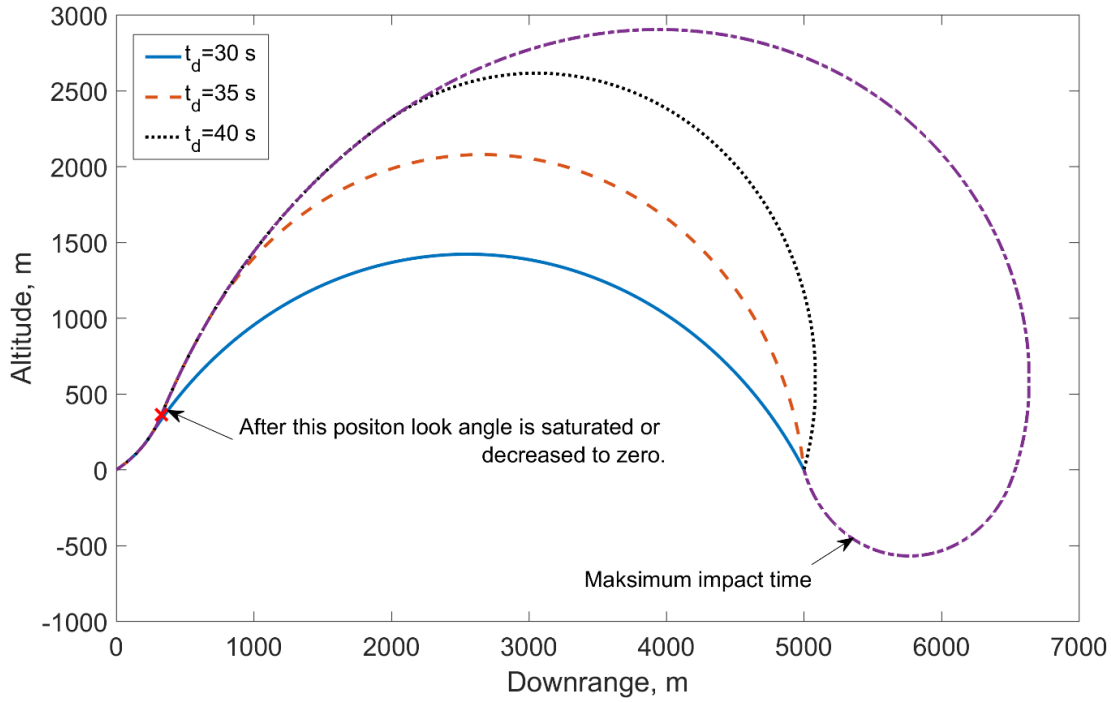

Figure 4.10 Trajectory histories produced by the constrained impact time control method.

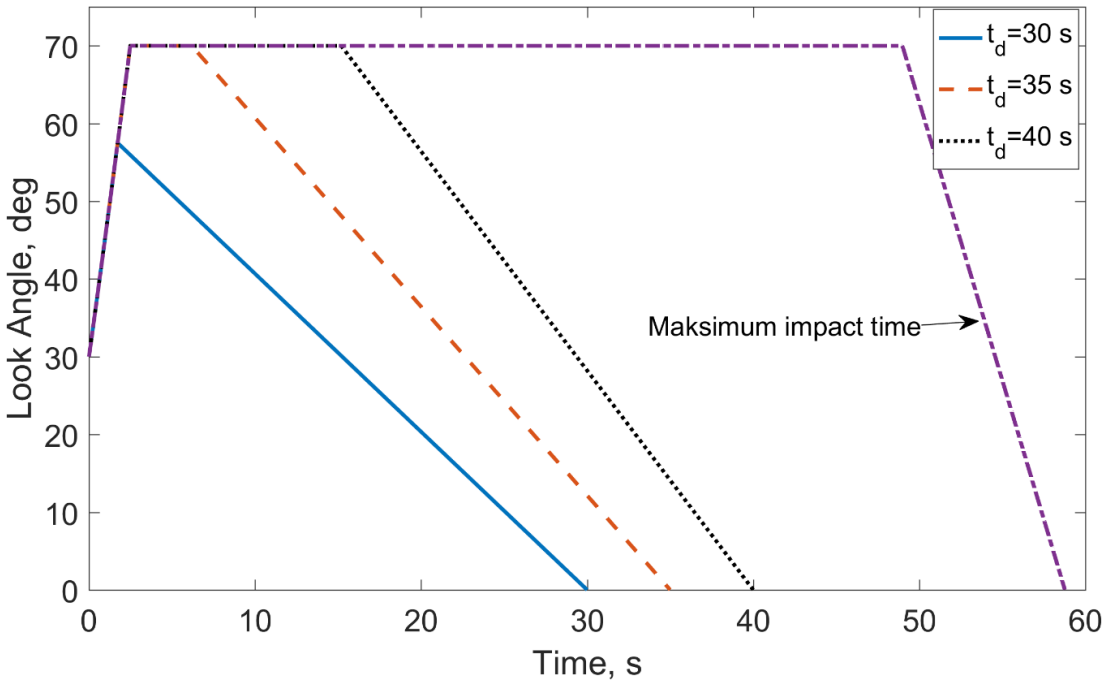

Figure 4.11 Look angle histories produced by the constrained impact time control method.

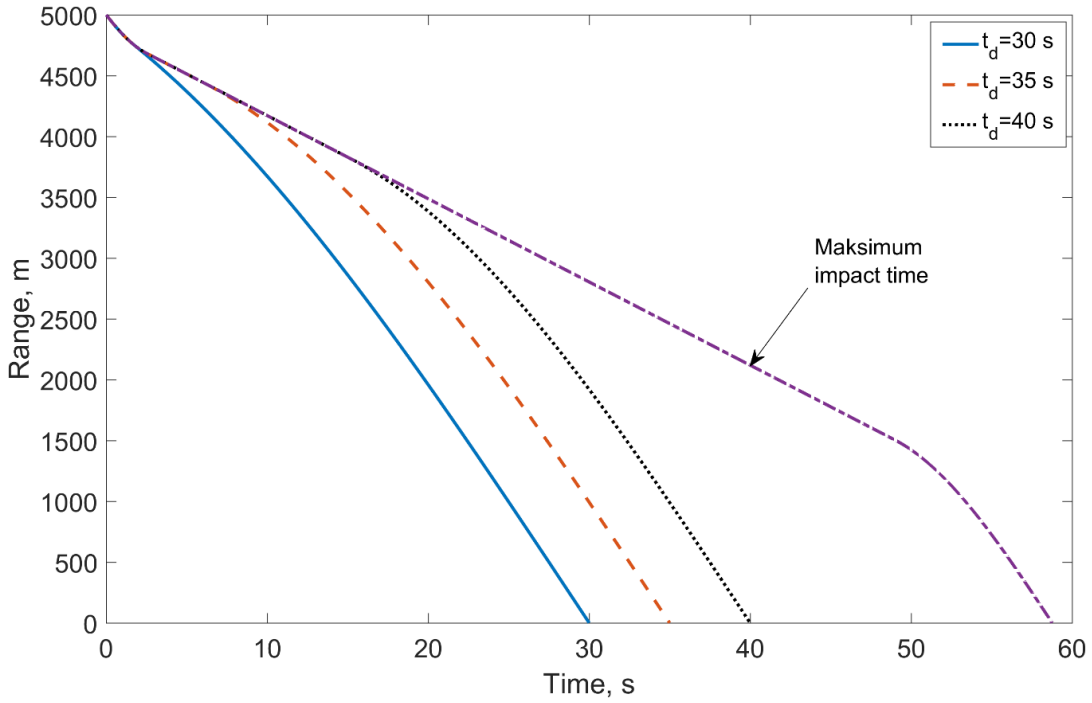

Figure 4.12 Range histories produced by the constrained impact time control method.

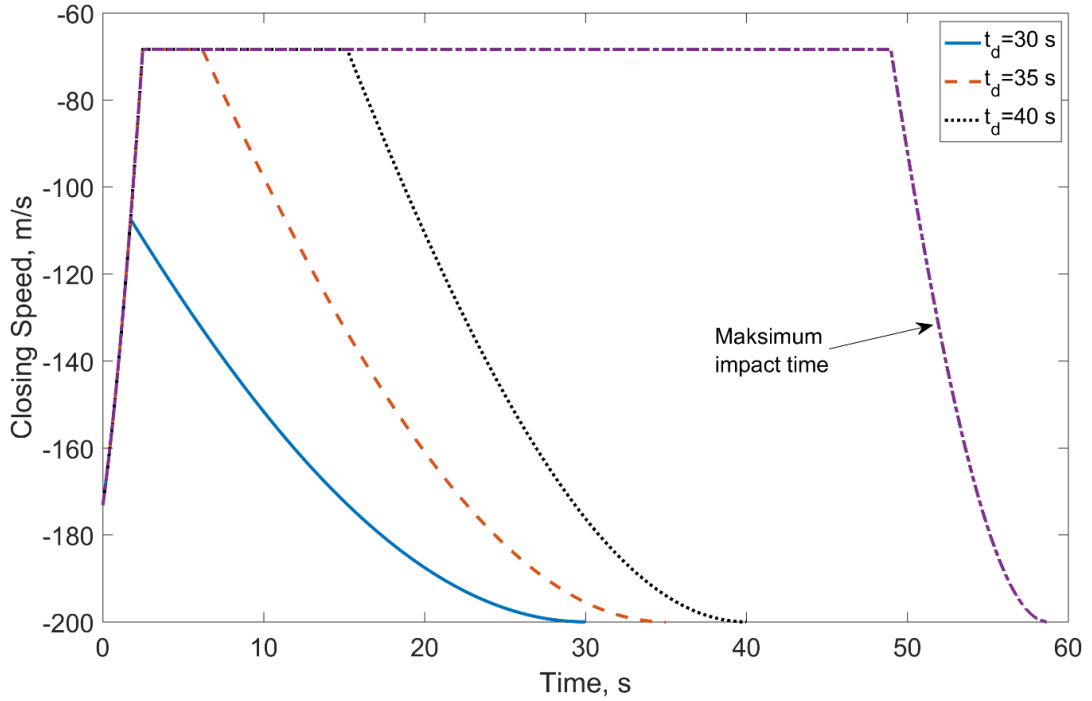

Figure 4.13 Closing speed histories produced by the constrained impact time control.

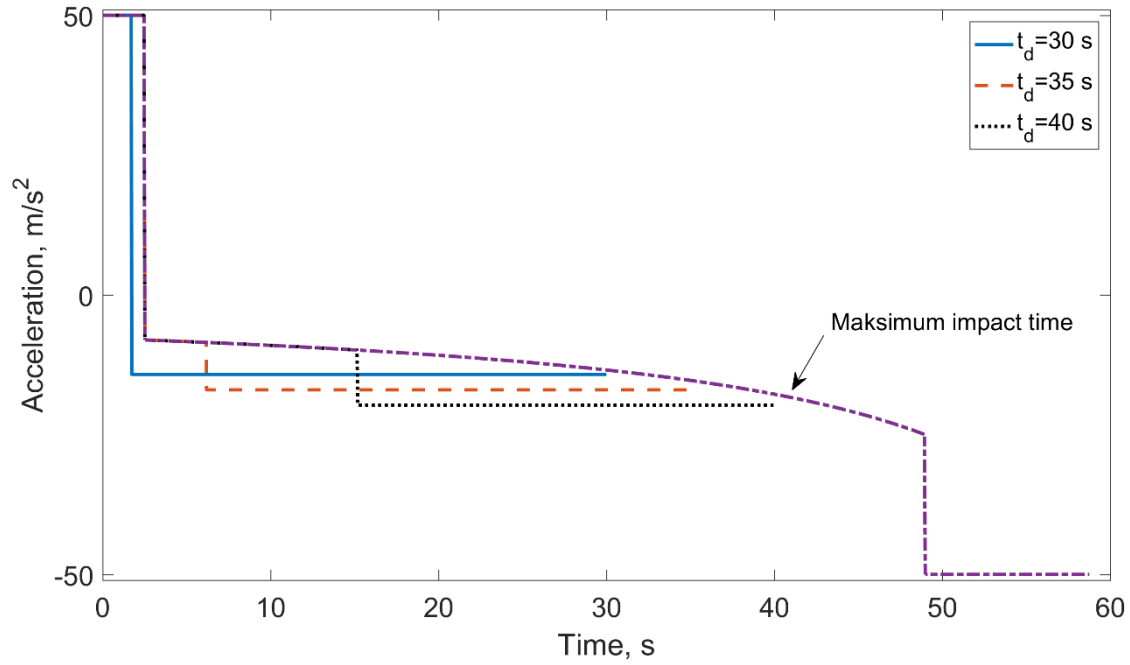

Figure 4.14 Acceleration histories produced by the constrained impact time control.

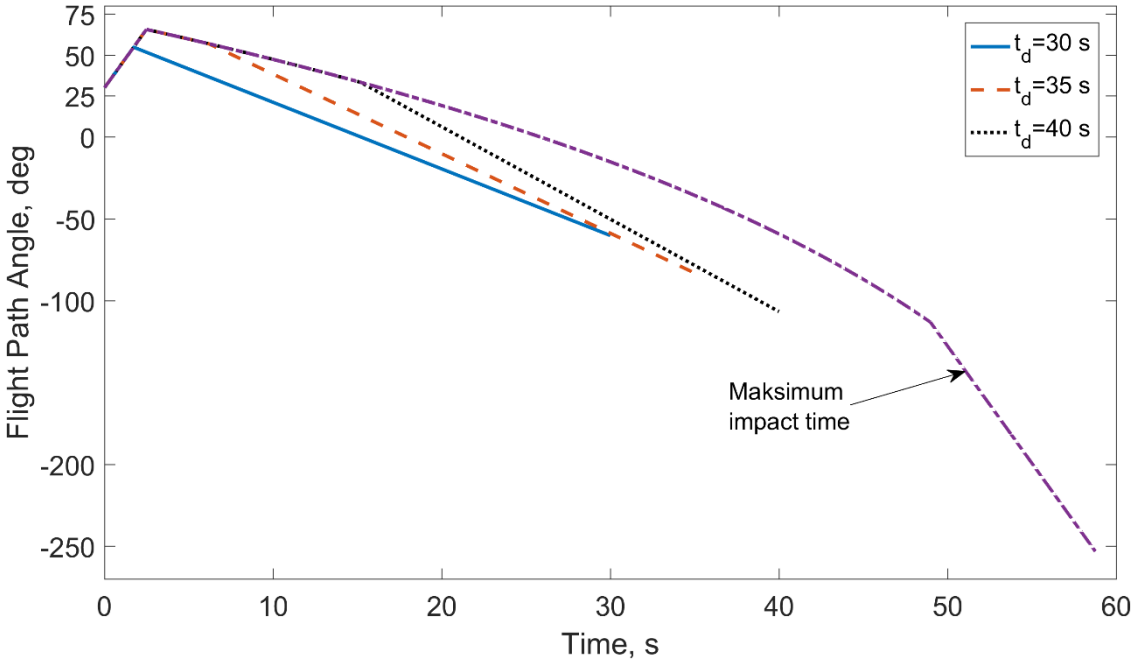

Figure 4.15 Flight path angle histories produced by the constrained impact time control.

For comparison purposes, the look angle shaping expressed in Section 4.1.1 and Section 4.2.2. are run with the same initial conditions of the previous simulation study. They are named as Method I and Method II, respectively. Here, the impact time is demanded to be 26 s. So, Method II will not increase the look angle, which falls into Case II.1. Otherwise, a comparison

would not be possible. Moreover, results of $t_{\min}$ and $t_{f,c}$ are also shown in order to provide a basic understanding. Figure 4.16 shows the trajectories, where they have not much difference unless it is the trajectory of the minimum impact time. The look angle histories shows the difference of the methods clearly. Regarding Eq. (4.61), Method II decreases the look angle in 0.2 seconds and then switches to PN. Unlike Method II, Method I decreases the look angle to zero directly and then keeps it constant until intercept as it can be observed in Figure 4.17. As expressed in Section 4.2.1, $t_{f,c}$ results in a linearly decreasing look angle profile. In correlation with the look angle, the acceleration histories are displayed in Figure 4.18. As seen, Method I does not demand the acceleration to be at its limit and commands zero acceleration for the second phase of the engagement. Meanwhile, Method II requires constant acceleration till the end. The costs $\left(\int a^2 dt\right)$ are 174.7 m^2/s^3 and 201.2 m^2/s^3, respectively. As it could be guessed, Method I has a better energy cost with respect to Method II. It is also shown that $t_{f,c}$ demands constant acceleration until capture as mentioned and $t_{\min}$ composes of maximum effort and no effort afterwards.

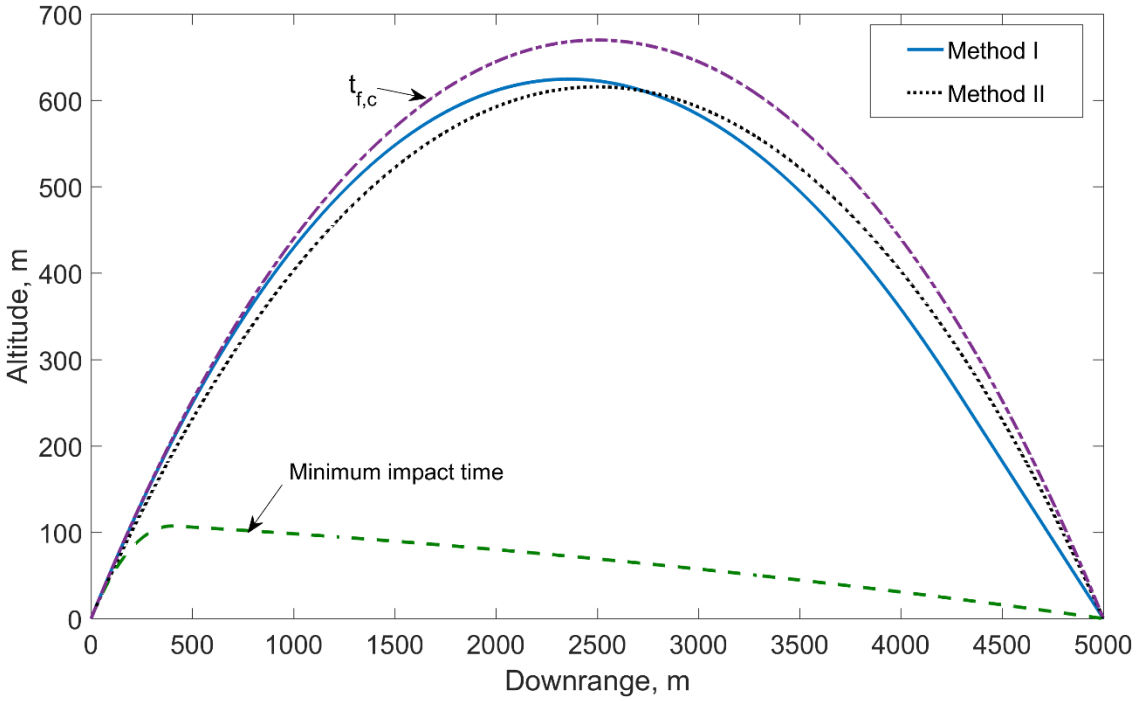

Figure 4.16 Trajectory histories of the comparison study between the first cases.

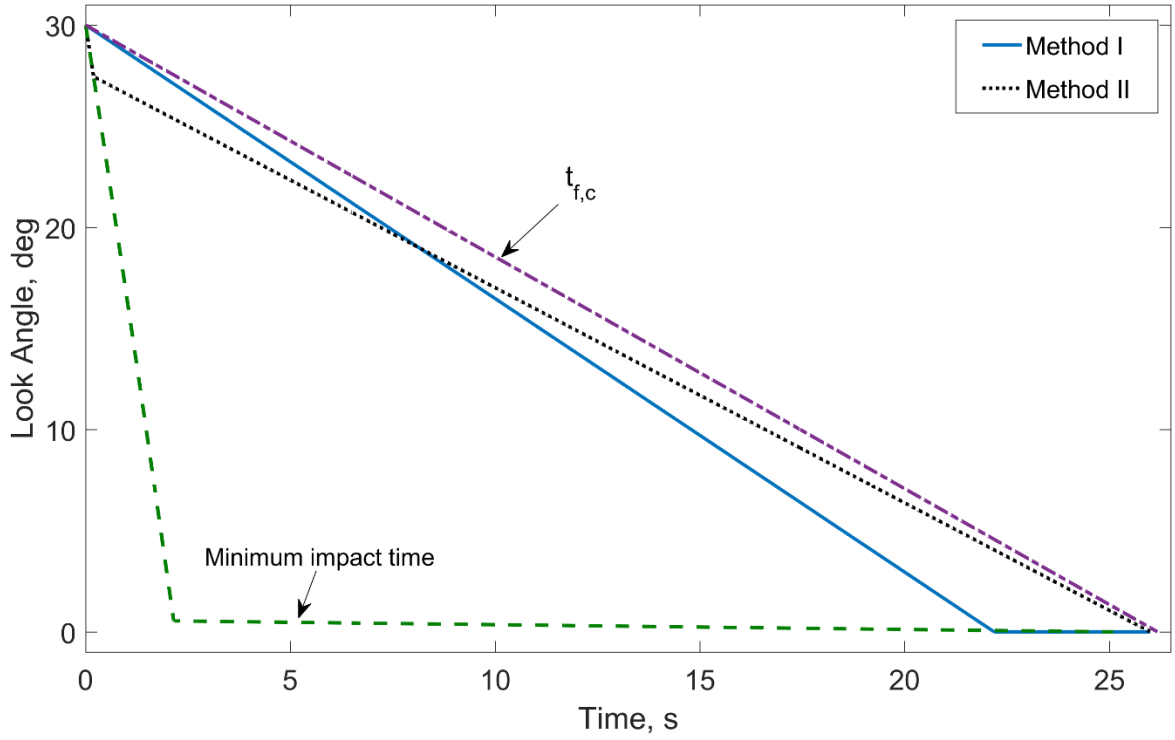

Figure 4.17 Look angle histories of the comparison study between the first cases.

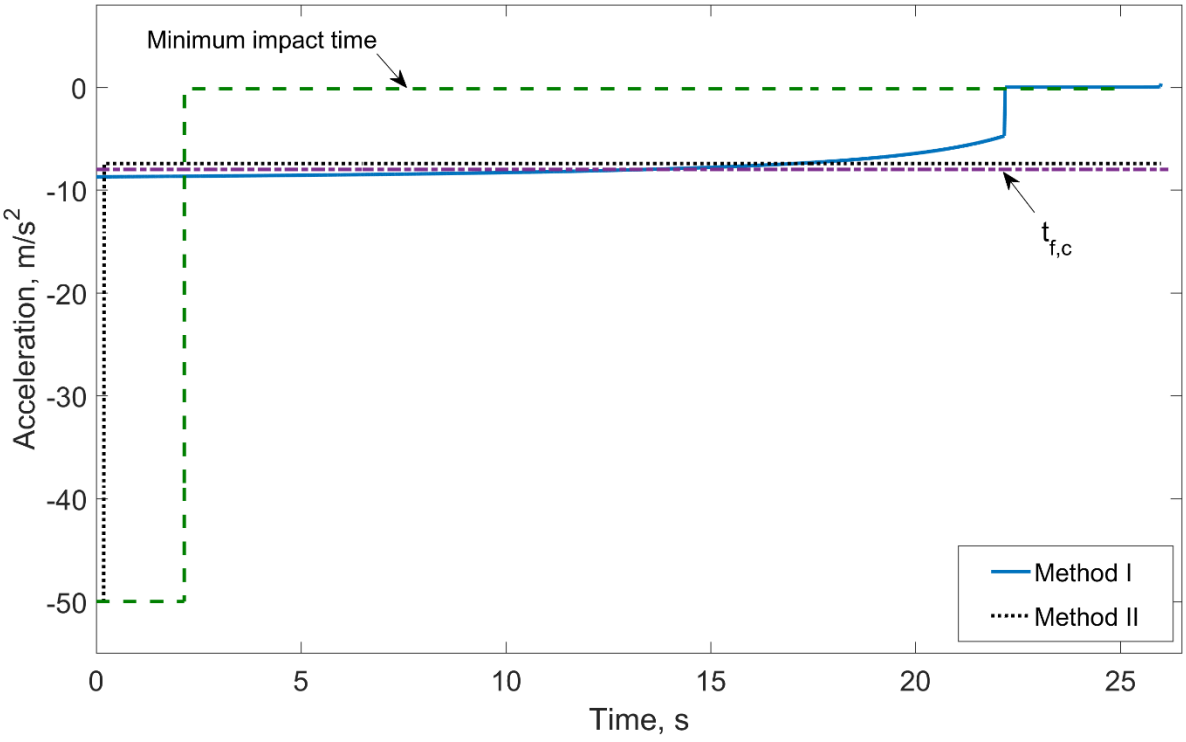

Figure 4.18 Acceleration histories of the comparison study between the first cases.

5 POLYNOMIAL LOOK ANGLE SHAPING FOR IMPACT TIME CONTROL

In the previous chapter, impact time control was accomplished via a switched structure of the look angle. Rather than such structure, during a typical trajectory shaping guidance process, the look angle firstly grows in magnitude and then it goes back, becoming identically zero at the end of the engagement [46]. Hence, a non-switching formulation must be applicable. As exemplified for the range shaping in Chapter 3 and with the experience gained in the previous chapter, a continuous function could be considered for the impact time problem over look angle shaping. Thus, in this chapter the look angle is formulated for the nonlinear kinematics, using a shaping function that is an n^{th} order time dependent polynomial. The suggested formulation leads to a guidance command, that depends on two coefficients; one of them is responsible for zero miss distance and the other is for shaping the trajectory to satisfy the desired impact time. However, it should be kept in mind that the analytical solution of Eq. (2.8) under such a look angle function is not available. Therefore, after the guidance command is derived for the nonlinear kinematics, the linearized kinematics is used to present an analytical solution of the guidance gains. Next, the look angle and the acceleration characteristics along with the impact time interval are investigated. Later, the Newton-Raphson method is applied to find the guidance gain for the nonlinear domain, where the initial guess is the linear domain solution. Several examples are provided to show the efficiency of the suggested guidance law. First, very high impact time results are presented with the required Newton-Raphson iteration. Next, the efficiency of using the linear domain guidance gain as an initial guess is discussed. Last, a comparison study is held with the energy optimal and sliding mode control based impact time control methods. Last, the optimality and the robustness issues are addressed.

5.1 Determination of the Guidance Command

The guidance design is based on the shape of the look angle that is defined as a time dependent polynomial:

$$\varepsilon = \kappa_n t^n + \kappa_{n-1} t^{n-1} + ... + \kappa_2 t^2 + \kappa_1 t + \kappa_0 \tag{5.1}$$

which has the same structure of the range as described in Eq. (3.1). Here, *n* is the order of the look angle polynomial and κ_i, where *i* = 1…*n*, are the coefficients of the polynomial. It has already been shown in Chapter 4, when *n* is one, then the linear look angle shaping provides only one impact time value, which was defined as the critical impact time. Thus, the minimum value of *n* must be two. The primary boundary conditions of Eq. (5.1) are

$$\varepsilon(t=0) = \varepsilon_0, \;\; \varepsilon(t=t_f) = 0 \tag{5.2}$$

These boundary conditions along with the range requirements must be fulfilled for a satisfactory engagement. However, Eq. (5.2) does not yet have any relation with the boundary conditions of the range, which are

$$r(t=0) = R_0, \quad r(t=t_f) = 0 \tag{5.3}$$

The boundary conditions defined in Eq. (5.2) only provide the following relations:

$$\begin{aligned} &\kappa_0 = \varepsilon_0 \\ &\kappa_n {t_f}^n + \kappa_{n-1} {t_f}^{n-1} + ... + \kappa_2 {t_f}^2 + \kappa_1 t_f + \kappa_0 = 0 \end{aligned} \tag{5.4}$$

It is apparent that the number of the boundary conditions have to be increased with respect to *n.* In the range shaping, the guidance command was designed to force $\dot{r}_f$ and its higher order derivatives to zero, which could also be imitated for the look angle shaping. Motivated by this approach, the final look angle rate could be demanded to be zero. Hence, if *n* is more than two, then the remaining conditions may be obtained from the higher derivatives of the look angle rate. In the end, the following equation for the look angle shaping is achieved:

$$\begin{bmatrix} \dot{\varepsilon} \\ \ddot{\varepsilon} \\ \dddot{\varepsilon} \\ . \\ . \\ \dot{\varepsilon}^{(n-2)} \end{bmatrix}_{t_f} = \begin{bmatrix} n\kappa_n {t_f}^{n-1} + (n-1)\kappa_{n-1} {t_f}^{n-2} + ... + \kappa_3 {t_f}^3 + \kappa_2 {t_f}^2 + \kappa_1 \\ n(n-1)\kappa_n {t_f}^{n-3} + (n-2)(n-1)\kappa_{n-1} {t_f}^{n-4} + ... + 3\kappa_3 {t_f}^2 + 2\kappa_2 t_f \\ n(n-1)(n-2)\kappa_n {t_f}^{n-3} + (n-3)(n-2)(n-1)\kappa_{n-1} {t_f}^{n-4} + ... + 6\kappa_3 t_f \\ . \\ . \\ n(n-1)(n-2)(n-3).....2\kappa_n t_f \end{bmatrix} = \bar{0} \quad (5.5)$$

If Eq. (5.5) was solved and the coefficients of Eq. (5.1) were already available, then the guidance command with the help of Eq. (2.9) and using the first time derivative of Eq. (5.1) would be:

$$\dot{\gamma} = \kappa_n t^{n-1} + (n-1)\kappa_{n-1} t^{n-2} + ... + 2\kappa_2 t + \kappa_1 + \dot{\lambda} \quad (5.6)$$

When Eq. (5.6) is roughly analyzed, it is seen that the guidance command is not singular in contrast to the guidance law in Chapter 3. However, it is not possible to provide a simple solution for the coefficients κ_i, which was the opposite for the range shaping. This result is not surprising as it was already expressed in Chapter 3 that not only the state selection, but also the formulation of the shaping function is also important.

5.2 Guidance Laws for the 2nd, 3rd and 4th Order Polynomials

After presenting the general form of the guidance command, now it is time to provide the coefficients and analyze the proposed method. It has already been mentioned that the minimum order of Eq. (5.1) must be two. Thus, the first solution is provided for the quadratic polynomial, where the quadratic look angle can be written as

$$\varepsilon_2 = \kappa_2 t^2 + \kappa_1 t + \kappa_0 \quad (5.7)$$

where κ_0 was already given in Eq. (5.4). Using the boundary conditions related to the initial and the final conditions of the look angle, the following relation is obtained for the second coefficient

$$\kappa_1 = -\left(\kappa_2 t_f + \frac{\varepsilon_0}{t_f} \right) \quad (5.8)$$

yielding the look angle function:

$$\varepsilon_2 = \kappa_2 t^2 - \left(\kappa_2 t_f + \frac{\varepsilon_0}{t_f} \right) t + \varepsilon_0 \tag{5.9}$$

where κ_2 is to be determined later to drive the range to zero at the desired impact time. Then, the look angle rate for the quadratic polynomial becomes:

$$\dot{\varepsilon}_2 = 2\kappa_2 t - \left(\kappa_2 t_f + \frac{\varepsilon_0}{t_f} \right) \tag{5.10}$$

Similarly, the cubic look angle would be as

$$\varepsilon_3 = \kappa_3 t^3 + \kappa_2 t^2 + \kappa_1 t + \varepsilon_0 \tag{5.11}$$

In addition to zero look angle at the final time, the additional boundary condition is defined as $\dot{\varepsilon}_f = 0$. If the coefficients are written in terms of κ_3

$$\begin{aligned} &f_1: \ \ \varepsilon_f = \kappa_3 {t_f}^3 + \kappa_2 {t_f}^2 + \kappa_1 t_f + \varepsilon_0 = 0 \\ &f_2: \ \dot{\varepsilon}_f = 3\kappa_3 {t_f}^2 + 2\kappa_2 t_f + \kappa_1 = 0 \Rightarrow \kappa_1 = -3\kappa_3 {t_f}^2 - 2\kappa_2 t_f \\ &f_3: \left(t_f f_2 - f_1 \right): 2\kappa_3 {t_f}^3 + \kappa_2 {t_f}^2 - \varepsilon_0 = 0 \Rightarrow \kappa_2 = -2\kappa_3 t_f + \frac{\varepsilon_0}{{t_f}^2} \end{aligned} \tag{5.12}$$

When κ_2 is replaced in κ_1, then the cubic look angle becomes:

$$\varepsilon_3 = \kappa_3 t^3 - \left(2\kappa_3 t_f - \frac{\varepsilon_0}{t_f^2} \right) t^2 + \left(\kappa_3 t_f^2 - \frac{2\varepsilon_0}{t_f} \right) t + \varepsilon_0 \tag{5.13}$$

Now κ_3 is the constant to be determined later to derive the range to zero at the desired impact time. The rate of the cubic look angle is then as follows:

$$\dot{\varepsilon}_3 = 3\kappa_3 t^2 - \left(4\kappa_3 t_f - \frac{2\varepsilon_0}{t_f^2} \right) t + \left(\kappa_3 t_f^2 - \frac{2\varepsilon_0}{t_f} \right) \tag{5.14}$$

Lastly, the quartic look angle would be as

$$\varepsilon_4 = \kappa_4 t^4 + \kappa_3 t^3 + \kappa_2 t^2 + \kappa_1 t + \varepsilon_0 \tag{5.15}$$

The quartic order look angle equation could be rewritten with the boundary conditions $\ddot{\varepsilon}_f = 0$ to $\dot{\varepsilon}_f = 0$ and $\varepsilon_f = 0$. The overall equation set to solve the coefficients is

$$\begin{aligned}
&f_1: \quad \varepsilon_f = \kappa_4 {t_f}^4 + \kappa_3 {t_f}^3 + \kappa_2 {t_f}^2 + \kappa_1 t_f + \varepsilon_0 = 0 \\
&f_2: \quad \dot{\varepsilon}_f = 4\kappa_4 {t_f}^3 + 3\kappa_3 {t_f}^2 + 2\kappa_2 t_f + \kappa_1 = 0 \\
&f_3: \quad \ddot{\varepsilon}_f = 12\kappa_4 {t_f}^2 + 6\kappa_3 t_f + 2\kappa_2 = 0 \Rightarrow \kappa_2 = -6\kappa_4 {t_f}^2 - 3\kappa_3 t_f \\
&f_4: \left(f_2 - t_f f_3\right): -8\kappa_4 {t_f}^3 - 3\kappa_3 {t_f}^2 + \kappa_1 = 0 \Rightarrow \kappa_1 = 8\kappa_4 {t_f}^3 + 3\kappa_3 {t_f}^2
\end{aligned} \tag{5.16}$$

When κ_1 and κ_2 are replaced in the first equation of (5.16), κ_3 becomes

$$\kappa_3 = -3\kappa_4 t_f - \frac{\varepsilon_0}{{t_f}^3} \tag{5.17}$$

Then, all of these coefficients are used in Eq. (5.15) and the following look angle function is obtained

$$\varepsilon_4 = \kappa_4 t^4 - \left(3\kappa_4 t_f + \frac{\varepsilon_0}{{t_f}^3}\right) t^3 + \left(3\kappa_4 {t_f}^2 - \frac{3\varepsilon_0}{{t_f}^2}\right) t^2 - \left(\kappa_4 {t_f}^3 + \frac{3\varepsilon_0}{t_f}\right) t + \varepsilon_0 \tag{5.18}$$

The corresponding look angle rate would be

$$\dot{\varepsilon}_4 = 4\kappa_4 t^3 - 3t^2 \left(3\kappa_4 t_f + \frac{\varepsilon_0}{{t_f}^3}\right) + 2t \left(3\kappa_4 {t_f}^2 - \frac{3\varepsilon_0}{{t_f}^2}\right) - \left(\kappa_4 {t_f}^3 + \frac{3\varepsilon_0}{t_f}\right) \tag{5.19}$$

It could be observed in Eq. (5.10), Eq. (5.14) and Eq. (5.19) that the look angle rate depends only on one coefficient, κ_n. The key idea of such a formulation is to have the look angle equation governed by a single unknown parameter by defining the coefficients recursively. So, the range will be driven to zero with this parameter. This outcome is valuable since the sum of the look angle rate and the LOS rate define the guidance command as presented in Eq. (2.9).

5.3 Closed Loop Guidance Formulation

The guidance formulations given in Eq. (5.10), Eq. (5.14) and Eq. (5.19) process only the current time and the initial conditions. Nonetheless, it is also possible to include the remaining time in the guidance command and the closed loop form of the guidance command can be constructed. This alternative form can be obtained by considering the fact that each time instant can actually be regarded as the initial time. Additionally the final time is also updated in accordance with Eq. (3.35) and Eq. (3.36). These modifications yield Eq. (5.10) as

$$\dot{\varepsilon}_2 = -\kappa_2 \left(t_f - t \right) - \frac{\varepsilon}{t_f - t} \tag{5.20}$$

for the quadratic look angle rate. Furthermore, Eq. (5.14) becomes

$$\dot{\varepsilon}_3 = \kappa_3 \left(t_f - t \right)^2 - \frac{2\varepsilon}{t_f - t} \tag{5.21}$$

for the cubic look angle rate. Last, Eq. (5.19) turns into

$$\dot{\varepsilon}_4 = -\kappa_4 \left(t_f - t \right)^3 - \frac{3\varepsilon}{\left(t_f - t \right)} \tag{5.22}$$

Motivated by the systematic structures of the look angle rates given in Eq. (5.20) - (5.22), the general form of the look angle rate can be expressed for the n^{th} order polynomial as

$$\dot{\varepsilon} = \left(-1 \right)^{(n-1)} \kappa_n \left(t_f - t \right)^{(n-1)} - \frac{(n-1)}{t_f - t} \varepsilon \tag{5.23}$$

The resulting look angle equation can then be shown to be as follows

$$\varepsilon = \left(t - t_f \right)^{n-1} \left(\frac{\varepsilon_0}{\left(-1 \right)^{(n-1)} t_f{}^{(n-1)}} + \kappa_n t \right) \tag{5.24}$$

which satisfies the same boundary conditions provided in Eq. (5.2). Based on Eq. (5.23), the guidance command can be identified as :

$$\dot{\gamma} = (-1)^{(n-1)} \kappa_n \left(t_f - t\right)^{(n-1)} - \frac{(n-1)}{t_f - t} \varepsilon + \dot{\lambda} \tag{5.25}$$

Actually, this guidance command is partially closed loop since the guidance gain is constant and does not have any regulation for the impact time error. On the other hand, it may be appreciated that Eq. (5.25) is in a compact form.

The next step is to find the guidance gain satisfying the zero range at intercept. Therefore, the following equation needs to be considered again

$$\dot{r} = -V \int \cos \varepsilon \left(t, \kappa_n\right) dt \tag{5.26}$$

where the look angle is expressed as a function of κ_n and *t*. When Eq. (5.26) is integrated from $t = 0$ to $t = t_f$ with the zero final range requirement, then the corresponding equation to find κ_n is obtained:

$$R_0 = V \int_0^{t_f} \cos \varepsilon \left(t, \kappa_n\right) dt \tag{5.27}$$

However, finding κ_n is not an easy task. The cause of this difficulty is that the right-hand side of Eq. (5.27) is not analytically integrable for such kind of functions. For example, when the look angle behaves as a quadratic polynomial, i.e. *n* = 2, this integral equation can be converted into an approximate transcendental equation through the use of Fresnel integrals (see Appendix E), which can then be solved via a numerical root finding algorithm such as the Newton-Raphson method. As for the higher polynomial orders, the way to calculate the gain is repeatedly evaluating the integral within a numerical iteration scheme. This approach would naturally be applicable to the former case as well. However, such a pure numerical routine might not be preferred. Moreover, as will be demonstrated later, multiple solutions for κ_n may exist depending on the engagement parameters, especially when the desired final time is much higher than R_0 / V. In such cases, some of the solutions may lead to very high look angles; so, the feasibility of each solution should be assessed before proceeding. Currently, the engagement can be analyzed in the linear domain, in case more information about the engagement and the guidance gains are available.

5.4 Linear Domain Analysis for Impact Time Control Formulation

First, the engagement geometry is linearized as illustrated in Figure 5.1 in order to obtain the guidance gain in Eq. (5.25) and to analyze the linear domain implications of having such polynomial variations. The linearization of the missile and the stationary target can be accomplished with the new quantities. *y* is the relative separation between the missile and the target perpendicular to the fixed reference. The range is $r = V\left(t_f - t\right)$, where t_f is constant. The linearized miss distance is taken to be the relative separation between the missile and the target, *y*, at the end of the flight as $\text{miss} = y\left(t_f\right)$. It is to be noted that the linearized miss is not computed from the distance formula, it is only an approximation to the actual miss [2].

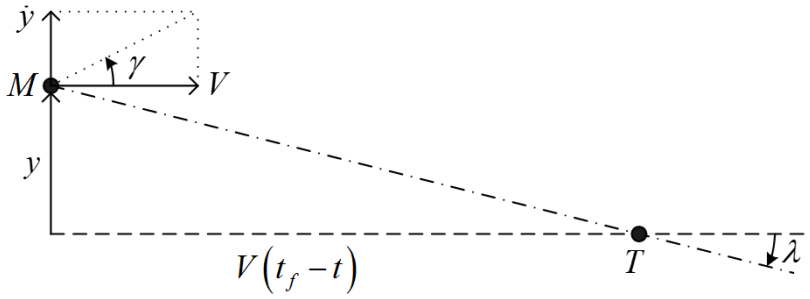

Figure 5.1 Linear engagement geometry.

Referring to this picture, the path and the LOS angles are respectively defined as

$$\gamma = \frac{\dot{y}}{V} \tag{5.28}$$

and

$$\lambda = -\frac{y}{V\left(t_f - t\right)} \tag{5.29}$$

by small angle approximation [2]. Accordingly, the LOS rate can be written as

$$\dot{\lambda} = -\frac{\dot{y}}{V(t_f - t)} - \frac{y}{V(t_f - t)^2} \tag{5.30}$$

This equation leads to

$$\dot{\lambda} = -\frac{\varepsilon}{t_f - t} \tag{5.31}$$

By using Eq. (5.29) and Eq. (5.28) via the geometric relation given in Eq. (2.4). Rewriting Eq. (2.4) with the related linear equations given in Eq. (5.28) and Eq. (5.29), the differential equation that follows is

$$\dot{y} + \frac{y}{t_f - t} = V\varepsilon \tag{5.32}$$

The time derivative of Eq. (5.32) and Eq. (5.31) are used to obtain $\ddot{y}$:

$$\begin{aligned} \ddot{y} &= V\dot{\varepsilon} - \dot{y}\left(t_f - t\right)^{-1} - y\left(t_f - t\right)^{-2} = V\dot{\varepsilon} + V\dot{\lambda} \\ \ddot{y} &= V\dot{\varepsilon} - V\frac{\varepsilon}{t_f - t} \end{aligned} \tag{5.33}$$

When Eq. (5.24) and Eq. (5.23) are used for the look angle and the look angle rate equations in Eq. (5.33), $\ddot{y}$ becomes as

$$\ddot{y} = V\left(-1\right)^{n-2}\left(t_f - t\right)^{n-2}\left(\kappa_n\left(nt - t_f\right) + \frac{n\varepsilon_0}{\left(-1\right)^{(n-1)}\, {t_f}^{n-1}}\right) \tag{5.34}$$

and $\dot{y}$ is as follows

$$\dot{y} = V\left(t_f - t\right)^{n-1}\left(\frac{n\varepsilon_0}{\left(n-1\right){t_f}^{n-1}} - \left(-1\right)^n t\kappa_n\right) \tag{5.35}$$

Before providing the general forms, three simple cases are presented to give a brief information about $\ddot{y}$. Eq. (5.34), when combined with Eq. (5.9) and Eq. (5.13) lead to the following acceleration solutions for the quadratic, the cubic and the quartic solutions

$$\ddot{y}_2 = V\left\{\kappa_2\left(3t - t_f\right) - \frac{2\varepsilon_0}{t_f}\right\} \tag{5.36}$$

$$\ddot{y}_3 = -V\left(t_f - t\right)\left\{\kappa_3\left(4t - t_f\right) + \frac{3\varepsilon_0}{t_f^2}\right\} \tag{5.37}$$

$$\ddot{y}_4 = V\left(t_f - t\right)^2\left\{\kappa_4\left(5t - t_f\right) - \frac{4\varepsilon_0}{t_f^3}\right\} \tag{5.38}$$

It is seen that each acceleration function turns out to be one order less than the corresponding look angle polynomial. Additionally, it is obvious that the final accelerations of the cubic and the quartic functions will be zero at intercept.

5.4.1 Time Domain Solutions of the Engagement States

The overall structure of the linearized engagement including the guidance law is illustrated in Figure 5.2.

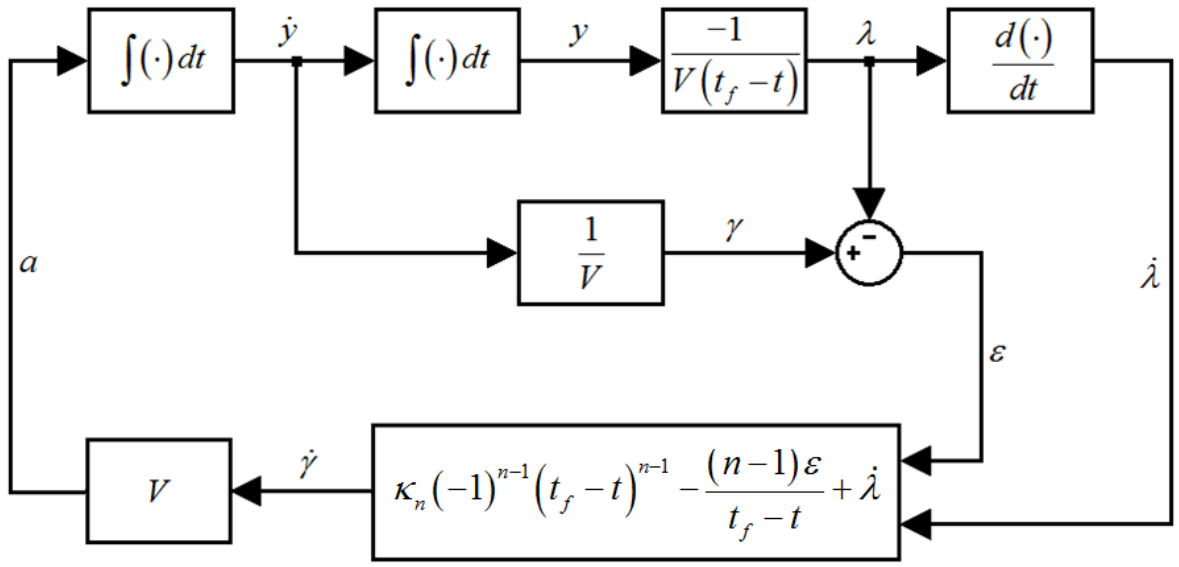

Figure 5.2 Linear guidance loop.

First, the guidance command defined for the nonlinear kinematics needs to be linearized. Using Eq. (2.9) and the LOS rate given in Eq. (5.31), the general form of the nonlinear guidance law is rewritten. Eq. (5.25) is seen to be equivalent to the following time-varying biased PN law in the linear domain, which is

$$\dot{\gamma} = N\dot{\lambda} + \kappa(-1)^{N-1}\left(t_f - t\right)^{N-1} \tag{5.39}$$

where $N = n$ is the PN gain. Thus, N in Eq. (5.39) and n in Eq. (5.25) can be regarded as the gains to derive the miss distance to zero, whereas $\kappa = \kappa_n$ is to be solved for shaping the trajectory for impact time control. For that purpose, Eq. (5.32) can be converted into the following differential equation using Eq. (5.24) to obtain the general form solution of the displacement:

$$\dot{y} + \frac{y}{t_f - t} = V\left(\frac{\varepsilon_0}{\left(-t_f\right)^{(n-1)}} + \kappa_n t\right)\left(t - t_f\right)^{(n-1)} \tag{5.40}$$

$\dot{y}$ was already given in Eq. (5.35). Then, the reorganizing of this equation yields the displacement:

$$y(t) = C\left(t - t_f\right) + V\left(\frac{\varepsilon_0}{(n-1)(-t_f)^{(n-1)}} + \kappa_n \frac{t_f + (n-1)t}{n(n-1)}\right)\left(t - t_f\right)^n \tag{5.41}$$

where C includes the initial displacement, y_0, as

$$C = -\left(\frac{y_0}{t_f} + \frac{V\varepsilon_0}{n-1} + (-1)^{(n-1)}\kappa_n \frac{V{t_f}^n}{n(n-1)}\right) \tag{5.42}$$

So far, the displacement equation for the general order polynomial has been identified. Fortunately, the linearized framework also makes the other states and the state derivatives available. One of them is the LOS rate:

$$\dot{\lambda} = \left(t - t_f\right)^{n-2}\left(\frac{\varepsilon_0}{(-1)^{(n-1)}\,{t_f}^{(n-1)}} + \kappa_n t\right) \tag{5.43}$$

which is found via Eq. (5.24) and Eq. (5.31). Afterward, the LOS angle can be obtained from Eq. (5.41) as described in Eq. (5.29)

$$\lambda(t)=\frac{C}{V}+\left(\frac{\varepsilon_0}{(n-1)\left(-t_f\right)^{(n-1)}}+\kappa_n\frac{t_f+(n-1)t}{n(n-1)}\right)\left(t-t_f\right)^{n-1} \tag{5.44}$$

Since the look angle and the LOS angle are available, it is easy to have the flight path angle via the geometric relation given in Eq. (2.4):

$$\gamma=\left(t-t_f\right)^{(n-1)}\left\{\kappa_n t+(-1)^{(1-n)}\varepsilon_0 {t_f}^{(1-n)}-\left(\frac{\varepsilon_0\left(-t_f\right)^{(1-n)}}{(n-1)}+\frac{\kappa_n\left\{t_f+t(n-1)\right\}}{n(n-1)}\right)\right\}-\frac{C}{V} \tag{5.45}$$

To give an example about the structure of the flight path angle and the LOS angle, they are written for the cubic polynomial. The flight path angle is:

$$\gamma(t)=t^3\frac{4\kappa_3}{3}-t^2\frac{\left(5\kappa_3{t_f}^3-3\varepsilon_0\right)}{2{t_f}^2}+t\frac{\left(\kappa_3{t_f}^3-3\varepsilon_0\right)}{t_f}+\frac{\varepsilon_0 t_f-y_0/V}{t_f} \tag{5.46}$$

and the LOS angle becomes

$$\lambda(t)=t^3\frac{\kappa_3}{3}-t^2\left(\frac{\kappa_3{t_f}^3-2\varepsilon_0}{2{t_f}^2}\right)-t\frac{\varepsilon_0}{t_f}-\frac{y_0}{Vt_f} \tag{5.47}$$

all of which are also third order polynomials. It needs to be reminded that these equations are available in the linear domain; therefore, there will be difference in the nonlinear domain when the system is away from the linear conditions. However, it is still beneficial to have the time domain solutions of the engagement.

5.4.2 Guidance Gain Determination

So far, the time domain solution of the engagement has been presented. However, in order to control the impact time, the length of the trajectory given in Eq. (2.15) is needed. It is rewritten as

$$S=\int_0^{x_f}\sqrt{1+\left(\frac{dy}{dx}\right)^2}\,dx=Vt_f \tag{5.48}$$

where x_f is the final downrange. Since Eq. (5.48) will not be analytically solvable, Taylor expansion is applied [24],

$$S \approx \int_0^{x_f} \left(1 + \frac{1}{2} \left(\frac{dy}{dx} \right)^2 \right) dx \tag{5.49}$$

In order to obtain the time domain solution of the length of the trajectory, the following assumption, which states the time and the downrange are linearly correlated, is made:

$$\frac{t}{t_f} \approx \frac{x}{x_f} \Rightarrow t \approx \frac{t_f}{x_f} x \Rightarrow dx \approx dt \frac{x_f}{t_f} \tag{5.50}$$

According to this assumption, the horizontal distance travelled in unit time will be more than the one in reality, when the flight path angle is not small. The solution could be set up by using Eq. (5.41) and meanwhile modifying Eq. (5.49) with respect to Eq. (5.50). Afterward, the approximate length of the trajectory would be obtained. Unfortunately, a general form solution is not directly available. Instead, the solution is first provided for n = 3, encouraged by the optimality of the PN guidance (PN is energy optimal in the linear domain for N = 3 [2]). In this case, the displacement is:

$$y(t) = \left(t_f - t \right) \left(-t^3 V \frac{\kappa_3}{3} + t^2 V \frac{\kappa_3 {t_f}^3 - \varepsilon_0}{2 {t_f}^2} + tV \frac{\varepsilon_0}{t_f} + \frac{y_0}{t_f} \right) \tag{5.51}$$

Using Eq. (5.51) in Eq. (5.49) along with the assumption given in Eq. (5.50) and evaluating the corresponding integral, the equation for determining the guidance gain κ_3 turns out to be

$$\frac{t_f^6}{21} \kappa_3^2 + \frac{\varepsilon_0 t_f^3}{3} \kappa_3^2 + \frac{10 x_f}{V t_f} \left(\frac{x_f}{V t_f} + \frac{y_0^2}{2 x_f} - 1 \right) + \varepsilon_0^2 = 0 \tag{5.52}$$

Eq. (5.52) provides two solutions satisfying the impact at the specified final time in the following form:

$$\kappa_3 = -\frac{7 \varepsilon_0}{2 {t_f}^3} \mp \sqrt{35} \frac{\sqrt{24 V t_f x_f - V^2 \varepsilon_0^2 {t_f}^2 - 24 {x_f}^2 - 12 y_0^2}}{2 V {t_f}^4} \tag{5.53}$$

It is to be noted that the missile will follow different trajectories with either of these two guidance gains. Furthermore, the following relation must be satisfied in order to have real valued guidance gains:

$$Vt_f x_f \geq \frac{V^2 \varepsilon_0^2 t_f{}^2}{24} + x_f{}^2 + 0.5 y_0^2 \tag{5.54}$$

which holds the positivity in the square root function of Eq. (5.53).

The last issue of the guidance gain determination is to find the guidance gain for any *n*. For that purpose, the method in Chapter 3 will be applied. To obtain the guidance gains for the chosen *n*, Eq. (5.41) along with Eq. (5.49) with respect to Eq. (5.50) must be solved. First, the solution for the even values of *n* are given:

$$\begin{aligned}
\kappa_2 &= \pm 5 \frac{6\left\{\left(\sqrt{\frac{2Vt_f x_f}{30} - \frac{2x_f{}^2}{30} - \frac{y_0{}^2}{30} - \frac{V^2 \varepsilon_0{}^2 t_f{}^2}{240}}\right) \pm V\varepsilon_0 t_f\right\}}{Vt_f{}^3} \\
\kappa_4 &= \pm 9 \frac{28\left\{\left(\sqrt{\frac{2Vt_f x_f}{252} - \frac{2x_f{}^2}{252} - \frac{y_0{}^2}{252} - \frac{V^2 \varepsilon_0{}^2 t_f{}^2}{4032}}\right) \pm V\varepsilon_0 t_f\right\}}{Vt_f{}^5} \\
&\vdots
\end{aligned} \tag{5.55}$$

and afterwards, the guidance gains for the odd values of *n* are presented:

$$\begin{aligned}
\kappa_3 &= \pm 7 \frac{15\left\{\left(\sqrt{\frac{2Vt_f x_f}{105} - \frac{2x_f{}^2}{105} - \frac{y_0^2}{105} - \frac{V^2 \varepsilon_0{}^2 t_f{}^2}{1260}}\right) \mp V\varepsilon_0 t_f\right\}}{Vt_f{}^4} \\
\kappa_5 &= \pm 11 \frac{45\left\{\left(\sqrt{\frac{2Vt_f x_f}{495} - \frac{2x_f{}^2}{495} - \frac{y_0^2}{495} - \frac{V^2 \varepsilon_0{}^2 t_f{}^2}{9900}}\right) \mp V\varepsilon_0 t_f\right\}}{Vt_f{}^6} \\
&\vdots
\end{aligned} \tag{5.56}$$

When the pattern is observed, it will be seen than these equations result in the following general form guidance gain solution

$$\kappa_n = \pm(2n+1)\frac{n(2n-1)\left\{\left(\sqrt{\frac{2Vt_f x_f}{A}-\frac{2x_f{}^2}{A}-\frac{y_0^2}{A}-\frac{V^2\varepsilon_0{}^2 t_f{}^2}{B}}\right)\pm(-1)^n V\varepsilon_0 t_f\right\}}{Vt_f{}^{(n+1)}} \tag{5.57}$$

where

$$\begin{aligned} A &= n(2n+1)(2n-1) \\ B &= 4n^2(2n+1)(2n-1) \end{aligned} \tag{5.58}$$

As seen in the equations, there are two solutions which would result in upward and downward trajectories. So, the preference of the gain selection will be discussed later.

5.4.3 Optimality Analysis for the Linear Domain

Before further analysis, a brief example and a comparison is exemplified for the linearized kinematics, since the linear solutions are not in the scope in the upcoming sections. For comparison purposes, an energy optimal trajectory is considered. The energy optimal impact time control problem based on the same linearized kinematics, as detailed in the Appendix F, can be formulated. The corresponding command is as follows

$$u = -2\mu\upsilon\sin\left(\upsilon\left(t_f - t\right)\right) \tag{5.59}$$

where μ and υ are constants to be determined. It should be noted that Eq. (5.59) is actually suboptimal since it follows from Eq. (5.49), not Eq. (5.48).

A missile is located at the origin and the target is at 5 km away. The initial flight path angle is zero and the speed is 200 m/s. Impact time is set to be 30 s. The related gain of the polynomial guidance is $\kappa_3 = 2.0002\cdot10^{-4}$. The constants of the guidance command given in Eq. (5.59) are μ = 76.36 and υ = 0.1498. Figure 5.3 presents the trajectories of the two impact time control approaches, where the maximum altitudes are approximately the same. In Figure 5.4, the look angle histories are shown, where the two are also quite comparable. The guidance command histories are presented in Figure 5.5, which are obtained by Eq. (5.39) and Eq. (5.59), respectively. At the beginning of the engagement, the optimal one requires less acceleration; however, starting from t = 15 s the polynomial approach requires less acceleration than the optimal one. Finally, at the end of the engagement they both demand zero acceleration. The

magnitudes of the cost, where the cost function is $\int a^2 dt$, are 7.78. 10^3 m^2/s^3 and 7.48. 10^3 m^2/s^3, respectively. Since this results gives an intuition about the near optimality of n = 3, it will be analyzed for the nonlinear kinematics in the further sections.

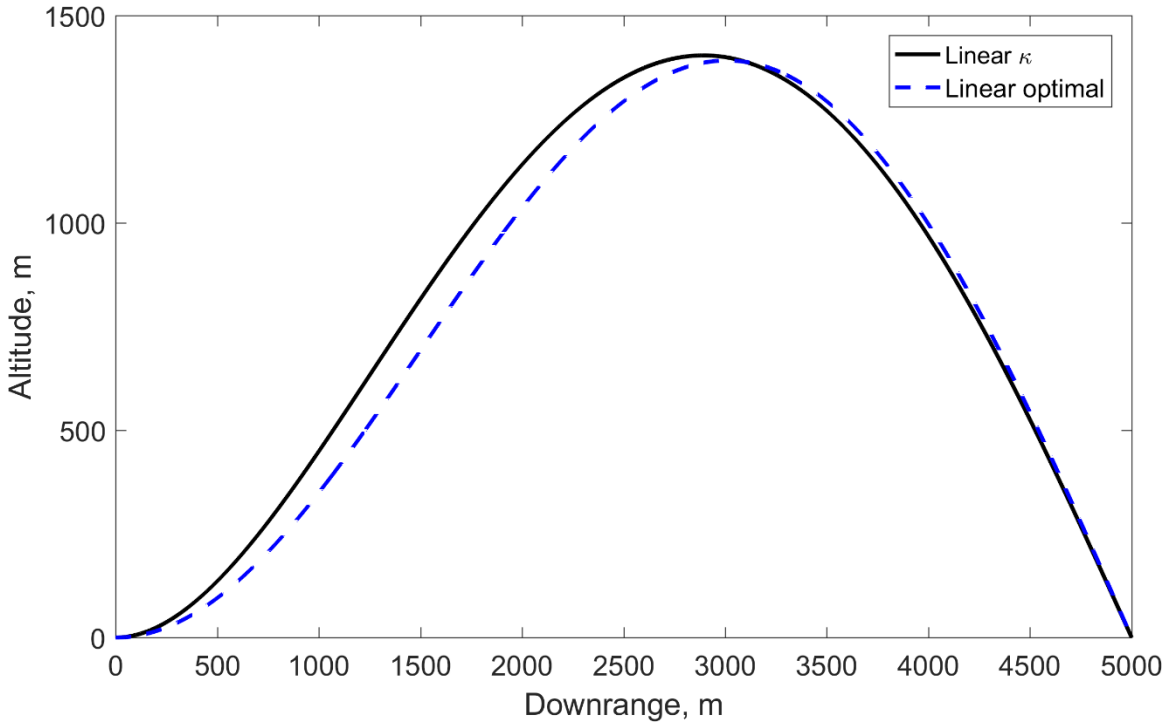

Figure 5.3 Comparison of the linear domain trajectories.

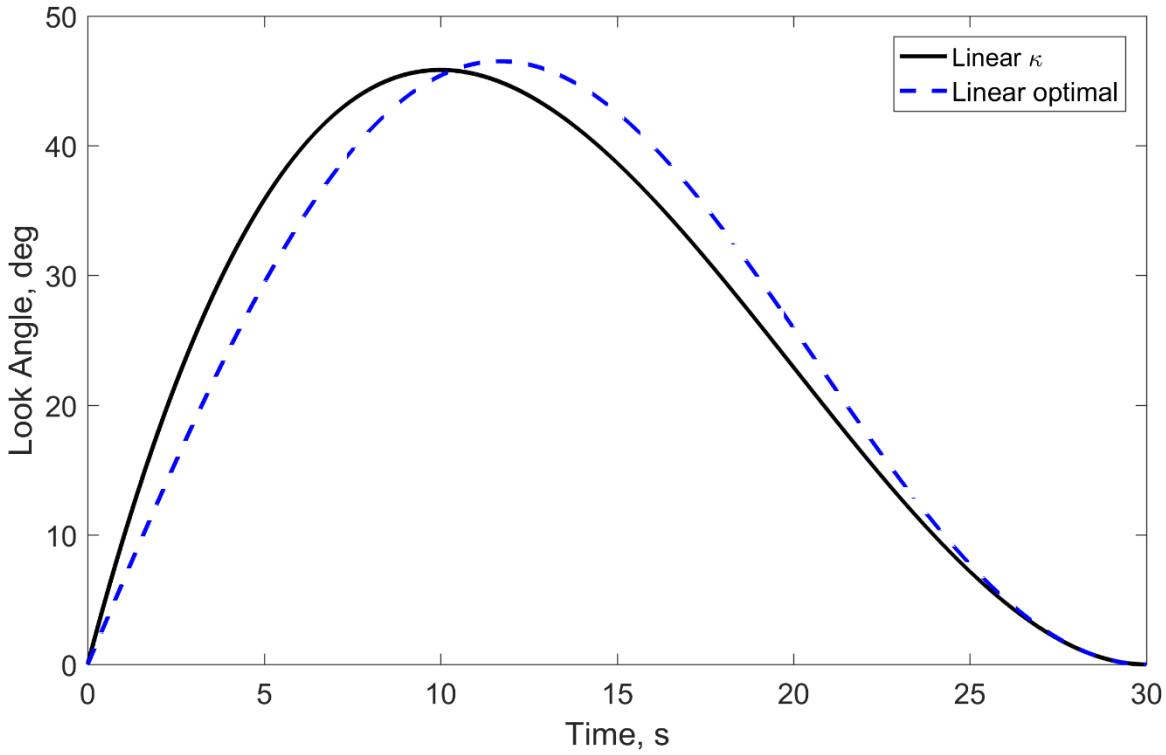

Figure 5.4 Comparison of the linear domain look angle histories.

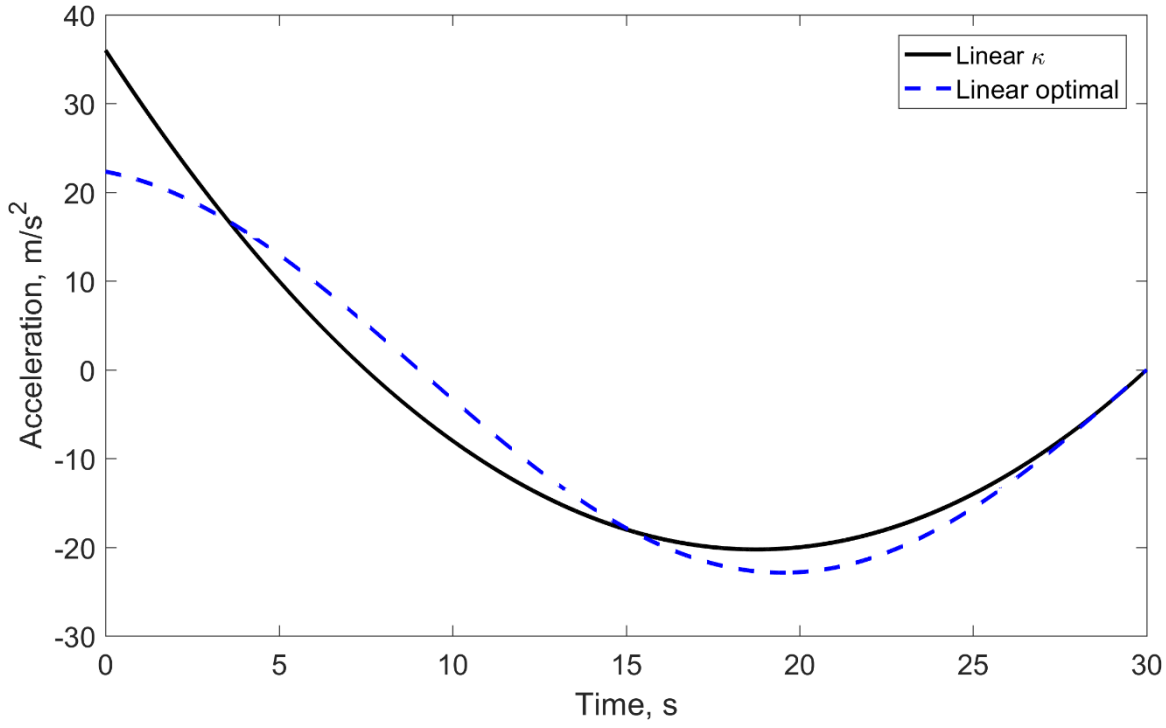

Figure 5.5 Comparison of the linear domain guidance command histories.

5.5 Characteristics of the Proposed Guidance Law

Depending on the application, there might be some physical considerations and limits. Thus, this section is reserved for analyzing the characteristics of the proposed impact time control method for the nonlinear kinematics as much as possible. The look angle is the first concern. Thereafter, the acceleration characteristics will be the second concern of the analysis. Afterwards, the final flight path angle and the impact time interval are explained.

5.5.1 Look Angle Characteristics

The proposed impact time control is designed over the look angle shaping. Thus, it would be relatively simpler to analyze the maximum look angle of the design and the look angle characteristics. As a rule of thumb, the maximum look angle could occur either at the initial time or at the local maximum point since the final look angle is zero.

First, the maximum magnitude of the look angle is assessed by equating Eq. (5.23) to zero to reveal the time instants where the look angle rate is zero:

$$\dot{\varepsilon} = \left(t - t_f\right)^{n-1}\left[\kappa_n - \frac{(n-1)}{t_f - t}\left(\frac{\varepsilon_0}{\left(-1\right)^{(n-1)} {t_f}^{(n-1)}} + \kappa_n t\right)\right] = 0 \tag{5.60}$$

As seen, there is more than one solution. One of them is represented as t^*, which is

$$t^* = \frac{\varepsilon_0\left(n-1\right) + \left(-1\right)^n \kappa_n {t_f}^n}{\left(-1\right)^n n \kappa_n {t_f}^{(n-1)}} \tag{5.61}$$

and the rest of the solutions are at $t^* = t_f$. However, the look angle is dictated to be zero at the final time by the design. Therefore, the only valid time instant where the look angle could be the maximum in this regard is given by Eq. (5.61). Replacing this time instant into Eq. (5.24) provides the maximum look angle:

$$\varepsilon_{\max} = -\frac{\kappa_n}{n-1}\left(\frac{\left(\varepsilon_0 - \left(-1\right)^n \kappa_n {t_f}^n\right)\left(n-1\right)}{\left(-1\right)^n \kappa_n n {t_f}^{(n-1)}}\right)^n \tag{5.62}$$

The next step is to determine if Eq. (5.62) or the initial look angle is the maximum look angle. A straightforward solution would depend on the behavior of the look angle. For instance, if the desired impact time requires more look angle, then the initial rate of the look angle must be positive. On the other hand, if the desired impact time requires the look angle to decrease from its initial condition to zero, this means that the initial look angle rate is negative, which could be represented as the following:

$$\dot{\varepsilon}\left(t=0\right)<0 \tag{5.63}$$

Eq. (5.23) is modified to reflect this property and it leads to the following condition:

$$\frac{\left(-1\right)^{(n-1)}\kappa_n {t_f}^n}{n-1}<\varepsilon_0 \tag{5.64}$$

If Eq. (5.64) is true, then the look angle decreases from its initial condition and the maximum look angle occurs at the initial time. Other than that, the maximum look angle is obtained at the time instant given in Eq. (5.61).

Table 5.1 Maximum look angle and the related time instants for n = 2, 3 and 4.

n	$\varepsilon_{\max}$	t^*
2	$-\frac{\left(\varepsilon_0-\kappa_2 {t_f}^2\right)^2}{4\kappa_2 {t_f}^2}$	$\frac{\varepsilon_0+\kappa_2 {t_f}^2}{2\kappa t_f}$
3	$\frac{4\left(\kappa_3 {t_f}^3+\varepsilon_0\right)^3}{27{\kappa_3}^2 {t_f}^6}$	$\frac{\kappa_3 {t_f}^3-2\varepsilon_0}{3\kappa_3 {t_f}^2}$
4	$-\frac{27\left(\varepsilon_0-\kappa_4 {t_f}^4\right)^4}{256\kappa_4^3 {t_f}^{12}}$	$\frac{3\varepsilon_0+\kappa_4 {t_f}^4}{4\kappa_4 {t_f}^3}$

Lastly, the maximum look angle definitions for n = 2, 3 and 4 are given in Table 5.1 for the cases when the look angle needs to be increased from its initial value. It is noted that the maximum look angle definitions are valid for the nonlinear domain. Whenever the guidance gain κ_n is calculated for the nonlinear engagement, Eq. (5.62) is applicable. Otherwise, there

happens to be an error when Eq. (5.57) is used as the linear guidance gain for the nonlinear domain.

5.5.2 Acceleration Characteristics

Acceleration characteristics will be considered in three parts. First the initial acceleration, then the final acceleration and last the extremum acceleration will be analyzed. The initial acceleration is obtained as

$$\dot{\gamma}_0 = (-1)^{(n-1)} \kappa_n {t_f}^{(n-1)} - \frac{(n-1)\varepsilon_0}{t_f} + \dot{\lambda}_0 \tag{5.65}$$

by replacing zero for t in Eq. (5.25). It could be stated that, since the look angle shaping forces the final look angle rate to be zero for $n > 2$, the guidance command curves the trajectory beforehand. So, the look angle is driven to zero before the impact sooner and sooner along with the increase in n. Thus, an increase in n would result in an increase in the initial acceleration regardless the guidance gain because of this physical interpretation.

In addition to the initial acceleration, the final acceleration can be evaluated using Eq. (2.7) and Eq. (2.9). However, the first term related to the LOS rate is indeterminate since $\varepsilon_f = r_f = 0$. Thus, L'Hôpital's rule can be applied to identify

$$\dot{\gamma}_f = \dot{\varepsilon}_f - V \lim_{t \to t_f} \frac{\sin \varepsilon}{r} = \dot{\varepsilon}_f - V \lim_{t \to t_f} \frac{\dot{\varepsilon} \cos \varepsilon}{\dot{r}} = 2\dot{\varepsilon}_f \tag{5.66}$$

using Eq. (2.8) for $\dot{r}$. For $n > 2$, as expressed previously $\dot{\varepsilon}_f$ is zero as forced by the guidance design. However, one needs to combine Eq. (5.66) with Eq. (5.10) when $n = 2$. These results lead to the following result

$$\lim_{t \to t_f} \dot{\gamma} = \begin{cases} 2\left(\kappa_2 t_f - \dfrac{\varepsilon_0}{t_f} \right), & n = 2 \\ 0, & n > 2 \end{cases} \tag{5.67}$$

showing that if the order of the look angle polynomial is more than 2, then the final acceleration will be zero. This property is quite advantageous since the system does not need maneuver at the end of the engagement.

The second issue is the extreme acceleration, which is important during the overall system design. Since the characteristic of the LOS rate is not known in the nonlinear domain and the analytical solution of the guidance gain is available only under the linearized kinematics, the designer must be careful while examining the extreme acceleration for the nonlinear domain. To find this acceleration, first the initial and the final values of the acceleration are examined. When $n > 2$, the case of final acceleration drops owing to Eq. (5.67). When $n = 2$, the maximum acceleration magnitude might be demanded at the end of the engagement if the following case holds

$$\left|\dot{\gamma}_f\right| > \left|\dot{\gamma}_0\right| \tag{5.68}$$

By replacing the initial and the final accelerations of the quadratic look angle shaping in Eq. (5.68), the corresponding condition turns into the following:

$$\left|2\left(\kappa_2 t_f - \frac{\varepsilon_0}{t_f}\right)\right| > \left|-\kappa_2 t_f - \frac{\varepsilon_0}{t_f} + \dot{\lambda}_0\right| \tag{5.69}$$

Next, the local extremum is investigated. For that, the first time derivative of Eq. (5.25) is equated to zero:

$$\ddot{\gamma} = \kappa_n \left(-1\right)^{(n-1)} \left(t_f - t\right)^{(n-1)} - \frac{(n-1)}{t_f - t}\varepsilon + \dot{\lambda} = 0 \tag{5.70}$$

When the LOS rate, which is given in Eq. (5.31) for the linearized kinematics, and the look angle in Eq. (5.24) are replaced in Eq. (5.70), Eq. (5.70) yields

$$\left(t - t_f\right)^{(n-3)} \frac{\varepsilon_0 n t_f \left(n-2\right) + \left(-1\right)^n \kappa_n {t_f}^n t\left(1-n^2\right) + \left(-1\right)^n \kappa_n {t_f}^{n+1}\left(2n-1\right)}{\left(-1\right)^{(n-1)} {t_f}^n} = 0 \tag{5.71}$$

As seen, the local extremum solution is obtained at $t = t_f$ and at the given time instant:

$$\hat{t} = \frac{n\varepsilon_0\left(2-n\right) + \left(-1\right)^n \kappa_n {t_f}^n \left(1-2n\right)}{\left(-1\right)^{(n-1)} {t_f}^{(n-1)} \kappa_n \left(n^2-1\right)} \tag{5.72}$$

When Eq. (5.72) is evaluated for $n = 2$, it is seen that $\hat{t} = t_f$. This result verifies that depending on the initial conditions and the desired impact time, the extreme acceleration might occur at the initial or at the final time for $n = 2$, which is not the case for higher orders. Nevertheless, if $t = \hat{t}$ is replaced in the guidance command given in Eq. (5.25), then the extremum of the guidance command will be:

$$\dot{\gamma}_{ext} = \frac{n\left(\varepsilon_0 - (-1)^n \kappa_n {t_f}^n\right)}{(-1)^{(n-1)}(n-1){t_f}^{(n-1)}} \left(\frac{n(n-2)\left(\varepsilon_0 - (-1)^n \kappa_n {t_f}^n\right)}{(-1)^n (n^2-1)\kappa_n {t_f}^{(n-1)}} \right)^{(n-2)} \tag{5.73}$$

Table 5.2 Extreme acceleration candidates and the related time instants for $n = 2$, 3 and 4.

n	**Extreme Acceleration Candidates, m/s²**	**Time of the Extreme Acceleration, s**
2	$a \approx 2V\left(\kappa_2 t_f - \frac{\varepsilon_0}{t_f}\right)$ $a = -V\left(\frac{2\varepsilon_0 + \kappa_2 {t_f}^2}{t_f}\right)$	$t = 0$ $t = t_f$
3	$a \approx V\left(\kappa_3 {t_f}^2 - \frac{3\varepsilon_0}{t_f}\right)$ $a \approx -\frac{9V\left(\varepsilon_0 + \kappa_3 {t_f}^3\right)^2}{16\kappa_3 t_f^4}$	$t = 0$ $t \approx \frac{5\kappa_3 {t_f}^3 - 3\varepsilon_0}{8{t_f}^2 \kappa_3}$
4	$a \approx -V\left(\kappa_4 {t_f}^3 + \frac{4}{t_f}\varepsilon_0\right)$ $a \approx -\frac{128V(\varepsilon_0 - \kappa_4 {t_f}^4)^3}{675{\kappa_4}^2 {t_f}^8}$	$t = 0$ $t \approx \frac{7\kappa_4 {t_f}^4 + 8\varepsilon_0}{15{t_f}^3 \kappa_4}$

It is noted that this result is found by Eq. (5.25) with the LOS rate defined for the linearized kinematics. As a consequence, if the engagement is far from the linear conditions, then degeneration from Eq. (5.73) will arise. The acceleration at $t = t_f$ is already presented in Eq.

(5.67). Now, the extreme acceleration analysis is completed since all of the candidates are provided. To decide which one is the maximum, they have to be checked with respect to the given engagement conditions. To illustrate the candidates and the related time instants, the results for the 2nd, 3rd and 4th orders are summarized in Table 5.2.

5.5.3 Flight Path Angle Characteristics

The time domain solution of the flight path angle is given in Eq. (5.45), which was derived using the linearized kinematics. When this equation is used to determine the final flight path angle, and $t = t_f$ is applied, the following equation is obtained

$$\gamma_f = -\left(\frac{y_0}{V t_f} + \frac{\varepsilon_0}{n-1} + (-1)^{(n-1)} \kappa_n \frac{{t_f}^n}{n(n-1)} \right) \tag{5.74}$$

which is actually the division of Eq. (5.42) by *V*. It is here noted that there will be an error for the nonlinear kinematics. However, instead of the linear guidance gain, using the guidance gain found for the nonlinear kinematics will provide a final flight path angle closer to the true one.

5.5.4 Impact Time Interval

The minimum impact time would cause high-*g* maneuvers whereas the maximum impact time would demand high look angles. However, generally speaking it is the case that if there is not any physical limit, then the proposed guidance law can accomplish a very large and an infeasible impact time since there is not a singularity in this guidance law. This issue will also be exemplified in the simulations. Therefore, the only consideration could be operational, i.e. high impact times might result in negative altitude against the ground targets, which is not desirable for such engagements. However, this may not be a problem; for instance, for loitering. Hence, the maximum impact time will not be examined for this impact time control method.

The minimum impact time definition can be proposed based on the linearized kinematics. For instance, the minimum impact time could be suggested as the impact time that results in the determinant of the guidance gains to be zero. Any desired impact time less than this value will cause the guidance gain to be imaginary. In other words, there will not be a solution. For instance, when Eq. (5.53) is examined, it is seen that the inner part of the square root function is zero if the following equality holds for $n = 3$

$$-V^2\varepsilon_0^2 t_{f,\min}^2 + 24Vt_{f,\min}x_f - 24{x_f}^2 = 0 \tag{5.75}$$

where y_0 is zero for the sake of simplicity. When this equation is solved, $t_{f,\min}$ may also provide a guidance gain in the nonlinear domain. However, the difficulty is the unknown relation between the linear and the nonlinear domain solutions. Therefore, it has to be checked before the engagement if a solution exists for the nonlinear domain. Nevertheless, in general it could be said that if there is a solution for the linearized kinematics, there can be a solution for the nonlinear domain. So that, the minimum impact time would be the solution of Eq. (5.75) or any value close to it.

It is to be noted that, since Eq. (5.75) is a quadratic function, there will be two solutions, one of which is infeasible. For instance, 25.13 s and 4899.1 s for an engagement with 20° of initial look angle of the base model. Hence, the minimum of the solutions must be considered. To sum up, because of the nonlinear nature of the problem, the minimum impact time for the nonlinear kinematics cannot exactly be found; however, an estimated value is provided based on the linearized kinematics.

5.6 Performance in the Nonlinear Domain

In the previous section, it was shown that an analytical solution of the guidance gain was available for the linearized kinematics. However, the linear domain solution will result in performance degradation in the nonlinear environment. Even for a constant speed missile, the guidance law in Eq. (5.25) with the gain obtained from Eq. (5.57) cannot be expected to lead to the desired impact time. It was stated afterwards that the guidance gain for the nonlinear domain could be found by a root-finding algorithm such as the Newton-Raphson method operating on Eq. (5.27) using the linear solution as the initial guess.

If the numerical search algorithm is briefly explained, it would be seen that first the partial derivative of Eq. (5.27) with respect to the guidance gain is required, which is

$$\frac{\partial r}{\partial \kappa_n} = r' = -V\int_0^{t_f} \frac{\partial \cos\varepsilon\left(t,\kappa_n\right)}{\partial \kappa_n} dt \tag{5.76}$$

The partial derivative within the integral is obtained using Eq. (5.24):

$$\frac{\partial \cos \varepsilon}{\partial \kappa_n} = \sin(\varepsilon)\left(t - t_f\right)^{n-1} t \tag{5.77}$$

After that, the new guidance is computed with the following scheme:

$$\kappa_{n,j+1} = \kappa_{n,j} - \frac{r}{r'} \tag{5.78}$$

where j is the iteration number. This routine could run until a threshold value of the miss distance is sustained, which is one meter for the scenarios given below.

In the following examples, several aspects of the proposed method are presented. The missile with a constant speed of 200 m/s engages a stationary target. The initial separation is 5 km and the guidance command is executed with no latency. The guidance gain is computed via the Newton-Raphson's method, where the initial guess is obtained from Eq. (5.57). Under these conditions; first, the results of very high impact times are discussed. Next, the effect of the initial guess for the search algorithm is examined. Since there are two guidance gains, the upward or the downward trajectories are presented. Afterwards, a comparison study is held, where n is varied; in addition, the energy optimal solution and the sliding mode control based impact time control, which is introduced in [29], are used for comparison purposes. Finally, several analysis studies are run; for instance, concerning optimality and robustness under autopilot lag.

5.6.1 High Impact Time Examples

Here, the purpose is to show the efficiency of the guidance law and the search algorithm starting with the linear gains. It is also noted that to present the behavior of the system under the hypothetic impact times such as 500 s and 750 s is the main aim. The initial look angle is 20° and n = 3. The iteration numbers, the guidance gains and the maximum look angles obtained via Eq. (5.62) are provided in Table 5.3. As seen, the number of the iterations even for such impact times are reasonable. Additionally, the gains obtained via Eq. (5.57) for the linearized kinematics and the ones for the nonlinear kinematics could also be observed.

Figure 5.6 shows the trajectories regarding these impact times, where the target is represented by a red cross. The missile moves around the target for some time with no apparent motive and in the end hits the target. This result shows that besides impact time control, the proposed impact time control method could also be used for loitering. In Figure 5.7, the smooth

look angle variations corresponding to such seemingly chaotic trajectories can be observed. Figure 5.8 displays the range histories that oscillate until the desired impact times are satisfied. Figure 5.9 illustrates the feasible acceleration histories without any high-g maneuvers. It is to be noted that due to the highly nonlinear engagement geometry, Eq. (5.73), which is derived under the assumption of the linearized kinematics, does not provide the true maximum acceleration magnitude.

Table 5.3 Important results of the hypothetic impact time simulations.

Impact Time, s	**Number of Iterations**	κ_{linear}	$\kappa_{nonlinear}$	**Max. Look Angle, deg**
500	4	$1.4104.\ 10^{-8}$	$2.8276.\ 10^{-7}$	308.99
750	7	$8.2867.\ 10^{-9}$	$8.2867.\ 10^{-8}$	305.73

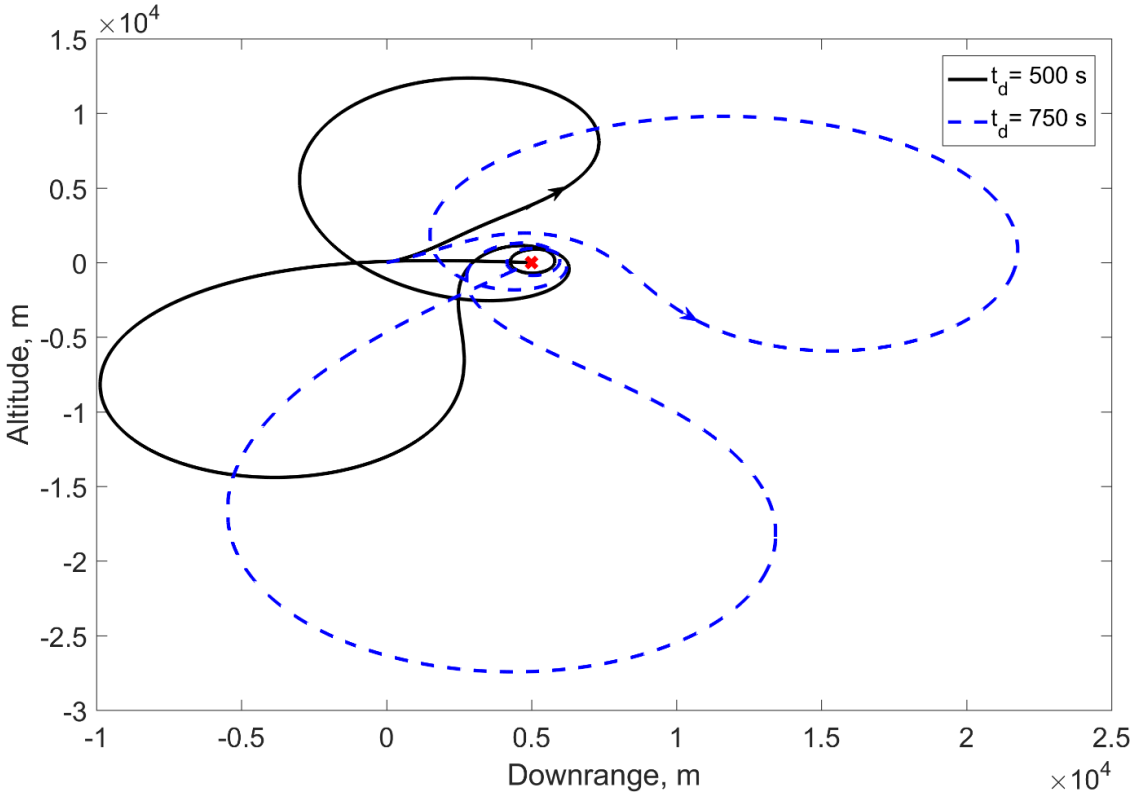

Figure 5.6 Trajectory histories for the high impact time simulations.

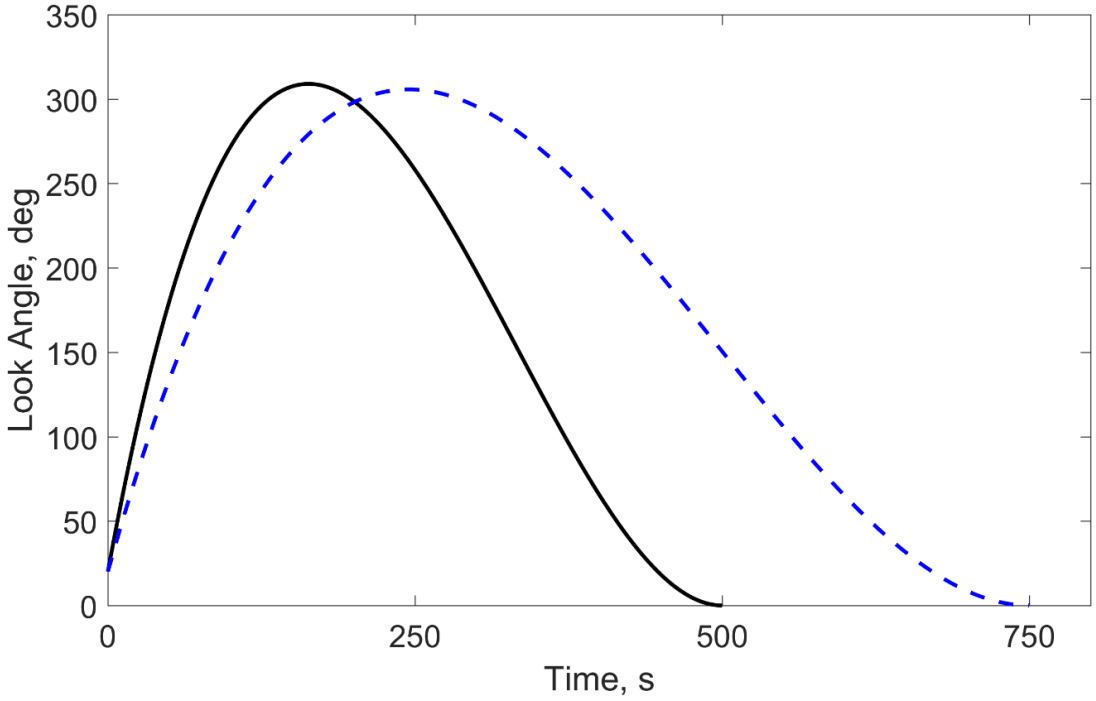

Figure 5.7 Look angle histories for the high impact time simulations.

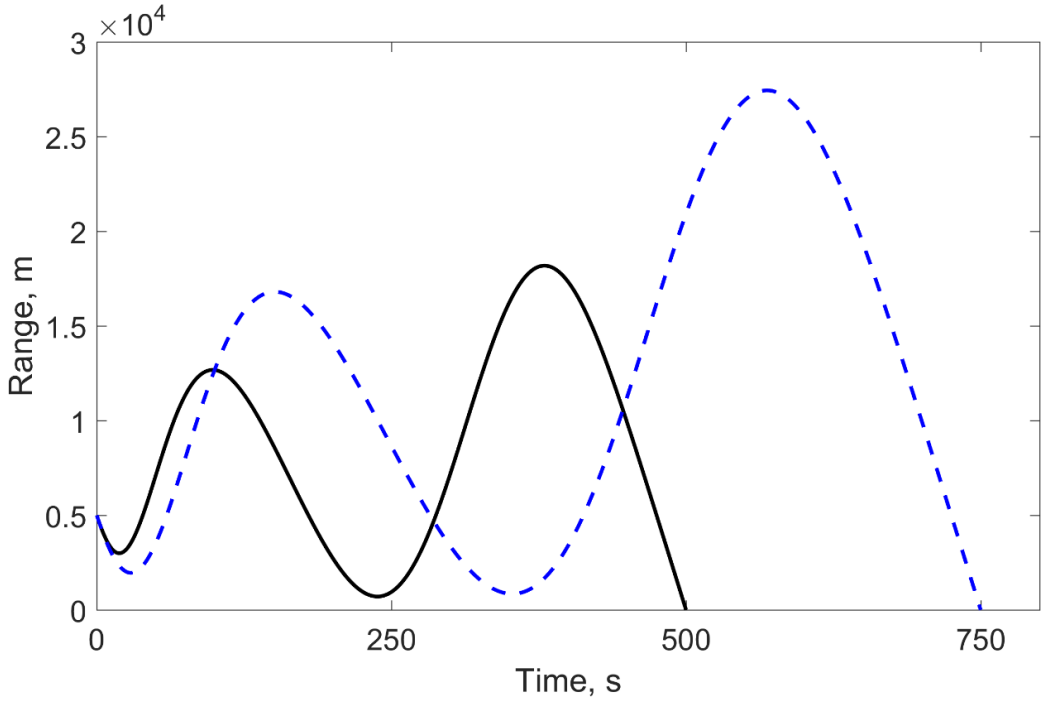

Figure 5.8 Range histories for the high impact time simulations.

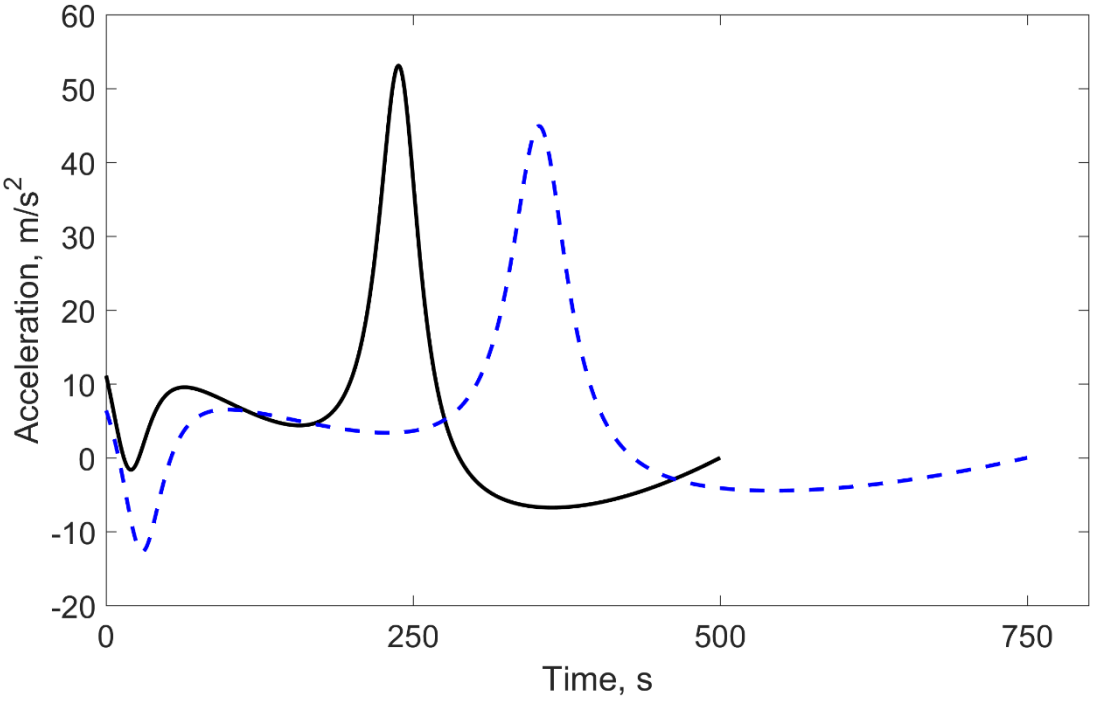

Figure 5.9 Acceleration histories for the high impact time simulations.

5.6.2 Example Scenarios

This subsection is reserved for presenting the efficiency of using the linear guidance gain as an initial guess of the Newton-Raphson method. Afterward, the results obtained by the two alternative guidance gains, which is given in Eq. (5.57), are presented.

5.6.2.1 Numerical Analysis of the Guidance Gains

First, the case with zero initial look angle is examined for 30 s of impact time. The guidance gain is varied from -0.02 to 0.02 and *n* is 3. The initial range is subtracted from the numerically obtained final range, in order to provide the range error as seen in Figure 5.10. The linear guidance gain, which is calculated via Eq. (5.57) and resulting in $\kappa_3 = 2.0002.10^{-4}$, presents a good approximation of the guidance gain of the nonlinear domain. Therefore, this value can be used as a starting point of the Newton-Raphson method. This linear guidance gain is also shown in the figure. Using this initial condition, the required number of iterations to terminate the Newton-Raphson root finding algorithm is 3.

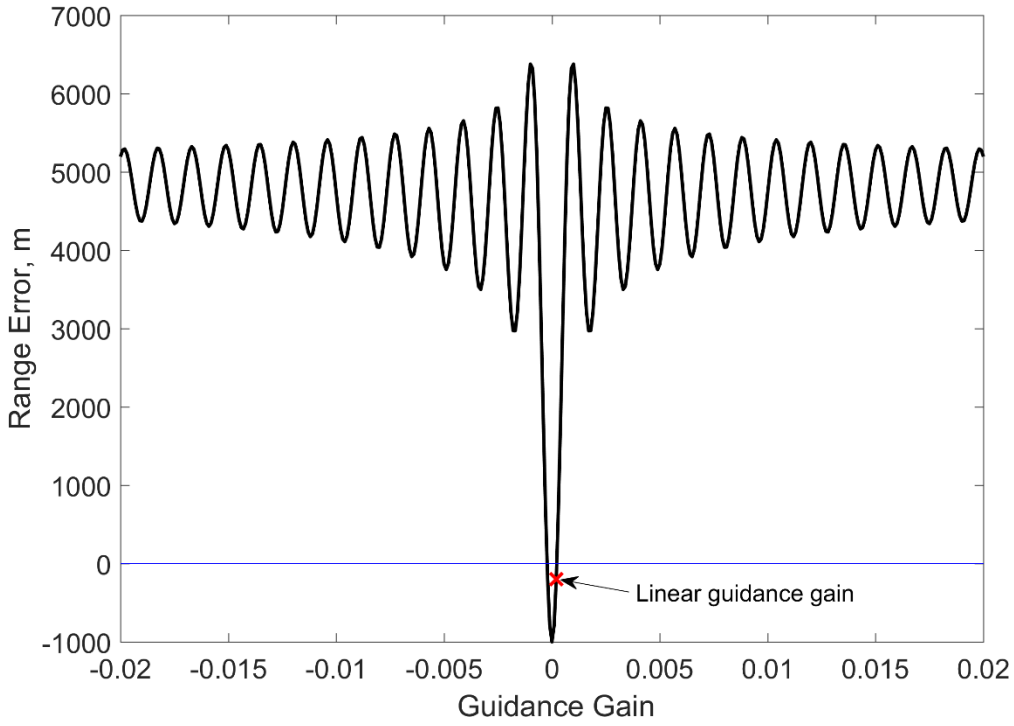

Figure 5.10 Range error versus guidance gain for $t_f = 30\ s$.

Afterward, the same analysis is done for 100 seconds, which is not a very realistic impact time. In contrast to t_f = 30 s, in this problem, there are ten guidance gains that can drive the range to zero as seen in Figure 5.11. The location of the linear guidance gain, which happens to be $6.275.10^{-6}$, could be also observed in Figure 5.11. This means that in general, there might be more than two guidance gains, which accomplish the desired impact time including the symmetrical trajectories. Therefore, the guidance gains have to be examined whether they are feasible or not. For instance, the positive guidance gains of this problem are $[1.45 \quad 4.14 \quad 5.33 \quad 8.91 \quad 9.06].10^{-5}$. As it is seen in Eq. (5.62), whenever the guidance gain increases, the maximum look angle increases linearly since the initial look angle is zero. For example, the maximum look angle will be four times greater if the second guidance gain selected. Therefore, it could be said that using the minimum one of the guidance gains is appreciated. The linear guidance gain would be notably helpful and practical in such cases. Additionally, even for a high impact time demand, the iteration number to find the guidance gain is 4.

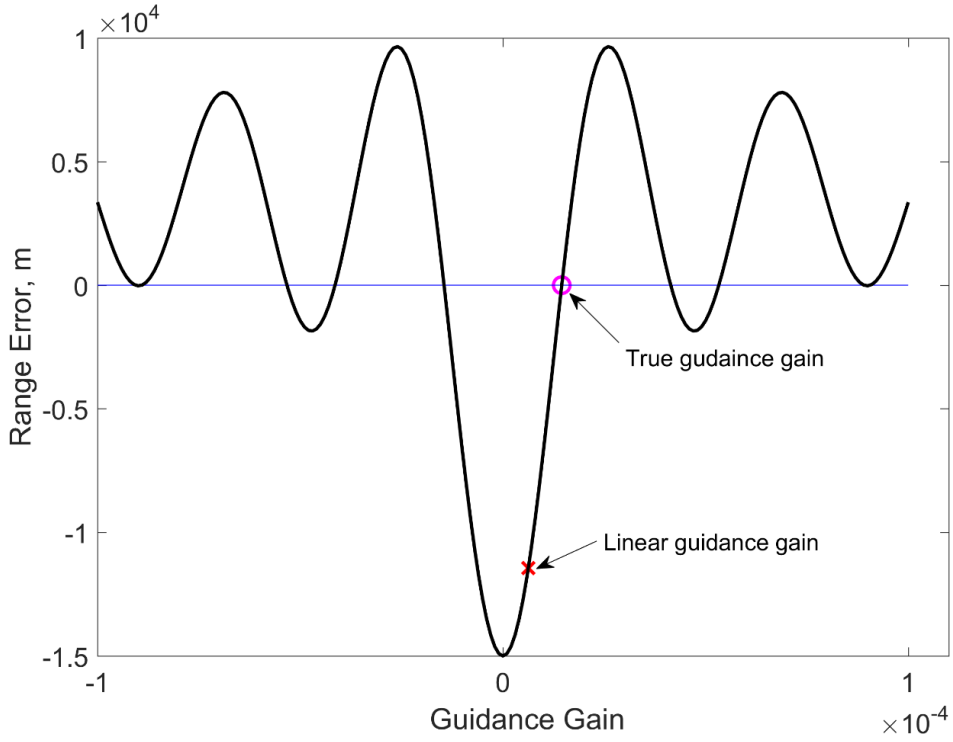

Figure 5.11 Range error versus guidance gain for $t_f = 100$ s.

5.6.2.2 Scenarios with Alternative Guidance Gains

Here, the results with the two gains obtained by Eq. (5.57) will be discussed for $n = 3$. The initial look angles are 0° and 20°. For quick referencing, the summary of the simulations is presented in Table 5.4. The scenario couples 1-1′ and 2-2′ are chosen with the intention of showing the effects of the different solutions of the guidance gain under the same conditions. When the initial look angle is zero as in scenarios 1 and 1′, the engagements happen to be exactly symmetric. However, when the initial value is different from zero as in scenarios 2 and 2′, the symmetry disappears as might be expected. One thing to note is that the negative guidance gain results in higher maximum look angle and acceleration magnitudes for the second scenario. The linear and the nonlinear gains are also given in Table 5.4 to remind the assumption in Eq. (5.50). As mentioned previously, this assumption causes longer traveled distance than reality. As a result, the guidance gains for the nonlinear domain are greater in magnitude than the guidance gains for the linear domain since the trajectory needs to be curved more.

Figure 5.12 displays how the trajectories are shaped with the gains of different sign. In Figure 5.13, the look angle histories of the scenarios are presented, where the downward trajectory results in a higher maximum look angle magnitude for the second scenario pair. When the guidance command histories are analyzed, it is seen that the downward trajectory requires more acceleration with respect to the upward trajectory for this asymmetric scenario pair as seen in Figure 5.14. In addition to the higher look angle and the acceleration magnitudes, since a downward trajectory is not desired for ground-to-ground scenarios, the positive guidance gain will be preferred in the simulations for $n = 3$.

Table 5.4 Simulations results for the two gains.

Scenario	**Direction**	$\mathcal{K}_{linear}$	$\mathcal{K}_{nonlinear}$	**Cost, m^2/s^3**	**Extreme Look Angle, deg**	**Extreme Acc., m/s^2**
1	Upward	$2.0002.10^{-4}$	$2.2468.10^{-4}$	4824	51.49	40.44
1′	Downward	$-2.0002.10^{-4}$	$-2.2468.10^{-4}$	4824	-51.49	-40.44
2	Upward	$1.5108.10^{-4}$	$1.7584.10^{-4}$	3195	49.86	24.26
2′	Downward	$-2.4158.10^{-4}$	$-2.6690.10^{-4}$	7088	-52.70	-55.43

Furthermore, in this section the linear domain solutions of the LOS angle and the flight path angle results will be compared with the nonlinear ones for the upward trajectories. Eq. (5.46) and Eq. (5.47) are employed with the nonlinear guidance gains. Figure 5.15 and Figure 5.16 show how the linear solutions and the nonlinear results look, where the dashed lines are used for the former. It could be said that unless the system is highly nonlinear, i.e. very high t_d, the linear solutions of the engagement states would be fairly consistent. This advantage could be applicable for the further guidance problems.

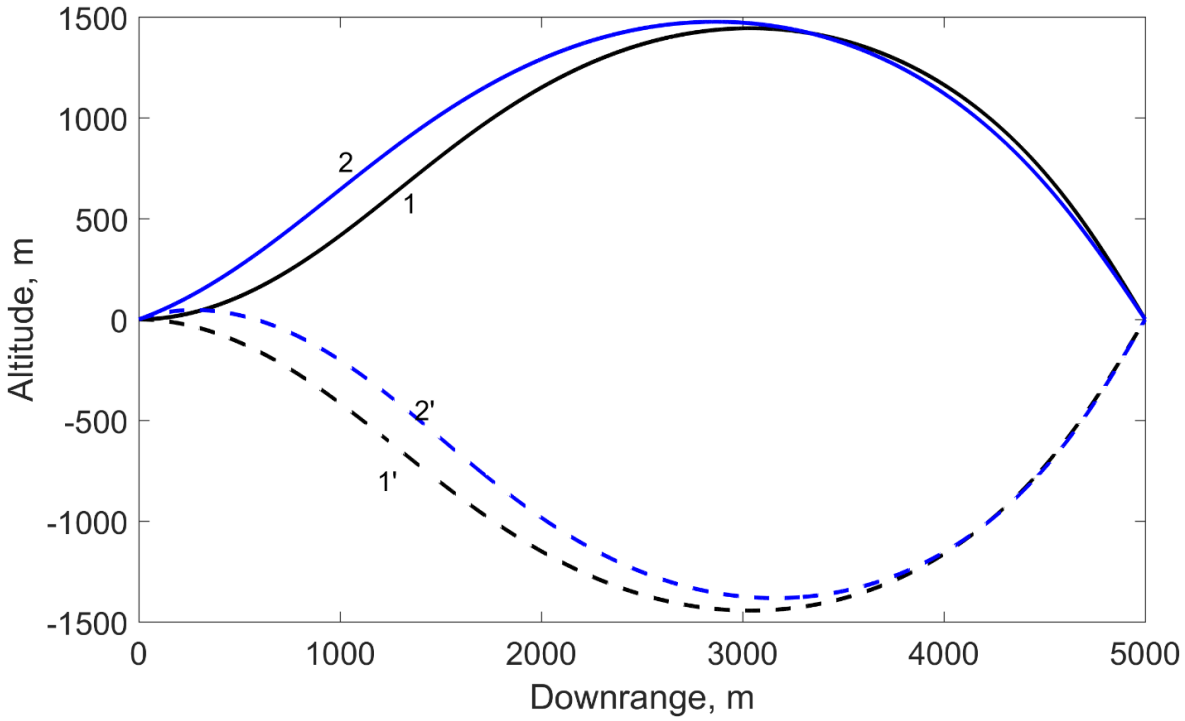

Figure 5.12 Trajectories for different κ_3 values.

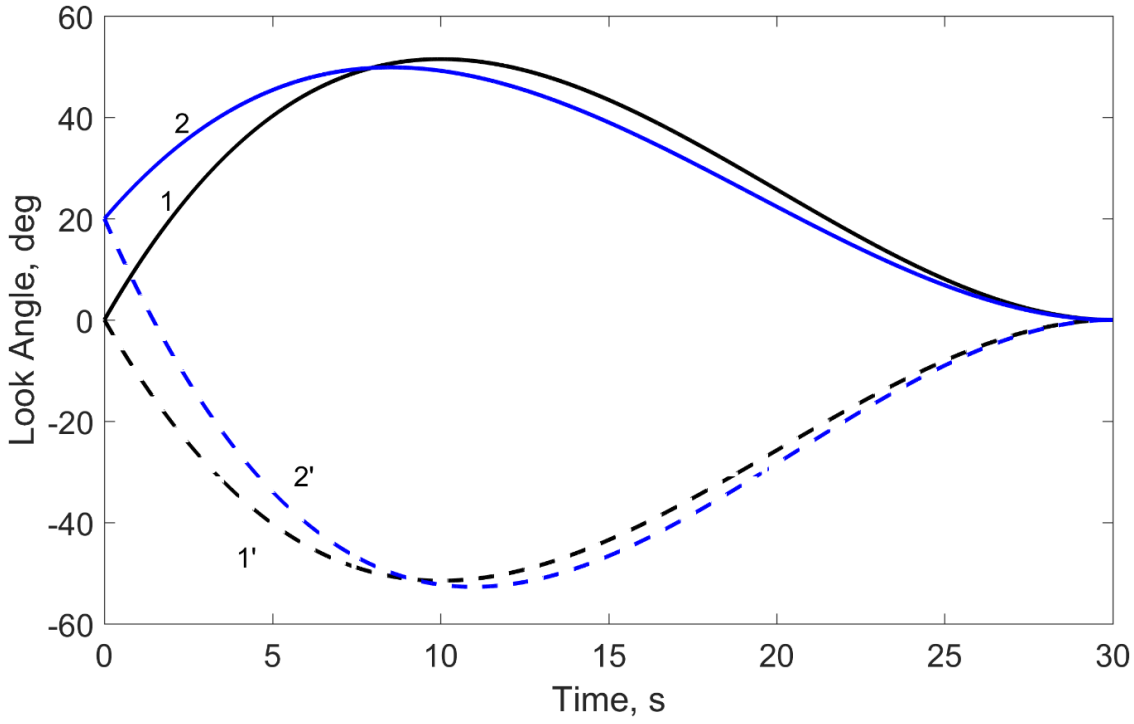

Figure 5.13 Look angle histories for different κ_3 values.

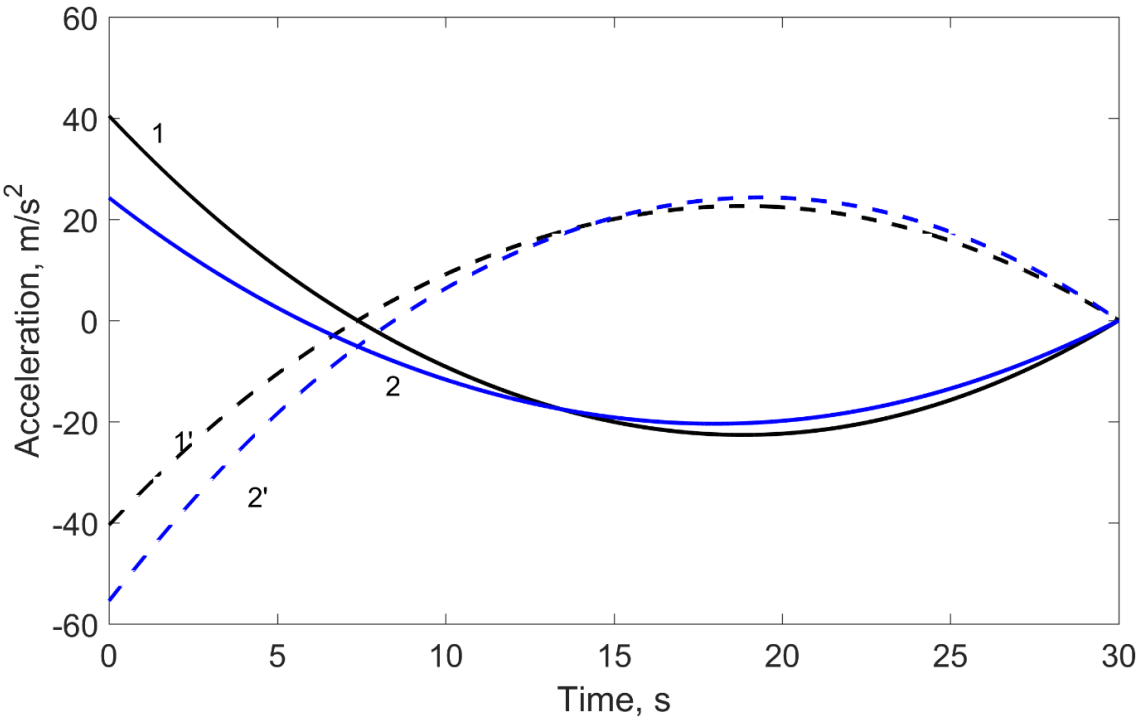

Figure 5.14 Guidance command histories for different κ_3 values.

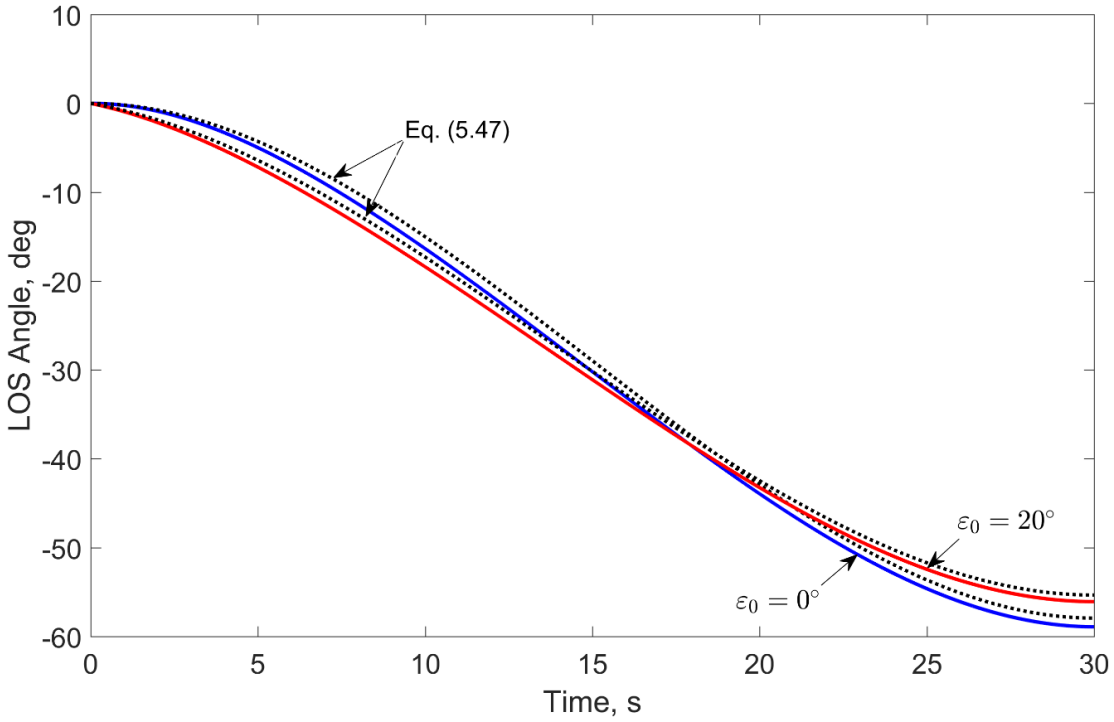

Figure 5.15 LOS angles for the linear and the nonlinear domains.

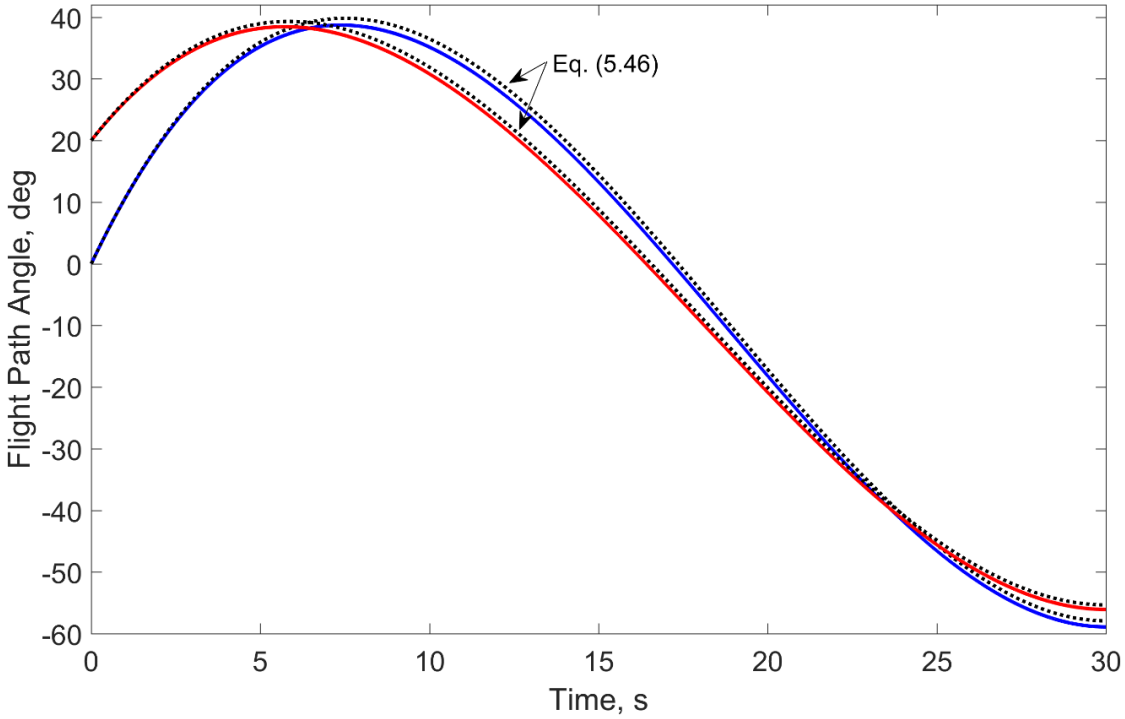

Figure 5.16 Flight path angles for the linear and the nonlinear domains.

5.6.2.3 Comparison Study

The performance of the proposed method is demonstrated for different n values and a comparison is held with [29] along with the energy optimal solution, where the cost function is $\int a^2 dt$. The same engagement model as in the previous study is used for 30 s, where the initial look angle is zero. The maximum of the guidance command is chosen as 10 g.

The quick summary of the simulations can be seen in Table 5.5, including a comparison of the true results obtained from the simulations and the analytical results from the corresponding equations. Additionally, the number of the required iterations is 3 for all of the orders. The maximum accelerations are obtained at the initial time for n = 3, 4 and 5, where the analytical solutions given in Eq. (5.65) provide the same results. On the hand, for n = 2 the maximum acceleration is obtained at the end of the engagement, as it is presented in Eq. (5.67). Among all the scenarios, [29] demands the maximum acceleration magnitude. The energy optimal one has by far less maximum acceleration magnitude. The maximum look angle of the proposed method is calculated from Eq. (5.62). When the guidance gain for the nonlinear domain is used, this equation provides the true maximum look angle as also seen in the table. [29] requires approximately 70° of look angle, which is again the maximum among the methods. The cubic

shaping and the optimal solution have almost the same maximum look angle. The final path angles are also compared using Eq. (5.74). When n = 2, the maximum error occurs. However, for the rest of the scenarios the results are quite similar. It is also possible to observe that the increase in the guidance gains results in higher maximum look angle values. However, such a statement is not valid for the cost functions. The cost function of n = 3 is the closest to the optimal one as the same statement holds for the maximum look angle. This result was expected since optimality was already examined for the linear domain.

Figure 5.17 illustrates the history of the trajectories, where the optimal one and the one with n = 3 have approximately the same maximum altitude. Figure 5.18 shows the acceleration histories, in which [29] demands the most among all, leading to saturation. In fact, [29] demands more than 20 g, which is too much for a missile with a speed of 200 m/s. In contrast, none of the guidance commands of the proposed method become saturated, not even when n = 5. Figure 5.19 shows the differences between the methods more clearly. [29] results in the maximum look angle requirement among all. As mentioned in Chapter 1, the Lyapunov and sliding mode based impact time control methods increase the look angle as soon as possible so that the remaining engagement could be covered with PN guidance. In Figure 5.20, the flight path angle histories of the simulations are presented. The maximum final flight path angle magnitude is obtained for n = 2. The rest remains more or less in a narrow band.

Table 5.5 Summary of the simulation results of the comparison study.

n	$\kappa_{nonlinear}$	**Extreme Acc., m/s^2** ***analytical***	**Extreme Acc., m/s^2** ***true***	**Max. ε, deg**	**Final γ, deg** ***analytical***	**Final γ, deg** ***true***	**Cost, m^2/s^3**
2	$-3.587.\ 10^{-3}$	-43.05	-43.05	46.246	-92.491	-96.73	13994.03
3	$2.2468.\ 10^{-4}$	40.44	40.44	51.494	-57.93	-58.9	9647.34
4	$-1.1664.\ 10^{-5}$	62.98	62.98	57.093	-45.11	-44.83	12206.28
5	$5.4803.\ 10^{-7}$	88.78	88.78	62.506	-38.151	-37.1	16554.41
-	Optimal	-	25.85	52.42	-	-60.75	9258
-	[29]	-	98.1	69.79	-	-39.31	27265.05

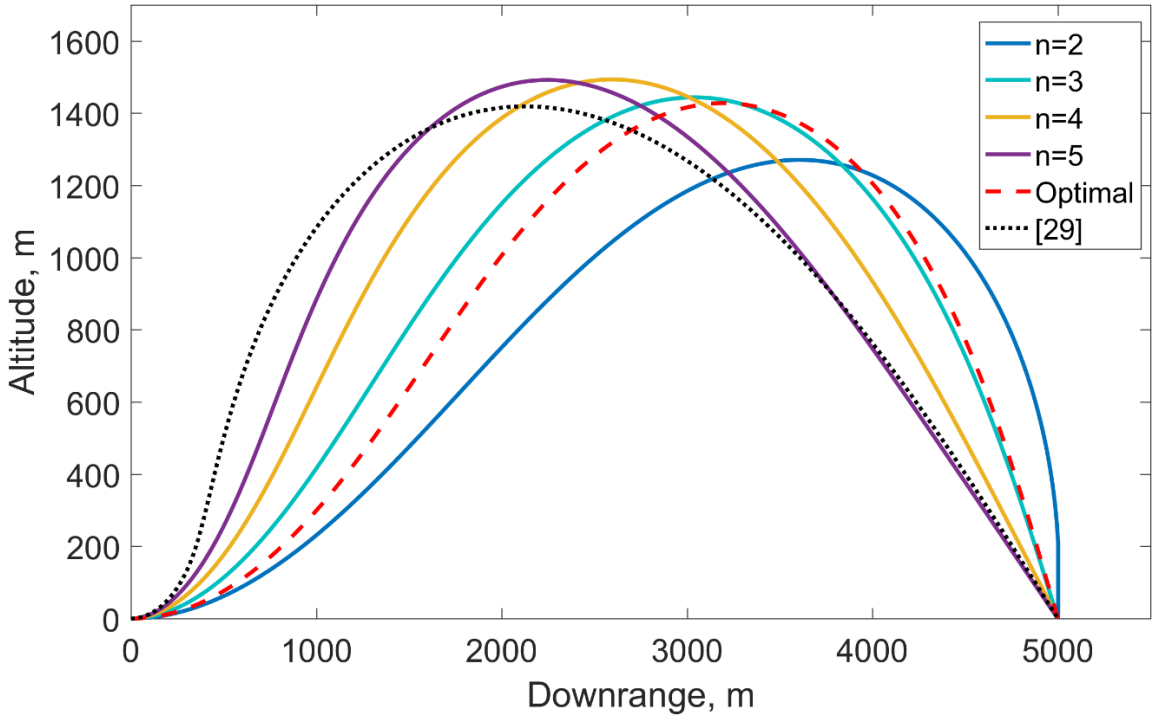

Figure 5.17 Trajectories histories of the comparison study.

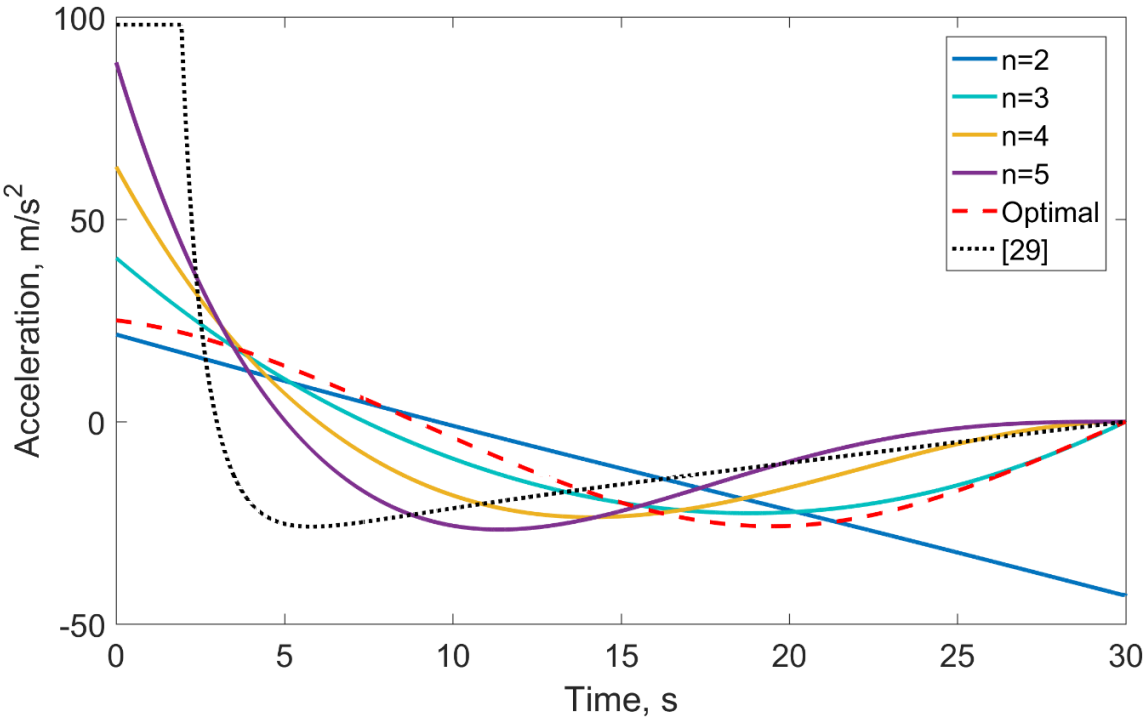

Figure 5.18 Acceleration histories of the comparison study.

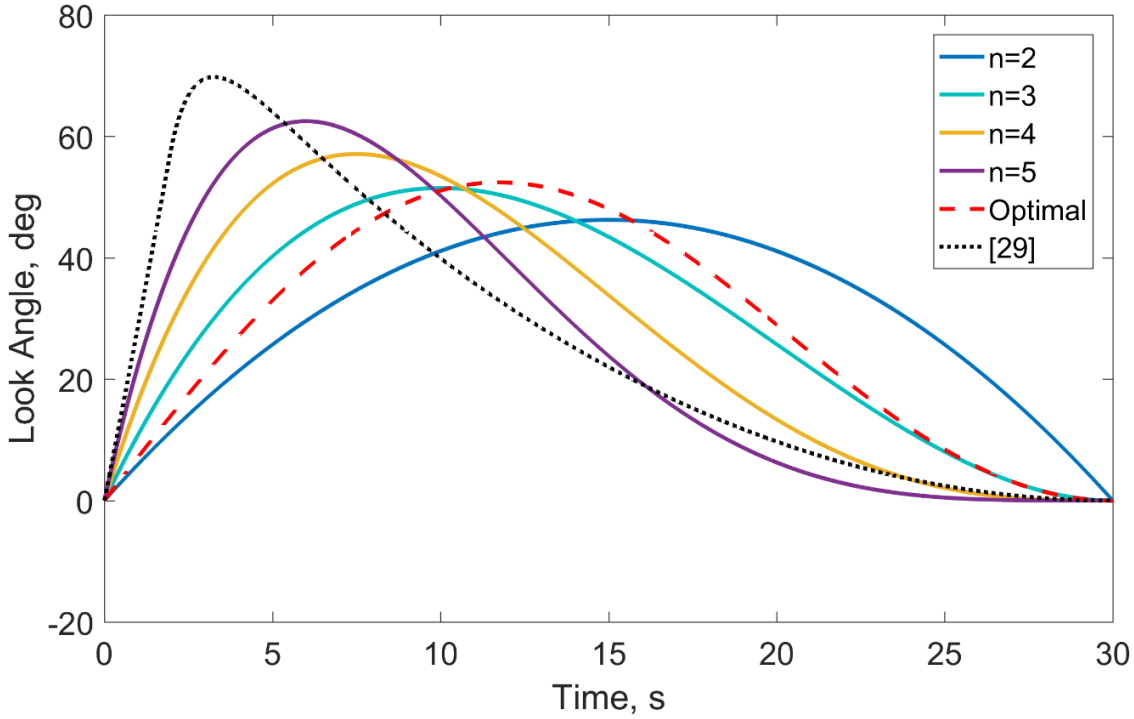

Figure 5.19 Look angle histories of the comparison study.

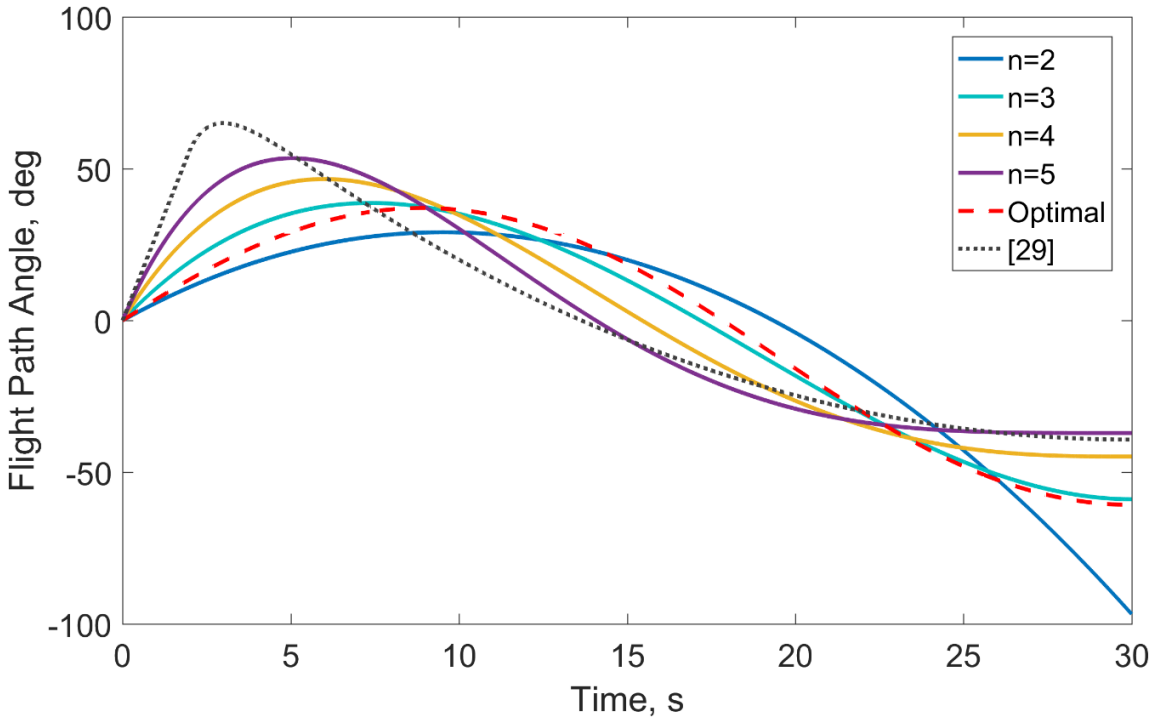

Figure 5.20 Flight path angle histories of the comparison study.

5.6.3 Optimality Analysis

The optimality of the polynomial guidance with n = 3 is explored for a wider impact time interval with the same model, where the variations of the initial look angles and the desired impact times are given in Table 5.6.

Table 5.6 Simulation variations for the optimality comparison.

Initial Look Angle, ε_0	$[0 \quad 10 \quad 20 \quad 30 \quad 40 \quad 50 \quad 60 \quad 70 \quad 80]^\circ$
Desired Impact Time, t_d	$[30 \quad 32 \quad 34 \quad 36 \quad 38 \quad 40]$ s

Figure 5.21 shows the costs of the optimal solution and the cubic look angle shaping, where the dashed lines represent the optimal one. It could be said that in general costs of the methods are very close to each other. Specifically, when the initial look angle is high, the optimal and the polynomial methods have almost the same cost.

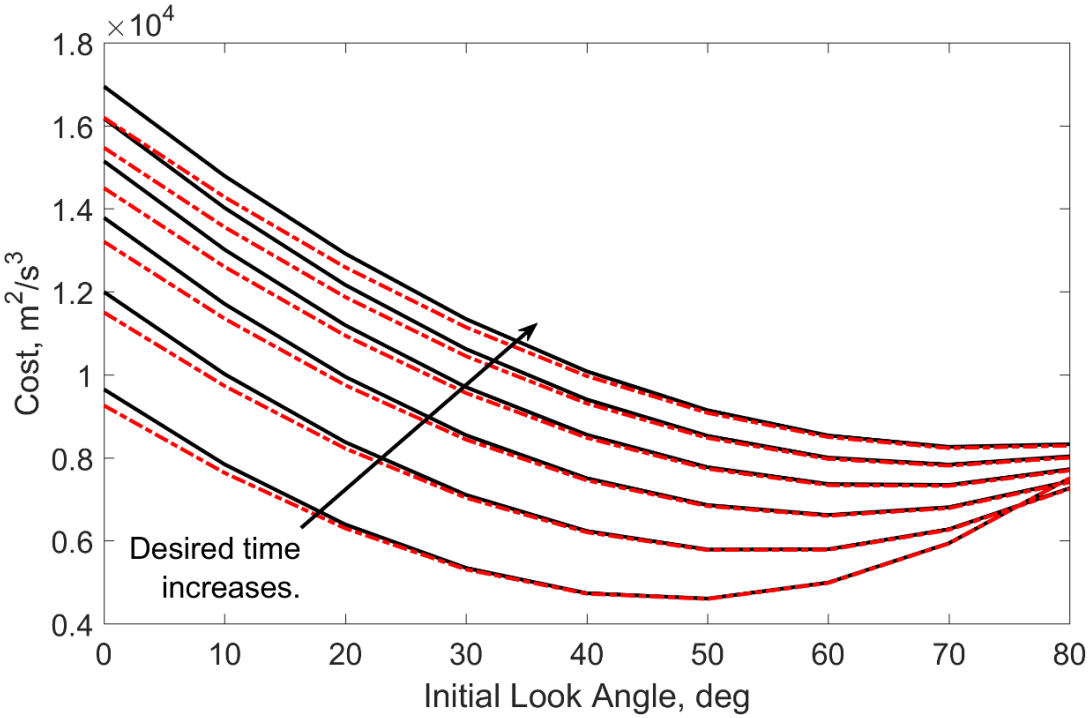

Figure 5.21 Costs of the proposed guidance law and the energy optimal solution.

Second, the difference of the maximum look angles is compared. It is computed as $\varepsilon_{3,\max} - \varepsilon_{o,\max}$. Figure 5.22 shows that the optimal solution demands slightly more look angle

with respect to the cubic look angle shaping. As seen, the difference increases when the desired impact time increases. However, the maximum difference is still less than 2.5 degrees and this difference decreases when the initial look angle increases. Next, the acceleration histories are discussed. $a_{3,\max} - a_{o,\max}$ is shown in Figure 5.23. When the initial look angle is zero, the maximum difference is obtained. The difference decreases to the ± 2 m/s^2 band when the initial look angle is more than 30°. As seen, the maximum acceleration of the optimal trajectory is less than the one obtained via the cubic shaping. However, during the most part of the engagement the cubic shaping method demands less acceleration with respect to the optimal one, and this behavior may help to explain the similarity of the costs.

After showing the main differences, another analysis is carried out for different speeds, where the ratio of the cost functions are computed via Eq. (5.79). The result to be stressed is: When the speed is low, then the similarity increases as seen in Figure 5.24.

$$\text{Cost Ratio} = \frac{\text{Cost Cubic}}{\text{Cost Optimal}} \tag{5.79}$$

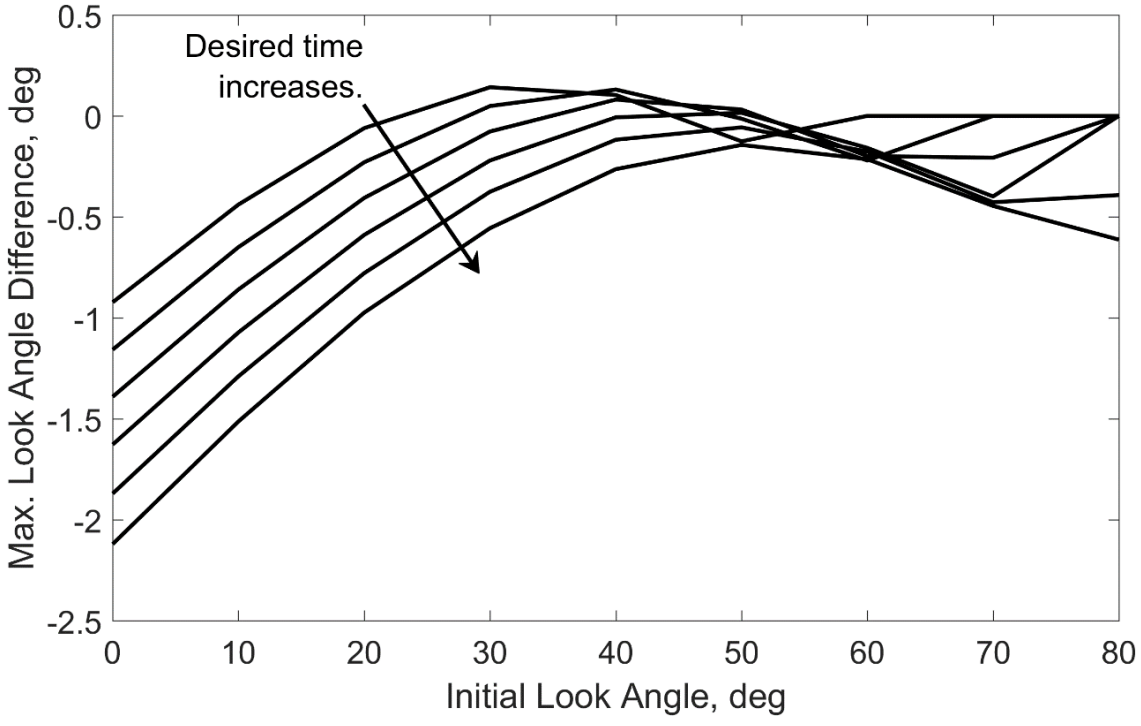

Figure 5.22 The difference of the maximum look angles between the proposed guidance law and the energy optimal solution.

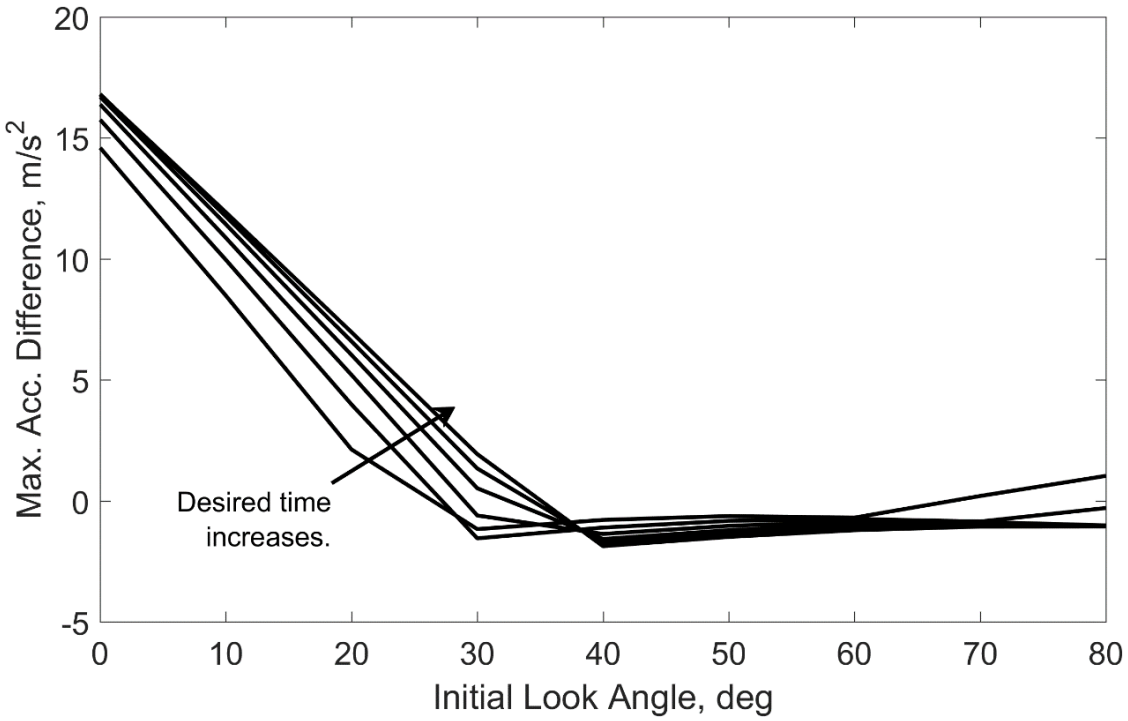

Figure 5.23 The difference of the maximum accelerations between the proposed guidance law and the energy optimal solution.

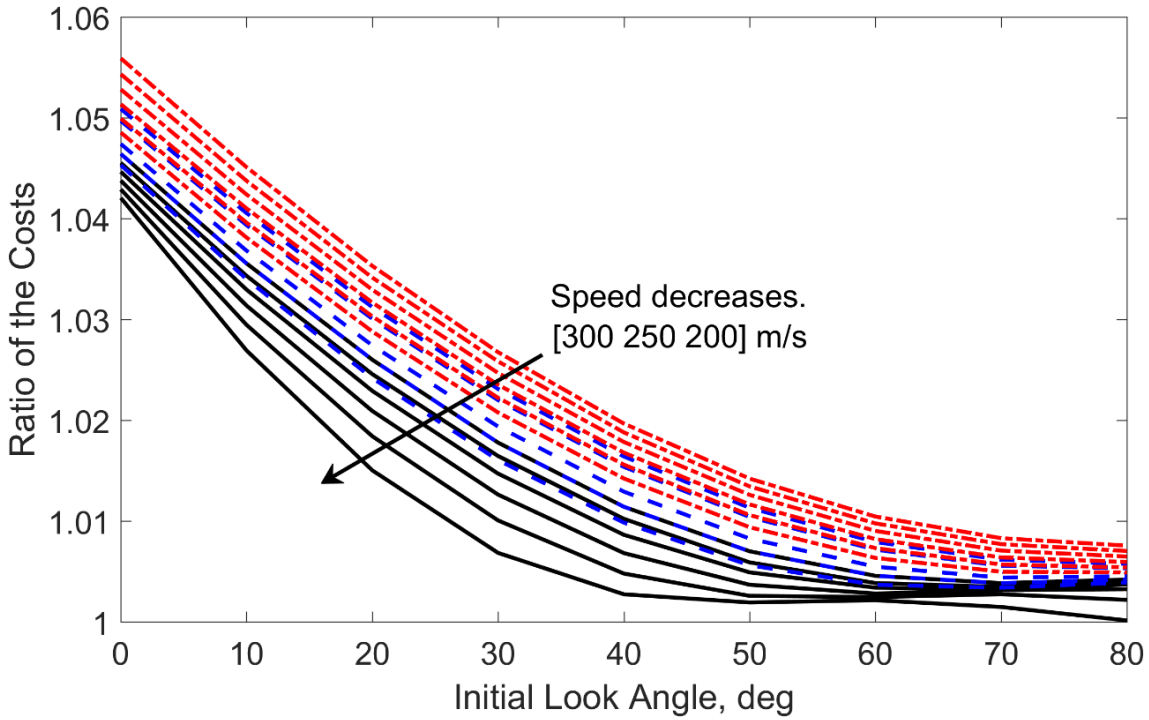

Figure 5.24 Ratio of the cost functions with respect to different speeds.

5.6.4 Performance Under Autopilot Lag

The other important issue related to the guidance design is the robustness under uncertainties, such as the autopilot lag. In this section, the impact time error will be analyzed under different autopilot lags. In Table 3.3, the variations of the initial look angle, the autopilot lag and the desired impact time are given. The same reference model is used to test the performance with one modification. When the range is less than 100 meters, the guidance command is held for the rest of the engagement. Figure 5.25 shows the histogram of the impact time error. It is seen that very few of the simulations end up with 0.5 seconds of impact time error. In general, impact time errors are negligible with respect to the desired values.

Table 5.7 Parameters for the robustness comparison.

Initial Look Angle, ε_0	$[0 \quad 10 \quad 20 \quad 30 \quad 40 \quad 50 \quad 60 \quad 70 \quad 80]^\circ$
Autopilot Lag, τ	$[0.1 \quad 0.2 \quad 0.3 \quad 0.4 \quad 0.5]$ s
Desired Impact Time, t_d	$[30 \quad 32 \quad 34 \quad 36 \quad 38 \quad 40]$ s

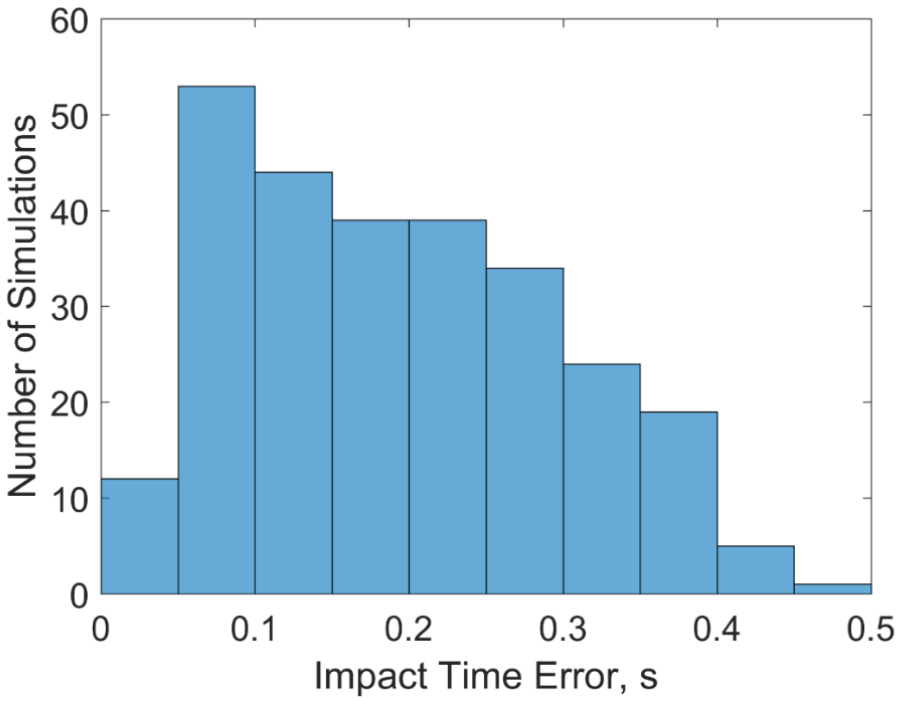

Figure 5.25 Histogram of impact time error under autopilot lag.

6 PREDICTIVE-ADAPTIVE IMPACT TIME CONTROL

The impact time control problem was thus far solved under the ideal conditions with the constant speed assumption for the nonlinear kinematics. The performance is satisfactory under the degrading conditions such as autopilot lag, noisy measurements and estimated range information. However, there is in fact another actor, which would be detrimental if not properly accounted for: Time varying speed. It was mentioned that almost all of the impact time control methods in the literature assume constant speed or demand speed control. Unfortunately, the speed of the missile will pose a serious challenge if it does not remain constant. One way to deal with this is to predict the mean speed. If the mean speed is known beforehand, the existing impact time control methods might provide better results under the varying conditions. On the other hand, predicting the mean speed of a trajectory is an effortful task since the trajectory, in other words, the guidance process plays an important role in how the speed changes. To the author's knowledge, the only study which provides a concept of mean speed for impact time control is [28]. In this paper, the impact time control method is same as the one for constant speed but instead of the instant speed, the mean speed is used to estimate the time-to-go. Afterwards, sliding mode control is applied to control the time of impact. However, the mean speed is presented only for the supersonic systems under several assumptions. For instance, in the sustain phase the speed is assumed to be constant and afterwards it behaves like an exponentially decreasing function without considering the gravity and the induced drag. Moreover, if a basic search is carried out in the literature of missile guidance, it would be seen that only the optimal guidance laws try to predict the mean speed since they mostly use time-to-go estimation in their guidance commands such as [51] and [52].

As mentioned in the introduction, one of the objectives of this dissertation is to present a solution for the case of time varying speed regardless of the application and without any preflight analysis. In the meantime, including as many actors as possible that change the speed

is appreciated. So far, three different impact time control algorithms have been presented. When they are examined for a possible solution under time varying speed, it can be seen that only the method of polynomial look angle shaping qualifies. Since gravity has an effect on the speed via the flight path angle, the time domain solution of the flight path angle is necessary for the mean speed prediction. The range shaping method will fail because it is not possible to have an analytical solution of the flight path angle even for the linearized kinematics. The second impact time control method could provide flight path angle under the linearized kinematics; however, it has a switched structure. Thus, an iterative scheme to compute the mean speed is infeasible. On the other hand, the polynomial shaping of the look angle, which provides the analytical equations of the engagement, could be used for mean speed prediction and the guidance law could be designed in such a way that impact time control under varying conditions is successful.

The organization of this chapter is as follows; first, the adaptation scheme is introduced to cope with disturbances such as autopilot lag, which are not included in the design process, for constant speed. Here, no connection with the conventional adaptive control is meant, but an adaptive guidance scheme based on updating the guidance gain is constructed. The distribution of the impact time error under autopilot lag is revisited, which was already shown in the previous chapter. Next, the efficiency of the adaptation is discussed. It is to be noted that the equations and the simulations are presented for $n = 3$ because of its near optimality, as also shown in the previous chapter. Next, since the adaptation is based on the linearized kinematics, it is shown that the sensitivity increases toward the end of the engagement and a simple remedy is proposed. Additionally, based on the adaptation scheme, the impact time control under the FOV constraint is presented. The rest of the chapter is reserved for impact time control under varying speed. First, the mean speed is predicted in an iterative structure for once at the beginning of the engagement, whereas the guidance gain is also computed along. Next, using this predictive algorithm and updating throughout the engagement in an adaptive scheme leads to a closed loop guidance for impact time control under the varying conditions. Afterward, the optimality of the predictive-adaptive guidance is investigated. Last, robustness against unknown drag coefficient is examined.

6.1 Adaptive Guidance Scheme

The basic idea of adaptation might be appreciated with the help of Figure 6.1, which shows the constant speed missile at two different points along its trajectory. The linear guidance gains to be calculated at each of these points will be different since the engagement is nonlinear. However, as the missile approaches the target, the calculated value will converge to a certain value since the assumption of linearity will become valid during the final part of the engagement owing to the fact that the look angle will eventually tend to zero. This general picture implies that the gain value needs to be updated as frequently as required until no further update might be necessary.

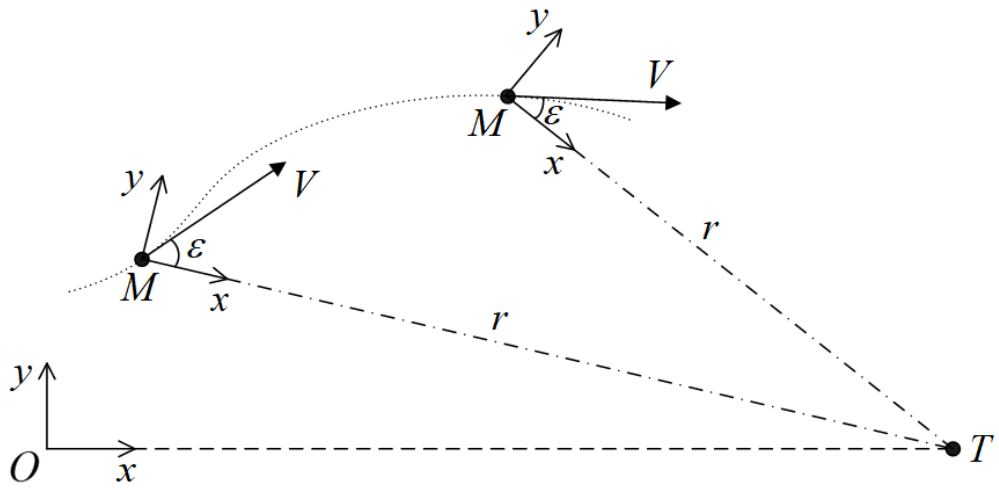

Figure 6.1 The idea of adaptation.

Instead of updating through Eq. (5.53), which would require the knowledge of the vertical position in addition to the final horizontal position, the calculation may be based on a more practical formulation based on the LOS frame. As seen in Figure 6.1, the vertical position is always zero in this frame, which is attached to the missile, i.e. $y_0 \to 0$. Furthermore, the final horizontal position can be interpreted as the range to the target, i.e. $x_f \to r$. Since instantaneous variables instead of the initial conditions, i.e. $\varepsilon_0 \to \varepsilon$, will be employed in this adaptive formulation, the impact time also needs to be updated, i.e. $t_f \to t_f - t$. With all these modifications, the impact time control method expressed in the previous chapter turns into a closed loop fashion, where Eq. (5.52) can now be written as

$$\frac{\left(t_f - t\right)^6}{21}\kappa_3^{\,2} + \frac{\varepsilon\left(t_f - t\right)^3}{3}\kappa_3 + 10\frac{r}{V\left(t_f - t\right)}\left(\frac{r}{V\left(t_f - t\right)^6} - 1\right) + \varepsilon^2 = 0 \tag{6.1}$$

which leads to the following solution:

$$\kappa_3 = -\frac{7\varepsilon}{2\left(t_f - t\right)^3} \mp \sqrt{35}\frac{\sqrt{24V\left(t_f - t\right)r - V^2\varepsilon^2\left(t_f - t\right)^2 - 24r^2}}{2V\left(t_f - t\right)^4} \tag{6.2}$$

The discriminant of Eq. (6.1) is

$$\Delta = \frac{5\left(t_f - t\right)^4\left\{-V^2\varepsilon^2\left(t_f - t\right)^2 + 24Vr\left(t_f - t\right) - 24r^2\right\}}{63V^2} \tag{6.3}$$

which will give imaginary solutions if it is less than zero. This can simply be avoided by setting a positive adaptation threshold.

6.1.1 Example Scenarios under Ideal Conditions

In order to show how the adaptation routine affects the trajectory and the performance, simulations are run with adaptive gain and with constant gain under no latency. The constant guidance gain is computed as in the previous chapter via the Newton-Raphson method. The model is run for 30 s and 35 s, where the initial look angle is zero. The adaptation is performed at 10 Hz and it is terminated when Δ is less than 2000 in order to avoid imaginary guidance gains. The nonlinear guidance gains are $2.2468.10^{-4}$ and $1.8896.10^{-4}$, respectively. Figure 6.2 shows the trajectories of the two different approaches. It is apparent that adaptive guidance gains result in a different trajectory than the constant gain guidance. Figure 6.3 explains the reason for such trajectories. The constant gain found via the Newton-Raphson method requires higher look angles while the adaptive application fulfills the task with smaller magnitudes. In Figure 6.4, the acceleration histories are shown. It is observed that the adaptive guidance acts later to decrease the acceleration magnitude towards the end. In addition, a bump might occur when the adaptive gain starts to remain constant. It is seen in Figure 6.5 that there is no adaptation approximately for more than 5 seconds regarding the chosen threshold value, in which the adaptive guidance gains remain constant. Hence, the guidance algorithm is partially

closed loop during this interval for the impact time control purpose. Despite this fact, the performance of the adaptive scheme is satisfactory. It is also shown in Figure 6.5 that the adaptive gains converge a certain value if Δ is chosen as zero, which was the main assumption of the adaptation as stated in Section 6.1.

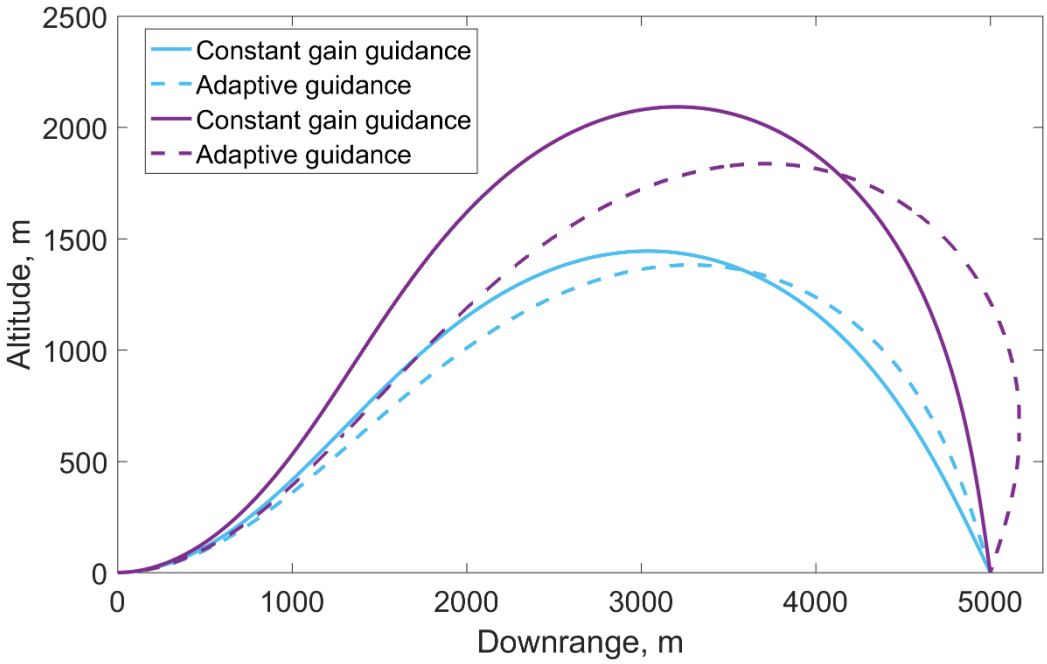

Figure 6.2 Trajectories with and without the adaptation routine.

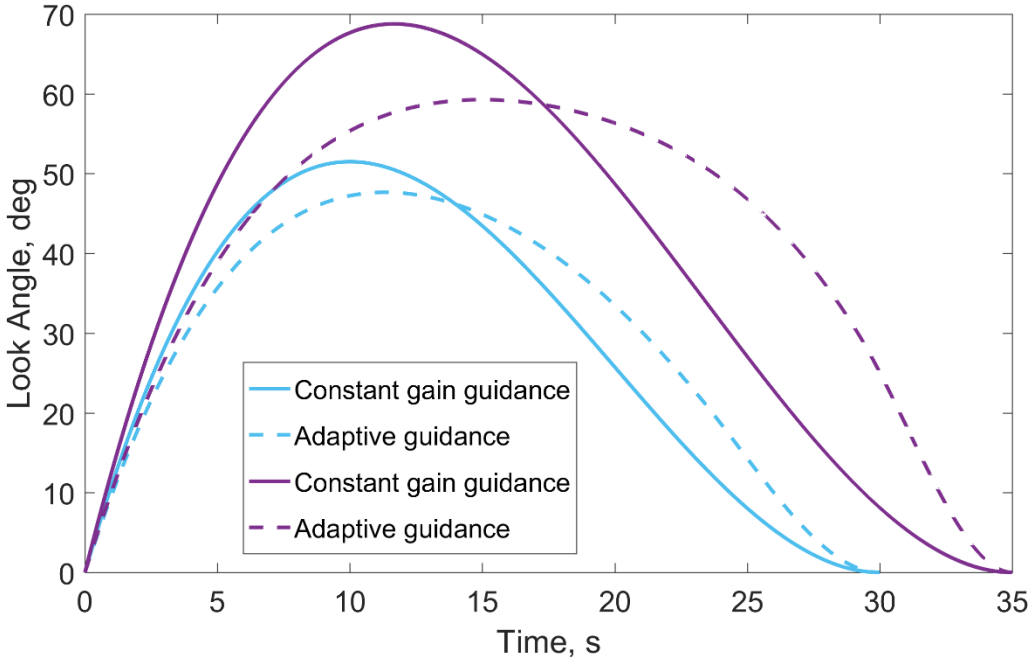

Figure 6.3 Look angles with and without the adaptation routine.

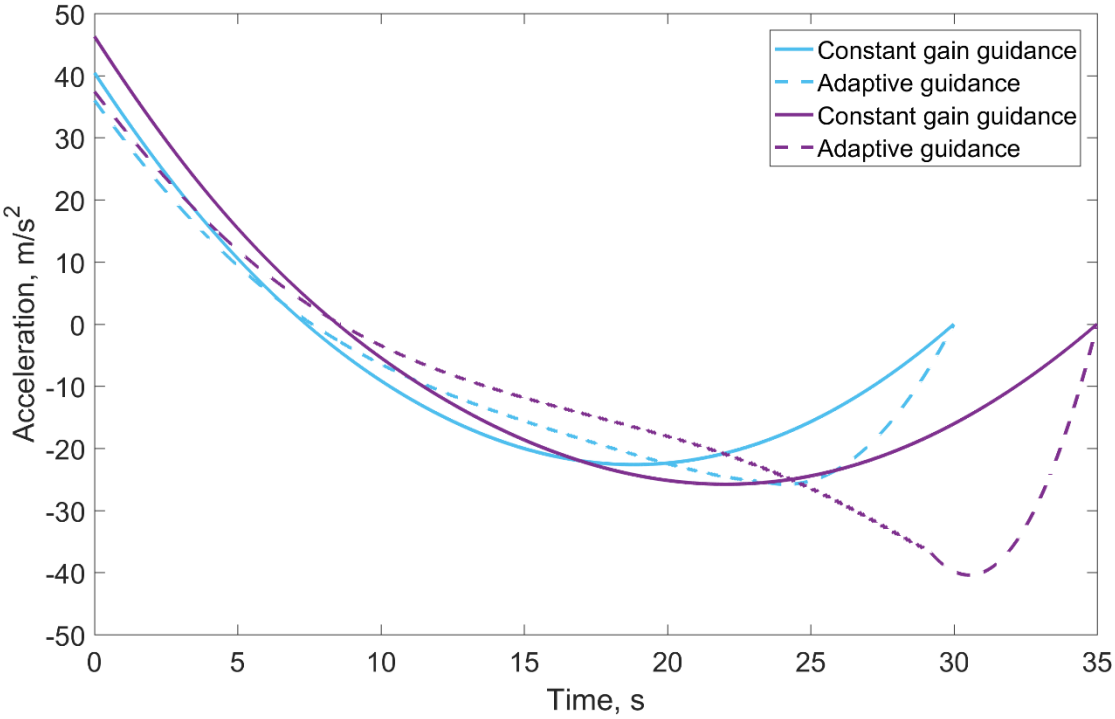

Figure 6.4 Acceleration histories with and without the adaptation routine.

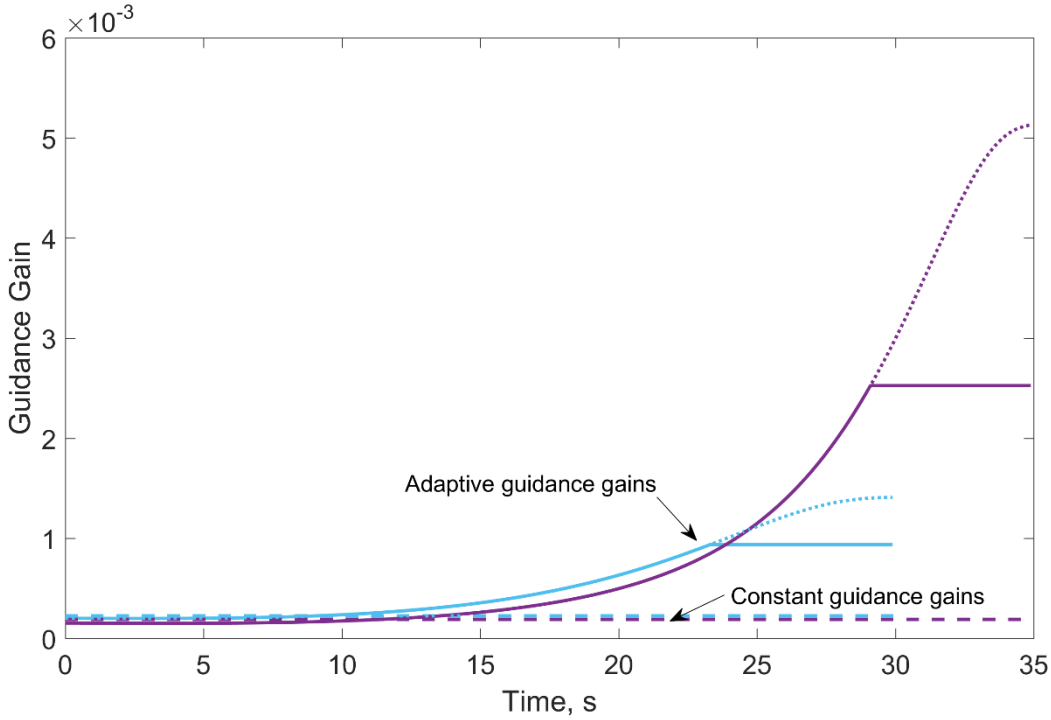

Figure 6.5 History of the guidance gains with and without the adaptation routine.

6.1.2 Performance under Autopilot Lag

In the previous chapter, the performance of the cubic look angle shaping under the autopilot lag was examined. In this section the adaptation routine is employed for the same test case and the distribution of the impact time error is revisited. When Figure 5.25 and Figure 6.6 are compared, the superiority of the adaptation can be observed such that the impact time error decreases more than 10 times.

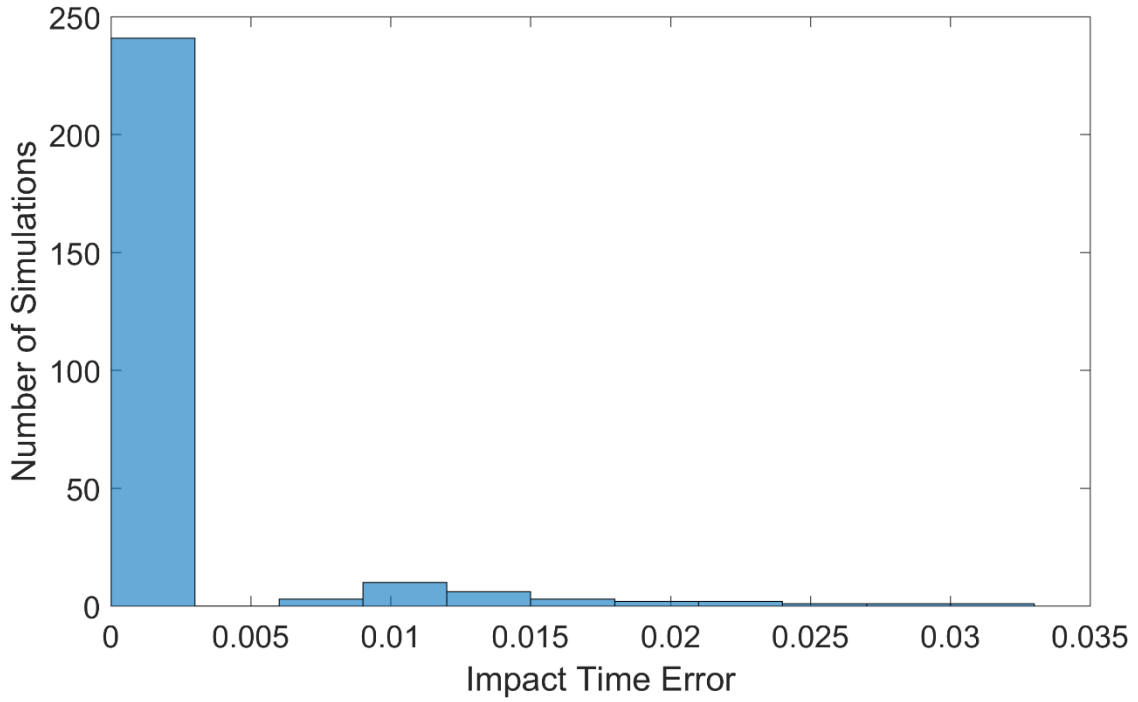

Figure 6.6 Histogram of the impact time error with the adaptive guidance.

6.1.3 Sensitivity of the Adaptation Routine

One important issue is the impact of the value of the threshold on the guidance performance. Here, the effect of the termination condition of the adaptation routine is investigated and the characteristic of the minimum threshold, $\Delta_{\min}$, is introduced. The discriminant of Eq. (6.1) is already given in Eq. (6.3). Since the determinant must be a positive value in order to avoid imaginary guidance gains, the following inequality must hold:

$$24V\left(t_f - t\right)r - 24r^2 > V^2\varepsilon^2\left(t_f - t\right)^2 \tag{6.4}$$

which is derived from Eq. (6.3). When the remaining range is close to the remaining trajectory length, i.e. $r \approx V(t_f - t)$, it can be easily inferred that Eq. (6.4) becomes false. Therefore, Eq. (6.3) converges to zero as the engagement nears the final time. This implies that the sensitivity of the gain calculation process will increase towards the end of the engagement. As a consequence, the adaptation needs to be stopped at a positive threshold, Δ_{min}.

The previous model is used to investigate the effect of the threshold value on the performance of the adaptive impact time control. The desired impact times are 30 s and 35 s. Δ_{min} is varied between 200 and 4000. Figure 6.7 shows the range-to-go when Δ_{min} is reached. It could be observed that the range-to-go at Δ_{min} is less for the engagement which lasts 35. The values of the range-to-go at the threshold value could not be accepted as negligible. Nevertheless, the simulations are satisfactory under this partially closed loop implementation. Therefore, depending on the application, the designer can determine a value, which does not result in unsatisfactory results.

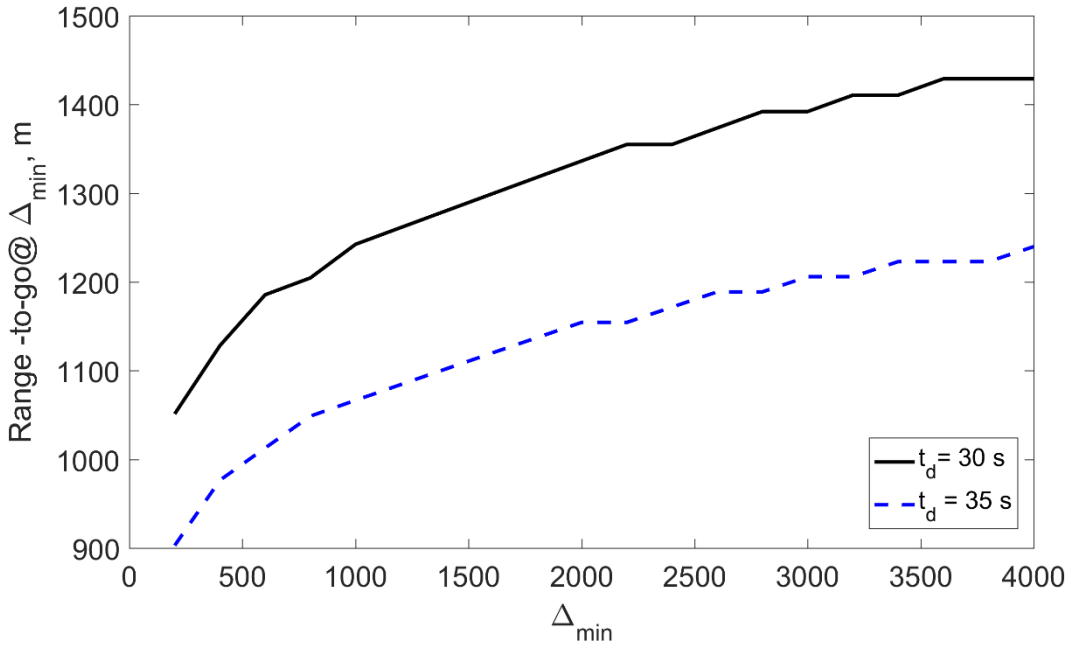

Figure 6.7 Range-to-go at Δ_{min}.

In Figure 6.8, two different but directly related parameters are presented. These are the discriminant given in Eq. (6.3), the difference between the length of the trajectory and the

range, and the last one is the adaptive guidance gain, all of which are normalized with respect to their initial values. The definition related to the normalized discriminant is

$$\Delta^* = \frac{\Delta}{\Delta_0} \tag{6.5}$$

where Δ_0 is initial value of the discriminant. The second normalized value is the difference between the length of the trajectory and the range is defined as

$$\Delta_S = \frac{V\left(t_f - t\right) - r}{Vt_f - R_0} \tag{6.6}$$

Moreover, the variation of Δ^* for each simulation is so negligible that the differences are not even visible. One might suggest that the threshold could be defined with respect to Δ_S. When Figure 6.8 is examined carefully, it is observed that Eq. (6.5) converges to zero faster than Eq. (6.6) for both of the desired impact times meaning that the sensitivity to calculate the guidance gain is already increased. So that, it is better if the threshold is defined over the discriminant given in Eq. (6.3), and not directly related with respect to the relation: $r \approx V(t_f - t)$. The variation of the adaptive gains are visible as presented in Figure 6.9. When these results are considered with Figure 6.7, $\Delta_{\min}$ = 2000 is selected for all of the simulations of this chapter.

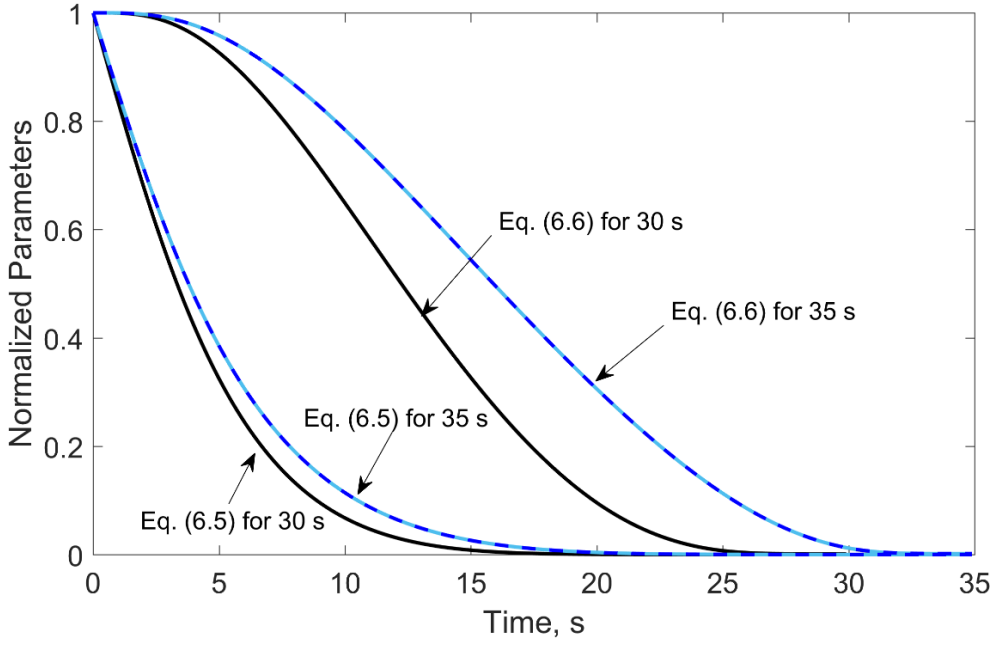

Figure 6.8 The histories of Eq. (6.5) and Eq. (6.6).

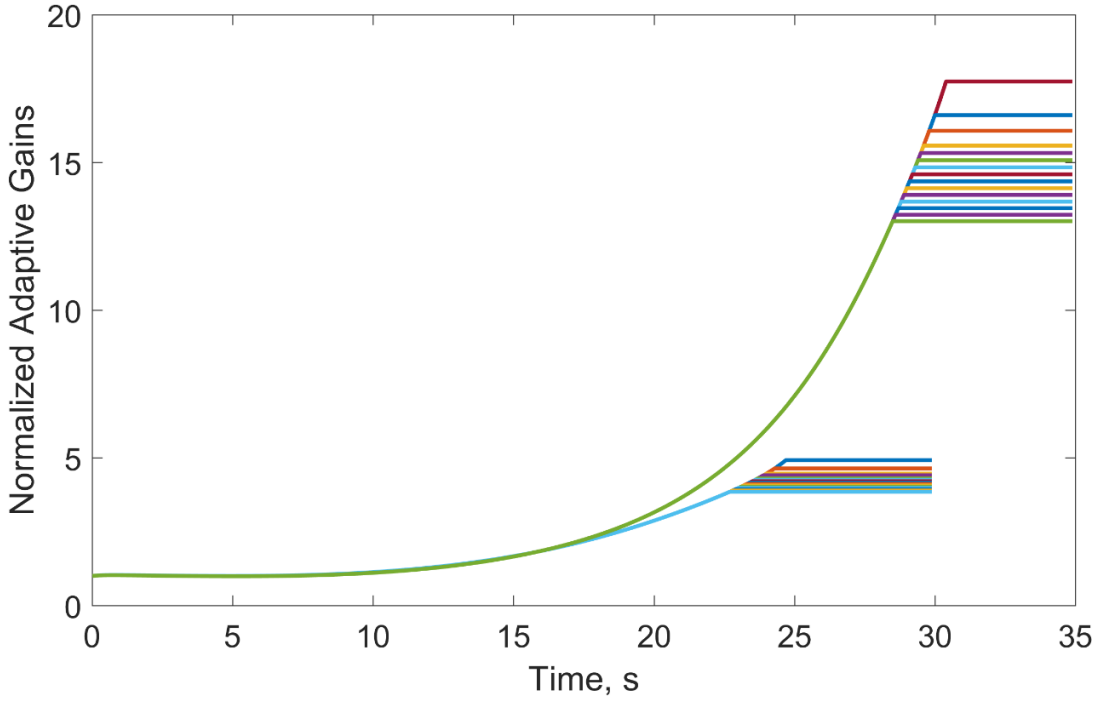

Figure 6.9 The histories of the normalized adaptive gains for different $\Delta_{\min}$.

6.2 Impact Time Control Under Field of View Constraint

After introducing the adaptation routine, impact time control under the FOV constraint can now be presented for the look angle shaping. As described in the range shaping, the guidance command is composed of three phases, which run sequentially:

$$\dot{\gamma} = \begin{cases} \bar{\kappa}_3 \left(t_d - t\right)^2 - \dfrac{2\varepsilon}{t_d - t} + \dot{\lambda} & \varepsilon \le \varepsilon_{\max} \\ \dot{\lambda} & \text{until } \dot{\varepsilon} < 0 \\ \bar{\kappa}_3 \left(t_d - t\right)^2 - \dfrac{2\varepsilon}{t_d - t} + \dot{\lambda} & \text{otherwise} \end{cases} \tag{6.7}$$

where $\bar{\kappa}_3$ represents the adaptive guidance gain and t_d is the desired impact time. The first phase continues until the time instant where the look angle reaches its limit. Afterwards, the constant look angle phase starts. This second phase continues until the commanded look angle rate becomes zero, which means that the look angle must be decreased to intercept the target. At that time instant, the final phase starts, which is the same guidance law as in the first phase. The analytical solutions of the switching time instants are not available for the nonlinear

domain. Therefore, the adaptive structure is considered for the constrained impact time control problem.

In order to demonstrate the impact time control under the FOV limit, several simulations are performed where the initial look angle is zero. The FOV limit is 50° and the desired impact times are 32 s and 34 s. The guidance commands are realized without latency. The trajectories can be seen in Figure 6.10, where the maximum altitudes are similar. However, the curvatures of the final phases are quite different. Figure 6.11 illustrates the look angle histories. Although the difference between the impact times is two seconds, the duration of the saturated phase is longer. The acceleration histories are in correlation with the look angle histories; thus, when the final phase starts, the second scenario demands more acceleration as it could be observed in Figure 6.12.

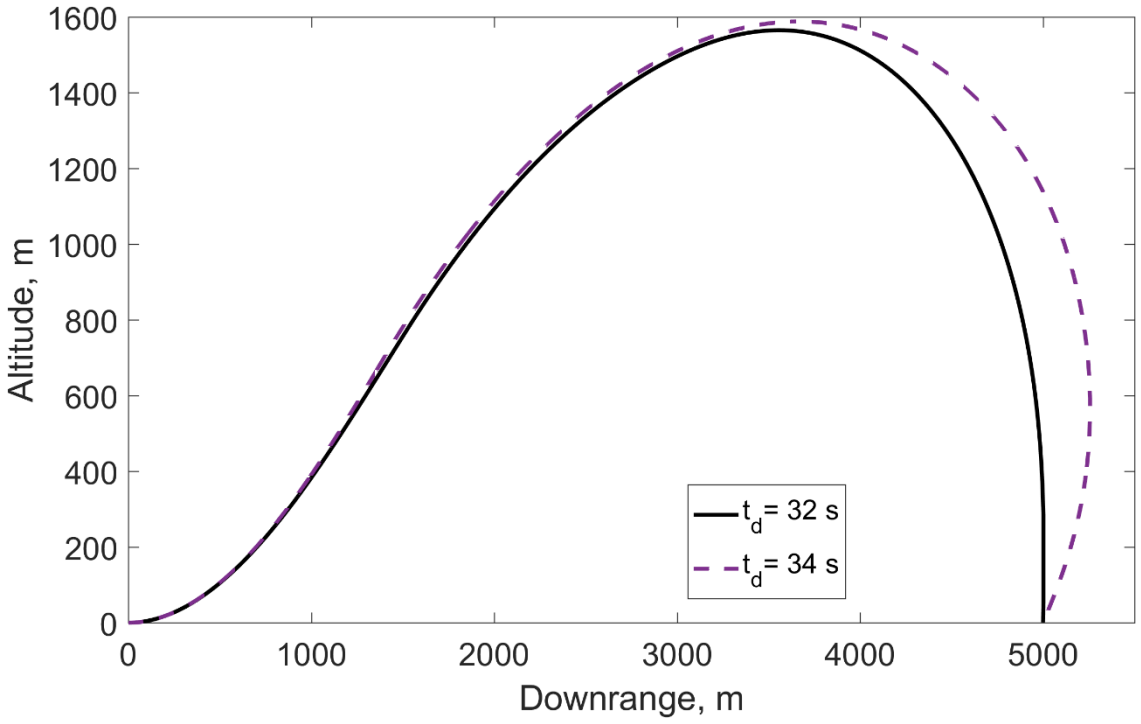

Figure 6.10 Trajectory histories under the FOV constraint obtained by adaptive guidance.

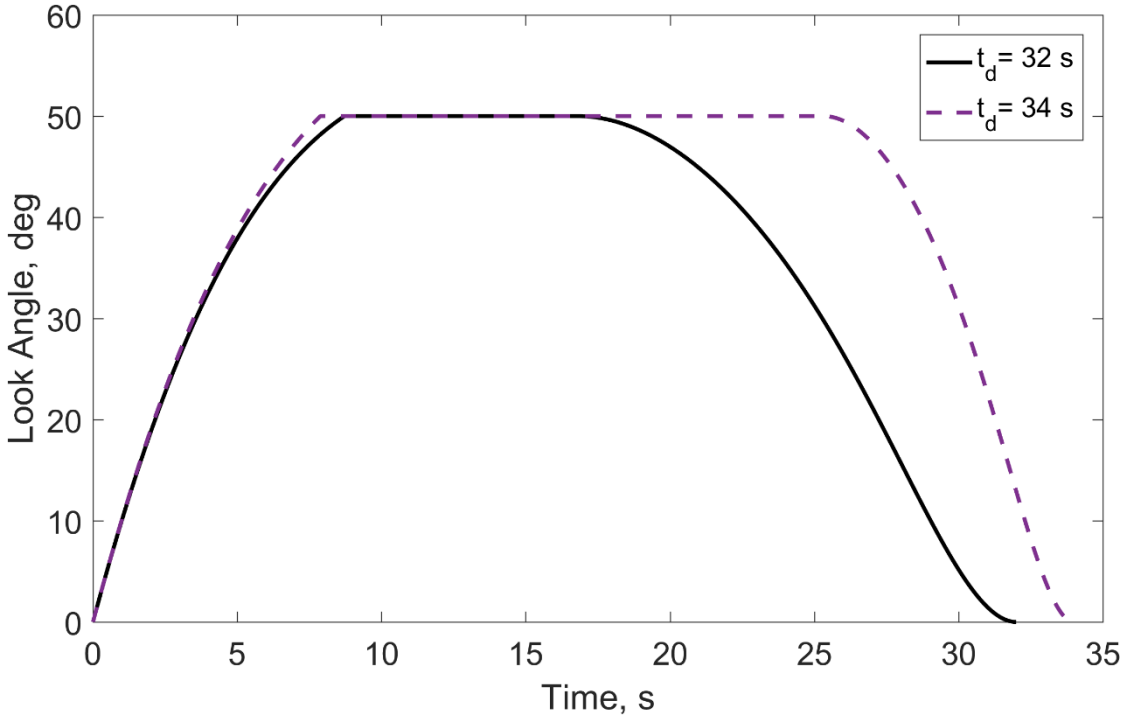

Figure 6.11 Look angle histories under the FOV constraint.

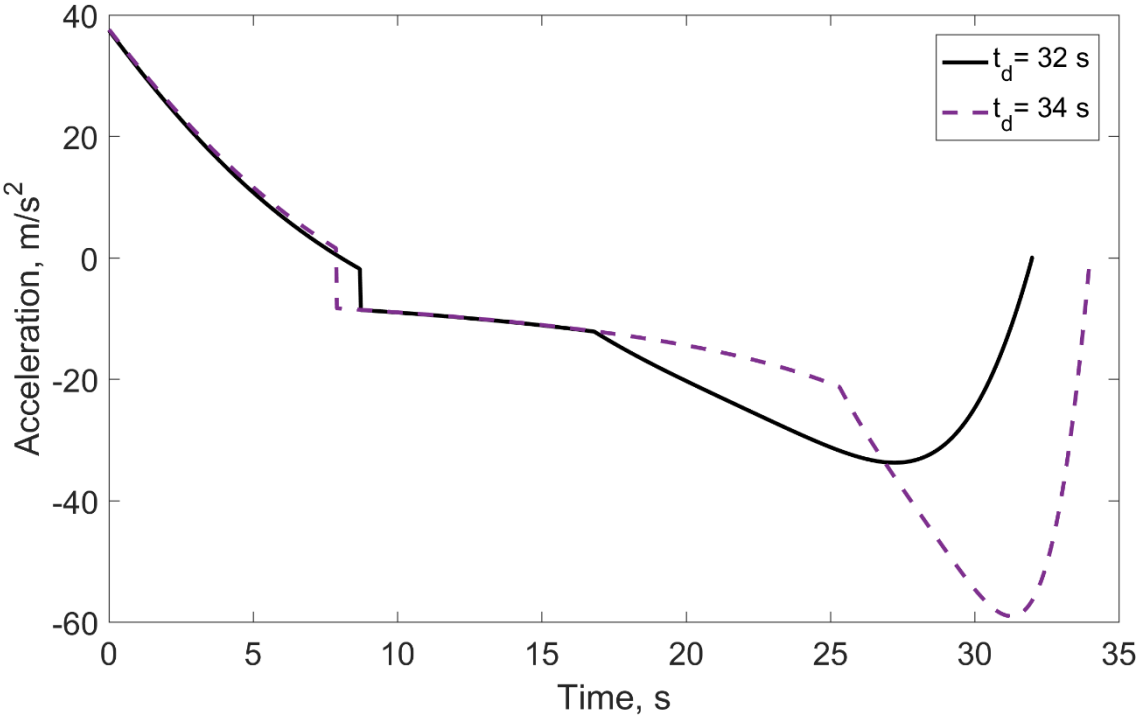

Figure 6.12 Acceleration histories under the FOV constraint.

6.3 Prediction of the Mean Speed

In this subsection, the adaptive guidance scheme will be extended to handle the case of non-constant missile speed. The first step is to rewrite Eq. (2.8) as

$$R = \int_{t}^{t_f} V \cos \varepsilon \left(\kappa_n, t \right) dt \tag{6.8}$$

where in general, the speed changes under the action of accelerations due to thrust, drag and gravity. This can be modeled as

$$\dot{V} = a_T - a_D - g \sin \gamma \tag{6.9}$$

Here, a_T and a_D represent the related components of the acceleration under the thrust and the drag forces, respectively. However, Eq. (6.8) may be approximated as

$$R \approx \bar{V} \int_{t}^{t_f} \cos \varepsilon \left(\kappa_n, t \right) dt \tag{6.10}$$

where $\bar{V}$ is the mean speed to be encountered throughout the engagement, i.e. the future mean speed.

Since the true value of the future mean speed is not available before the flight, the next question is how to predict it so that the guidance gain can be calculated properly. The key to speed prediction is the ability to integrate Eq. (6.10). The challenge here comes from the fact that the speed change will be governed by the yet-undetermined shape of the trajectory. This may be so; but, the thrust profile as a function of time and the drag model as a function of several states would usually be available. It is common that the drag model is composed of both base and induced components. Unlike the former, which is only dependent on the speed, the latter might further complicate the prediction process since it correlates the drag force with the lateral acceleration. Likewise, the effect of gravity also complicates the process since it enters the system through the flight path angle. The technical approach adopted in this study to overcome such complications is to make use of the analytical foundations laid out in the polynomial look angle shaping method. In Chapter 5, the profile of the flight path angle and

the lateral acceleration, if required, were made available for the linearized kinematics to be used in the prediction algorithm.

The algorithm for the proposed prediction scheme is presented in Table 6.1 in pseudo-code form. The algorithm takes the old (or user-defined initial) value of the predicted mean speed and checks whether the discriminant in Eq. (6.3) is higher than the threshold. If not, the old value of the guidance gain is preserved. If the opposite condition is true, the guidance gain will be calculated using Eq. (6.2). Then, the speed profile of the missile from the current time until the final time is predicted by means of Euler integration. The derivative of the speed required for the integration process is obtained from Eq. (5.46), which assuming no induced drag for the sake of simplicity, involves the flight path angle profile predicted by Eq. (5.46). This profile must be shifted by the instantaneous LOS angle value so as to change the frame of reference from the LOS frame to the inertial frame as depicted in Figure 6.1. After the predicted speed profile is obtained, its mean value is calculated by integrating the profile and dividing it by the remaining flight time. The final step is to get an updated version of the predicted mean speed. This is done by obtaining the difference between the predicted mean speed and the previous value of the updated version, scaling this difference, and adding it to the previous value of the updated version. The difference between the predicted mean speed and its updated version is important since the whole iteration is driven by this quantity. The iteration stops when the difference goes below a specified tolerance.

It should be noted that there are several parameters that determine the performance of the algorithm. Firstly, the utility of $\Delta_{\min}$ must be mentioned. Then, as for the integration step, h, its importance is self-evident; the value should be sufficiently small to be able to generate an accurate speed profile. Nonetheless, the impact on computational costs should be kept in mind. Next, the iteration gain, σ, which is used in updating the predicted mean speed, plays a central role since it decides how much the old value will change. Lastly, the tolerance, ϑ, which acts on the magnitude of the difference between the predicted mean speed and its updated version, is the quantity that determines if the iteration will continue or stop. Like the integration step, it should be set sufficiently small; however, it is evident that a smaller value would lead to more number of iterations.

Table 6.1 Pseudocode for mean speed prediction.

assign $\bar{V} = \bar{V}_{old}$

assign $\bar{V}'$ // a sufficiently small value than $\bar{V}$

while $\left|\bar{V} - \bar{V}'\right| > \vartheta$ // ϑ : a specified tolerance

calculate Δ from Eq. (6.3)

if $\Delta > \Delta_{\min}$

calculate κ_3 from Eq. (6.2)

for t to t_f // with a sufficiently small integration step, *h*

calculate $\gamma(t)$ from Eq. (5.45) with $y_0 = 0$

$\gamma(t) \leftarrow \gamma(t) + \lambda$ // change from LOS frame to Inertial frame

calculate $\dot{V}(t)$ from Eq. (6.9)

calculate $V(t)$ with Euler integration

end // speed profile from t to t_f is available

$\bar{V} = \int_t^{t_f} V(t)dt / (t_f - t)$ // predicted mean speed

$\bar{V}' = \bar{V}'_{old} + \sigma\left(\bar{V} - \bar{V}'_{old}\right)$ // σ : iteration gain

else

$\kappa_3 = \kappa_{old}$

end

end

6.3.1 Performance of the Mean Speed Prediction

Here, efficiency of the prediction will be analyzed for several impact times. For that purpose, instead of adaptation throughout the engagement, a constant guidance gain is preferred. This guidance gain is computed for once with the Newton-Raphson method, which means another line after finding κ_3 from Eq. (6.2) in Table 6.1 as described in Section 5.6. The initial look angle is zero and the autopilot time constant is $\tau = 0.3\,s$. The parameters of the

prediction algorithm is given in Table 6.2. The speed is varying under gravity and base drag, $a_D = C_{D,0}V^2$ where $C_{D,0} = -2.10^{-5}$.

Table 6.2 Parameters for the prediction algorithm.

Symbol	Magnitude	Definition
$\Delta_{\min}$	2000	Threshold
ϑ	0.01 m/s	Specified tolerance
σ	0.25	Iteration step
$\bar{V}'$	150 m/s	Sufficiently small value than the initial speed
$\bar{V}_{old}$	200 m/s	Initial guess of the predicted mean speed
h	0.001 s	Euler integration step

Table 6.3 presents the summary of the prediction performance and the guidance gain for the nonlinear engagement. The predicted and the true mean speeds are quite comparable. The maximum impact time error is less than 1.5 seconds. Nevertheless, in a varying and nonlinear environment without any update throughout the engagement, it could be said with confidence that the proposed impact time control method under varying speed is a promising approach.

Table 6.3 Prediction performance of the proposed method with the nonlinear domain.

Desired Impact Time, s	$\bar{V}$, m/s (predicted)	$\bar{V}$, m/s (true)	κ_3	Impact Time	Iteration Number
30	171.94	172.3	$9.264.10^{-5}$	29.98	11
35	155.51	156	$9.245.10^{-5}$	34.55	14
40	142.10	142.7	$7.37.10^{-5}$	38.66	15

Figure 6.13 shows the histories of the predicted and the true speeds for the first scenario. Although these look quite similar, more difference is observable in Figure 6.14, which is the second scenario. Last, in Figure 6.15, it is more apparent that the predicted speed is less than the true one. The cause of this difference is the increased look angle for accomplishing a longer impact time. As the geometry is getting far from the linear conditions, the flight path angle

equation, which is obtained in the linear domain results in performance degradation. In addition, the error caused by numerical integration of range is also a degrading factor for such a problem. However, although there is this much difference for the last scenario, the impact time error could be said to be acceptable. Additionally, the predicted speeds are always less than the true speeds for this specific examples. However, this behavior cannot be generalized. Moreover, the proposed method gives the time history of the speed beforehand, which is also precious. For instance, the minimum speed would be also important to complete a mission successfully in real applications.

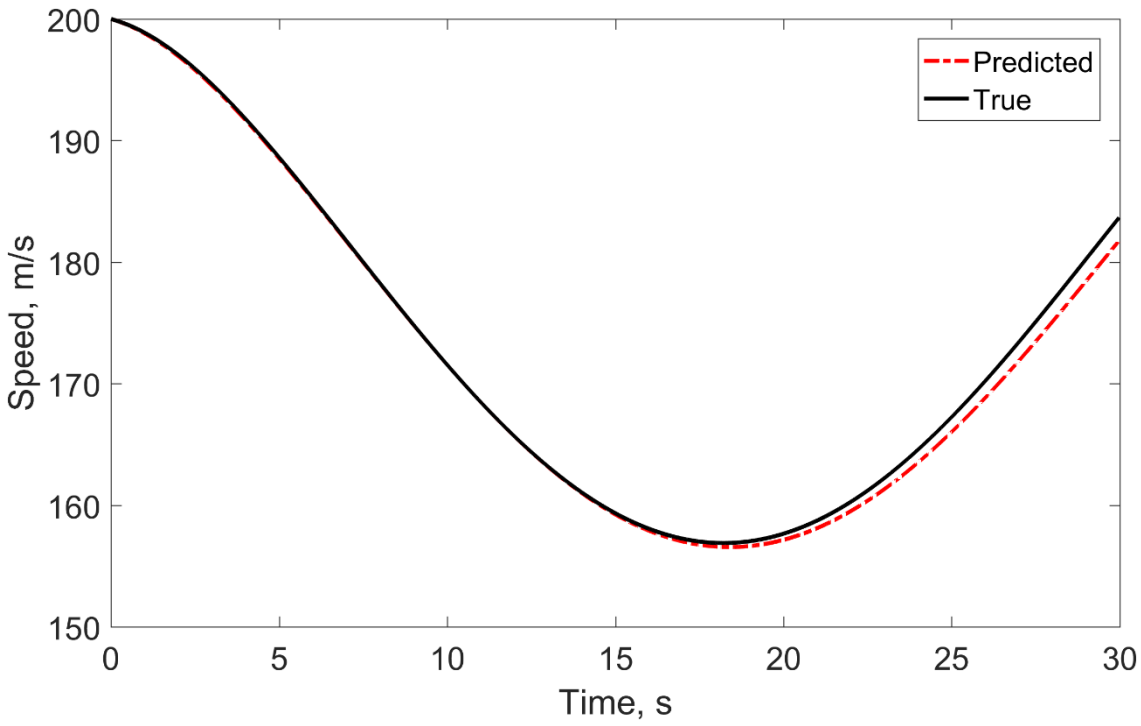

Figure 6.13 Predicted and the true speed histories for 30 s.

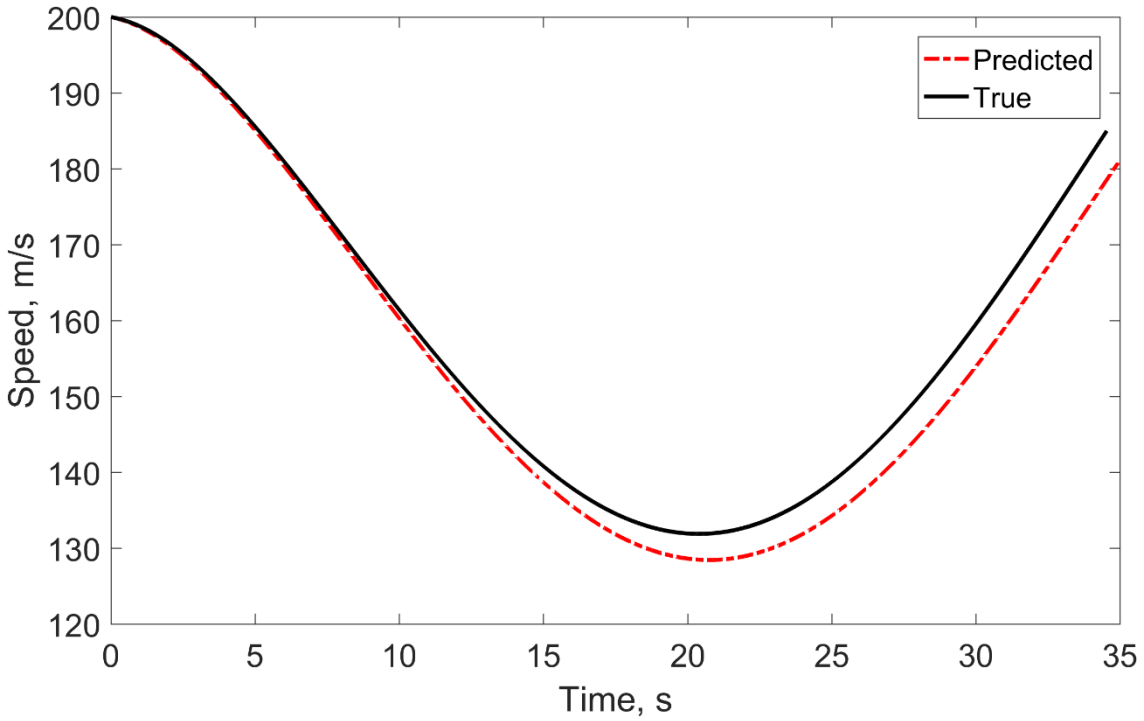

Figure 6.14 Predicted and the true speed histories for 35 s.

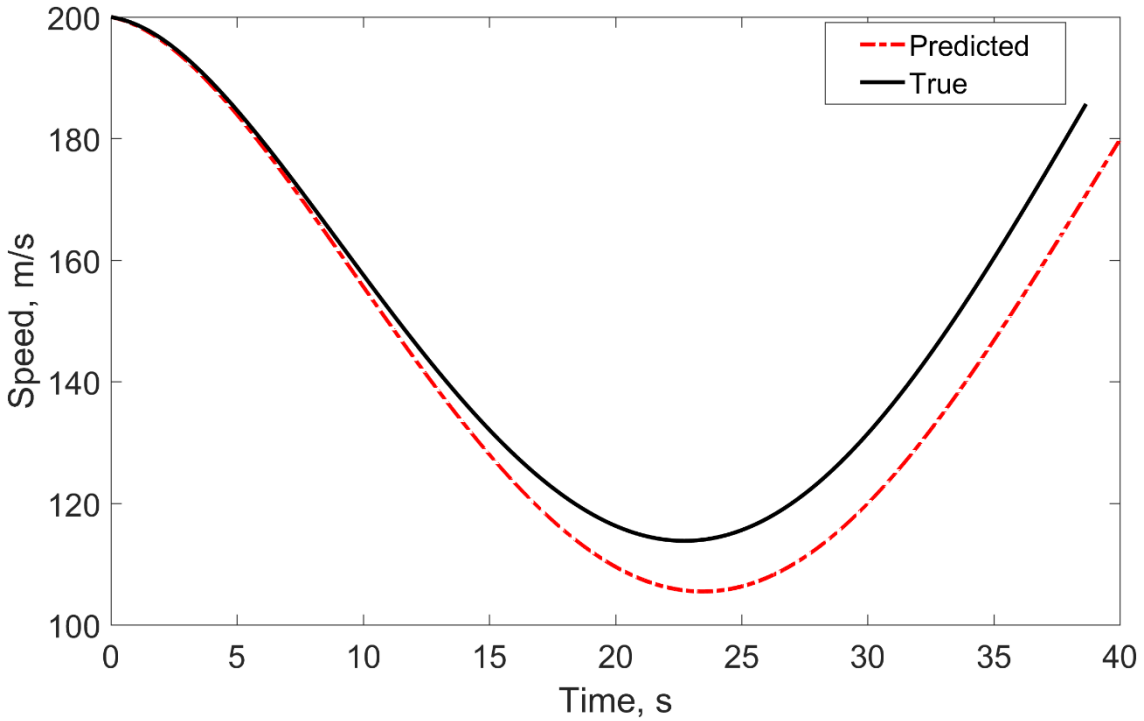

Figure 6.15 Predicted and the true speed histories for 40 s.

6.4 Predictive-Adaptive Guidance Scheme for Impact Time Control

In this section, impact time control with a predictive-adaptive structure is introduced, where the mean speed and the guidance gain will be updated during the engagement. This way, the guidance algorithm can handle uncertainties and variations throughout the engagement in a closed loop fashion, which is the main advantage of the predictive-adaptive structure. The disadvantage, on the other hand, is the increased computational effort. Nonetheless, it is to be noted that if the guidance gain is calculated via Eq. (6.2), the computational burden of the algorithm given in Table 6.1 could be acceptable.

In this chapter, no information about the impact time interval is given. Since with the predicted mean speed, the same procedure described in Section 5.5.4. would be applicable. In addition to the mean speed, the minimum speed will be the most important factor to define the impact time interval for realistic applications, since the minimum speed is related with the aerodynamic efficiency of the system. Fortunately, the minimum speed could also be extracted from the prediction algorithm as the time history of the speed is already available.

In order to show the efficiency of the method, a ground-to-ground attack scenario is performed for the same desired impact time ranges as in the previous subsection. The update rate of the algorithm is 10 Hz. All of the simulations satisfy the desired impact time and the miss distance. However, this was not the case for the non-adaptive application as it could be seen in Table 6.3. The trajectory and the acceleration histories of the simulations are presented in Figure 6.16 and Figure 6.17. The acceleration histories shown are always the aerodynamic acceleration, in which gravity is not included; that is the maneuver response of the missile. In Figure 6.18, the speed histories are displayed, where the deviation from the initial speed is not negligible. Figure 6.19 illustrates that the look angle reaches up to 50° for the last scenario. As seen, it is quite difficult to talk about the linear kinematics anymore; in contrast, the engagement geometry is highly nonlinear. Figure 6.20 is an important figure, which shows the efficiency of the predictive-adaptive impact time control. Although the predicted and true mean speeds are similar for the first scenario, it could be observed that the difference increases when the engagement lasts longer. When Figure 6.20 is considered together with Figure 6.19, it is seen that the difference of the predicted and the true mean speed increases when the look angle is high. The adaptive gains can be examined in Figure 6.21. It shows that approximately the last 10 seconds of each engagement does not involve any prediction and adaptation, which means partially closed loop application in terms of impact time control. Nevertheless, the

scenarios are successfully terminated. Finally, the iteration numbers are presented in Figure 6.22. The maximum iteration numbers are 12, 16 and 18 for the corresponding scenarios. It could be said that in general the maximum iteration number occurs at the initial time, where the algorithms start with a blind information of the mean speed, which is the initial speed. If it could be set to a more trustworthy initial value, then the initial iteration number would significantly decrease. Additionally, the immediate decrease of the number of the iterations after the initial time verifies that a successful initial prediction is done.

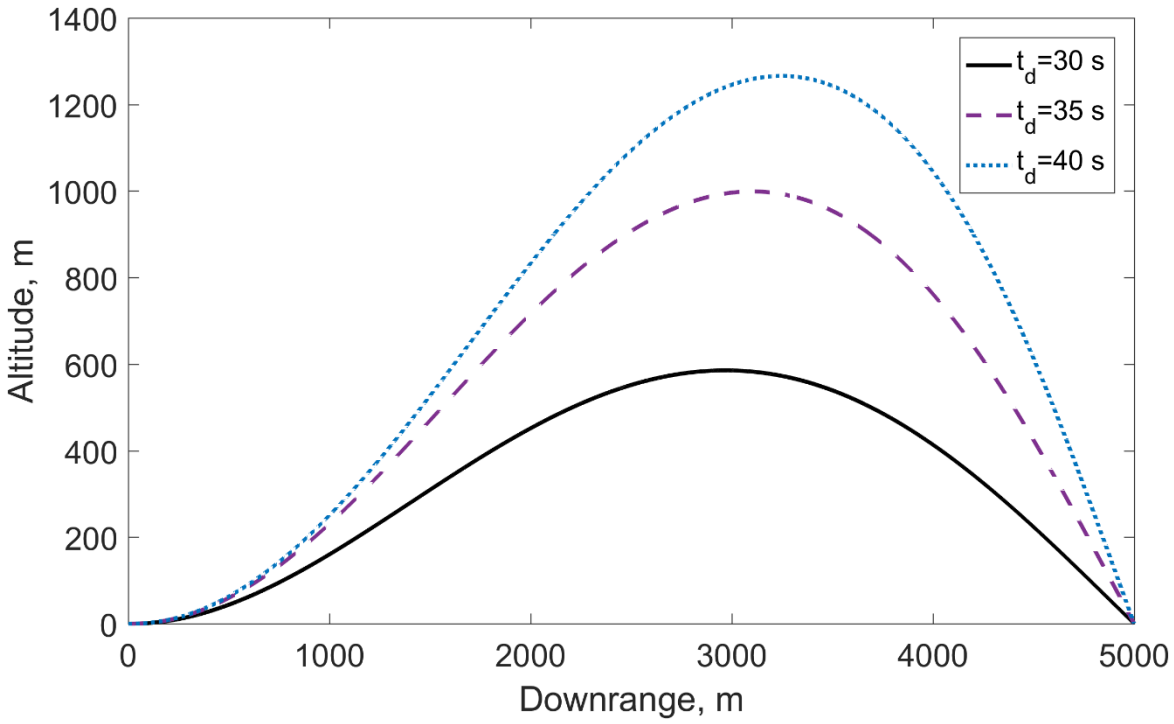

Figure 6.16 Trajectory histories of the realistic scenarios for several impact times.

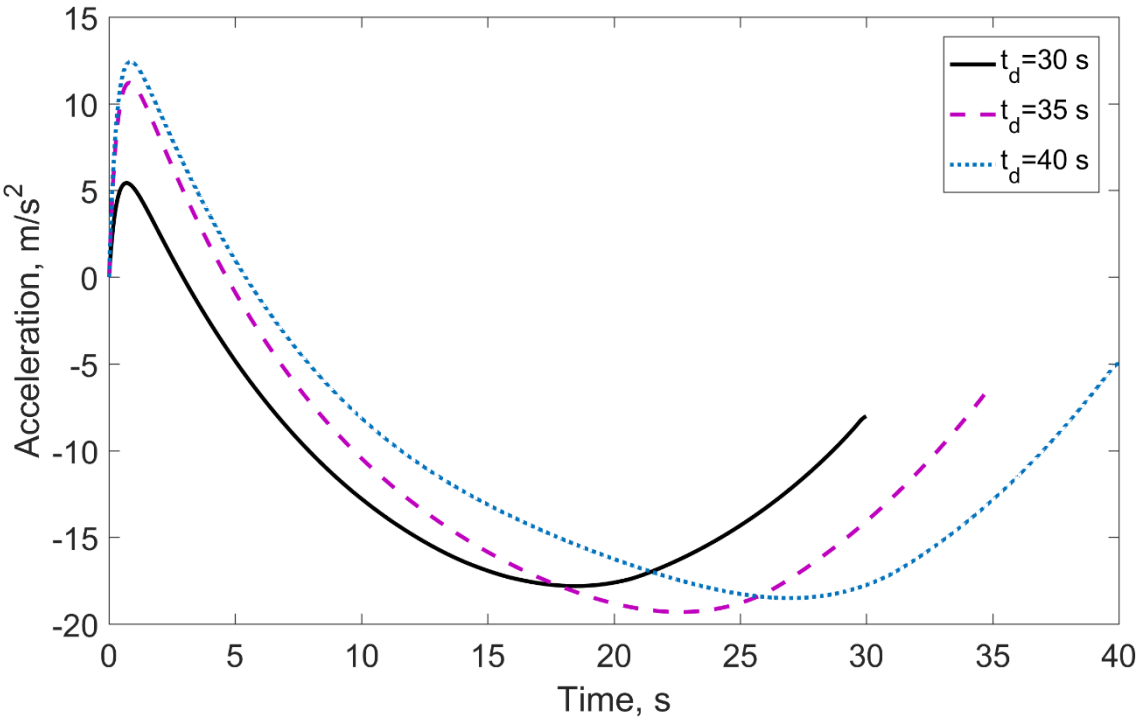

Figure 6.17 Acceleration histories of the realistic scenarios for several impact times.

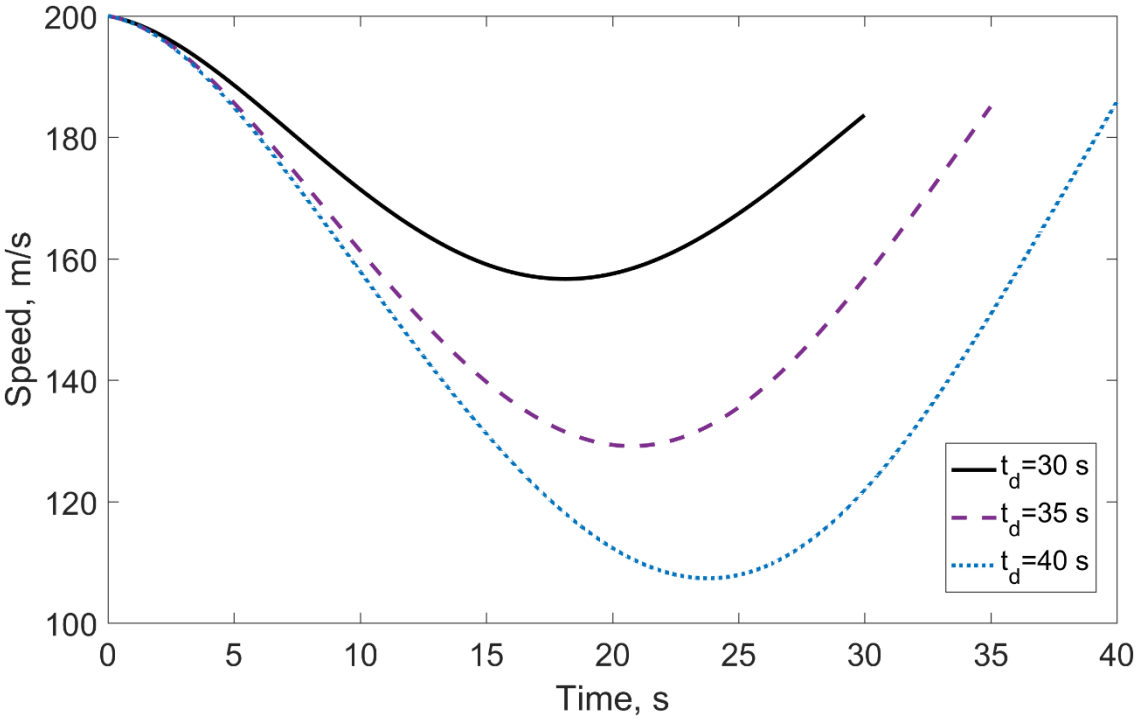

Figure 6.18 Speed histories of the realistic scenarios for several impact times.

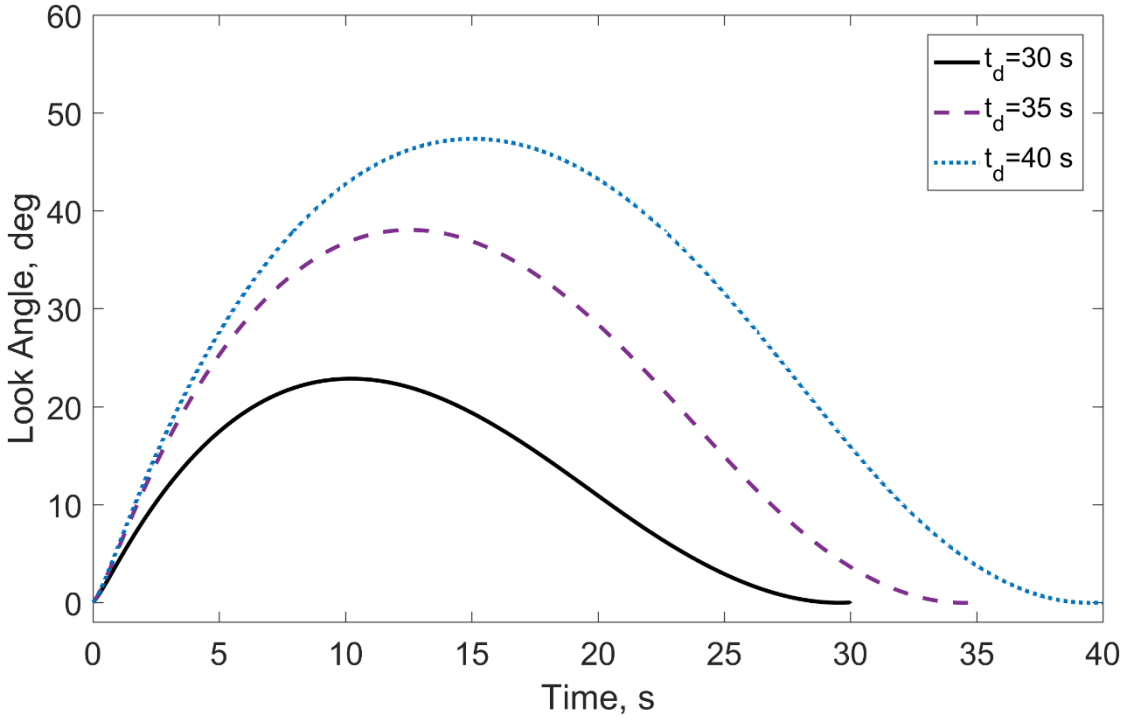

Figure 6.19 Look angle histories of the realistic scenarios for several impact times.

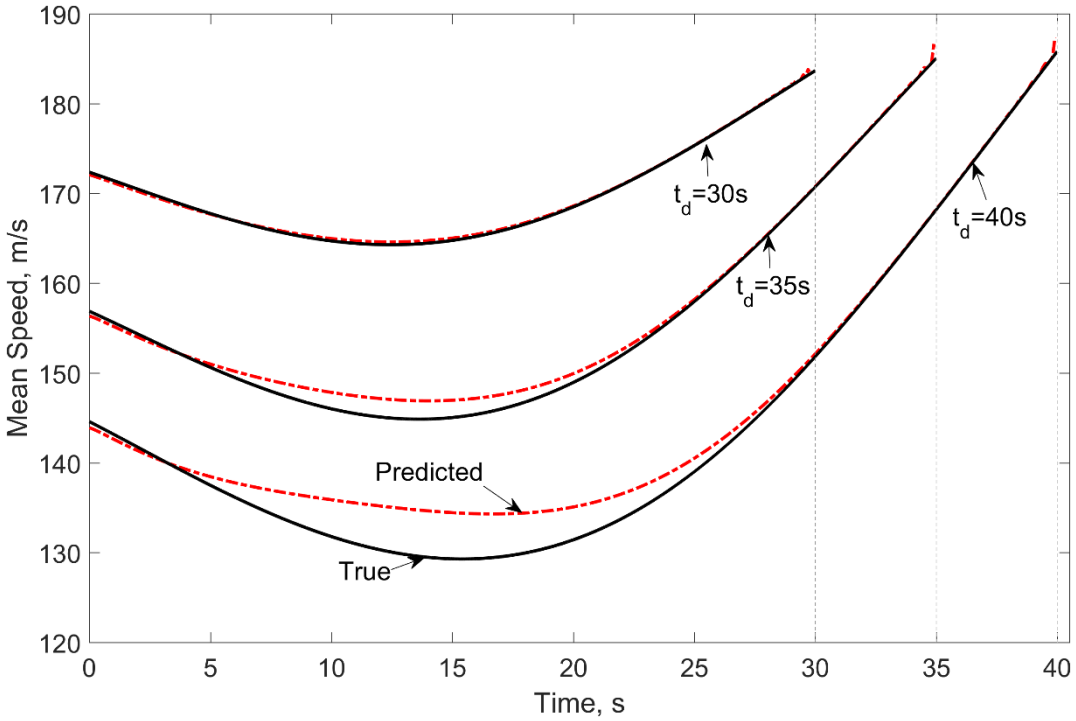

Figure 6.20 Mean speed histories of the realistic scenarios.

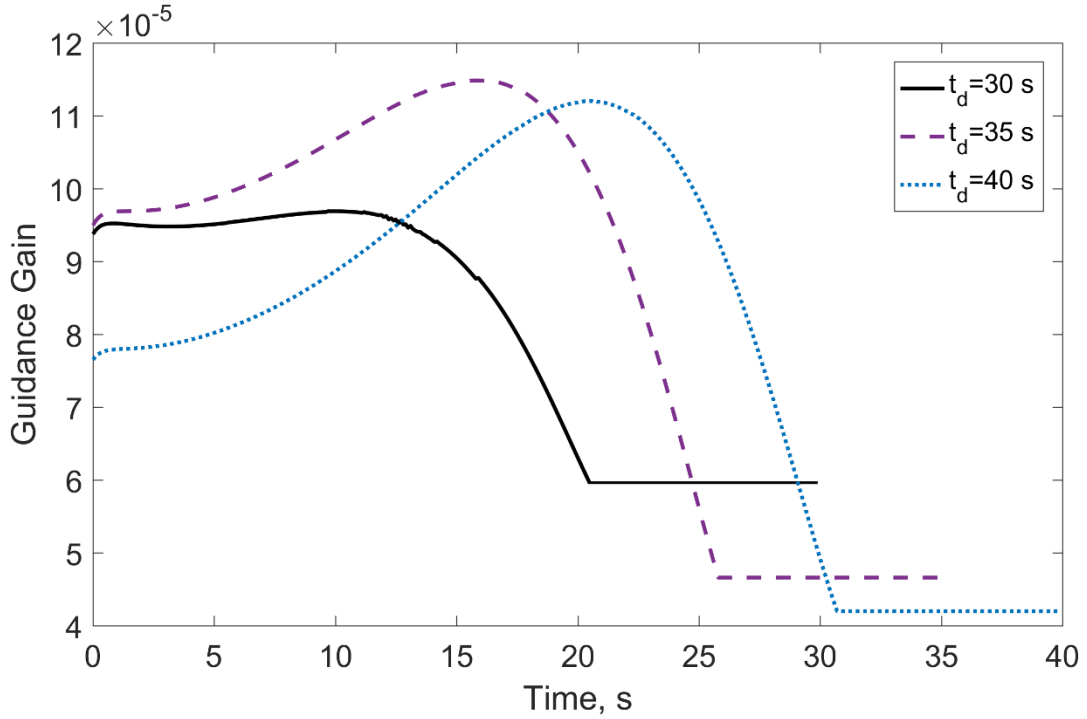

Figure 6.21 Adaptive guidance gains of the realistic scenarios.

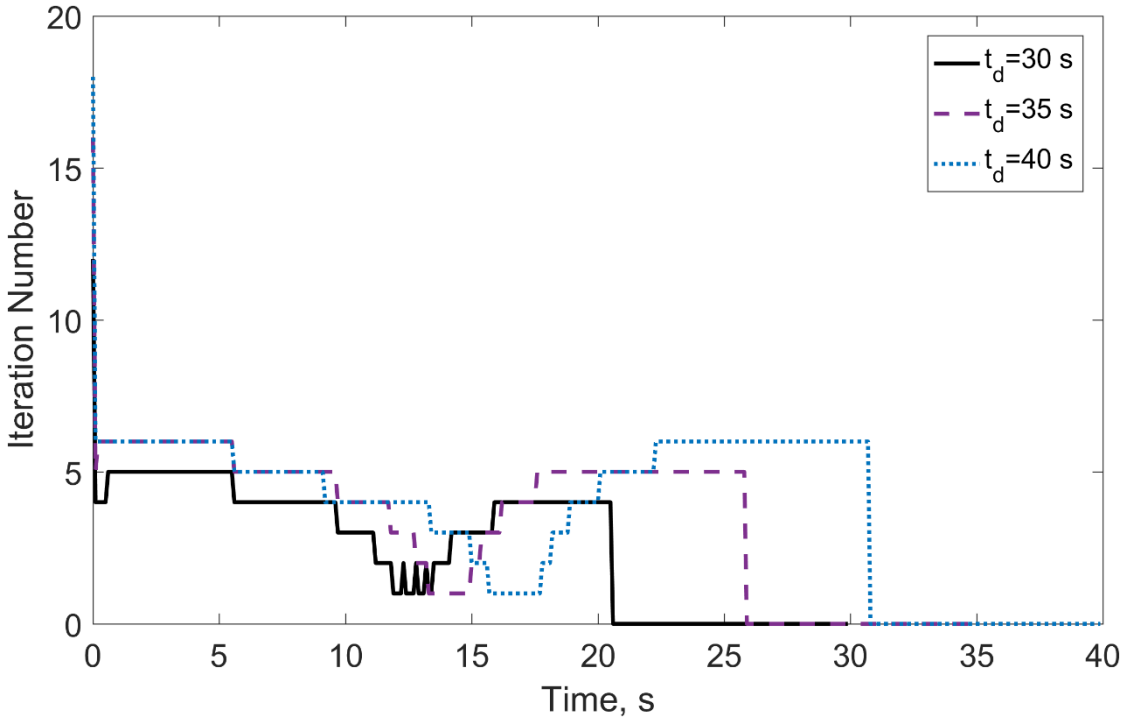

Figure 6.22 Iteration numbers of the predictive-adaptive algorithm for the realistic scenarios.

Next, the effects of the tolerance and the integration step on the guidance performance is investigated. For this purpose, the last scenario, which is the worst case of the previous

examples, is selected. The variations of the speed tolerance and the integration step are given in Table 6.4. The simulations are terminated either when the range is less than one meter or the desired impact time is reached to present the range-to-go at the desired impact time without capturing the target. It needs to be reminded that the range-to-go at intercept is not meant to be the miss distance because there is not any effort for avoiding the miss distance. For instance, simply switching to PN when the adaptation stops could be suggested. However, the performance of the proposed algorithm is to be emphasized so that no switching or a different implementation are suggested. The predictive-adaptation routine is run as in the previous examples with 10 Hz. The initial guess of the mean speed is now the outcome of the previous simulation result, which is 143 m/s. So, the effect of a better initial guess for the prediction algorithm could also be observed.

Table 6.4 The parameter variation of the predictive-adaptive algorithm.

ϑ : Speed Tolerance	$[0.01 \quad 0.05 \quad 0.1 \quad 0.2 \quad ..... \quad 0.9 \quad 1 \quad 2]$ m/s
h : Integration Step	$[0.001 \quad 0.01 \quad 0.02 \quad 0.1 \quad 0.2 \quad ..... \quad 0.9 \quad 1]$ s

Figure 6.23 shows the impact time error, which is obtained by dividing the range-to-go at the desired impact time by the final velocity. As it is seen, under the worst tolerance values, the impact time error is less than 1.2 s. In Figure 6.24, it is seen that when the integration step is increased, the range-to-go at the desired impact time increases drastically. On the other hand, ϑ does not have a significant role on the range-to-go at intercept. The iteration number of this scenario was 18 for ϑ = 0.01 m/s and h = 0.001 s. It is now 10 for the same simulation parameters and with the new initial guess of the mean speed. As it could be guessed, the iteration number decreases with the increased ϑ. It is possible to say that the integration step does not have a major effect on this behavior. Figure 6.25 is another prospect of the same results. Now, the main effector of the range-to-go at intercept is seen more clearly, i.e. almost linearly increasing behavior with the integration step. Meanwhile, the integration step results in an increase on the iteration number; nonetheless, ϑ is the most dominant parameter for the required iteration number.

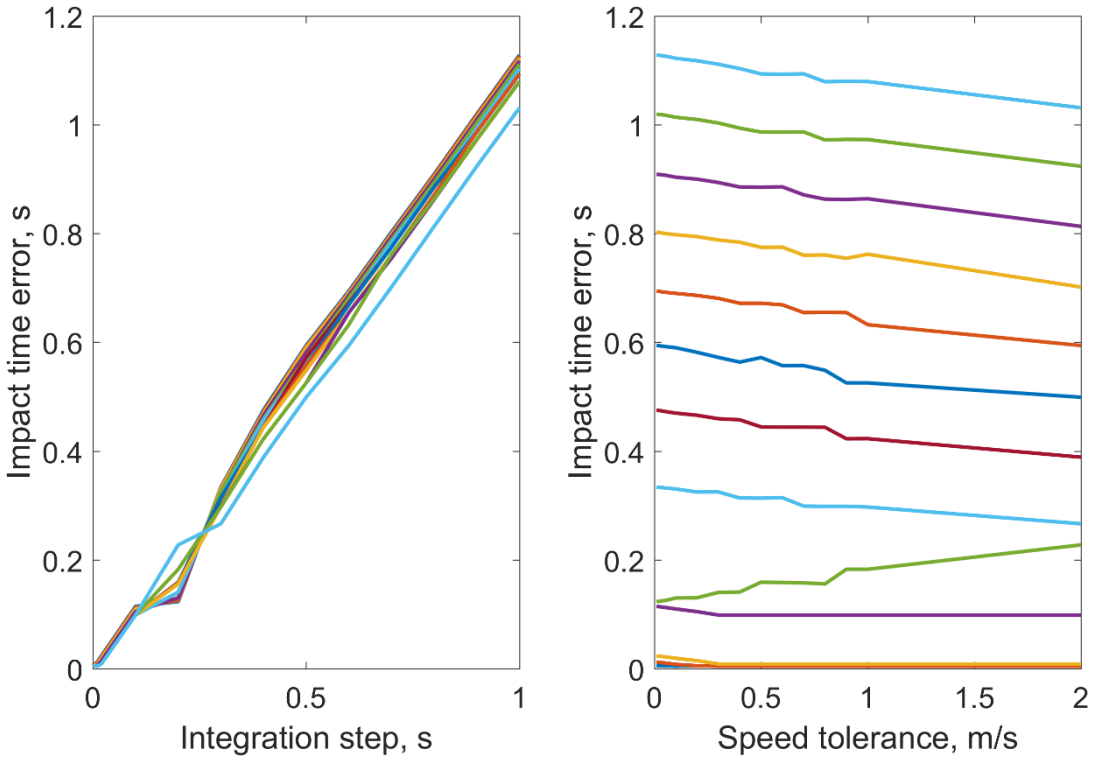

Figure 6.23 Impact time error under different tolerance values.

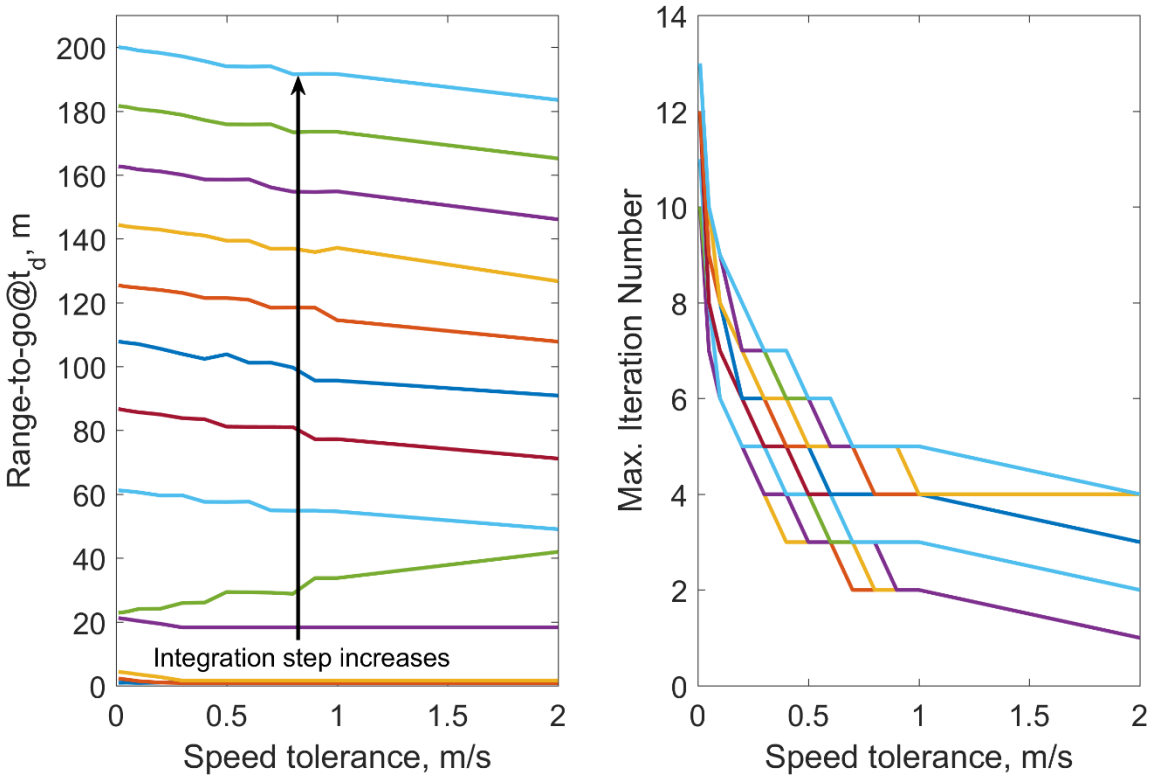

Figure 6.24 Effect of the speed tolerance on the guidance performance.

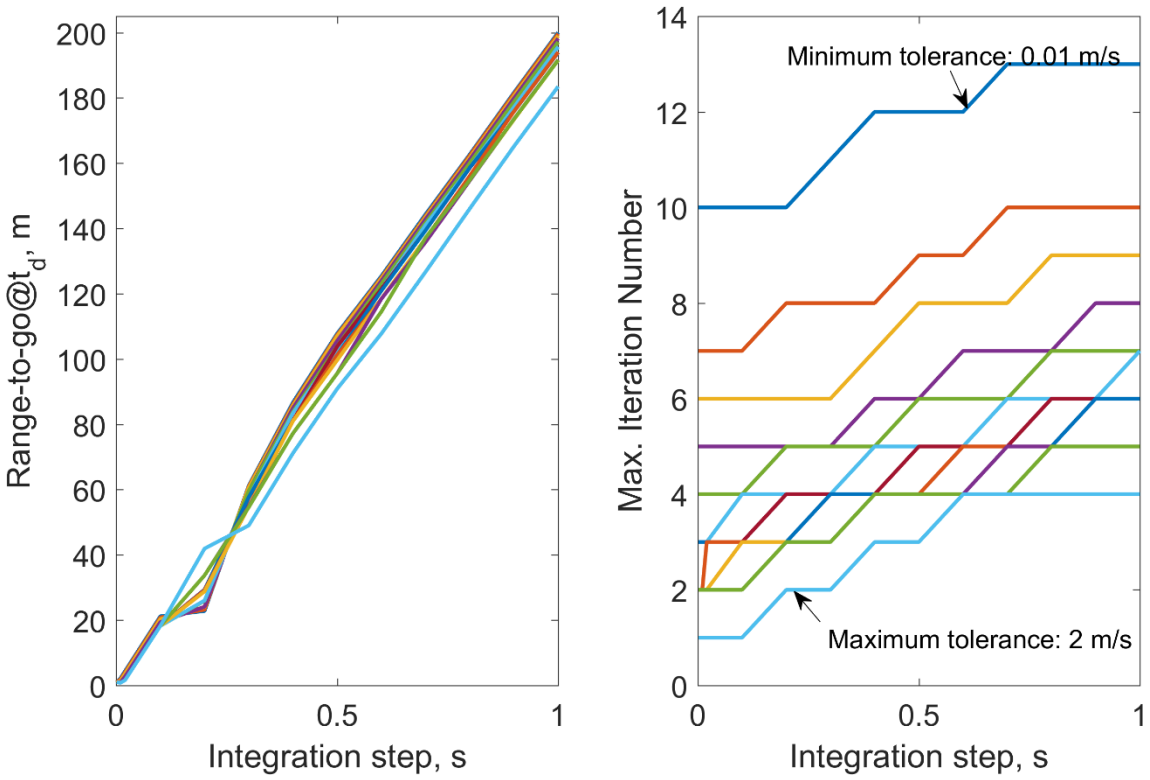

Figure 6.25 Effect of the integration step on the guidance performance.

6.4.1 Optimality Analysis of the Predictive-Adaptive Impact Time Control

The optimality of the cubic look angle shaping was investigated for the constant speed case in Chapter 5. The ratio of the cost functions was not far from unity; thus, a similar study is carried out for the varying speed problem. This time, the optimal guidance command is computed offline with a software program [63] named as FALCON, which is a free tool to solve optimal control problems.

The mathematical representation of the cost function is

$$J = \frac{1}{2}\int_0^{t_f} a^2 dt \tag{6.11}$$

The states are the downrange, the altitude, the speed, the flight path angle and its rate represented as

$$\bar{x} = \begin{bmatrix} X & Z & V & \gamma & \dot{\gamma} \end{bmatrix}^T \tag{6.12}$$

The control input is

$$u = \dot{\gamma}_c \tag{6.13}$$

The autopilot lag is also modelled with the following relation of the guidance command and the flight path angle rate:

$$\dot{\gamma} = \frac{1}{\tau s + 1}\dot{\gamma}_c \tag{6.14}$$

The initial conditions are

$$\bar{x}_0 = \begin{bmatrix} X_0 & Z_0 & V_0 & \gamma_0 & \dot{\gamma}_0 \end{bmatrix}^T \tag{6.15}$$

and except for the downrange and the altitude, the final states are defined to be free:

$$\bar{x}_0 = \begin{bmatrix} X_f & Z_f & \text{free} & \text{free} & \text{free} \end{bmatrix}^T \tag{6.16}$$

First, a sample comparison is presented between the optimal and the predictive-adaptive impact time control. The initial look angle is zero and the desired impact time is 30 s. The time constant of the autopilot is τ = 0.3 s. In addition, the guidance commands are held when the range is less than 50 meters. The cost functions turn out to be 678.6 m^2/s^3 and 643.3 m^2/s^3. In Figure 6.26, the trajectory and the speed histories are shown. Since the cost functions are so close, these histories are not far from each other, either. The optimal solution decreases the speed slightly more whereas the final speeds are the same. The look angles and the accelerations can be observed in Figure 6.27. The maximum look angle of the optimal solution is slightly more than that of the proposed look angle shaping method. When the accelerations are compared, it is seen that the initial acceleration of the look angle shaping is more than that of the optimal one. However, for the maximum acceleration comparison the opposite is true.

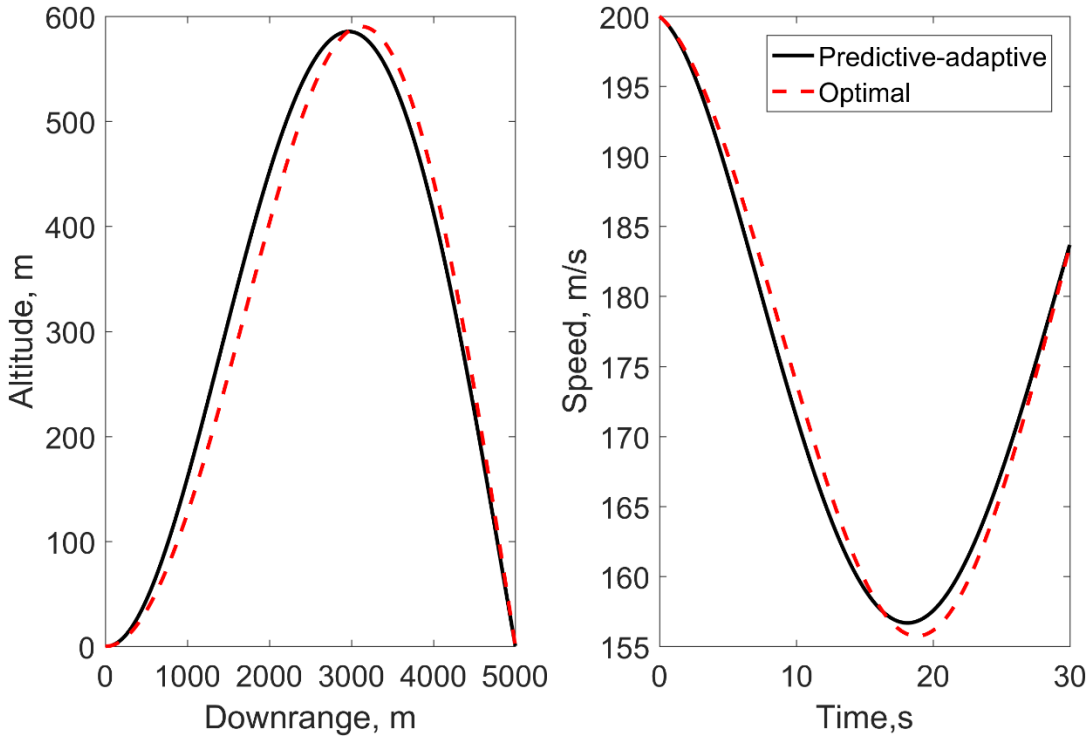

Figure 6.26 Trajectory and speed histories of the predictive-adaptive and the optimal solutions.

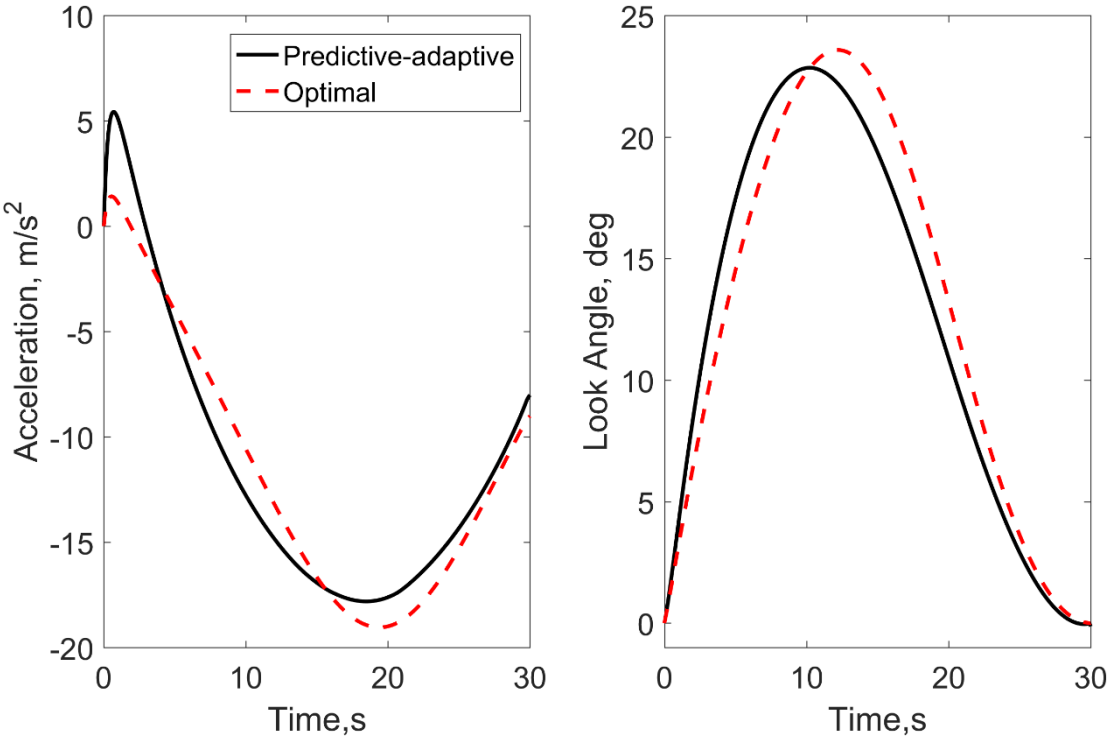

Figure 6.27 Acceleration and look angle histories of the predictive-adaptive and the optimal solutions.

Next, in order to extend the analysis of the optimality, more simulations are executed. Initial look angle is varied from 0 to 40 degrees and the desired impact time changes between 30 s to 40 s. The rest of the simulation parameters is as before. The cost functions could be seen in Figure 6.28. When the initial look angles are small, a tendency of diverging from optimality could be seen. Other than that, the overall agreement is encouraging. Also, the ratios of the cost functions are presented in Figure 6.29 with respect to Eq. (5.79). It could be said that the worst case is less than 20 %. It needs to be reminded that the worst case of the constant speed was less than 5 % as presented in Section 5.6.3. When the maximum look angle difference is analyzed, $\varepsilon_{3,\max} - \varepsilon_{o,\max}$, it would be observed as in Figure 6.30 that the optimal solution demands more look angle than the look angle shaping method, where the maximum difference is 8°. Last, $a_{3,\max} - a_{o,\max}$ is illustrated in Figure 6.31 and again the optimal solution also demands higher maximum accelerations in general. Nevertheless, these differences are not more than ± 4 m/s^2. Despite the fact that the look angle shaping demands smaller magnitudes, the optimal solution cannot be outperformed from the prospect of the running cost.

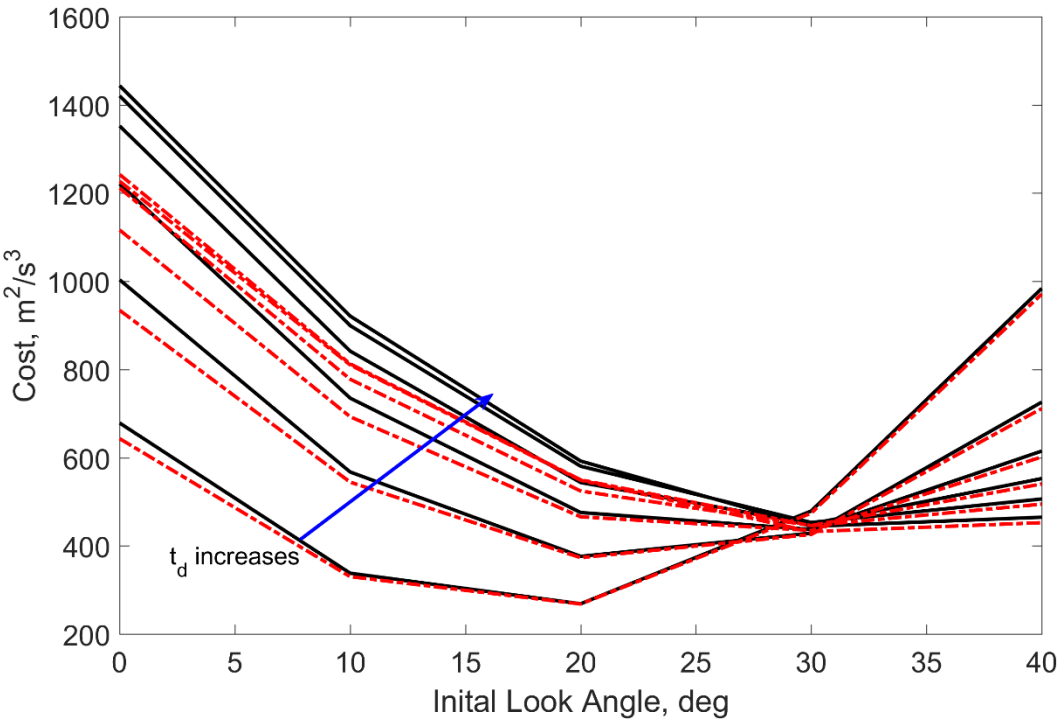

Figure 6.28 Cost functions of the guidance laws for varying speed scenarios.

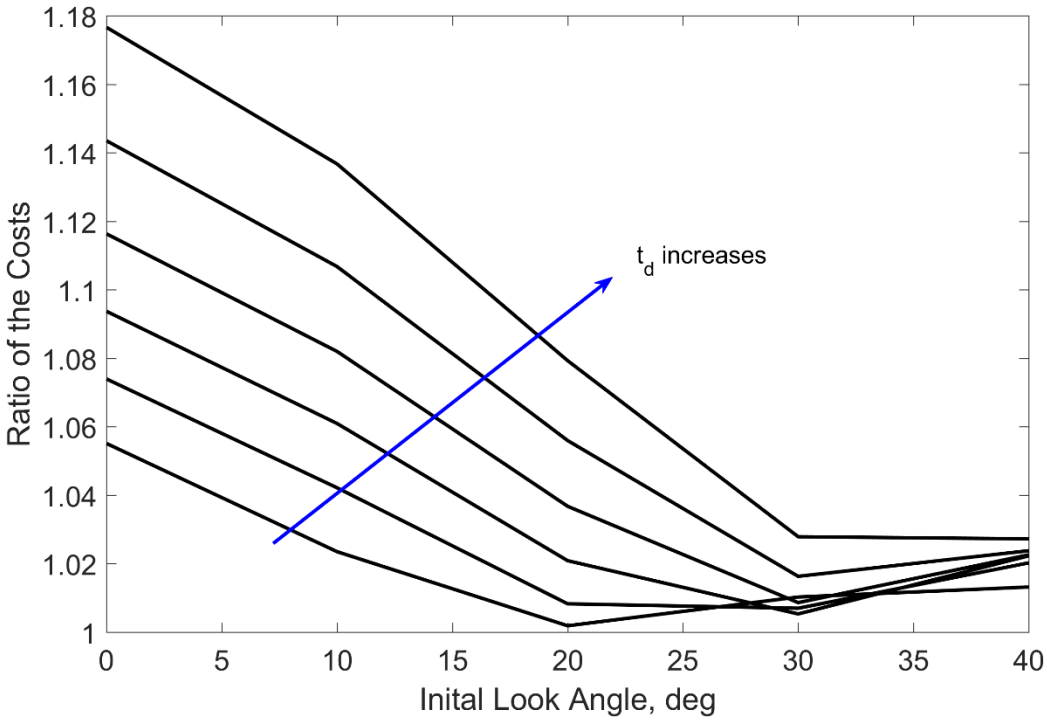

Figure 6.29 The ratio of the cost functions for varying speed scenarios.

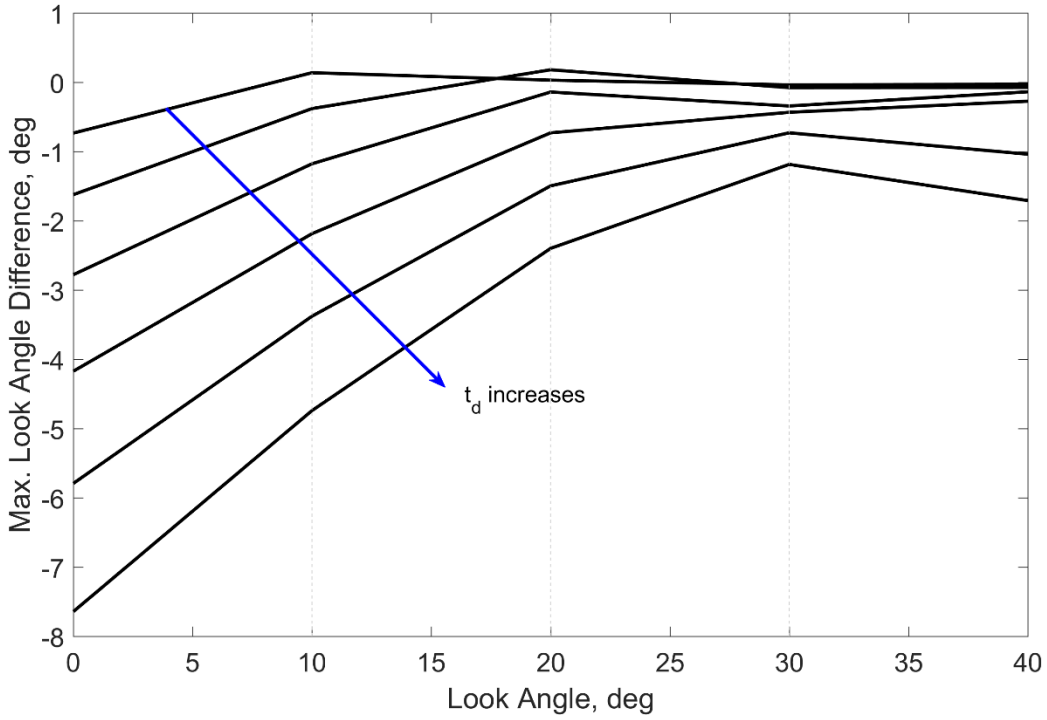

Figure 6.30 The difference of the maximum look angles for varying speed scenarios.

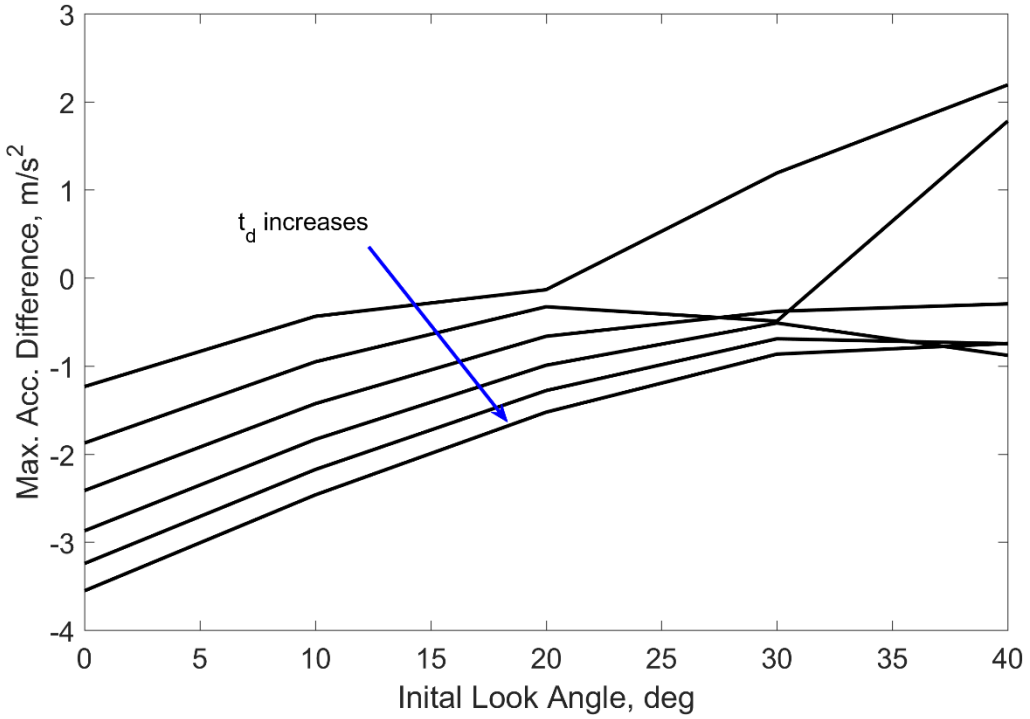

Figure 6.31 The difference of the maximum accelerations for varying speed scenarios.

6.4.2 Robustness Analysis Under Uncertain Drag Coefficient

In this final section, the predictive-adaptive algorithm is tested under uncertain drag coefficient. The details of the parameters used in the simulation are given in Table 6.5. The histogram of the obtained range-to-go at the desired impact time is shown in Figure 6.32. The majority of the simulations terminate with success. The maximum range-to-go is obtained for only one case, which is 31 meters, and the rest is mostly less than 10 m.

Table 6.5 Simulation parameters for uncertain drag coefficients.

Initial look angle, ε_0	$[0 \quad 10 \quad 20 \quad 30 \quad 40]^\circ$
Desired impact time, t_d	$[30 \quad 32 \quad 34 \quad 36 \quad 38 \quad 40]$ s
Drag uncertainty	$[-25 \quad -15 \quad -5 \quad 5 \quad 15 \quad 25]$%

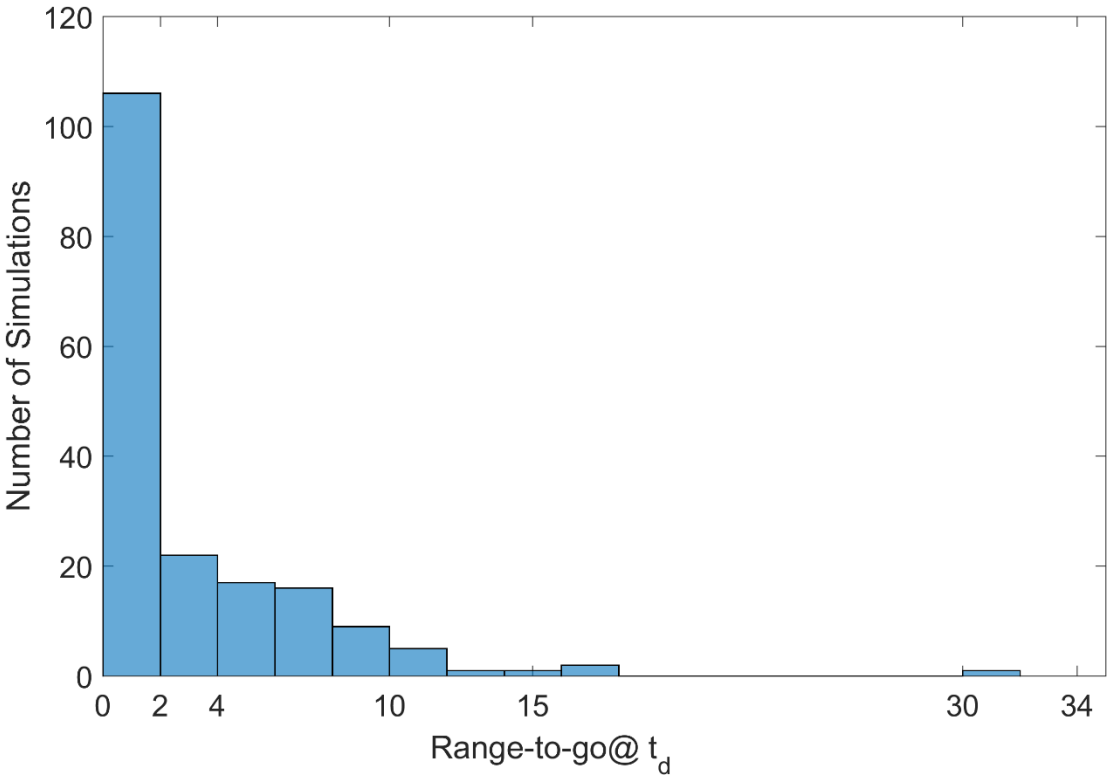

Figure 6.32 Histogram of the range-to-go at the desired impac time.

It is to be noted that, the uncertain drag coefficient could also be considered as an uncertainty caused by the induced drag and the air density varying with altitude, which are not included for the sake of simplicity. Studies have been carried on with the base and the induced drag. The performance is not affected much more than the uncertainties exemplified above. Thus, the results are not duplicated.

7 CONCLUSION

The guidance laws may require more information in contrast to the basic capture algorithms under the aim of satisfying extra objectives. Thus, there will be a price to be paid for objectives regarding the control of impact time, impact angle, or both simultaneously. Therefore, extra knowledge to be supplied. For instance, time-to-go estimation is typically needed to fulfill the objectives of trajectory shaping algorithms; in contrast, PN requires only the LOS rate.

Given infinite resources, it can be expected that any trajectory shaping method will be able to fulfill its objectives. In practice, however, feasibility is often what is needed for engineering problems and there are almost always a number of details that must be considered first. The availability of the information required by a guidance law is one concern. For example, time-to-go signals, which frequently appear in impact time control methods, generally require some sort of estimation. Since even the simplest estimation process will introduce additional complications, a guidance law that does not require such inputs would be advantageous. Another concern is associated with the control effort. A guidance law that does the same job with less total control effort would be a better choice. The third concern is the physical constraints. One constraint common to all missiles is the acceleration limit whereas the look angle limit is applicable to systems with seekers. If a control scheme is likely to violate these constraints, it will not be a feasible alternative. All of these concerns have been addressed in this dissertation in a way that is justified within the field of the guidance design.

7.1 Summary

The main outcome of the study is three different guidance laws for impact time control obtained through a common design framework. This new design approach is named as "shaping of the fundamental engagement states". The literature is dominated by methods based on PN and the nonlinear control theory, all of which require time-to-go estimation and/or high-g maneuvers at the beginning of the engagement. This work demonstrates that focusing on the

fundamental states enables guidance laws without these disadvantages. In this framework, the trajectory does not evolve into a PN trajectory since no time-to-go estimation. This brings the additional benefit that the guidance law would be difficult to predict as opposed to well-known guidance laws.

The range and the look angle are introduced as the fundamental states, which are shaped for impact time control. As well as the determination of the state to be shaped, it is also emphasized that designing the shaping function is also crucial. For instance, shaping the LOS angle as a function of downrange-to-go could result in complex and infeasible structures. However, since the ultimate objective is to capture the target at a specific time, a time dependent polynomial could be viewed as a natural choice for the shaping function. As the first method to control the impact time, a general polynomial formulation of the range that leads to a closed loop guidance formulation is introduced. Second, multi-phased look angle shaping is proposed, which can also be formulated with optimal control. Here, the global minimum and maximum impact time values are derived under given look angle and acceleration constraints. The third method is based on a general polynomial formulation of the look angle. In this guidance law, one gain has to be determined for impact time control. After selecting the order of the polynomial, this guidance gain is solved numerically for the nonlinear kinematics. Additionally, the analytical solution of the guidance gain for the linearized kinematics is presented. Using this analytical solution, an adaptive guidance scheme is presented to provide robustness under uncertainties. It is also shown that with a proper selection of the order of the polynomial, it is possible to have results, which are quite close to the energy optimal trajectories.

Another topic under investigation is the constrained impact time control. The approaches presented in this dissertation provide the time domain solutions of the engagement states. For instance, the LOS rate, the LOS angle and/or the flight path angle are made available. These time domain solutions offer many advantages, such that the maximum look angle or the maximum acceleration to be encountered could be known before the engagement. In addition, these solutions are used for constrained impact time control. In the first method, a solution considering the look angle constraint is introduced. In the second method, firstly the impact time intervals are determined with respect to the acceleration constraint. Next, both of the constraints associated with the acceleration and the look angle are handled in the design process. In the third method, the problem of impact time control under the look angle constraint is solved using the adaptive scheme.

Thus far, the speed is assumed to be constant for the guidance design process. Although some systems have the authority to control their speed, most of them do not have this feature. The last outcome of the dissertation is to present a solution for the problem of impact time control under varying speed, where the literature is short in this sense. The challenging issue in this problem is that the speed profile eventually depends on the guidance law itself. Yet in this case, the knowledge of the future mean speed of the missile could be effective. Following this direction, a predictive-adaptive scheme is designed and applied to the third impact time control method. It could be said that the gap in the literature related to the varying speed is filled without the need of the pre-flight analysis or unbounded acceleration demand. The results of the simulations involving gravity, autopilot lag, and uncertain drag show that such disturbing factors do not impede the performance. It must here be stated that the similarity of the obtained results with those of the energy optimal impact time control is a noteworthy byproduct. Last to mention, the prediction algorithm developed in this study can also be used in conjunction with any guidance law that provides the time domain solutions of the flight path angle and the guidance command.

7.2 Future Work

This study tries to address various aspects of the impact time control problem by proposing a feasible framework. By “feasible”, it is meant that the methods described here should be implementable under realistic circumstances. In this respect, the author hopes that this thesis will make a meaningful contribution to the literature. However, it is also true that it is not a complete treatment of the subject. For instance, the solutions are valid against stationary targets and they could be extended to cover moving targets. Second, since several numerical or analytical solutions for the final impact angle are available in this framework, simultaneous control of the impact angle and the impact time could be considered. This is an important and challenging topic that deserves overall attention in itself. Apart from these, as the third suggestion, this shaping framework could also be considered for the impact angle control problems. Although there is already a vast literature on this topic, the approach presented in this dissertation could be a new asset for designers.

8 REFERENCES

[1] Shneydor, N. A., Missile Guidance and Pursuit, Horwood, Chichester, West Sussex, 1998, p. 59, p.70, p. 77, p. 101, pp. 102–103, p. 218.

[2] Zarchan, P., Tactical and Strategic Missile, 6th ed., AIAA, Reston, VA, 2012, p.13, pp. 24–25, pp. 569–601, pp. 777–789.

[3] Yang, C.-D., and Yang, C.-C., "A Unified Approach to Proportional Navigation", IEEE Transactions on Aerospace and Electronic Systems, Vol. 33, No. 2, 1997, pp. 557–567.

[4] Murtaugh, S. A., and Criel, H. E., "Fundamentals of Proportional Navigation", IEEE Spectrum, Vol. 3, No. 12, 1966, pp. 75–85.

[5] Guelman, M., "A Qualitative Study of Proportional Navigation", IEEE Transactions on Aerospace and Electronic Systems, Vol. AES-7, No. 4, 1971, pp. 637–643.

[6] Shukla, U. S., and Mahapatra, P. R., "The Proportional Navigation Dilemma—Pure or True?", IEEE Transactions on Aerospace and Electronic Systems, Vol. 26, No. 2, 1990, pp. 382–392.

[7] Becker, K., "Closed-Form Solution of Pure Proportional Navigation", IEEE Transactions on Aerospace and Electronic Systems, Vol. 26, No. 3, 1990, pp. 526–533.

[8] Yuan, P.-J., and Chern, J.-S., "Ideal Proportional Navigation", Journal of Guidance, Control, and Dynamics, Vol. 15, No. 5, 1992, pp. 1161–1165.

[9] Kim, M., and Grider, K. V., "Terminal Guidance for Impact Attitude Angle Constrained Flight Trajectories," IEEE Transactions on Aerospace and Electronic Systems, Vol. AES-9, No. 6, 1973, pp. 852–859.

[10] Ryoo, C.-K., Cho, H., and Tahk, M.-J., "Optimal Guidance Laws with Terminal Impact Angle Constraint," Journal of Guidance, Control, and Dynamics, Vol. 28, No. 4, 2005, pp. 724–732.

[11] Erer, K. S., "Biased Proportional Navigation Guidance for Impact Angle Control with Extension to Three-Dimensional Engagements," Ph.D. dissertation, Mechanical Engineering Department, Middle East Technical University, Ankara, Turkey, 2015.

[12] Park, B.-G., Kim, T.-H., and Tahk, M.-J., "Optimal Impact Angle Control Guidance Law Considering the Seeker's Field-of-View Limits," Proceedings of the Institution of Mechanical Engineers, Part G: Journal of Aerospace Engineering, Vol. 227, No. 8, 2013, pp. 1347–1364.

[13] Tekin, R., and Erer, K. S., "Switched-Gain Guidance for Impact Angle Control under Physical Constraints," Journal of Guidance, Control, and Dynamics, Vol.38, No. 2, 2015, pp. 205–216.

[14] Erer, K. S., Tekin, R., and Özgören, M. K., "Look Angle Constrained Impact Angle Control Based on Proportional Navigation", AIAA Guidance, Navigation, and Control Conference, Kissimee, FL, 2015.

[15] Jeon, I.-S., Lee, J.-I., and Tahk, M.-J., "Impact-Time-Control Guidance Law for Anti-Ship Missiles," IEEE Transactions on Control Systems Technology, Vol. 14, No. 2, 2006, pp. 260–266.

[16] Chia, H. K., "A Simulation of a Combined Active and Electronic Warfare System for the Defense of a Naval Ship Against Multiple Low Altitude Missiles Threat," Master Thesis, Naval Postgraduate School September, 1989.

[17] https://en.wikipedia.org/wiki/Close-in_weapon_system, [cited 1 June 2017].

[18] http://www.thefreedictionary.com/salvo, [cited 1 June 2017].

[19] Jeon, I.-S., Lee, J.-I., and Tahk, M.-J., “Impact Time Control Guidance with Generalized Proportional Navigation Based on Nonlinear Formulation,” Journal of Guidance, Control, and Dynamics, Vol. 39, No. 8, 2016, pp. 1187–1892.

[20] Kim, T. H., Lee, C. H., Tahk, M. J., and Jeon, I. S., "Biased PNG Law for Impact Time Control," Transactions of Japan Society for Aeronautics and Space Sciences, Vol.56, No.4, Jun. 2013, pp. 205-214.

[21] Cho, N., and Kim, Y., " Modified Pure Proportional Navigation Guidance Law for Impact Time Control," Journal of Guidance, Control, and Dynamics, Vol. 39, No. 4, 2016, pp. 852–872.

[22] Shiyu, Z., Rui, Z., Chen, W., and Quanxin, D., “Design of Time-Constrained Guidance Laws via Virtual Leader Approach,” Chinese Journal of Aeronautics, Vol. 23, No. 1, 2010, pp. 103–108.

[23] Shiyu, Z., and Rui, Z., “Cooperative Guidance for Multi-Missile Salvo Attack,” Chinese Journal of Aeronautics, Vol. 21, No. 6, 2008, pp. 533–539.

[24] Jeon, I.-S., Lee, J.-I., and Tahk, M.-J., “Homing Guidance Law for Cooperative Attack of Multiple Missiles,” Journal of Guidance, Control, and Dynamics, Vol. 33, No. 1, 2010, pp. 275-280.

[25] Kim, M., Jung, B., Han, B., Lee, S., and Kim, Y., “Lyapunov-Based Impact Time Control Guidance Laws Against Stationary Targets,” IEEE Transactions on Aerospace and Electronic Systems, Vol. 51, No. 2, 2015, pp. 1111–1122.

[26] Saleem, A., and Ratnoo, A., “Lyapunov-Based Guidance Law for Impact Time Control and Simultaneous Arrival,” Journal of Guidance, Control, and Dynamics, Vol. 39, No. 1, 2016, pp. 164–173.

[27] Kumar, S. R., and Ghose, D., “Sliding Mode Control Based Guidance Law with Impact Time Constraints”, Proceedings of the American Control Conference, IEEE, 2013, pp. 5760–5765.

[28] Kumar, S. R., and Ghose, D., “Impact Time Guidance for Large Heading Errors Using Sliding Mode Control”, IEEE Transactions on Aerospace and Electronic Systems, Vol. 51, No. 4, 2015 pp. 3123 - 3138.

[29] Cho, D., Kim, H. J, and Tahk, M.-J., “Nonsingular Sliding Mode Guidance for Impact Time Control,” Journal of Guidance, Control, and Dynamics, Vol. 39, No. 1, 2016, pp. 61–68.

[30] Zhang, Y., Wang, X., and Wu, H., “Impact Time Control Guidance Law with Field of View Constraint,” Aerospace Science and Technology, Vol. 39, ,2014, pp. 361–369.

[31] Zhang, Y., Wang, X., and Wu, H., “Impact Time Control Guidance with Field of View Constraint Accounting for Uncertain System Lag,” Proceedings of the Institution of Mechanical Engineers, Part G: Journal of Aerospace Engineering, Vol. 230, No. 3, 2016, pp. 515–529.

[32] Jeon, I. S., and Lee, J. I, “Impact-Time-Control Guidance Law with Constraints on Seeker Look Angle,” IEEE Transactions on Aerospace and Electronic Systems, Vol. 99, 2017, pp. 361–369.

[33] Tahk, M. J., Ryoo, C. K., and Cho, H., “Recursive Time-To-Go Estimation for Homing Guidance Missiles,” IEEE Transactions on Aerospace and Electronic Systems, Vol. 38, No. 1, Jan. 2002, pp. 13–24.

[34] Dhananjay, N., and Ghose, D., “Accurate Time to Go Estimation for Proportional Navigation Guidance,” Journal of Guidance, Control, and Dynamics, Vol. 37, No. 4, 2014, pp. 1378–1383.

[35] Ghosh, S, Ghose, D., and Raha, S., “Unified Time-to-Go Algorithms for Proportional Navigation Class of Guidance,” Journal of Guidance, Control, and Dynamics, Vol. 39, No. 6, 2016, pp. 1118–1205.

[36] Tekin, R., Erer, K. S., and Holzapfel, F., “Control of Impact Time with Increased Robustness via Feedback Linearization,” Journal of Guidance, Control, and Dynamics, Vol. 39, No. 7, 2016, pp. 1678 –1684.

[37] Tekin, R., Erer, K. S., and Holzapfel, F., “Polynomial Shaping of the Look Angle for Impact Time Control,” Journal of Guidance, Control, and Dynamics, Vol. 40, No. 10, 2017, pp. 2668-2673.

[38] Gutman, S., “Impact-Time Vector Guidance,” Journal of Guidance, Control, and Dynamics, Vol. 40, No. 8, 2017, pp. 2110-2114.

[39] Tekin, R., Erer, K. S., and Holzapfel, F., “Quartic Range Shaping for Impact Time Control,” 25th Mediterranean Control and Automation Conference, Valetta, Malta, 2017.

[40] Tekin, R., Erer, K. S., and Holzapfel, F., “Impact Time Control with Generalized-Polynomial Range Formulation,” Journal of Guidance, Control, and Dynamics, Vol. 41, No. 5, 2018, pp. 1190-1195.

[41] Lee, J.-I., Jeon, I.-S., and Tahk, M.-J., “Guidance Law to Control Impact Time and Angle,” IEEE Transactions on Aerospace and Electronic Systems, Vol. 43, No. 1, 2007, pp. 301–310.

[42] Harl, N., and Balakrishnan, S. N., “Impact Time and Angle Guidance with Sliding Mode Control,” IEEE Transactions on Control Systems Technology, Vol. 20, No. 6, 2012 pp. 1436–1449.

[43] Kim, T.-H., Lee, C.-H., Jeon, I.-S., and Tahk, M.-J., “Augmented Polynomial Guidance with Impact Time and Angle Constraints,” IEEE Transactions on Aerospace and Electronic Systems, Vol. 49, No. 4, 2013, pp. 2806–2817.

[44] Kim, T.-H., “Polynomial Function Based Guidance for Impact Angle and Time Control,” Journal of the Korea Society for Industrial and Applied Mathematics, Vol. 19, No. 3, 2015, pp. 305-325.

[45] Arita, S., and Ueno, S., “Optimal Feedback Guidance for Nonlinear Missile Model with Impact Time and Angle Constraints,” Guidance, Navigation, and Control and Co-located Conferences, August 19-22, 2013, Boston, MA, AIAA 2013-4785.

[46] Erer, K. S., and Tekin, R., “Impact Time and Angle Control Based on Constrained Optimal Solutions,” Journal of Guidance, Control, and Dynamics, Vol. 39, No. 10, 2016, pp. 2448–2454.

[47] Lennox, D., “Cruise Missile Technologies and Performance Analysis,” Jane's Strategic Weapon Systems, Vol. 40, Jane's Defense Data, 2004.

[48] Bezick, S., Rusnak, I., and Gray, W. S., “Guidance of a Homing Missile via Nonlinear Geometric Control Methods,” Journal of Guidance, Control, and Dynamics, Vol. 18, No. 3, 1995, pp. 441–448.

[49] Snyder M., Qu, Z., Hull, R., and Prazenica, R., “Quad-Segment Polynomial Trajectory Guidance for Impact-Time Control of Precision-Munition Strike,” IEEE Transactions on Aerospace and Electronic Systems, Vol. 52, No. 6, 2016, pp. 3008-3023.

[50] Zhou J., Wang, Y., and Zhao, B., “Impact-Time-Control Guidance Law for Missile with Time-Varying Velocity,” Mathematical Problems in Engineering, Vol. 2016, 2016, pp. 1-14.

[51] Jeon, I.-S., Lee, J.-I., and Tahk, M.-J., “Closed –Form Optimal Guidance Law for Missiles of Time Varying Velocity,” Journal of Guidance, Control, and Dynamics, Vol. 19, No. 5, 1996, pp. 1017–1022.

[52] Cho, H., Ryoo, C.K., and Tahk, M.-J., “Implementation of Optimal Guidance Laws Using Predicted Missile Velocity Profiles,” Journal of Guidance, Control, and Dynamics, Vol. 22, No. 4, 1999, pp. 579-588.

[53] Lu, P., Doman, D. B., and Schierman, J. D., “Adaptive Terminal Guidance for Hypervelocity Impact in Specified Direction,” Journal of Guidance, Control, and Dynamics, Vol. 29, No. 2, 2006, pp. 269–278.

[54] Tyan, F., “Adaptive PPN Guidance Law with Impact Angle Constraint,” American Control Conference, Washington, DC, 2013.

[55] Tekin, R., Erer, K. S., and Holzapfel, F., “Adaptive Impact Time Control via Look Angle Shaping Under Varying Velocity,” Journal of Guidance, Control, and Dynamics, Vol. 40, No. 12, 2017, pp. 3247–3255.

[56] Tsiotras, P., Mesbahi, M., “Toward an Algorithmic Control Theory,” Journal of Guidance, Control, and Dynamics, Vol. 40, No. 2, 2017, pp. 194-196.

[57] Lu, P., “Introducing Computational Guidance and Control,” Journal of Guidance, Control, and Dynamics, Vol. 40, No. 2, 2017, pp. 193.

[58] Ohlmeyer, E. J., and Phillips, C. A., “Generalized Vector Explicit Guidance,” Journal of Guidance, Control, and Dynamics, Vol. 29, No. 2, 2006, pp. 261–268.

[59] Zarchan, P., and Nesline, F. W., “A New Look at Classical vs Modern Homing Missile Guidance,” Journal of Guidance, Control, and Dynamics, Vol. 4, No. 1, 1981, pp. 78–85.

[60] Kim, T. H., Park, B. G., and Tahk, M. J., “Bias-Shaping Method for Biased Proportional Navigation with Terminal-Angle Constraint”, Journal of Guidance, Control, and Dynamics, Vol. 36, No. 6, 2013, pp. 1810–1816.

[61] Sang D. K., and Tahk, M. J, “Guidance Law Switching Logic Considering the Seeker’s Field-of-View Limits,” Proceedings IMechE, Part G: Journal of Aerospace Engineering, Vol. 223, 2009, pp.1049–1058.

[62] Tekin, R., and Erer, K. S., "Considerations on Boost Phase Modeling and Guidance Command Generation", AIAA Guidance, Navigation, and Control Conference, Kissimmee, 2015.

[63] Rieck, M., Bittner, M., Grüter, B., and Diepolder, J., FALCON.m User Guide, online available at www.falcon-m.com, [cited 7 June 2017].

[64] Kirk, D. E., Optimal Control Theory: An Introduction, Dover, Mineola, NY, 1998, pp. 184–209.

[65] Wang, X., "Solving Optimal Control Problems with MATLAB — Indirect Methods", Technical Report, ISE Dept., NCSU, 2009.

[66] Aidala, V. J., "Kalman Filter Behavior in Bearings-Only Tracking Applications", IEEE Transactions on Aerospace and Electronic Systems, Vol. AES-15, No. 1, 1979, pp. 29–39.

[67] Taur, D.-R., and Chem, J.-S., "Passive Ranging for Dog-Fight Air-to-Air IR Missiles", AIAA Guidance, Navigation, and Control Conference, Portland, 1999, pp. 1737–1751.

[68] Ogata, K., Modern Control Engineering, Prentice-Hall, Upper Saddle River, NJ. 2002, pp. 288-293.

[69] Ross, I. M., A Primer in Pontryagin's Principle in Optimal Control, Collegiate Publishers, Carmel, CA, 2009, pp. 22–33.

[70] Gopalan, A., Ratnoo, A., and Ghose, D., "Time-Optimal Guidance for Lateral Interception of Moving Targets," Journal of Guidance, Control, and Dynamics, Vol.39, No. 3, 2016, pp. 510–525.

APPENDIX A

DERIVATION OF TIME-TO-GO APPROXIMATION OF PN GUIDANCE

[24] presents a time-to-go estimation solution of PN guidance. Since time-to-go estimation of PN is often mention in the dissertation, it is briefly explained. The differential equations governing the engagement between a pursuer and a stationary target are

$$\dot{x} = V\cos\gamma, \quad \dot{y} = V\sin\gamma \tag{A.1}$$

where the guidance command is

$$\dot{\gamma} = \frac{a}{V} \tag{A.2}$$

which is perpendicular to the velocity vector. The PN guidance command is

$$a = NV\dot{\lambda} \tag{A.3}$$

Under the small angle assumption and constant speed V, substituting x/V for t yields

$$dx = Vdt \tag{A.4}$$

and the differential equations can be written as

$$y' = \gamma, \quad \gamma' = a/V^2 \tag{A.5}$$

Here, prime denotes the derivative with respect to *x*. The LOS angle in the linear domain is approximated as

$$\lambda = -\frac{y}{\left(x_f - x\right)} \tag{A.6}$$

Then, using Eq. (A.6) for λ', Eq. (A.3) turns out to be

$$a\left(x\right) = -\frac{NV^2}{\left(x_f - x\right)^2} y - \frac{NV^2}{\left(x_f - x\right)} y' \tag{A.7}$$

Replacing Eq. (A.7) into Eq. (A.5), then the following Cauchy equation is obtained

$$y'' + \frac{N}{\left(x_f - x\right)} y' + \frac{N}{\left(x_f - x\right)^2} y = 0 \tag{A.8}$$

where the initial conditions are $y\left(0\right) = 0,\ y'\left(0\right) = \gamma_0$. The solution of this equation is

$$y\left(x\right) = \frac{\gamma_0}{N-1}\left(x_f - x\right)\left(1 - \left(1 - \frac{x}{x_f}\right)^{N-1}\right) \tag{A.9}$$

Differentiating Eq. (A.9) with respect to *x* leads to

$$\gamma\left(x\right) = -\frac{\gamma_0}{N-1}\left(1 - N\left(1 - \frac{x}{x_f}\right)^{N-1}\right) \tag{A.10}$$

The length of the trajectory is

$$S = Vt_f = \int_0^{x_f} \sqrt{1 + y'^2}\, dx \tag{A.11}$$

If $y'\ \left(= \gamma\right)$ is assumed to be small, then Eq. (A.11) can be approximated using Eq. (A.10) as

$$Vt_f \approx \int_0^{x_f} \left(1+0.5y'\right)^2 dx = x_f \left(1+\frac{\gamma_0^2}{2\left(2N-1\right)}\right) \tag{A.12}$$

Finally, the time-to-go estimation of PN

$$t_f \approx \frac{x_f}{V}\left(1+\frac{\gamma_0^2}{2\left(2N-1\right)}\right) \tag{A.13}$$

t_f can be regarded as the time-to-go estimation at the initial time. It is always possible to set the inertial coordinate system at the initial time as a specific coordinate system with *x* axis consistent with the current LOS angle. Therefore, γ_0 coincides with ε_0. Hence, the time-to-go estimation of PN in terms of R_0 and ε_0 is as given in [24]

$$t_{go} \approx \frac{R_0}{V}\left(1+\frac{\varepsilon_0^2}{2\left(2N-1\right)}\right) \tag{A.14}$$

and for the instantaneous time, the time-to-go estimation of PN becomes

$$t_{go} \approx \frac{r}{V}\left(1+\frac{\varepsilon^2}{2\left(2N-1\right)}\right) \tag{A.15}$$

APPENDIX B

NONSINGULAR SLIDING MODE IMPACT TIME CONTROL

For comparison purposes, a nonlinear sliding mode impact time control method is chosen, whose details can be read in [29]. The sliding surface is defined as

$$s = t_f - t_d = t + t_{go} - t_d = t_{go} - t_{go,d} \tag{B.1}$$

where $t_{go,d}$ represents the desired time-to-go. The time derivative of the switching surface is

$$\dot{s} = \dot{t}_{go} - \dot{t}_{go,d} \tag{B.2}$$

Using the time-to-go estimation in Eq. (A.15), Eq. (B.2) turns out to be:

$$\dot{s} = \frac{\dot{r}}{V}\left\{1 + \frac{1}{2(2N-1)}\varepsilon^2\right\} - \frac{r\varepsilon}{V(2N-1)}\dot{\lambda} + 1 + \frac{r\varepsilon}{V^2(2N-1)}a \tag{B.3}$$

with the help of Eq. (2.4). Using Lyapunov-based nonlinear control theory, the guidance command can be written as

$$a = a^{eq} + a^{con} \tag{B.4}$$

One of the two components of the guidance command is

$$a^{eq} = \frac{V^2(2N-1)}{r}\frac{(\cos\varepsilon - 1)}{\varepsilon} + \frac{0.5V^2}{r}\varepsilon\cos\varepsilon + V\dot{\lambda} \tag{B.5}$$

for $\dot{s}=0$. The second guidance component is for satisfying the Lyapunov stability conditions.

$$a_{con} = -\frac{k}{\varepsilon} s \tag{B.6}$$

Here, k is a positive constant and s is the sliding surface defined in Eq. (B.1). The authors express that the interception by impact happens when $r \neq 0$ due to a certain size of the target; therefore, the condition of zero range does not cause singularity. However, the command has a singularity when the look angle is zero, which will cause unbounded acceleration. Here, to avoid singularity, a_{con} is modified as

$$\hat{a}_{con} = -\frac{h(\varepsilon)}{\varepsilon} ks \tag{B.7}$$

$h(\varepsilon)$ is a continuous function, which is defined as

$$h(\varepsilon) = \begin{cases} \operatorname{sgn}(\varepsilon)\varepsilon & \text{if } |\varepsilon| < e_1 \\ \dfrac{1-e_1}{e_2-e_1}|\varepsilon| + \dfrac{e_1(e_2-1)}{e_2-e_1} & \text{if } e_1 \le |\varepsilon| \le e_2 \\ 1 & \text{otherwise} \end{cases} \tag{B.8}$$

where e_1 and e_2 are small positive constants. However, this new guidance command cannot satisfy the impact time when $\varepsilon = 0$ and $s \neq 0$. To overcome this problem, an additional guidance term is added to Eq. (B.4):

$$a_{sw} = -M\left(p\operatorname{sgn}(\varepsilon)+1\right)\operatorname{sgn}(s) \tag{B.9}$$

where $p>1$ and $M>0$. Finally, the final guidance command for impact time control is the sum of Eq. (B.5), Eq. (B.7) and Eq. (B.9):

$$a^{eq} = \frac{V^2(2N-1)}{r}\frac{(\cos\varepsilon-1)}{\varepsilon} + \frac{0.5V^2}{r}\varepsilon\cos\varepsilon + V\dot{\lambda} - \frac{h(\varepsilon)}{\varepsilon}ks - M\left(p\operatorname{sgn}(\varepsilon)+1\right)\operatorname{sgn}(s) \tag{B.10}$$

APPENDIX C

NONLINEAR OPTIMAL CONTROL SOLUTION

Starting from a set of initial conditions, the optimal control enabling the achievement of a set of specified final conditions in some planar engagement geometry can be obtained by following the guidelines outlined in [64]. The states of the optimal control problem are selected as

$$x_1 = r \tag{C.1}$$

$$x_2 = \varepsilon \tag{C.2}$$

which are the fundamental states used in this dissertation. Referring to Eq. (2.7) and Eq. (2.8), the state equations below can be written for constant speed with the help of Eq. (2.4):

$$\dot{x}_1 = -V\cos x_2 \tag{C.3}$$

$$\dot{x}_2 = V\frac{\sin x_2}{x_1} + u \tag{C.4}$$

where u is the control: $\dot{\gamma}$. The cost function of the final time boundary value problem is defined as

$$E = \frac{1}{2}\int_0^{t_f} u^2 \mathrm{d}t \tag{C.5}$$

With α denoting the costate, the Hamiltonian can be constructed as

$$H = -V\alpha_1\cos x_2 + V\alpha_2\frac{\sin x_2}{x_1} + \alpha_2 u + \frac{1}{2}u^2 \tag{C.6}$$

Exploiting the facts that $\mathrm{d}\bar{x}/\mathrm{d}t = \partial H/\partial \bar{\alpha}$ and $\mathrm{d}\bar{\alpha}/\mathrm{d}t = -\partial H/\partial \bar{x}$ and using Eq. (C.3) and Eq. (C.4), the differential equation set corresponding to the optimal control problem can be derived as

$$\begin{bmatrix} \dot{x}_1 \\ \dot{x}_2 \\ \dot{\alpha}_1 \\ \dot{\alpha}_2 \end{bmatrix} = \begin{bmatrix} -V\cos x_2 \\ V\dfrac{\sin x_2}{x_1} - \alpha_2 \\ V\alpha_2 \dfrac{\sin x_2}{x_1^2} \\ -V\alpha_1 \sin x_2 - V\alpha_2 \dfrac{\cos x_2}{x_1} \end{bmatrix} \tag{C.7}$$

The boundary conditions are

$$\begin{bmatrix} \bar{x}(0) & \bar{x}(t_\mathrm{f}) \end{bmatrix}^\mathrm{T} = \begin{bmatrix} R_0 & \varepsilon_0 & 0 & 0 \end{bmatrix}^T \tag{C.8}$$

The third and fourth conditions are seen to be zero, which follows from the fact that the final values of the range and the look angle must be zero in order to capture a stationary target with a finite acceleration. For a given initial condition set, final time is user specified, which is a control parameter that determines the shape of the trajectory. The boundary conditions given in Eq. (C.8) are sufficient to initiate the solution process because the final time is fixed. The solution of Eq. (C.7) with Eq. (C.8) necessitates numerical techniques. One convenient way to overcome this problem is to utilize the MATLAB command “bvp4c” [65]. The following is the MATLAB code used to solve the problem:

```
function sol=TimeControl
solinit     = bvpinit(linspace(0,tf),[10;1;0;0]);
sol         = bvp4c(@odefun,@bcfun,solinit);

function dydt=odefun(t,y)

dydt = [ -cos(y(2))
         sin(y(2))/y(1)-y(4)
         y(4)*sin(y(2))/y(1).^2
        -y(3)*sin(y(2))-y(4)*cos(y(2))/y(1) ];

function res=bcfun(ya,yb)
epsi0 = 20*pi/180;     %  Initial look angle
```

```
R0    = 5000;          %  Initial range
V     = 200;           %  Missile speed
Res   =[ ya(1)-R0/V;   %  Minimum time
         ya(2)-eps0    %  Initial look angle
         yb(1)         %  Final range
         yb(2) ];      %  Final look angle
```

The states and their derivatives can be extracted from the solution as follows:

```
dt= 0.001;            %  Sample time
t = 0:dt:tf;
sxint = deval(sol,t);
u = -sxint(4,:);
U = [t;u];
```

APPENDIX D

RANGE OBSERVER

The “passive ranging” problem is typically solved for moving targets through the use of Kalman filters as in [66] and [67] and the missile trajectory is often modified to enhance observability. The range observer, which is based on the state observer methodology in [68], is structured on the nonlinear kinematics against a stationary target in [11]. It also addresses the observability issue through a simple switching action that stops the pseudo range measurement from being fed back to the system when required.

The nonlinear engagement model including the system and the measurement model is

$$\dot{r} = u = -V\cos\varepsilon \tag{D.1}$$

$$r = y = -\frac{V\sin\varepsilon}{\dot{\lambda}} \tag{D.2}$$

where u is the input and y is the measurement. In fact, y is the pseudo measurement because the range is not measured directly. An approximation is obtained by combining the outputs from the inertial navigation system and the seeker. The block diagram of the proposed range observer is presented in Figure D.1. $\tilde{r}$ is the range estimate and *K* is the observer gain, which could be constant or varying.

The range becomes unobservable when the missile is in the collision course as mentioned in [66] and [67]. In this structure, when the LOS rate is zero, the un-observability manifests itself in the pseudo-measurement equation. The observability switch shown in the figure is to address this problem. However, due to the noisy signal provided by the seeker, this

phenomenon would show itself not when the LOS angle rate becomes identically zero but when its absolute value drops below a certain threshold, which depends on the system being studied.

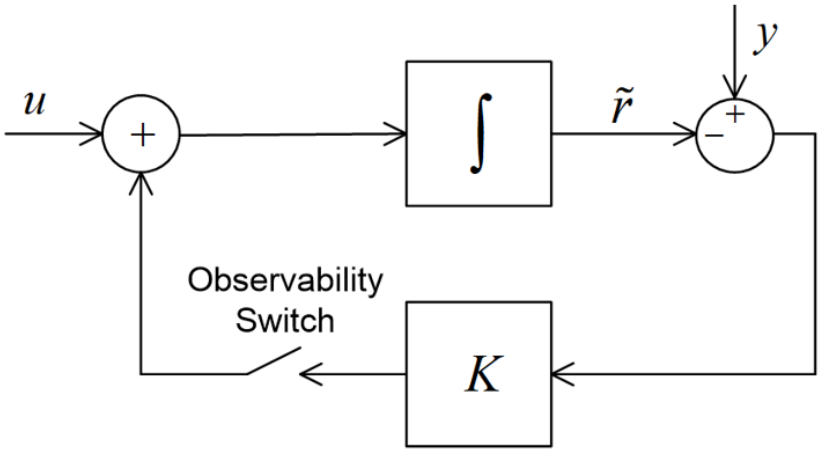

Figure D.1 Range observer structure.

So; if this situation is realized, the error feedback could be simply switched off. It is to be noted that the system flows through the open-loop route in this situation. In addition, if the observability switch goes off after the range estimation has converged, even the system model without the erroneous measurement might still yield acceptable estimates.

The transfer function relating the output to the inputs can be written as

$$\tilde{R}(s) = \frac{1}{s+K} U(s) + \frac{K}{s+K} Y(s) \tag{D.3}$$

It is seen that the observer essentially acts as a low-pass filter for both the input and the measurement. The proposed range estimator/observer could be implemented with only two user defined parameters: The gain to adjust the bandwidth and the threshold to prevent the estimation process from collapsing. The method operates independent of the guidance law and can be used in conjunction with any law that would benefit from the range information. For more details and examples, [11] could be read.

APPENDIX E

CONSTRAINED IMPACT TIME CONTROL REFORMULATION VIA OPTIMAL CONTROL

[46] presents impact time and impact angle control problem based on constrained optimal solutions. Here, only the impact time solution is briefly expressed. The investigated system is under the effect of physical constraints $\dot{\gamma}_{\max}$ and $\varepsilon_{\max}$, respectively associated with the rotation rate and the look angle capacities. To keep the solution less complicated, only the rotation rate constraint will be considered firstly, after which the look angle constraint will be incorporated into the solution.

Subject to the dynamic constraints in Eq. (2.8) and Eq. (2.9), the state equations could be written as

$$\begin{bmatrix} \dot{\alpha}_1 \\ \dot{\alpha}_2 \\ \dot{\alpha}_3 \end{bmatrix} = \begin{bmatrix} -\cos\alpha_2 \\ \dfrac{\sin\alpha_2}{\alpha_1} + u \\ u \end{bmatrix} \tag{E.1}$$

Here, the states are defined as $\alpha_1 = r/V$, $\alpha_2 = \varepsilon$ and $\alpha_3 = \gamma$ whereas the input is $u = \dot{\gamma}$. The boundary conditions are

$$\begin{bmatrix} \bar{\alpha}(0) \\ \bar{\alpha}(t_f) \\ \Downarrow \\ free \end{bmatrix} = \begin{bmatrix} \alpha_{1,0} & \alpha_{2,0} & \alpha_{3,0} & 0 & 0 & \text{free} \end{bmatrix}^T \tag{E.2}$$

Under the influence of the input constraint

$$|u| \leq u_{\max} \tag{E.3}$$

The problem is to minimize either of the following costs

$$J = \pm t_{\mathrm{f}} \tag{E.4}$$

As seen in Eq. (E.2), the final values of the range and the look angle must be zero for the stationary target to be captured. On the other hand, the impact time is free to assume any values dictated by the solution that is to be obtained. The nature of the problem, i.e. whether the quantity of interest is to be minimized or maximized, is determined by the sign multipliers seen in Eq. (E.4). For example, if the final time is to be maximized, the cost function should be $J = -t_{\mathrm{f}}$. The Hamiltonian associated with this problem valid for the both cost functions may be formed as

$$H = -\beta_1 \cos\alpha_2 + \beta_2 \frac{\sin\alpha_2}{\alpha_1} + (\beta_2 + \beta_3)u \tag{E.5}$$

which is to remain constant because of the fact that it does not explicitly depend on time. Then, using the relation $\dot{\bar{\beta}} = -\partial H / \partial \bar{\alpha}$, the differential equations associated with the costates are obtained

$$\begin{bmatrix} \dot{\beta}_1 \\ \dot{\beta}_2 \\ \dot{\beta}_3 \end{bmatrix} = \begin{bmatrix} \beta_2 \dfrac{\sin\alpha_2}{\alpha_1^2} \\ -\beta_1 \sin\alpha_2 - \beta_2 \dfrac{\cos\alpha_2}{\alpha_1} \\ 0 \end{bmatrix} \tag{E.6}$$

Noting from the previous equation that the third costate is unchanging, Eq. (E.5) implies that the control that minimizes the Hamiltonian ($\partial H / \partial u = 0$) can be written as

$$u = \begin{cases} u_{\max}, & \beta_2 < -\beta_{3,\mathrm{f}} \\ -u_{\max}, & \beta_2 > -\beta_{3,\mathrm{f}} \\ u_{\mathrm{s}}, & \beta_2 = -\beta_{3,\mathrm{f}} \end{cases} \tag{E.7}$$

where the singular interval is denoted by subscript *s*. To find out whether the last condition in this equation may be realized over a finite time interval, the differential equation associated with the second costate and the Hamiltonian itself are evaluated. This gives the second costate

$$\dot{\beta}_{2,\mathrm{s}} = -\beta_{1,\mathrm{s}} \sin\alpha_{2,\mathrm{s}} + \beta_{3,\mathrm{f}} \frac{\cos\alpha_{2,\mathrm{s}}}{\alpha_{1,\mathrm{s}}} = 0 \tag{E.8}$$

and the Hamiltonian

$$H_{\mathrm{s}} = -\beta_{1,\mathrm{s}} \cos\alpha_{2,\mathrm{s}} - \beta_{3,\mathrm{f}} \frac{\sin\alpha_{2,\mathrm{s}}}{\alpha_{1,\mathrm{s}}} = h \tag{E.9}$$

where $\beta_{3,\mathrm{f}}$ is 0 and *h* is ∓ 1 as per the terminal transversality and Hamiltonian value conditions [69], respectively.

Using Eq. (E.8) and Eq. (E.9) the following can be shown: A singular interval may exist when $\sin\alpha_2 = 0$. The physical interpretation of this result is that the pursuer, utilizing zero control, moves either towards or away from the target over a straight line trajectory. This situation is naturally applicable to the minimum time scenarios, where $J > 0$. As for the maximum time scenarios, where $J < 0$, neither a direct course to the target is feasible nor moving in the opposite direction is allowed; so, no singular interval can exist in this case. Now, the general forms of the control laws may be deduced based on the information gathered above. For the minimum time problem, it makes sense that the pursuer captures the target using a straight line trajectory, which happens to be the singular solution. Yet before that, the look angle must be brought to zero as soon as possible, which can be realized by exerting the full control effort. For the maximum time problem, on the other hand, it makes sense that the purser captures the target using the least direct trajectory, which can only be achieved by firstly increasing the look angle and then decreasing it under the action of full control effort.

It is now convenient to discuss the effect of the look angle constraint on the optimal solutions. One may immediately appreciate that the constraint is ineffective in the minimum time problem. However, the situation is different for the maximum time problem. The look

angle will sooner or later reach it. Once this happens, the optimal strategy is to keep the look angle at the constraint value. This policy needs to be carried out until such an instant that the target can finally be captured by applying the full control effort in the opposite direction.

Based on the discussion above, the two-phased open loop control profile of the minimum time problem can be written as

$$u = \begin{cases} -u_{\max}, & t \le \hat{t} \\ 0, & t > \hat{t} \end{cases} \tag{E.10}$$

where $\hat{t}$ is the time instant, at which the look angle becomes zero, which is in fact $\hat{t}_c$ as described in Section 4.2.1. As might be expected, such a strategy will produce a Dubin's path [70]. It is to be noted that Eq. (E.10) is the same Eq. (4.60), where the LOS rate is zero for the minimum time problem. Based on the discussion above, the three-phased open loop control profile for the maximum time problem can be deduced as

$$u = \begin{cases} -u_{\max}, & t \le \tilde{t} \\ -\dfrac{\sin\alpha_2}{\alpha_1}, & \tilde{t} < t \le \breve{t} \\ u_{\max}, & t > \breve{t} \end{cases} \tag{E.11}$$

where $\tilde{t}$ is the instant, at which the look angle reaches its limit and $\breve{t}$ denotes the latest time for the beginning of the terminal maneuver. These time instants are the critical time instants as previously described. If the switching from the second phase to the third phase occurs later than $\breve{t}$, it will not be possible to reach the target without violating the acceleration limit. Moreover, if the switching occurs earlier than $\breve{t}$, the target can be captured, but without exerting the full control effort. These time instants are actually the critical switching instants as described in Section 4.2.1. It is necessary to remind that Eq. (E.11) has the same structure with Eq. (4.63) for the maximum time problem.

It would also be helpful to have a look at some general trajectories. Figure E.1 shows two different trajectories, each of which belongs to one of the optimal families just discussed. The portions of the trajectories where the control becomes saturated are highlighted in bold curves whereas the remaining portions are presented in plain curves. The circles with a radius of $V/\dot{\gamma}_{\max}$ acting as maneuvering boundaries are drawn in dashed lines. As seen, the two-phased

minimum time trajectory rapidly converges towards the target, finishing over a straight line. On the other hand, the three-phased maximum time trajectory is seen to rapidly diverge from the target until it hits the look angle limit. Then, it follows a path that maintains a constant look angle before finishing over a circular arc.

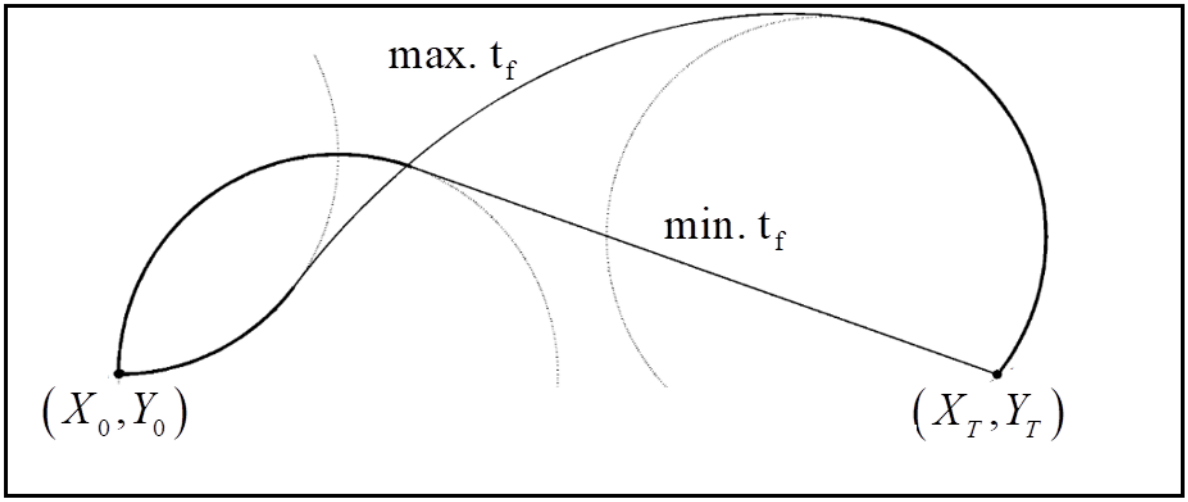

Figure E.1 Optimal trajectories.

APPENDIX F

FRESNEL INTEGRALS FOR IMPACT TIME CONTROL

The indefinite integral without the integration constant of the cosine of Eq. (5.9) can compactly be written as

$$I = \sqrt{\frac{1}{\kappa_2}}\left(\cos\phi F_c - \sin\phi F_s\right) \tag{F.1}$$

where ϕ

$$\phi = \varepsilon_0 - \frac{(\kappa_2 {t_f}^2 + \varepsilon_0)^2}{4\kappa_2 {t_f}^2} \tag{F.2}$$

F_c and F_s are the Fresnel cosine and the Fresnel sine integrals, respectively. These are defined as

$$F_c = \int_0^f \cos\zeta^2 d\zeta = \sum_{n=0}^{\infty}(-1)^n \frac{f^{4n+1}}{(2n)!(4n+1)} \tag{F.3}$$

and

$$F_s = \int_0^f \sin\zeta^2 d\zeta = \sum_{n=0}^{\infty}(-1)^n \frac{f^{4n+3}}{(2n)!(4n+3)} \tag{F.4}$$

in which

$$f = \sqrt{\frac{1}{\kappa_2}}\left(\kappa_2 t - \frac{\kappa_2 {t_f}^2 + \varepsilon_0}{2t_f}\right) \tag{F.5}$$

As seen, the integrals can be represented in terms of infinite summations. Then, the definite integral given in Eq. (5.27) may approximately be written as

$$\frac{R_0}{V} \approx \sqrt{\frac{1}{\kappa_2}}\left\{\cos\phi\left(\hat{F}_{c,f} - \hat{F}_{c,0}\right) - \sin\phi\left(\hat{F}_{s,f} - \hat{F}_{s,0}\right)\right\} \tag{F.6}$$

where $\hat{F}_c$ and $\hat{F}_s$ denote approximations to the Fresnel integrals obtained by keeping a finite number of terms in Eq. (F.3) and Eq. (F.4). Hence, the guidance gain may be calculated by solving the approximate transcendental equation presented in Eq. (F.6) instead of solving the integral equation in Eq. (5.27). It is important to note that, because Eq. (F.6) is only an approximation to Eq. (5.27), it might happen that the numerical algorithm operating on the former converges to a solution that does not satisfy the latter. In such a case, the guidance gain obtained in the linearized domain could be used as the initial guess.

APPENDIX G

OPTIMAL IMPACT TIME SOLUTION IN THE LINEAR DOMAIN

The differential equations related to the impact time problem for the linearized kinematics can be written as follows:

$$\begin{bmatrix} \dot{x}_1 \\ \dot{x}_2 \\ \dot{x}_3 \end{bmatrix} = \begin{bmatrix} x_2 \\ u \\ \beta\left\{1+0.5\left(x_2/\beta\right)^2\right\} \end{bmatrix} \tag{G.1}$$

where the states are defined as $x_1 = y$, $x_2 = \dot{y}$, $x_3 = \dot{S}$. u is the control input and $\beta = x_f / t_f$ is a known constant. The objective is to find the control input which minimizes

$$J = \frac{1}{2}\int_0^{t_f} u^2 dt \tag{G.2}$$

The Hamiltonian associated with this problem can be constructed as

$$H = \zeta_1 x_2 + \zeta_2 u + \zeta_3 \beta\left\{1+\frac{1}{2}\left(\frac{x_2}{\beta}\right)^2\right\} + \frac{1}{2}u^2 \tag{G.3}$$

where ζ_1, ζ_2 and ζ_3 are the costates. The optimal control must satisfy $\partial H/\partial u = 0$, which resolves into

$$u = -\zeta_2 \tag{G.4}$$

Then, using the relation $-\partial H/\partial \bar{x} = \dot{\bar{\zeta}}$, the differential equations associated with the costates are obtained as

$$\begin{bmatrix} \dot{\zeta}_1 \\ \dot{\zeta}_2 \\ \dot{\zeta}_3 \end{bmatrix} = \begin{bmatrix} 0 \\ -\zeta_1 - \zeta_3 x_2/\beta \\ 0 \end{bmatrix} \tag{G.5}$$

which shows that first and the third costates are constant. The final value of the second state is free, so the following must hold: $u_f = \zeta_{2,f} = 0$. Thus, the boundary conditions of the optimal control problem can be written as

$$\begin{bmatrix} x_{1,0} & x_{2,0} & x_{3,0} & x_{1,f} & u_f & x_{3,f} \end{bmatrix} = \begin{bmatrix} x_{1,0} & x_{2,0} & 0 & x_{1,f} & 0 & Vt_f \end{bmatrix} \tag{G.6}$$

Generally speaking, the initial and the final values of the first state can be anything. However, $x_{1,0} = x_{1,f} = 0$ is assumed here for simplicity with no loss of generality. Merging the second item in Eq. (G.1) with the second item in Eq. (G.5), the following differential equation can be obtained:

$$\ddot{x}_2 = \zeta_1 + \frac{\zeta_3 x_2}{\beta} \tag{G.7}$$

It can be shown that this equation leads to the following solution for the states:

$$\begin{bmatrix} x_1 \\ x_2 \\ x_3 \end{bmatrix} = \begin{bmatrix} \frac{1}{\alpha}\left(C_1 e^{\alpha t} - C_2 e^{-\alpha t}\right) + \rho t + C_3 \\ C_1 e^{\alpha t} + C_2 e^{-\alpha t} + \rho \\ \left\{\frac{1}{\beta}\left(C_1 C_2 + \frac{\rho^2}{2}\right) + \beta\right\} t + \frac{\rho t_f}{\alpha\beta}\left(C_1 e^{\alpha t} - C_2 e^{-\alpha t}\right) + \frac{1}{4a\beta}\left(C_1^2 e^{2\alpha t} - C_2^2 e^{-2\alpha t}\right) + C_4 \end{bmatrix} \tag{G.8}$$

Here, C_{1-4} are the integration constants, $\rho = -\beta\zeta_1/\zeta_3$, and $\alpha = \sqrt{\zeta_3/\beta}$. The optimal control then becomes

$$u = \alpha\left(C_1 e^{\alpha t} - C_2 e^{-\alpha t}\right) \tag{G.9}$$

The problem with this representation is that although u is real-valued, the coefficients are not. Therefore, the following manipulation is suggested:

$$\alpha = \upsilon i,\ C_{1,2} = -\mu e^{\mp i\left(\upsilon t_f\right)} \tag{G.10}$$

When Eq. (G.10) is replaced in Eq. (G.9) where necessary, the control input yields

$$u = \mu\upsilon i\left(e^{i\upsilon\left(t_f - t\right)} - e^{-i\upsilon\left(t_f - t\right)}\right) \tag{G.11}$$

Then, Euler`s formula is written for the related functions:

$$\begin{aligned} e^{i\upsilon\left(t_f - t\right)} &= \cos\left(\upsilon\left(t_f - t\right)\right) + i\sin\left(\upsilon\left(t_f - t\right)\right) \\ e^{-i\upsilon\left(t_f - t\right)} &= \cos\left(\upsilon\left(t_f - t\right)\right) - i\sin\left(\upsilon\left(t_f - t\right)\right) \end{aligned} \tag{G.12}$$

When Eq. (G.12) is used in Eq. (G.11), it becomes

$$u = \mu\upsilon i\left\{2i\sin\left(\upsilon\left(t_f - t\right)\right)\right\} \tag{G.13}$$

Finally, the optimal guidance command turns into the following form:

$$u = -2\mu\upsilon\sin\left(\upsilon\left(t_f - t\right)\right) \tag{G.14}$$

where μ and υ are real-valued constants to be determined numerically.